

Dissertation
submitted to the
Combined Faculties for the Natural Sciences and for Mathematics
of the Ruperto-Carola University of Heidelberg, Germany
for the degree of
Doctor of Natural Sciences

Presented by:

Diplom-Biologe Eike Christoph Kienle

Born in: Worms (Germany)

Oral Examination: 11. November 2014

**Secrets to finding the ideal mate:
New insights into parameters that govern
successful Adeno-associated virus (AAV)
vector evolution**

Referees: Prof. Dr. Hans-Georg Kräusslich
Dr. Dirk Grimm

Contents

Contents	5
Abbreviations	8
Summary	10
Zusammenfassung.....	12
1 Introduction.....	14
1.1 Gene Therapy - targets and vectors	15
1.2 Adeno-associated Virus.....	18
1.2.1 AAV classification and genome structure.....	18
1.2.2 AAV capsid structure	20
1.2.3 Receptors and tropisms of AAV serotypes	21
1.2.4 AAV infection and intracellular processing	25
1.2.5 Recombinant AAV (rAAV) vectors	28
1.3 Molecular AAV vector evolution	31
1.3.1 DNA Family Shuffling	33
1.3.2 Peptide display	34
1.4 Objectives	37
2 Materials and Methods	38
2.1 Materials.....	38
2.1.1 Cell lines and viruses	38
2.1.2 Cell Culture Media and Additives	39
2.1.3 Nucleotides.....	39
2.1.4 Standard markers	39
2.1.5 Enzymes.....	40
2.1.6 Kits	40
2.1.7 Buffers and solutions.....	40
2.1.8 Bacteria:.....	41
2.1.9 Chemicals and reagents.....	42

2.1.10	Equipment	43
2.1.11	Materials.....	44
2.1.12	Software:	45
2.2	Methods	45
2.2.1	Standard microbiological methods	45
2.2.2	Standard molecular biological methods.....	46
2.2.3	Cell biological methods	49
2.2.4	Cloning procedures.....	50
2.2.5	DNA family shuffling.....	60
2.2.6	AAV virus production.....	62
2.2.7	Selection procedures.....	66
2.2.8	Flow Cytometry	68
2.2.9	Bioinformatic analysis of shuffled sequences	68
3	Results	69
3.1	AAV DNA Family Shuffling	69
3.1.1	Optimization of the protocol for generation of shuffled AAV libraries.....	70
3.1.2	Analysis of parameters influencing AAV library selection.....	77
3.1.3	<i>In vivo</i> biopanning of an AAV15689 library	98
3.2	AAV peptide display	103
3.2.1	Engineering of alternative AAV serotypes for peptide display	103
3.2.2	Characterization of AAV serotype-peptide panels	109
3.2.3	AAV peptide display screens	113
3.2.4	Consensus sequence NXXRXXX	117
3.2.5	Specific applications of AAV peptide display.....	119
4	Discussion	131
4.1	AAV capsid shuffling	132
4.1.1	An optimized shuffling protocol is key to generation of diverse AAV libraries	132
4.1.2	The selection process is equally decisive for the success of the shuffling approach..	134

4.2	Peptide display	145
4.2.1	Expansion of peptide display to 11 AAV serotypes other than AAV2	145
4.2.2	Implications of peptide display on AAV transduction	147
4.2.3	AAV peptide mutants can be readily exploited for specific applications.....	150
4.3	Advantages, challenges and perspectives of AAV evolution technology.....	152
5	Appendix.....	157
5.1	Supplementary heatmaps	157
5.1.1	Transduction pattern of AAV1-12 with peptides P1-P6	157
5.1.2	Transduction pattern of AAV1-12 with peptides of the MP	160
5.2	Supplementary data on AAV library selection schemes	162
5.3	Supplementary electronic Data.....	163
6	References.....	164
	Remarks.....	192
	Danksagung	193

Abbreviations

μ	Micro
μg	Microgram
μl	Microliter
mM	Millimolar
aa	Amino acid
AAV	Adeno-associated virus
Ad5	Adenovirus type 5
ATP	Adenosine triphosphate
bp	Base pair
BSA	Bovine serum albumin
cDNA	Complementary DNA
ddH ₂ O	Double-distilled water
DMEM	Dulbecco's modified Eagle medium
DNA	Deoxyribonucleic acid
dNTP	Deoxynucleoside triphosphate
DRG	Dorsal root ganglion
<i>E. coli</i>	<i>Escherichia coli</i>
EDTA	Ethylendinitrilo-N, N, N', N'-tetraacetate
FBS	Fetal bovine serum
g	Relative centrifugal force
h	Hour(s)
ITR	Inverted terminal repeat
kb	Kilobases (unit for DNA and RNA - 1000 nucleotides)
kDa	Kilo Daltons (unit for protein mass)
LB media	Lysogeny broth media
M	Molar
mA	Milliampere
MCS	Multiple cloning site
mg	Milligram
min	Minute(s)
miRNA	microRNA
ml	Milliliter

Abbreviations

mM	Millimolar
MOI	Multiplicity of infection
mRNA	Messenger ribonucleic acid
NEAA	Non-essential amino acids
nt	Nucleotide
o.n.	Over night
OD	Optical density
oligo	Oligonucleotide
ORF	Open reading frame
P/S	Penicillin/streptomycin
PAGE	Polyacrylamide gel electrophoresis
PBS	Phosphate buffered saline
PCR	Polymerase chain reaction
PEI	Polyethyleneimine
PFA	Paraformaldehyde
qRT-PCR	Quantitative real-time PCR
rAAV	Recombinant AAV
RNA	Ribonucleic acid
RNAi	RNA interference
rpm	Revolutions per minute
RT	Room temperature
scAAV	Self-complementary AAV
SDS	Sodium dodecyl sulfate
sec	Seconds
ss	single-stranded
ssAAV	single-stranded AAV
ssDNA	single-stranded DNA
TBS	Tris buffered saline
TBST	Tris buffered saline + Tween
TEMED	Triethylmethylethyldiamine
Tris	Tris (hydroxymethyl) aminomethane
UV	Ultraviolet
V	Volt
wt	Wild type
α	Anti

Summary

The success of human gene therapy - the treatment of hereditary or acquired diseases with a genetic cause - depends on potent, safe and specific gene delivery vectors. Amongst the large variety of currently available non-viral or viral vectors, those derived from Adeno-associated viruses (AAV) are particularly attractive due to a unique combination of assets: the virus/vector is apathogenic, poses little risk of insertional mutagenesis, has a broad host and cell range, and can easily be modified and produced in large quantities. However, no natural AAV fulfills all the requirements for clinical use in humans, raising a need for new technologies and strategies to engineer synthetic “designer” vectors.

Accordingly, the central aim of this work was to improve and apply two fundamental methods for molecular AAV vector evolution, DNA family shuffling and peptide display. The first technology relies on fragmentation and homology-based recombination of capsid genes from closely related AAV serotypes, resulting in libraries of AAV chimeras from which capsids with desired properties can be enriched via subsequent selection. Here, we initially assessed and optimized the key steps for AAV shuffling, culminating in a robust and standardized new protocol for AAV library generation. Next, we used this protocol to shuffle AAV2, 8 and 9, and exploited the resulting library to analyze two major parameters for AAV selection - helper virus and anti-AAV-antibodies. Interestingly, we found that AAV capsids selected in the presence of a helper virus give stronger gene expression, implying that their intracellular processing is enhanced. Moreover, comparative analyses of AAVs isolated under various conditions with human antisera showed that the degree of negative selection pressure determines the balance between infectivity and immunity of the viral particles. Finally, we also performed a helper virus-free *in vivo* biopanning with a library comprising AAV1, 5, 6, 8 and 9 in murine pancreas. Intriguingly, gene expression from the single clone emerging after three selection rounds was low, supporting our conclusion that the presence of a helper virus is key for potent AAV vector evolution.

Unlike shuffling, AAV vector improvement through peptide display starts with a single viral serotype (traditionally AAV2) whose capsid is expanded by insertion of 7-9 aa into an exposed loop, with the aim to alter vector tropism towards desired target cells. Here, we extended this strategy to 11 alternative AAV serotypes and demonstrate their tremendous, previously unrecognized potential as scaffolds for viral peptide display. Therefore, we first implemented a simple PCR protocol for rapid cloning of peptide-encoding sequences into AAV capsid genes, which replaces the original stepwise mutagenesis. We then used our new approach to insert 6 distinct peptides into all 12 AAV serotypes, resulting in a collection of 84 YFP-encoding vectors (12 wildtypes & 72 mutants). While screening this panel in a large array of human and non-human cell lines and primary cells, we made three

important observations: i) AAV vector transduction is not determined by the peptide alone but largely depends on the capsid context; ii) alternative AAV serotypes with certain peptides frequently outperform the AAV2 prototype and its peptide derivatives; and iii) some serotype-peptide combinations even allow to transduce cells previously considered refractory to AAV infection. Subsequent analysis of further peptides showed that a common motif, NxxRxxx, is enriched in the best performing candidates and particularly enhances AAV1, 7-9 and rh.10. Based on these findings, we assembled a “Master panel” of vectors including the superior serotype-peptide combinations from our various screens, and used it in collaborative studies to select potent new AAV vectors in clinically relevant cell types, such as myeloid cell lines, primary human myeloma cells, or dorsal root ganglia and proprioceptive neurons.

As a whole, the work in this thesis makes a number of essential contributions to the fields of AAV biology, AAV vector development and human gene therapy. First, it resulted in optimized protocols and tools that substantially simplify, standardize and accelerate the future generation of tailored AAV capsids for vector engineering. Second, it also yielded a wide variety of new AAV variants - either in the form of shuffled libraries or as panels of specific capsid-peptide combinations - that can now be screened in further cell lines, primary cells or even directly *in vivo*. Third, the data obtained in this thesis with the various wildtype, shuffled or peptide-modified capsids greatly improve our knowledge of fundamental steps in cellular AAV infection. Most importantly, our results consistently exemplify that the function of AAV capsids is not determined by single residues, but rather results from very complex interactions of different regions that are dispersed throughout the viral shell. Altogether, the present thesis fuels the belief that AAV is one of the most versatile, powerful and robust viral vector systems available today and that it provides unique benefits for clinical translation in humans.

Zusammenfassung

Der Erfolg humaner Gentherapie - die Behandlung angeborener oder erworbener Erkrankungen mit genetischen Ursachen - hängt ab von wirksamen, sicheren und spezifischen Vektoren zum Transport von „fremdem“ genetischem Material. Unter den gegenwärtig verfügbaren nicht-viralen und viralen Vektoren erweisen sich solche basierend auf Adeno-assoziierten Viren (AAV) dank einer einzigartigen Kombination günstiger Eigenschaften als besonders attraktiv: Virus und Vektor sind apathogen, haben ein geringes Risiko für Mutationen durch Integration, zeigen ein breites Wirtszell-Spektrum, sind leicht modifizierbar und in großem Maßstab produzierbar. Allerdings erfüllt kein natürlich vorkommendes AAV alle Bedingungen für die klinische Anwendung im Menschen, weshalb neue Technologien und Strategien für die Entwicklung synthetischer „Designer“- Vektoren notwendig sind.

Zentrales Ziel dieser Arbeit war demgemäß die Optimierung und Anwendung zweier prinzipieller Methoden zur molekularen AAV-Vektor-Evolution, „DNA-Family-Shuffling“ und „Peptid-Display“. Die erste Technologie basiert auf der Fragmentierung und homologen Rekombination von Kapsidgenen verwandter AAV-Serotypen, gefolgt von der Selektion von Kapsiden mit gewünschten Eigenschaften aus den resultierenden Bibliotheken chimärer AAVs. In dieser Arbeit wurden zunächst die wichtigsten Schritte des Shuffling-Prozesses ermittelt und optimiert, um basierend darauf ein neues, robustes und standardisiertes Protokoll festzulegen. Nach dessen Verwendung zum „Shuffling“ der Serotypen AAV2, 8 und 9 wurden anhand der erzeugten Bibliothek zwei wichtige Aspekte der AAV-Selektion studiert - Helfervirus und anti-AAV-Antikörper. Interessanterweise konnte gezeigt werden, dass in Anwesenheit des Helfervirus selektierte AAV-Kapside eine stärkere Genexpression vermitteln, was auf bessere intrazelluläre Prozessierung hinweist. Weiterhin zeigte die vergleichende Untersuchung von AAV-Isolaten nach Selektion unter verschiedenen Bedingungen in Anwesenheit von humanem Antiserum, dass das Ausmaß des negativen Selektionsdrucks das Verhältnis zwischen Infektiösität und Immunogenität bestimmt. Abschließend wurde eine Bibliothek aus den Serotypen AAV1, 5, 6, 8 und 9 in Abwesenheit von Helferviren im Pankreas von Mäusen selektioniert. Überraschenderweise zeigte der nach drei Selektionsrunden angereicherte Klon eine geringe Expression, was unsere These unterstützt, dass eine erfolgreiche AAV-Vektor-Evolution die Anwesenheit von Helferviren erfordert.

Anders als beim Shuffling startet die AAV-Vektor-Optimierung durch Peptid-Display mit nur einem Serotyp (meist AAV2), dessen Kapsid durch den Einbau von 7-9 Aminosäuren in eine exponierte Region verändert wird. Ziel ist dabei die Anpassung des Vektor-Tropismus an einen gewünschten Zelltyp. Diese Strategie wurde hier auf 11 weitere Serotypen erweitert, was zur Entdeckung ihres enormen, bisher unbeachteten Potenzials als Gerüst für Peptid-Display geführt hat. Hierzu wurde zuerst ein PCR-Protokoll etabliert, das die schnelle und einfache Klonierung Peptid-kodierender

Sequenzen in AAV-Kapsidgene ermöglicht und das die bisherige schrittweise Mutagenese-Strategie ersetzt. Dieser Ansatz wurde nachfolgend zum Einbau von sechs definierten Peptiden in alle 12 AAV-Serotypen verwendet, was zu einer Kollektion von 84 YFP-kodierenden Vektoren geführt hat (12 Wildtypen & 72 Mutanten). Das 'Screening' dieser Kollektion auf einer Vielzahl humaner und nicht-humaner Zelllinien und primären Zellen ergab drei wichtige Befunde: i) AAV-Vektor-Transduktion wird nicht nur durch das Peptid bestimmt, sondern hängt stark vom Kapsid-Kontext ab; ii) alternative Serotypen mit bestimmten Peptiden übertreffen häufig den AAV2-Prototyp und davon abgeleitete Derivate; und iii) einige Serotyp-Peptid-Kombinationen erlauben sogar die Transduktion von Zellen, die bisher als resistent gegenüber AAV galten. Die Analyse dieser und weiterer Peptide führte zur Identifikation des Motivs NxxRxxx, das in den effizientesten Peptiden angereichert ist und besonders AAV1, 7-9 und rh.10 verbessert. Aufgrund dieser Ergebnisse wurde ein 'Master Panel' (MP) erstellt, welches die besten Serotyp-Peptid-Kombinationen aus den verschiedenen Screens umfasst. Dieses MP wurde in Kooperation mit anderen Gruppen verwendet, um potente neue AAV-Vektoren in diversen klinisch relevanten Zellen zu identifizieren, darunter myeloide Zelllinien, primäre humane Myelomzellen, sowie neuronale Zellen der dorsalen Wurzelganglien und propriozeptive Neuronen.

Zusammengefasst leistet die vorliegende Arbeit wichtige Beiträge für das Feld der AAV-Biologie, der AAV-Vektor-Entwicklung und der humanen Gentherapie. Erstens erlauben die optimierten Protokolle und Konstrukte künftig die einfachere, standardisierte und rapidere Generierung maßgeschneiderter AAV-Vektoren. Zweitens erbrachte die Arbeit vielfältige neue AAV-Varianten - in Form chimärer Bibliotheken oder spezieller Kapsid-Peptid-Kombinationen - die nun in weiteren Zelllinien, primären Zellen oder *in vivo* getestet werden können. Drittens haben die in dieser Arbeit mit verschiedenen natürlichen, chimären oder Peptid-modifizierten AAV-Kapsiden erzielten Daten unser Verständnis fundamentaler Schritte der zellulären AAV-Infektion erweitert. Eine zentrale Erkenntnis war, dass die Funktion von AAV-Kapsiden nicht durch einzelne Aminosäuren bestimmt wird, sondern durch komplexe Interaktionen verschiedener verteilter Regionen. Insgesamt unterstützt die vorliegende Arbeit die Ansicht, dass AAV eines der vielseitigsten, leistungsfähigsten und robustesten viralen Vektor-Systeme ist, welches einzigartige Vorteile für die klinische Anwendung im Menschen bietet.

1 Introduction

Over four decades ago, the term “gene therapy” was coined to describe the fundamental concept to treat human disorders by correcting the underlying genetic defect(s). For the first time in the history of medicine, it promised the option to tackle hereditary diseases at their core, *i.e.*, the genes that are either mutated or missing in pathologically altered cells. Accordingly, the first gene therapies aimed at introducing functional versions of these genes into a patient’s cells *ex* or *in vivo*, in order to reconstitute an intact genome and to restore proper expression of the affected protein. Immediately it became clear, however, that pivotal to the success of any such strategy is the availability of gene delivery vehicles, so-called vectors that can potently, safely and specifically transfer the therapeutic nucleic acids into the target cells. Moreover, it also soon became evident that mere delivery of ectopic DNAs (or RNAs) would not suffice to treat all variants of human disorders with a genetic component. This is because many of these are caused by an inherent over-abundance of disease-associated genes, exemplified by pathogen infections or many cancers, creating a need to extend gene therapies to strategies that also suppress or eliminate nucleic acids, rather than adding them.

Fortunately, the past decade has yielded a flurry of new developments and powerful technologies that nowadays make the realization of clinical gene therapy likelier than ever. Most crucial advances include the discovery that RNA interference (RNAi), an endogenous process of gene silencing through short double-stranded RNAs, is active in human cells and can be harnessed for deliberate knockdown of disease-associated gene expression [1]–[5]. Together with the latest generations of designer nucleases (zinc finger nucleases, TALEns or, most recently, the CRISPR system) that provide potent and specific modalities for gene/genome engineering [6], these novel technologies now offer unprecedented possibilities to treat human diseases not only by gene over-expression, but also by suppression or repair of underlying genetic defects. In parallel, vector systems for delivery of therapeutic cassettes have undergone steady and substantial improvement, culminating in today’s availability of a collection of non-viral or viral tools many of which are under extensive clinical evaluation. Amongst these, most notable candidates are vectors derived from Adeno-associated viruses (AAV), due to a unique combination of beneficial features such as their inherent apathogenicity and their amenability to genetic engineering. These vectors were also in the center of the present thesis, whose essential aim it was to devise and validate novel approaches to enhance the efficiency and specificity of AAV gene therapy vectors through molecular engineering and stringent selection.

Before describing the results of this work, the following chapters will provide a more profound overview over gene therapy and the vectors used thus far, and then focus on AAV biology as well as on the presently available techniques for AAV vector optimization through directed evolution.

1.1 Gene Therapy - targets and vectors

To date, over 2000 clinical trials - from phase I to IV - have been conducted world-wide to assess the concept of gene therapy in human volunteers and patients. According to the database at www.abedia.com/wiley/index.html, the vast majority of these trials - roughly two thirds - took place in the United States, whereas a quarter was centered in Europe and 4.2% in Germany (Figure 1A-B).

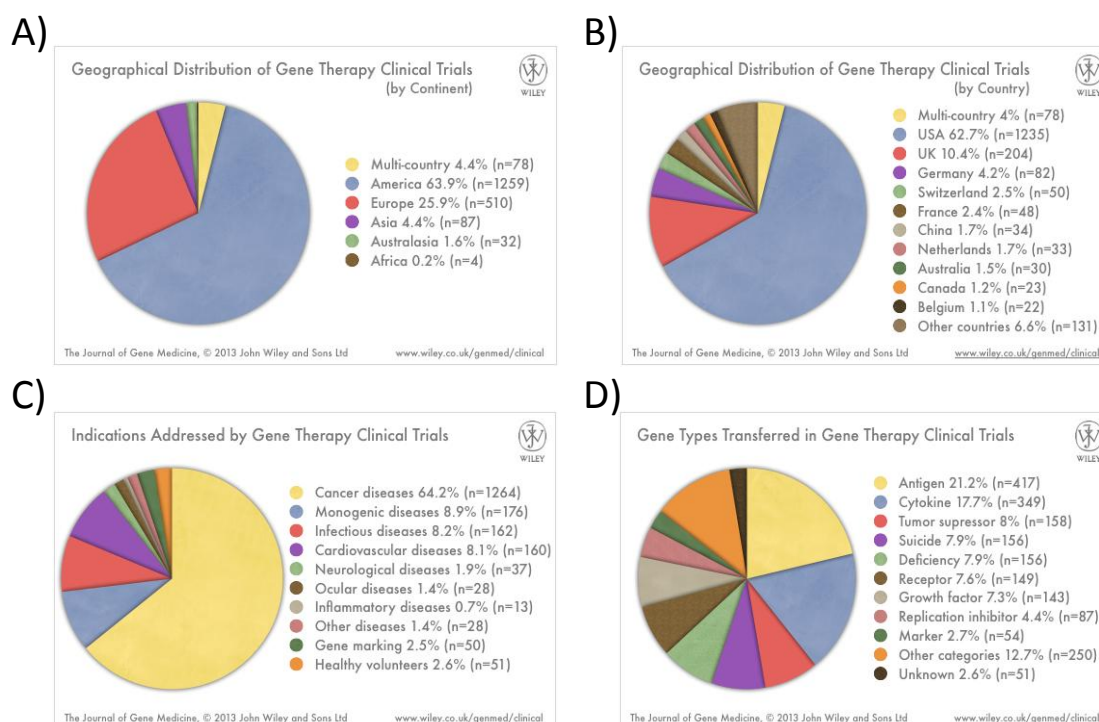


Figure 1: Overview over gene therapy trials conducted until 2013. Shown are the geographical distribution of all world-wide gene therapy trials by continent (A) or country (B), as well as the indications studied (C) and genes delivered (D) thus far. The four panels were taken from the freely accessible gene therapy database at www.abedia.com/wiley/index.html.

Of all these trials, about two thirds tackled cancers, while the rest focused on a large variety of hereditary or acquired human diseases (Figure 1C). Equally diverse is the list of therapeutic or reporter/marker genes that have been transferred in all these trials thus far (Figure 1D).

Because the individual approaches and trials have already been discussed in great detail in the literature (*e.g.*, [7], [8]), and because the focus of the present thesis was on the vector aspect of human gene therapy, it should suffice to highlight a few hallmark studies in the following. Particularly notable are early attempts which triggered serious adverse events but nonetheless significantly

advanced our knowledge. These include one unfortunate fatality during a 1999 gene therapy trial aimed at curing ornithine transcarbamylase deficiency (an X-linked genetic liver disease). The 18-year old patient who died had been treated with a high dose of a recombinant Adenovirus vector expressing a correct version of the defect gene, which resulted in a rapid and massive immune response and multiple organ failure [9]–[12]. Additional concern over the safety of gene therapy arose when multiple children that had received genetically modified cells to treat X-linked severe combined immunodeficiency (X-SCID) developed leukemia-like conditions (that were treatable by conventional means) [13], [14]. For obvious reasons, these and other adverse events during the early days of gene therapy not only resulted in halts of the corresponding clinical trials, but also provided major setbacks for the entire field.

Fortunately, the continuous improvements in the safety and specificity of gene therapy vectors (see below) have recently allowed numerous impressive clinical successes which have now renewed the interest in this promising technology. One example are gene therapies for hemophilia B, a potentially fatal blood clotting disorder caused by defects in, or the absence of, human factor IX. In a remarkable study that is widely recognized in the gene therapy field, Nathwani and colleagues infused six hemophilia B patients with a single dose of an optimized AAV serotype 8 vector encoding factor IX [15]. Strikingly, as presented in detail at the 2013 annual meetings of the American or European Gene & Cell Therapy Societies, respectively, all six patients continue to express detectable factor IX over two years after gene therapy vector administration, in the absence of serious adverse events. Another important group of human disorders where gene therapies were highly successful are inherited blinding diseases of the eye, such as Leber's congenital amaurosis (LCA, caused by defects in the *RPE65* gene). A series of high-profile papers from the past few years have reported safe improvements in the vision of LCA patients treated with AAV vectors encoding a correct version of the mutated gene [16]–[18]. Finally, yet another example highlighting the increasing success rates of gene therapies are two recent *Science* papers describing very promising clinical data from children treated with lentiviral vectors, who originally suffered from metachromatic leukodystrophy or Wiskott-Aldrich syndrome [19], [20].

As noted, all these latest breakthroughs in human gene therapy trials were only made possible by the steady improvements in vector design that have alleviated multiple safety concerns, by increasing the efficiency and specificity of gene delivery, by reducing the immunogenicity and by advancing the options to control vector gene expression within the treated cell. In general, currently used vectors for gene therapy can broadly be segregated into non-viral or viral vectors. Non-viral vectors comprise *e.g.* complexes of cationic polymers or lipids with the DNA or RNA that has to be delivered. The negative charge of nucleic acids allows binding of the cationic polymers and lipids, resulting in so-

called polyplexes or lipoplexes that have still a positive net charge and bind anionic cellular surface receptors, such as heparan sulfate proteoglycans (HSPG). Cellular uptake of these complexes is mediated by endocytosis or, more specifically, by phagocytosis [21]–[27]. Inside the cell, the DNA is then released from the endosomes either by destabilization of the endosomal membrane by the complexed lipids [28], or by rupture of the endosomal membrane by the cationic polymers [29]. Major advantages of these polyplexes or lipoplexes are that they can be formed with DNA/RNA of any size and can be easily produced in large scale, and that they have a low immunoreactivity [30]. However, the latter is only true for very plain complexes that lack cellular ligands and that are thus also unable to mediate efficient and specific cell binding. More advanced recent formulations instead typically contain moieties that allow their targeting to desired cells, which increases their specificity and thus *in vivo* applicability. Yet, it also complicates their production and provides epitopes for immune recognition, and hence counteracts two of the main advantages of non-viral vectors.

In contrast, viral vectors have the genuine advantage that viruses have already naturally evolved the ability to potently and specifically enter cells through receptor ligands on their capsid or lipid surface. Moreover, viruses and thus also vectors derived thereof are inherently efficient at intracellular processing and expression of their genes. As depicted in Figure 2 and briefly described below, a large variety of viruses have already been engineered as recombinant gene therapy vectors, including Lentivirus, Adenovirus and AAV [31], [32].

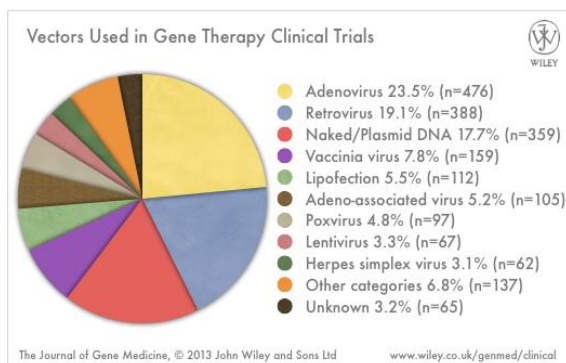


Figure 2: Vector types used in gene therapy trials until 2013. The chart was taken from the freely accessible gene therapy database at www.abedia.com/wiley/index.html.

Lentiviruses belong to the family of *Retroviridae* and comprise viruses like HIV or SIV (human or simian immunodeficiency virus, respectively). They have a nucleocapsid that is enveloped by a lipid bilayer harboring the envelope glycoproteins (Env proteins) which mediate viral attachment to cellular receptors. Upon receptor binding, the envelope fuses with the cellular membrane to release the nucleocapsid into the cytosol (albeit other uptake mechanisms are also discussed [33], [34]). The tropism of lentiviral vectors can be modified because the lipid bilayer is accessible to incorporation of selected glycoproteins as new receptor ligands [35], [36]. Other notable features are that lentiviruses

can transduce quiescent cells and can integrate their genome to mediate long-term gene expression; however, this can be associated with a risk of insertional mutagenesis. Additional drawbacks of the lentiviral vector system are the complex genome structure, the rather inefficient protocols for vector production, as well as safety concerns about reversion of vectors to replication-competent viruses. **Adenoviruses** used in gene therapy belong to the family of *Adenoviridae* and the genus *Mastadenoviruses*. They are non-enveloped viruses with an icosahedral capsid comprising a double-stranded DNA genome. The capsid consists of 240 homotrimeric hexons and 12 pentons from which trimeric fiber proteins extend; their C-terminal domain mediates binding to cellular receptors [37], [38]. Accordingly, modification of the hexons and fibers allows to re- or de-target virions to or from specific cell types, respectively [37], [39]–[41]. Obstacles in the use of Adenovirus as gene therapy vector are related to pre-existing immunity against the virus, cytotoxicity, and, akin to lentiviruses, the general nature of wildtype Adenovirus as a disease-causing pathogen. **Adeno-associated viruses (AAV)** are non-enveloped viruses with an icosahedral capsid and a single-stranded DNA genome. Because they are in the center of the present thesis, their biology as wildtype viruses or recombinant vectors will be described in more detail in the following paragraphs. Here, it should already be mentioned that AAV is one of the leading vector systems for gene therapy due to numerous inherent assets, and that it forms the basis for the first and so far only gene therapeutic that was approved in Europe (EMEA/H/C/002145, 2012, European Medicines Agency London). The specific vector underlying this product (“Glybera”, uniQure biopharma, Amsterdam, Netherlands) is derived from AAV serotype 1 and is intended to deliver an intact lipoprotein lipase gene (LPL) to muscle cells of patients with lipoprotein lipase deficiency (LPLD) upon local administration.

1.2 Adeno-associated Virus

1.2.1 AAV classification and genome structure

Adeno-associated viruses (AAV) are members of the family *Parvoviridae* and the sub-family *Parvovirinae*. This sub-family further segregates into Amdoviruses, Bocaviruses, Dependoviruses, Erythroviruses and Parvoviruses. AAV is a replication-defective virus from the genus Dependovirus which - as the names implies - depends on functions provided by “helper” viruses to complete its replication cycle [42]. The fact that AAVs were first discovered as a contaminant of Adenovirus preparations [43], [44] gave AAV its name and reflects that Adenoviruses represent potent AAV helpers (their early gene products facilitate AAV gene expression and replication). Still, helper functions can also be provided by other viruses, e.g. Herpes simplex virus type 1 (HSV-1) [45]–[47].

Typical for Parvoviruses, AAV has a single-stranded (ss) DNA genome with a length of only about 4.7 kb. During viral replication, both plus and minus strands are packaged with comparable efficiencies. The genome comprises two open reading frames (ORF) flanked by two T-shaped palindromic sequences, the so-called inverted terminal repeats (ITR). The ITRs are the only (partially) double-stranded parts of the genome and function *in cis* as origin of replication, are required for genome packaging and are important for viral integration into the host genome in the absence of helper virus functions [48], [49]. Expression of AAV genes is driven from three promoters within the viral genome, p5, p19 and p40, named according to their relative map position in AAV serotype 2 (the entire genome is divided into 100 map units; 1 map unit corresponds to roughly 47 nt). The *rep* ORF encodes four non-structural proteins (Rep), termed Rep78, Rep68, Rep52 and Rep40 based on their apparent molecular weight in SDS-polyacrylamide gels. The mRNAs encoding Rep78 and Rep52 are transcribed from p5 or p19, respectively, while Rep68 and Rep40 are generated by splicing of a single intron from the mRNAs for Rep78 or Rep52. Rep proteins function in genome replication, as well as in transcriptional control and packaging of AAV genomes. In the absence of a helper virus, Rep proteins also play a critical role in AAV integration into the host genome (in the case of AAV2, the long arm of chromosome 19) [50]–[54]. The *cap* ORF encodes the structural proteins VP1 (90kDa), VP2 (72kDa) and VP3 (62kDa) (sizes are given for AAV2) that form the viral capsid. The fact that all three proteins originate from the single p40 promoter is explained by the use of three different start codons combined with alternative splicing. Notably, a fourth protein - the assembly-activating protein AAP - has recently been discovered that is also encoded in the *cap* ORF and that is essential for efficient capsid assembly [55], [56].

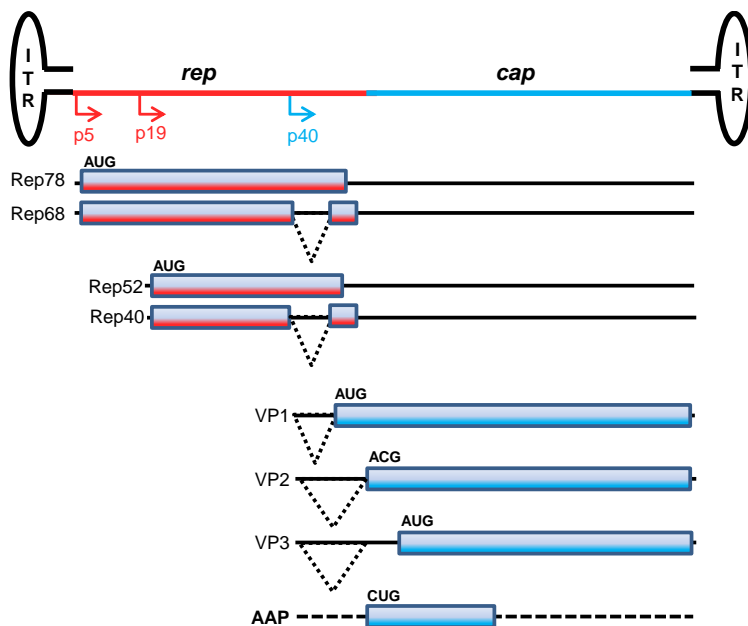


Figure 3: AAV genome structure. Top: The 4.7 kb genome comprises the two *rep* and *cap* ORFs that are flanked by ITRs. Below: Four non-structural Rep proteins are encoded by the *rep* ORF, and three VP proteins as well as AAP by the *cap* ORF. Also shown are the various alternative start codons (either consensus AUG or weaker ACG/CUG) and the central intron (indicated by the caret; the two different sizes imply the use of two alternative splice acceptor sites).

1.2.2 AAV capsid structure

AAV has a small icosahedral and non-enveloped capsid of approximately 18-25 nm in diameter that encapsidates a single copy of the genome (plus or minus strand, as noted). The capsid is composed of 60 copies of the structural proteins VP1, VP2 and VP3 in a ratio of about 1:1:10. All VP proteins share the same C terminus but have unique N-terminal ends (see Figure 3 above). VP1 contains a conserved phospholipase-A2 (PLA2) domain in its N-terminal part that is important for endosomal escape and infection [57]. In the N-terminal part that is common to VP1 and VP2, several nuclear localization signals have been identified [57]–[60]. Neither VP1 nor VP2 are essential for capsid assembly, but particles lacking VP1 are non-infectious [61]–[63]. VP3, which constitutes roughly 90% of the protein content of the capsid, mostly forms the outer part of the capsid with loops and variable regions (see below) that are important for cell and antibody binding [64]. In addition to the nucleotide and protein sequences of numerous AAV isolates (>100, [65]), the three-dimensional structures of nine AAV serotypes, AAV1 to AAV9, have been determined either by cryo-electron microscopy or X-ray crystallography, or by both [64], [66]–[78]. However, only the C-terminal part common to all VP proteins (except for the 15aa at the N terminus of VP3) has been found ‘stable’ and can be visualized (Figure 4). These amino acids comprise the outer part of the capsid, while the remaining residues including the entire VP1 and VP2 sequences are located within the capsid. According to data acquired with AAV2 - the best characterized serotype to date in any respect - the basic capsid structure consists of one α -helix and nine β -barrel motifs named β -A at the N terminus, to β -I at the C-terminal end. The β -barrels starting from β -B on are connected by loops that are named according to the β -barrels they connect (*e.g.*, the HI-loop connects barrels H and I). Located within these loops, especially those in the C-terminal VP part, are the aforementioned variable regions that constitute the largest sequence differences between the serotypes. Through sequence comparisons between AAV2 and AAV4 (one of the most unique AAV serotypes), a total of nine so-called hypervariable regions (VR-I to VR-IX, Figure 4) were identified [66]. Mostly, these hypervariable regions determine cellular receptor binding and antibody recognition (see also the following chapter 1.2.3).

Through interactions of VP monomers at two-, three- and five-fold axes, the AAV capsid assumes the structure of a T=1 icosahedron (Figure 5A) [79]. While the conserved α -helix and the last loop after β -I form the two-fold axis, the BC-, EF- and GH-loop are all part of the three-fold axis. The GH-loop, which is the largest loop, forms a protrusion that surrounds a depression at the three-fold axis. Variable regions cluster at the tip of these protrusions, such as VR-VIII which comprises the primary receptor binding site in AAV2. The five-fold axis is composed of the HI-loop that forms depressions around a pore built by the DE-loop (Figure 5B-D). The pore constitutes a channel between the inside and the outside of the capsid, and functions in genome packaging and PLA2 activation [80] [79].

Albeit the description above refers to AAV2, the basic structure with β -barrels and connecting loops is similarly conserved in all AAV serotypes whose structure has been analyzed and resolved thus far.

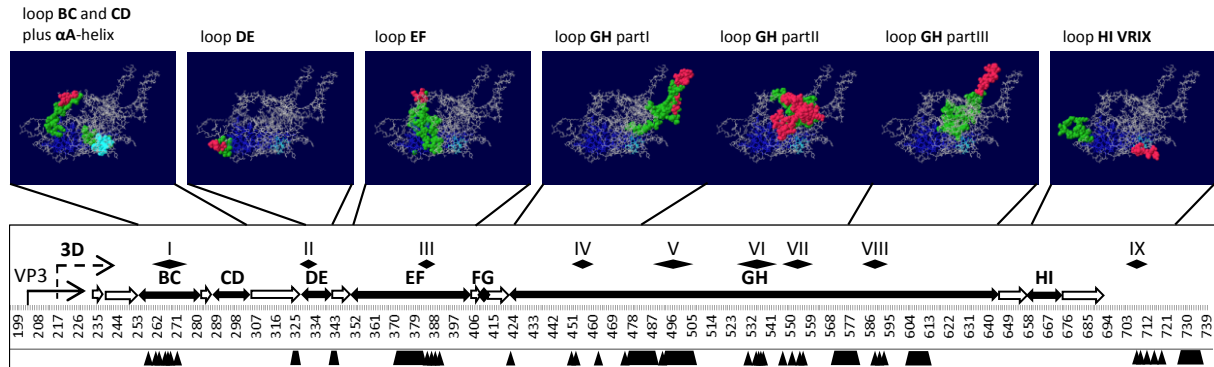


Figure 4: Overview over the C-terminal part of the AAV capsid. The lower part shows a linear alignment of the C-terminal amino acids that are shared by all three VP proteins. Numbers indicate amino acids based on the AAV2 VP1 sequence. Indicated on the left is the start of the VP3 protein as well as the beginning of the 3D crystal structure. Black and white arrows mark loops (BC to HI) in the capsid or intermediate β -sheets (A to I, labels were omitted for clarity), respectively. Black diamonds indicate hypervariable regions within the capsid (I to IX), labels were omitted for clarity, respectively. Black triangles show binding sites of different polyclonal and monoclonal antibodies of nonhuman origin or of antibodies from polyclonal human sera (IVIG) [81]–[86]. Antibody binding sites are described in more detail by Bartel *et al.* [87]. The upper part depicts the 3D crystal structure of the VP3 protein. β -sheets are shown in dark blue, while the alpha helix (α A) is shown in light blue. That α A-helix is conserved among parvoviruses. Highlighted in green and linked to the linear alignment are six of the seven loops, with their hypervariable regions marked in red. Note that the loops CD and FG do not contain hypervariable regions (not shown because of its small size of only 2-3 aa), and that the C-terminal VR-IX is located outside all loops.

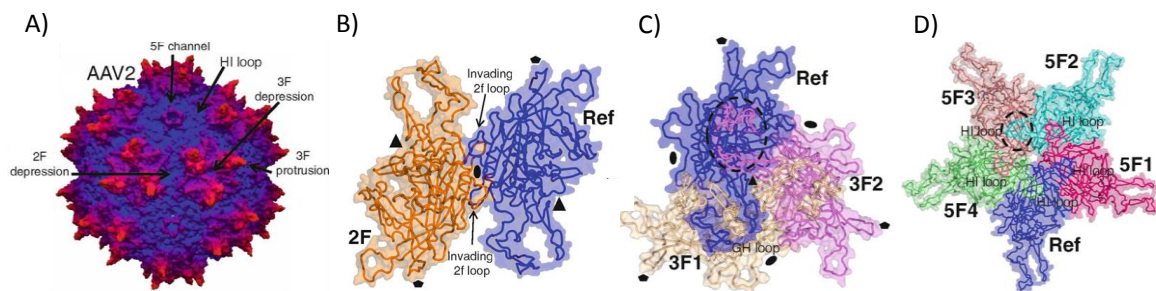


Figure 5: AAV capsid structure. **A)** Depth-cued surface representation of the AAV2 capsid crystal structure. Indicated are the two-fold (2F) and three-fold (3F) depressions, the 3F protrusion, the five-fold (5F) pore/channel and the HI-loop. **B)-D)** Coil diagrams of VP3 from AAV2. Shown are the VP3 monomers with the reference monomer (Ref) in blue and the related monomers 2F, 3F and 5F, respectively. The interaction sites at the icosahedral two-fold (black oval), three-fold (black triangle), and five-fold axes (black pentagon) are indicated. The loops that invade the neighboring monomer at the 2F axes and the protruded HI loop (dashed circles) are also labeled. (taken from: [79])

1.2.3 Receptors and tropisms of AAV serotypes

The AAV capsid proteins mediate cellular receptor binding and determine the serological properties of the particle that in turn define the AAV serotype. Today, at least 12 distinct AAV serotypes and

more than one hundred isolates (usually only the *cap* gene) are known, all of which have been found in vertebrates. According to their capsid genome homology and similarity, these serotypes and isolates were grouped into clades (Figure 6) [65]. Moreover, AAV serotypes can be segregated based on their species origin. Serotypes AAV2, 3, 5 and 6 are isolates from human tissue, whereas serotypes AAV1, 4, 7, 8, 10-12 and AAVrh10 originate from non-human primates. AAV9 is identical to AAVhu.14 and was found in both humans and non-human primates [65], [88]. AAV1 and AAV6, both part of clade A, differ in only 16 nucleotides and 6 amino acids from each other [89], and it is believed that AAV6 is actually a recombinant between AAV1 and AAV2. AAV4 and AAV5, which have not yet been assigned to a particular clade, have the least similarity to one another (around 60%) and to the other serotypes (around 65%). In contrast, all other known AAV serotypes show sequence similarities between 75% and 99% [65], [88], [90]–[92].

Interestingly, even these relatively small sequence differences produce unique receptor binding properties and tropisms (*i.e.*, cell/tissue specificities). Heparan sulfate proteoglycan (HSPG) was the first primary receptor identified for AAV [93], more specifically, for AAV2, AAV3 and AAV6 [89], [94]. Still, our knowledge of the exact HSPG binding motif(s) is largely restricted to AAV2 where amino acids at positions R484, R487, K532, R585 and R588 (R, arginine; K, lysine) were found to be critical [81], [95]–[97]. Among these, R585 and R588 are most essential, as mutation of each ablates HSPG binding. Both are located at the very tip of the GH-loop in VR-VIII (see also Figure 4 above) [95], [96]. Comparisons of AAV2 with the HSPG binder AAV6 and the HSPG non-binder AAV1 permitted to identify the AAV6 HSPG binding site at a position relative to that of AAV2 [73], [98]. Another common attachment receptor for AAV is sialic acid which is recognized by AAV1 and AAV6 that both bind α 2-3- and α 2-6-N-linked sialic acid. In contrast, AAV5 only attaches to α 2-3-N-linked sialic acid, and AAV4 specifically to its 3-O-linked conformation [98], [99]. Accordingly, AAVs can also be grouped based on their primary receptor: AAV2, AAV3 and AAV6 bind HSPG, while AAV1, AAV4, AAV5 and AAV6 bind sialic acid (in various conformations). While AAV9 is the only known isolate which binds N-terminal galactose, the primary receptors for AAV7, AAV8, AAV10, AAVrh10, AAVpo.1, AAV11 and AAV12 remain unknown. In addition to primary receptor attachment, virus uptake requires binding to secondary receptors. For AAV2, the following co-receptors have been proposed: α v β 5 and α 5 β 1 integrin, fibroblast growth factor receptor 1, hepatocyte growth factor receptor and laminin R receptor [100]–[104].

All known primary and secondary receptors are also summarized in Table 1, together with the tropisms (*i.e.*, cell specificities) resulting from these different virus-receptor interactions and selected clinical studies in which these tropisms have already been exploited.

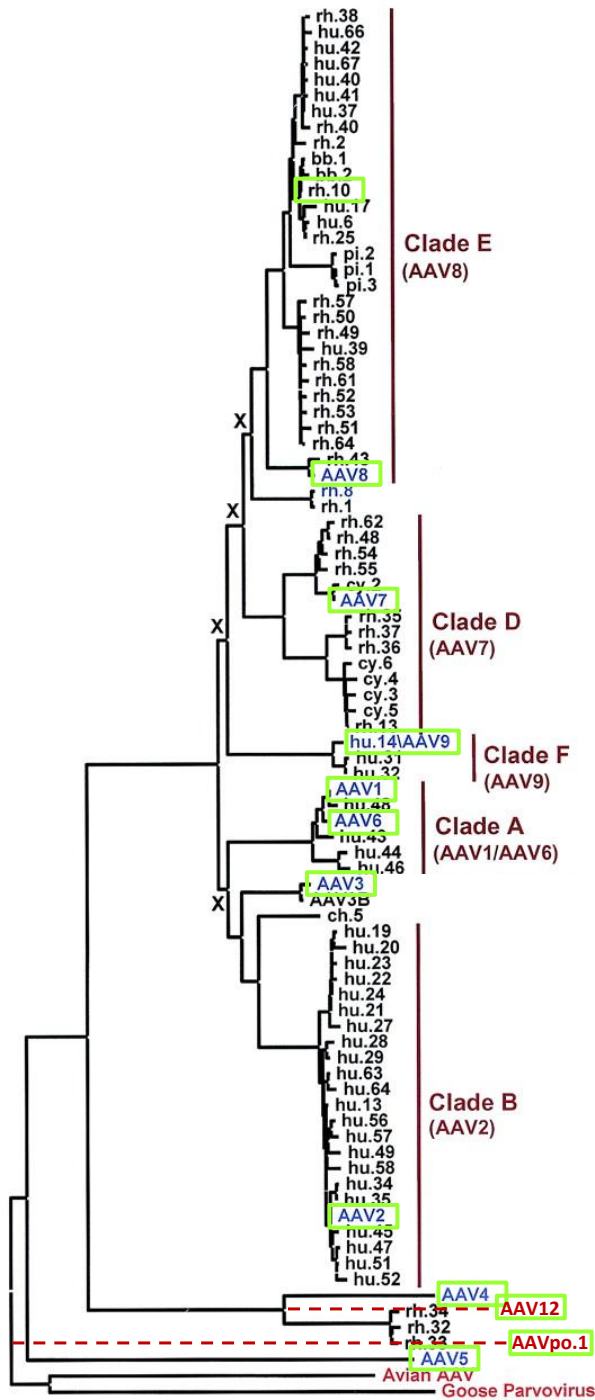


Figure 6: Phylogenetic tree of primate AAVs according to the VP1 sequence. Taxa are named either by serotype or according to the species from which they were isolated (hu, human; rh, rhesus macaque; cy, cynomolgus macaque; bb, baboon; pi, pigtailed macaque; ch, chimpanzee; numbers indicate the order in which they were sequenced). Different taxa are grouped in clades and named A, B, or D-F, and additionally according to a typical representative of the clade. This figure is modified from [65]. The AAV2-AAV3 hybrid clade C from the original figure is not shown here. In addition, serotypes AAV12 and AAVpo.1 were added. The green boxes highlight the serotypes that were used in our experiments.

Table 1: AAV receptors and tropisms

Serotype	Receptor (Glycan)	Co-receptor	Tropism (on local delivery, unless otherwise mentioned)	Origin	References	Clinical studies
AAV1	$\alpha 2,3/\alpha 2,6$ N-linked sialic acid	not known	SM, CNS, Retina, Pancreas	NHP (Rhesus monkey)	[43]	Heart failure, A1ATD, LGMD2D, LPLD
AAV2	HSPG	FGFR1, HGFR, LamR, CD9 tetraspanin, $\alpha V\beta 5/\alpha 5\beta 1$	VSMC, SM, CNS, Liver, Kidney	human	[44]	Alzheimer, Batten, Canavan, Parkinson, LCA, Inflammatory arthritis, hemophilia B, CF, A1ATD
AAV3b	HSPG	FGFR1, HGFR, LamR,	Hepatocarcinoma, SM	human	[44]	
AAV4	$\alpha 2,3$ O-linked sialic acid	not known	CNS, Retina	NHP (African green monkey)	[105]	
AAV5	$\alpha 2,3$ N-linked sialic acid	PDGFR	SM, CNS, Lung, Retina	human	[106]	
AAV6	HSPG , $\alpha 2,3/\alpha 2,6$ N-linked sialic acid	EGFR	SM (also i.v.), Heart, Lung	human	[107]	
AAV7	not known	not known	SM, Retina, CNS	NHP (Rhesus monkey)	[88]	
AAV8	not known	LamR	Liver, SM, CNS, Retina, Pancreas, Heart	NHP (Rhesus monkey)	[88]	Hemophilia B
AAV9	N-linked galactose	LamR	Liver, Heart (i.v.), Brain (i.v.), SM (i.v.), Lung, Pancreas, Kidney (i.v.)	human	[65]	
AAVrh10	not known	not known	not known	NHP (Rhesus monkey)	[88]	
AAVPo.1	not known	not known	not known	pig	[108]	
AAV12	not known	not known	not known	NHP (African green monkey)	[109]	

The column 'origin' names the species from which the respective serotype was isolated. The column 'clinical studies' refers to diseases for which clinical studies were conducted using the respective AAV serotype. NHP, non-human primate; i.v., intravenous; CNS, central nervous system; EGFR, epidermal growth factor receptor; FGFR1, fibroblast growth factor receptor 1; HGFR, hepatocyte growth factor receptor; HSPG, heparan sulfate proteoglycan; PDGFR, platelet-derived growth factor receptor; SM, skeletal muscle; VSMC, vascular smooth muscle cell. The shown information was gathered from various original literature as well as from publications [110] and [111].

1.2.4 AAV infection and intracellular processing

As just noted, the AAV capsid determines the first step in viral infection which is attachment to cell surface receptors. Interestingly, AAV serotypes also differ in the subsequent steps of internalization and intracellular processing, which are complex mechanisms that are again best understood for the AAV2 prototype. For this isolate, it was shown that binding to the primary HSPG receptor triggers a conformational change that allows capsid interaction with co-receptors that further facilitate structural rearrangements and ultimately mediate virus uptake (so-called “click-and-fit” mechanism [71], [100]). For AAV2 and most other serotypes studied thus far, this uptake requires clathrin-coated pit formation and is dynamin-dependent [112]. Still, AAV2 can also enter cells in a clathrin-independent manner through carriers/GPI-enriched endocytic compartments (CLIC/GEEC) [113]. Moreover, for AAV5, caveolin-dependent internalization was described [111], [114], [115]. Once internalized, AAV particles are transported along microtubules and microfilaments in endosomal compartments. Data with AAV2 suggest a predominant virion release from early endosomes, albeit it was also reported to occur in late endosomes, recycling endosomes or in the *trans*-Golgi network [114]–[122]. In addition to the influence of the viral serotype, the compartment from which AAV finally escapes may also be dose-dependent and/or cell type-specific [118], [123]. In any case, a crucial step is the acidification of the compartment that leads to a conformational change in the AAV capsid. For AAV2, a low pH was shown to trigger conformational changes of side chains of the capsid and exposure of the N terminus of VP1 that carries the PLA2 domain [57], [58], [124]. The same process is further described in more detail in the context of AAV8. Here, transitions during endosomal trafficking at the exterior surface close to the icosahedral 2-fold depression leads to a release of the PLA2 domain of VP1 [125]. This PLA2 release is important for endosomal escape and AAV infectivity in general [57], [126]–[128].

Once released from the endosome, the virions are further processed in ways that have also not been fully resolved thus far. To some extent, AAV capsids are subject to ubiquitination and degradation, as evidenced by findings that inhibition of the proteasome enhances cell transduction with several AAV serotypes [121], [129]–[134]. Moreover, mutation of tyrosines at exposed capsid positions in AAV2 - Y444, Y500 and Y730 - was shown to result in decreased phosphorylation and concurrently increased transduction. The improvements were 10-fold in HeLa cells and 30-fold in murine hepatocytes *in vivo*, even at a 10-fold lower vector dose as compared to wildtype AAV2 [135]. Likewise, tyrosine mutation in AAV6 at amino acid position 445 (Y445F) led to an improvement of transduction of skeletal muscle after intramuscular injection. Compared to a wildtype (wt) AAV6 vector, an 8-fold increase in luciferase activity in living mice and a 6-fold higher abundance of viral genomes in muscle sections were achieved when delivered with AAV6Y445F. Comparable results were obtained with an AAV8 tyrosine mutant (Y733F). Subretinal injection of mice with AAV8Y733F carrying a gene to

correct a mutation of the β -subunit of rod cGMP-phosphodiesterase restored visual acuity and contrast sensitivity to normal levels. The effect with AAV8Y733F was visible six months post-infection, whereas treatment with AAV5 and AAV8 vectors had almost no effect even in long-term follow-ups. In contrast, a single tyrosine mutation at position Y447F or Y733F in AAV8, or Y446F or Y731F in AAV9, respectively, was found insufficient to improve gene delivery to skeletal muscle and heart as compared to wtAAV8 and wtAAV9 vectors [136]–[138].

Capsid uncoating as the next step in AAV infection/transduction is again a complex and multifaceted process whose details remain unclear. In addition to the previously described conformational change at the exterior surface, changes at the interior surface at the icosahedral 3-fold axis likely trigger genome uncoating [125]. Certain proteins were also reported to interact with the AAV capsid to further mediate uncoating. For instance, cleavage by cathepsins B and L was found essential for AAV2 as well as AAV8 cell transduction [139]. Although many studies suggest encapsidated genomes in the nucleus, it still remains debatable to date whether the capsids uncoat in the cytoplasm or at a perinuclear region, or whether they enter the nucleus intact. Evidence for the latter is that AAV2 capsids within the nucleus have been observed by several groups [116], [117], [119], [123], [140], [141]. Still, others postulated that uncoating occurs before or during nuclear entry [140], [142]. It is furthermore uncertain whether the nuclear pore complex (NPC) is involved in AAV transduction [58], [123], [143]. While the discovery of nuclear localization signals in the N terminus of VP1 and VP2 supports a NPC-dependent mechanism, mutation of NPC-unrelated domains in the N-terminal region impairs nuclear transport [60], [62].

The single-stranded (ss) AAV DNA genomes must be converted into double-stranded (ds) DNA prior to transcription. This is achieved by either synthesis of the complementary strand or by annealing of one plus and one minus strand in cells infected with multiple virions. Together with the process of uncoating, *i.e.* the release of the genome from the capsid, this conversion step was found rate-limiting for AAV infection which has consequences for the use of AAV vectors [144], [145]. In the case of AAV8, viral genomes are released quickly and ss genomes can anneal rapidly to form expression-competent ds DNA. Therefore, transduction with AAV8 is more potent in murine liver *in vivo* as compared to AAV2, whose uncoating occurs at a much slower rate. Evidence for the latter is that AAV2 genomes remain DNase-resistant for longer periods in the nuclei of transduced hepatocytes, implying that they were encapsidated even six weeks after administration to the mice. Consequently the kinetics of capsid uncoating determine the fate of the viral genomes. Slow uncoating leads to degradation of the genomes that persist as single strands, which could readily explain the relatively inefficient liver transduction with AAV2, as compared to the more rapidly uncoating AAV8 [142].

Finally of note is that several steps in AAV infection, replication and gene expression are governed by the presence or absence of helper virus functions. In a latent infection in the absence of a helper virus, dsAAV genomes concatemerize and form circular episomes or integrate into the host genome (at very low frequencies). In contrast, during a lytic helper virus co-infection, AAV is actively transcribed and replicates, resulting in production and release of progeny particles.

In summary, the AAV capsid sequence influences every step in virus infection, from cell attachment, co-receptor binding and virus uptake, to endosomal release, virion processing and finally nuclear transport and uncoating. This broad relevance of the AAV capsid explains why major efforts in the AAV vector field aim at modifying the capsid sequence and structure, as described in the following chapters, and why the central goal of the present thesis was to improve the underlying technologies.

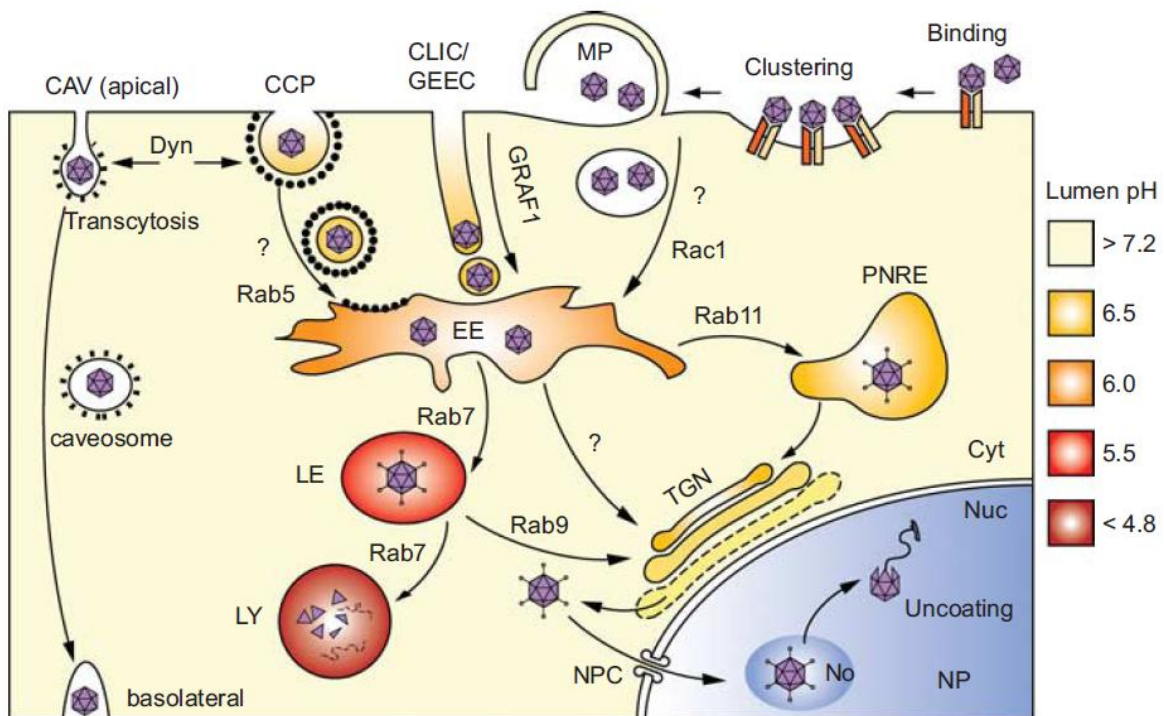


Figure 7: Postulated entry and intracellular trafficking of AAV vectors. Bound and clustered AAV particles enter the cell via different pathways. Internalization via macropinocytosis (MP) is strongly affected by the Rac1 GTPase [116]. Endocytosis via the clathrin-independent carriers/GPI-enriched endocytic compartment CLIC/GEEC is characterized by a GTPase Regulator Associated with Focal Adhesion Kinase 1 (GRAF1) dependency [113]. Clathrin-dependent endocytosis (CCP) is another possibility of AAV uptake. Internalization via caveolar (CAV) mediated endocytosis leads to transcytosis. CCP and CAV both involve dynamin (Dyn). Except for the CAV pathway, internalized AAV capsids traffic through early endosomes (EE) followed either by late endosomes, by perinuclear recycling endosomes (PNRE), or by both, and are transported to the trans-Golgi network. From LE, AAV particles can also be degraded in lysosomes (LY). Different compartments are characterized by distinct members of the family of RAS-related GTP-binding proteins (Rab5, 7, 9, 11). Conformational capsid changes due to acidification (see text) lead to cytoplasmic release from the Golgi apparatus or the ER, and nuclear import via the nuclear pore complex (NPC) (the pH of the lumen is indicated by color code; release of the PLA2 domain is indicated by spikes). Once in the nucleus (Nuc), intact capsids accumulate in the nucleolus (No) followed by genome release in the nucleoplasm (NP). Figure taken from [111].

1.2.5 Recombinant AAV (rAAV) vectors

For use in gene therapy, AAV provides a unique combination of advantages that make it highly useful as recombinant vector system. A first important asset is that AAV is entirely non-pathogenic in humans and replication-defective (in the absence of a helper virus), which offers an unmatched degree of safety. The latter is further increased by the fact that the only *cis*-acting elements within the AAV genome that are required for replication and packaging are the ITRs (Figure 8). Accordingly, for AAV vector production, the complete viral genome between the ITRs including *rep* and *cap* genes can be replaced by the desired transgene. As *rep* and *cap* products are still needed for recombinant particle production, however, they as well as Adenovirus helper functions must be provided *in trans*. Typically, Hek293T cells that stably express the Adenovirus E1 gene (another important helper function) are therefore triple-transfected with plasmids containing 1) *rep* and *cap* genes, 2) the remaining Adenovirus helper genes (E2A, VA RNA and E4orf6) and 3) the desired transgene flanked by ITRs [146]–[148]. Because the resulting recombinant AAV vector is gutless, *i.e.*, devoid of all viral genes, it has a maximal packaging capacity for foreign DNA sequences of roughly 5 kb (Figure 8). This is less than that of other viral vector systems used in gene therapy (*e.g.*, 30 kb for gutless Adenoviruses), but still enough for the vast majority of therapeutically relevant sequences, especially for RNAi or CRISPR cassettes.

Another key feature of AAV vectors is the ability to be packaged as “self-complementary” genomes that overcome the rate-limiting step of ssDNA to dsDNA conversion in the nucleus (see chapter 1.2.4 above). To understand their design and function, it is essential to point out that once the complementary DNA strand has been synthesized during AAV replication, the original strand is cleaved at a “terminal resolution site” (*trs*) within the ITR. This allows separation of the two strands (which would otherwise remain joined at one ITR) and thus permits the replication cycle to continue. To create self-complementary genomes, the *trs* in one of the two ITRs is mutated, yielding a concatemer of two complementary sequences that can directly fold back onto each other to form a double-stranded genome which gives rapid and potent gene expression in the infected cell. While a drawback of the self-complementary vector design is the reduction of the packaging capacity to half of that of single-stranded vectors (roughly 2.2 kb, Figure 8), the substantial gain in efficiency over conventional AAV vectors usually outweighs this limitation [149], [150].

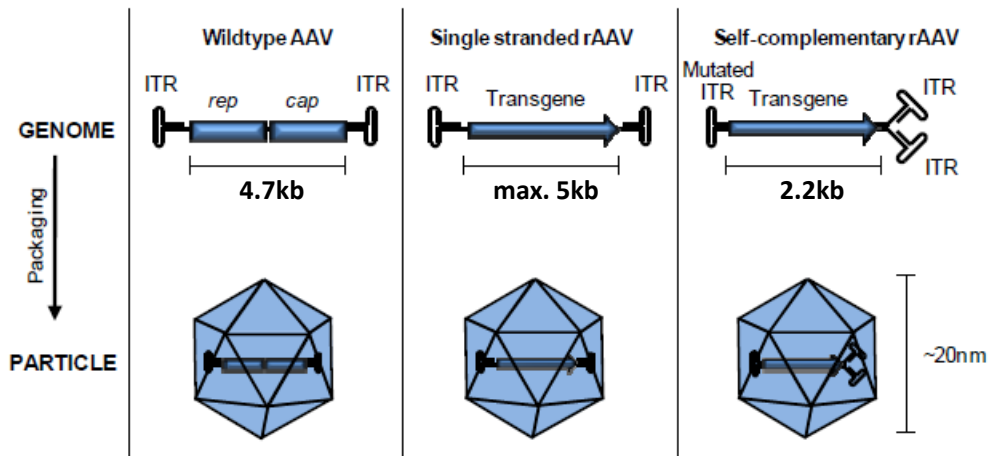


Figure 8: AAV wildtype virus and recombinant vectors. Shown is a direct side-by-side comparison of wildtype AAV (left) with conventional ssDNA- (center) or self-complementary dsDNA-containing (right) AAV vectors. The numbers underneath the genomes indicate the maximum size of foreign sequences that can be packaged in the different configurations. (Figure adapted from [151].

Moreover beneficial is that recombinant AAV vectors rarely ever integrate into the host genome since they lack expression of the Rep proteins which are required for this step. This alleviates concerns about genotoxicity (which are particularly prominent with retro/lentiviral vectors) but it also implies that the vector will be lost in dividing cells. Nonetheless, in clinically relevant cells and tissues that do not undergo frequent cycling, such as hepatocytes/livers, AAV vectors can persist as extra-chromosomal episomes and yield long-term and safe transgene expression.

Most important in the context of the present thesis is yet another advantage of AAV vectors, namely, the wealth of naturally occurring AAV serotypes and isolates to choose from. This is critical since this variety of capsids offers a huge range of receptor binding abilities and thereby tropisms as well as intracellular processing efficiencies (see also Table 1). Fortunately, the *rep* genes and ITRs from serotype AAV2 function in conjunction with any *cap* gene, independent of its origin [146], [148], [152]–[154]. Hence, transgenes flanked by ITRs from AAV2 can easily be packaged into virtually all available AAV capsids (serotypes, isolates or mutants), by simply encoding the desired *cap* gene on the AAV helper plasmid. Because the viral capsid mediates all functions in transduction (see chapters 1.2.3 and 1.2.4 above), the resulting so-called pseudotyped vectors then display all the properties - specificities and efficiencies - of the serotype from which the capsid originates. Notably, vector behavior can be further modulated through a variety of parameters, such as the dose or route of administration [155]. For many pseudotypes, the most frequently infected organ after intravenous injection into small animals is the liver [155]–[160]. In fact, the liver is the main target for AAV2

(>90% of peripherally injected vector ends up there), and also AAV8 and AAV9 transduce this organ robustly after tail vein injection of mice [155], [161]. Unlike AAV2 though, AAV9 also potently infects skeletal muscle, and together with AAV4, AAV6, AAV7 and AAV8, it has the highest transduction rate in the heart after systemic application [155], [162]–[164]. Intraperitoneally injected AAV8 can even pass the blood-brain-barrier, infect muscle and heart as well as dorsal root ganglia and lower motor neurons; besides, it is also very efficient in the pancreas [165]–[167]. Other serotypes, such as AAV1 and AAV6, are highly potent in skeletal muscle upon local administration [168]–[170]. The same serotypes, AAV1 and AAV6, are also efficient at heart transduction [171]–[173]. Likewise, AAV5 was found to be efficient in the CNS including the brain upon targeted delivery [174]–[177]. Serotype AAV5 together with AAV4 further has the potential to infect the eye [178]–[180]. Other, less commonly used serotypes like AAVrh10 and AAV12 are also capable of infecting organs such as brain, lung or muscle [92], [181], [182].

Notably, many of these findings were not only obtained in small animals (mice or rats) but also confirmed in larger species (dogs and monkeys). For example, AAV1, AAV2 as well as AAV6, AAV8 and AAV9 were shown to lead to long-term transgene expression after transfer to the liver and muscle in dogs [183]–[187]. In a study from 2010 that compared the efficiency of serotypes AAV1, 5 and 8 in neuron transduction in monkeys, AAV1 and AAV5 outperformed serotype 8 [188]. Systemic injection of AAV9 in macaques led to transduction of glia cells within the brain and dorsal root ganglia in the CNS [189]. Moreover, serotype AAV4 was shown to display tropism towards the retinal pigmented epithelium in the eye of dogs at efficiencies comparable to AAV2 [190].

While all these data (and many others that were omitted for space reasons) are highly promising, there are also a few remaining limitations of the AAV vector system that still hamper the direct translation of results from animal studies into humans and that thus need to be overcome. A first major problem is the high prevalence of some AAV serotypes in the human population and the ensuing abundance of pre-formed neutralizing antibodies (nAB) [191]–[194]. In fact, more than 80% of the human populations are seropositive for AAV2, closely followed by AAV1. Also, pre-formed nAB against some of the most potent (in mice) and thus most promising serotypes, like AAV7, AAV8 and AAV9, have been detected in humans [192], [193]. The potential issue of pre-existing immunity against AAV vectors was clearly exemplified by observations in a clinical trial using AAV2-based vectors, where patients with hemophilia B showed a CD8⁺ T-cell response that was most likely mediated by T-memory cells [18], [195]–[199]. A second related problem is that even if a patient lacks nAB to a certain serotype, she/he will become nAB-positive after a single AAV dose and thus resistant to the same sero-/pseudotype.

In addition to concerns about pre-existing or induced anti-AAV immunity, there are uncertainties about the comparability between data in cell culture, animals and humans. In fact, some of the most potent serotypes *in vivo* (small or large animals), such as AAV8, are almost inert in cell culture. *Vice versa*, while AAV2 transduces many cultured cells very potently, it mostly infects the liver after *in vivo* application, and rather inefficiently (as compared to other serotypes). Together, this largely hampers the thorough pre-clinical evaluation of novel AAV capsid variants. It is also because of these discrepancies (and because of general safety considerations) that in most clinical applications to date, AAV vectors are administered locally, *e.g.*, to the liver or muscle as in the hemophilia B patients, or to the eye for therapy of Leber's congenital amaurosis [200]–[202]. Likewise, the aforementioned AAV1 gene therapy product Glybera is intended for direct application into the muscle, rather than for systemic delivery.

As a whole, these restrictions which result from the limitations of naturally occurring AAV capsids define the aims for the development of newer and improved clinical AAV vectors, namely, increases in specificity and efficiency, and concurrent decreases in immunogenicity. The final chapter of this Introduction will describe the main approaches that have been pursued thus far to reach these goals, before the advanced strategies that were implemented and validated in this thesis will be presented.

1.3 Molecular AAV vector evolution

Towards the aim to refine the specificity of AAV vectors, two basic experimental means to alter AAV cell binding can be distinguished in the literature - 1) biochemical crosslinking of AAV to cellular receptors, or 2) direct genetic modification of the AAV capsid sequence. Examples for the first category include biotinylation of AAV which links the capsids to streptavidin-tagged proteins with defined cell binding abilities [203]. Another example are bi-specific antibodies that function as adapters between the AAV capsid and moieties on the cell surface. For instance, such an antibody was used to re-target AAV2 to α 1B β 3-integrin on cells that were inherently resistant to AAV2 [204]. Further approaches combined adapter molecules with genetic capsid modification, such as in a study where adapter-antibodies mediated binding of CD29, CD117 and CXCR4 to an IgG binding domain. The latter was genetically inserted into the AAV2 capsid, thereby permitting transduction of hard-to-infect cells of hematopoietic origin [205]. Problems with the techniques described so far are their low efficiency, poor stability of the agents *in vivo* and the difficult production of sufficient vector titers. Moreover, adapter molecules introduce yet another target for humoral or cellular immune responses.

For all these reasons, direct genetic engineering of the AAV capsid may be a more promising strategy to achieve AAV vector (re-)targeting. Again, one can distinguish numerous approaches in the past literature, including the generation of mosaic capsids that consist of parts from different serotypes and combine the binding abilities of the parental viruses [206]–[210]. One way to create these mosaic viruses is through rational domain swapping as already reported for a small number of serotypes and domains [211]. However, this technique is hampered by the limited knowledge of the function of AAV domains and of their relationship with each other during the various steps in AAV infection. A similar, but more powerful and versatile approach is AAV capsid DNA shuffling, whereby the *cap* genes of multiple AAV isolates are first fragmented and then re-assembled into chimeras that ideally combine numerous assets of the parental capsids. This technology, which was first introduced into the AAV field in a seminal 2008 paper by Grimm and colleagues [212], was further expanded and applied in the present thesis and will thus be described in more detail in the following chapter 1.3.1. The same is true for an alternative strategy for direct capsid engineering called viral display, in which short peptides are introduced into an exposed region of the viral capsid, hoping that this will ablate primary tropism and mediate binding to previously resistant cell types (chapter 1.3.2) The following Figure 9 shows a summary of all methods for genetic AAV capsid engineering reported thus far.

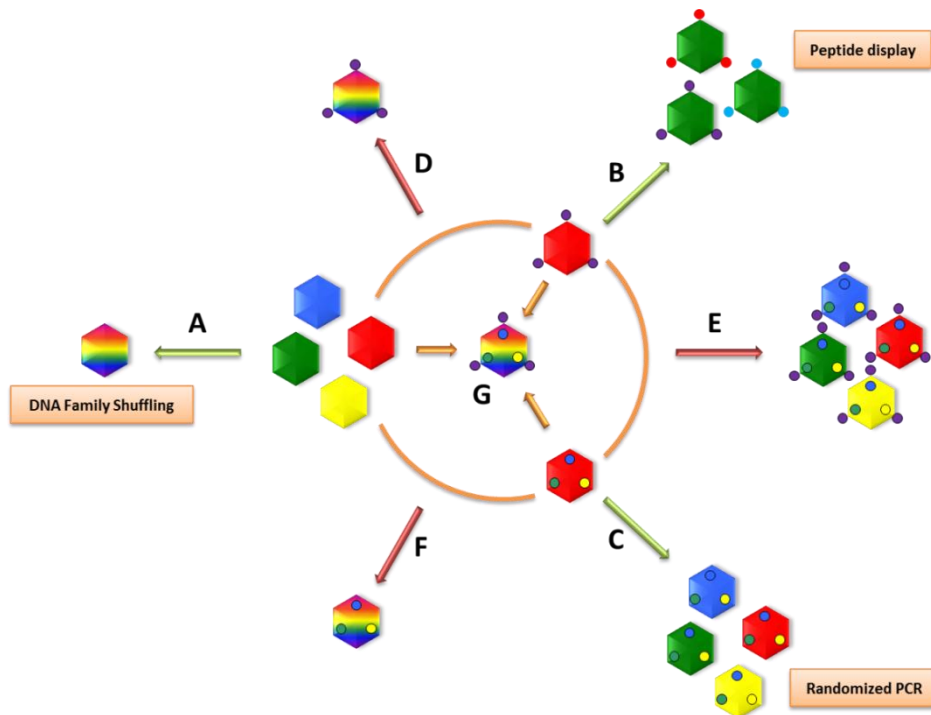


Figure 9: Methods for AAV vector evolution. Shown are the three main strategies that have been reported thus far: A) DNA family shuffling, B) peptide display, and C) randomized PCR. The first two have been used and further refined in the present thesis, and are therefore described in more detail in chapters 1.3.1 and 1.3.2. The third strategy relies on the introduction of random point mutations during error-prone PCR amplification of AAV capsid genes. As the frequency of these mutations is typically very low, and as only a minor fraction will actually improve capsid features, only few groups use this strategy. Also indicated is that all three main approaches can be combined, either in pairs (D-F) or all three (G).

1.3.1 DNA Family Shuffling

As outlined in chapter 1.2 above, naturally occurring AAV capsids differ broadly in multiple aspects such as cell and tissue specificity and efficiency as well as immunogenicity. All these features are mostly determined by numerous residues and domains that are dispersed throughout the sequences of VP1 to VP3, and that remain largely unidentified. While this complicates the rational design of hybrids between different natural serotypes, it provides an excellent starting point for the method of DNA family shuffling (DFS). This technique, which was first reported by Stemmer and colleagues in the 90's [213], enables the generation of large libraries of chimeric DNA sequences from closely related genes. A prerequisite is that the parental DNAs share at least 50% sequence homology, which fortunately applies to all known AAV isolates (including the diverse AAV4 and AAV5, see chapter 1.2.1). Briefly, these DNAs are first enzymatically fragmented (typically using DNase I) and then reassembled into chimeras in a series of two PCRs. The first lacks external primers in order to foster self-priming of partially homologous parental DNAs, and the second serves to amplify the resulting library for subsequent subcloning into an expression plasmid. This in turn allows to express all chimeras and to screen for those that exhibit a desired phenotype.

In the case of AAV, this method was originally introduced into the AAV field by Dirk Grimm and colleagues who reported the first chimeric AAV library generated by DFS in 2008 [212]. This library, comprising about 7×10^5 different hybrids, was generated by shuffling eight different AAV isolates, AAV2, AAV4, AAV5, AAV8, AAV9, avian AAV, bovine AAV and caprine AAV. It was then iteratively amplified in human hepatocytes in the presence of pooled human antisera (IVIG), with the aim to isolate new chimeras that would combine a high efficiency in these therapeutically relevant cells with the ability to evade pre-existing anti-AAV nAB that occur in the human population (and that are represented in IVIG). Indeed, this resulted in the enrichment of a single chimera - termed AAV-DJ - after 5 amplification rounds. Interestingly, AAV-DJ is only composed of shuffled sequences from AAV2, AAV8 and AAV9 and has lost the five other serotypes that were present in the original library. Notably, it combines the most beneficial assets of these three serotypes: like AAV2, AAV-DJ has the ability to bind HSPG and even shows a superior efficiency in cell lines of hepatic origin as well as in many other cells in culture. Like AAV8 and AAV9, it greatly outperforms AAV2 transduction efficiency *in vivo*, yet it preferentially transduces the liver (whereas AAV8 and AAV9 show substantial extra-hepatic targeting). Finally, AAV-DJ exhibits a decreased reactivity with nAB as compared to AAV2, most likely due to protruded loops in its capsid that originate from AAV8 and AAV9. As a whole, this study and this clone thus clearly exemplify the great power of the DNA family shuffling technology to create novel AAV chimeras that unite the best features of several parental viruses in a single capsid, and that can even outperform its parents. It is thus not surprising that a vast number of groups have rapidly adapted this technology after the original paper by Grimm *et al* [212]., have produced

additional libraries based on other serotype combinations and have executed further selection schemes to isolate clones that perform under specific conditions. For instance, shortly after the first AAV shuffling paper, another AAV chimeric library was reported that was generated from the parental serotypes AAV1, 2, 4, 5, 6, 8 and 9. The resulting clones showed a broad tropism in several cell lines comparable to AAV2 and an increased (up to 400-fold) resistance to human antibodies (IVIG) as compared to AAV2. Similar to the Grimm study, one clone which contained surface loops from multiple serotypes was found to be highly efficient at liver and also heart transduction after tail vein injection *in vivo* [214]. In another exemplary study, a shuffled AAV library comprising chimeras of AAV2, 7 and 8 was selected in HepG2 cells (human hepatoma line). The lead candidate had an increased efficiency specifically on HepG2 cells compared to AAV2 [215]. As a third example, an AAV library derived from AAV1, 6, 7 and 8 was selected *in vivo* to target the myocardium. One emerging clone transduced murine heart more efficiently than AAV6, and concurrently displayed a decreased tropism towards liver and other organs [216]. Moreover, further interesting examples of the power of AAV DNA shuffling include clones that were derived from AAV1, 3, 8 and 9 and that exhibit the potential to cross the (chemically compromised) blood-brain barrier in [217] rats. Finally, clones were selected from a library made of AAV1, 2, 4, 5, 6, 8 and 9 [218] in human embryonic stem cells (hESCs), and the same group isolated chimeric particles generated by pairwise shuffling of the AAV2 *cap* gene with AAV4, 5, 6 or 8 that mediated increased transduction of neuronal stem cells [6], [219].

Remarkably, albeit these and other papers differed in details regarding the library composition and target cells, three particular parameters were frequently similar which highlights their importance for AAV vector evolution: 1) The libraries were either amplified in the target cells via co-infection with a helper Adenovirus, or the capsid genes were rescued from the infected cells by PCR and then re-cloned to generate a new library for the next infection round; 2) selection occurred only under positive pressure (*i.e.*, enrichment for particles that can infect a given cell type), or it also included a negative pressure (*i.e.*, typically elimination of capsids that react with nAB/IVIG, as in the original Grimm paper [212]); and 3) many final clones were largely composed of serotype 2 in combination with potent (*in vivo*) capsids such as AAV8 or AAV9, strikingly reminiscent of the AAV-DJ chimera. Altogether, these curious observations provided the rationale for the experiments in the first part of this thesis, whose aim it was to more thoroughly dissect the influence of adenoviral co-infection and IVIG pressure, and to better understand the predominance of a few serotypes in typical final hybrids.

1.3.2 Peptide display

The second approach to alter AAV tropisms that was studied here is genetic modification of the AAV capsid aa sequence through the introduction of additional short peptides. The underlying idea is that these peptides will hinder binding of the capsid to its natural receptor(s) and concurrently mediate

attachment to other molecules that are specifically expressed on the surface of a target cell. This method, which is similar to phage display and hence called viral display, was originally established in the AAV2 context because the AAV2 structure was the first to be resolved [64], [124]. Accordingly, short peptides of seven residues were inserted into the AAV2 capsid at positions that were supposed to 1) be exposed at the capsid surface, 2) mediate binding to the natural AAV2 receptor(s), and 3) accept the insertion of additional amino acids without disrupting functions essential for the viral life cycle [84], [220], [221]. Of the insertion sites tested, position 587 and later 588 were confirmed to fulfill these criteria, as they accept peptides of different lengths (ideally seven amino acids, but also 14 and more were reported [61]) and to mediate the desired AAV2 retargeting, *i.e.*, ablation of the primary tropism and introduction of a new cell specificity. Indeed, peptide display at these positions was found to avert HSPG binding of the underlying AAV2 wildtype virus [222]. Moreover, a vast array of publications from the past decade has validated the power of this technology to create novel tropisms based on the AAV2 scaffold. Again, as for DNA family shuffling, only a few selected examples will be mentioned. Müller and colleagues were the first to select 7mer peptide libraries in the context of AAV2. Their selection scheme in human primary endothelial cells led to the enrichment of the peptides NSSRDLG and NDVRAVS. Both peptides have the potential to increase the transduction efficiency in their target cells substantially as compared to wtAAV2, but were inefficient in HeLa cells [221]. Another *in vitro* selection scheme in primary breast cancer cells from PymT mice identified two peptides, RGDMSRE and RGDGLLS that share the RGD motif and roughly double the transduction efficiency of wtAAV2 in primary PymT cancer cells. In the same paper, *in vivo* biopanning and selection in murine lungs identified two peptide motifs, PRSADLA and PRSTSDP, that increase transduction in the lung but also in other organs after intravenous administration (up to 233-fold with peptide PRSTSDP as compared to the unmodified wtAAV2 control, 28 days post-infection) [223]. In two more recent approaches, the previously generated AAV2 peptide library [221] was selected in hESCs and neuronal stem cells (NSCs). In the latter case, this led to the identification of an AAV2 clone that displayed the motif TQVGOKT and that carried an additional point mutation at position 719 (V719M). The peptide-displaying clone gave up to 50-fold increased NSC infection as compared to wtAAV2 and wtAAV5 (curiously, correction of the point mutation did not alter the efficiency of this clone) [6], [219].

Obviously, an important prerequisite for the success of this strategy is a detailed knowledge of the structure of the AAV capsid that is used for peptide display. This readily explains why up until very recently, peptide display and selection approaches have been restricted to the AAV2 prototype, as structures for alternative AAV serotypes have only been resolved lately. Accordingly, very few papers have thus far started to assess the potential of non-2 AAV serotypes as scaffolds for peptide display [224], [225], despite the fact that these capsids are very interesting candidates. This is because

peptide insertion into AAV2 will not alter the majority of epitopes on the capsid surface that are recognized by nAB in the population; accordingly, even the best retargeted AAV2 vector may ultimately fail in human gene therapy trials once it is neutralized. In addition, as highlighted above (chapters 1.2.2 - 1.2.4), the capsid not only affects cell attachment but also influences subsequent steps during vector transduction. Again, this suggests that inherently more potent capsids such as those from AAV8 or AAV9 may represent better scaffolds for peptide display, than the AAV2 prototype.

Finally, it was also suggested that it is not only the peptide *per se* which mediates target specificity, but that the combination with the AAV capsid backbone further contributes to an altered tropism. Arguing for the influence of the underlying serotype, Müller and colleagues already proposed in their original 2003 paper that direct peptide selection within the virus context is preferable over *e.g.* phage display and subsequent transfer of enriched peptides into AAV, since the peptide confirmation may be altered in the precise virus protein context [221]. One could accordingly postulate that capsid and peptide should be viewed as an entity rather than a combination of two parts. Along this line, Grimm and co-workers made observations that further support the concept that the capsid backbone is essential for peptide display. In their 2008 study, they performed an *in vivo* biopanning of a peptide library in the AAV-DJ context, and surprisingly isolated the exact same peptides in murine lungs that had previously been selected in coronary arterial and venous endothelial cells *in vitro* in the context of AAV2 [212], [221], [226]. This again highlights the importance of the capsid and raises the question whether the specificity of peptides displayed in AAV is truly due to the peptide alone, or whether it rather results from a complex, not yet fully understood, peptide-backbone interplay.

1.4 Objectives

This study had two closely related overarching goals, namely, (i) to improve and apply two essential technologies for AAV vector evolution, and (ii) to concurrently exploit these methods and the ensuing data in order to expand our understanding of AAV biology. One specific objective in the first part was to streamline the methodology of AAV DNA family shuffling, a process whereby capsid genes from distinct AAV isolates are first fragmented and then re-assembled based on partial homologies, thus yielding libraries of AAV chimeras for selection of desired candidates. Therefore, critical steps of the underlying protocol needed to be optimized, and constructs carrying the different capsid genes for shuffling or vector production had to be standardized. In addition, we aimed to thoroughly analyze two key parameters for AAV library selection, *i.e.*, the role of helper Adenovirus and the influence of the source and dose of neutralizing anti-AAV antibodies (IVIG). Similarly, another goal was to also improve the second fundamental AAV evolution method, viral peptide display, which is based on the presentation of short retargeting peptides on the surface of a genetically modified AAV capsid. Here, our specific aim was to assess the amenability of 11 non-AAV2 serotypes that were present in the lab as scaffolds for peptide display, which was intriguing as these alternative isolates provide a variety of assets for clinical use in humans. For both methodologies - DNA family shuffling and peptide display - a common goal was to finally apply the viral libraries and novel capsid-peptide combinations for selection of new and enhanced AAV vectors in a variety of cells *in vitro* and *in vivo*. Ideally, the lead candidates emerging from this work would not only represent optimal templates for future gene transfer/therapy applications, but would concomitantly allow us to dissect the individual residues and domains that determine the features of an AAV capsid and that hence govern AAV biology.

2 Materials and Methods

2.1 Materials

2.1.1 Cell lines and viruses

2.1.1.1 Cell lines:

Cell line	Origin	Tissue/Cell Type	References
RPMI 8226	H. sapiens	B-lymphocyte/ myeloma	[227]
A375	H. sapiens	Skin/ malignant myeloma	[228]
AMO-1	H. sapiens	Myeloma, plasmacytoma	[229]
H-4-II-E	M. musculus	Liver/ hepatoma	[230]
HEK293T	H. sapiens	Embryonic kidney cells	[231]
HeLa	H. sapiens	Cervix/ adenocarcinoma	[232]
HepG2	H. sapiens	Liver/ hepatocellular carcinoma	[233]
HepA1-6	M. musculus	Liver/ hepatoma	[234]
hiPSC	H. sapiens	Foreskin/ fibroblast Induced pluripotent stem cell	[235]
HT144	H. sapiens	Malignant melanoma	[236]
Huh7	H. sapiens	Liver/ hepatoma cell line	[237]
JAWSII	M. musculus	Bone marrow/ immature DC, monocyte	[238]
Jurkat	H. sapiens	T-lymphocyte/ acute leukemia	[239]
K-562	H. sapiens	Bone marrow/ lymphoblast	[240]
Karpas	H. sapiens	lymphoma	[241]
KG1	H. sapiens	Bone marrow/ macrophage, acute leukemia	[242]
KMS-11	H. sapiens	myeloma	[243]
KMS-12BM	H. sapiens	myeloma	[243]
L363	H. sapiens	Plasma cell leukemia	[244]
MCF10A	H. sapiens	Mammary gland, breast/ fibrocystic disease	[245]
MCF7	H. sapiens	Mammary gland, breast/ metastatic site	[246]
MDA-MB-231	H. sapiens	Mammary gland, breast/ adenocarcinoma	[247]
MDA-MB-436	H. sapiens	Mammary gland, breast/ adenocarcinoma	[247]
MolP2	H. sapiens	Multiple myeloma	[248]
MolP8	H. sapiens	Multiple myeloma	[249]
MT4	H. sapiens	T-lymphocyte/ T-cell leukemia	[250]
NIH3T3	M. musculus	Embryo fibroblast	[251]
NKL	H. sapiens	NK-cell/ leukemia	[252]
OPM	H. sapiens	Myeloma, leukemia	[253]
OVCAR-3	H. sapiens	Ovary/ adenocarcinoma	[254]
Panc-1	H. sapiens	Pancreas, duct/ carcinoma	[255]
PC3	H. sapiens	Prostate carcinoma	[256]
Raji	H. sapiens	Burkitt lymphoma	[257]
Raw264.7	M. musculus	Macrophage, monocyte	[258]
SF-539	H. sapiens	Gliosarcoma	[259]
SH-SY5Y	H. sapiens	Neuroblastoma	[260]

SK-MEL2	H. sapiens	Skin/ malignant melanoma	[236]
SKW6.4	H. sapiens	B-lymphoblast/ EBV derived	[261]
SupT1	H. sapiens	T-lymphocyte/ T-cell lymphoma	[262]
T98G	H. sapiens	Brain/ glioblastoma	[263]
THP-1	H. sapiens	Monocyte/ leukemia	[264]
U266	H. sapiens	Multiple myeloma	[265]
U373	H. sapiens	Glioblastoma, astrocytoma	[266]
U937	H. sapiens	Histiocytic lymphoma	[267]
WM266-4	H. sapiens	Skin/ melanoma, metastatic site	[268]

2.1.1.2 Viruses:

Virus type	Description	Source
rAAVx	Recombinant Adeno-associated virus type x (x= <i>cap</i> genes from AAV serotypes 1 to 9, rh10, po.1, 12) with different transgenes	produced in this study
rAAVDJ	Recombinant Adeno-associated virus type DJ vector with different transgenes	produced in this study
Ad5	Adenovirus type 5	provided by D. Nettelbeck, DKFZ

2.1.2 Cell Culture Media and Additives

Product	Company
1x PBS	PAA, GE Healthcare (München, Germany)
Dulbecco's modified eagle medium (DMEM) High Glucose (4,5 g/l) without L-Glutamine	PAA, GE Healthcare (München, Germany)
Fetal Bovine Serum Gold (FBS)	PAA, GE Healthcare (München, Germany)
L-Glutamine	Life Technologies GmbH (Paisley, UK)
MEM Non-Essential Amino Acids (NEAA)	Life Technologies GmbH (Paisley, UK)
Penicillin/ Streptomycin (Pen/Strep)	PAA, GE Healthcare (München, Germany)

2.1.3 Nucleotides

Name	Company
dNTPs (dATP, dCTP, dGTP, dTTP)	NEB (Frankfurt am Main, Germany)
NTPs (ATP, CTP, GTP, UTP)	Fermentas (St. Leon-Rot, Germany)

2.1.4 Standard markers

Marker	Company
100 bp DNA ladder	Life Technologies GmbH (Paisley, UK)
1 kb DNA ladder	Life Technologies GmbH (Paisley, UK)
PageRuler™ Plus Prestained Protein Ladder	Fermentas (St. Leon-Rot, Germany)

2.1.5 Enzymes

Enzyme	Company
Antarctic Phosphatase	NEB (Frankfurt am Main, Germany)
Benzonase	MERCK (Darmstadt, Germany)
DNaseI	Life Technologies GmbH (Paisley, UK)
HotStar Hifidelity Polymerase	QIAGEN (Hilden, Germany)
Phusion Hot Start II DNA Polymerase	Finnzymes (Espoo, Finland)
Proteinase K	Roche (Penzberg, Germany)
Restriction Enzymes	NEB (Frankfurt am Main, Germany) / Fermentas (St. Leon-Rot, Germany)
T4 DNA Ligase	NEB (Frankfurt am Main, Germany)

2.1.6 Kits

Kit	Company
DNA 1000 Kit	Agilent Technologies (Santa Clara, US)
PureLink® HiPure Plasmid Maxiprep Kit	Life Technologies GmbH (Paisley, UK)
PureYield™ Plasmid Midiprep System	Promega (Madison, USA)
QIAquick Gel Extraction Kit	QIAGEN (Hilden, Germany)
QIAquick Nucleotide Removal Kit	QIAGEN (Hilden, Germany)
QIAquick PCR Purification Kit	QIAGEN (Hilden, Germany)
SensiMix™II Probe Kit	Bioline (London, UK)
QIAamp Min Elute Virus Spin Kit	QIAGEN (Hilden, Germany)
Western Lightning® PLUS-ECL	PerkinElmer (Waltham, USA)

2.1.7 Buffers and solutions

Name	Composition	
DNA loading dye (10x)	50 mM 50% 0.25%	Tris pH 7.6 Glycerin bromophenol blue
Iodixanol (15%)	15% dilute in	Iodixanol (Optiprep) PBS-MK-NaCl
Iodixanol (25%)	25% dilute in 0.25%	Iodixanol (Optiprep) PBS-MK Phenol red → red color
Iodixanol (40%)	40% dilute in	Iodixanol (Optiprep) PBS-MK
Iodixanol (60%)	60% 0.25%	Iodixanol (Optiprep) Phenol red → yellow color
LB (lysogenic broth) medium	1% (w/v) 0.5% (w/v) 1% (w/v) <i>for LB plates:</i> 1.5% (w/v)	Bacto Tryptone Bacto Yeast Extract NaCl Bacto Agar
Na-HEPES-Resuspension buffer	50 mM 0.15 M 25 mM	HEPES NaCl EDTA
P1 buffer (Mini prep)	50 mM	Tris/HCl pH 8.0

	10 mM 100 µg/ml	EDTA RNase A → pH 8.0
P2 buffer (Mini prep)	200 mM 1%	NaOH SDS
P3 buffer (Mini prep)	2.8 M	KAc → pH 5.1
PBS-MK	1x 1 mM 2.5 mM	PBS MgCl ₂ KCl
PBS-MK-NaCl	1x 1 mM 2.5 mM 1 M	PBS MgCl ₂ KCl NaCl
Protein sample buffer (2x)	2 mM 100 mM 4% 20% 10% 0.02%	EDTA Tris/HCl pH 7.5 SDS Glycerin β-mercaptoethanol bromophenol blue
Proteinase K buffer	200 mM 25 mM 300 mM 2% (w/v)	Tris/HCl pH 7.5 EDTA NaCl SDS
SOB medium	2% (w/v) 0.5% (w/v) 10 mM 2.5 mM 10 mM	Bacto Tryptone Bacto Yeast extract NaCl KCl MgCl ₂ → pH 7.0
SOC medium	2% (w/v) 0.5% (w/v) 10 mM 2.5 mM 10 mM 20 mM	Tryptone Yeast extract NaCl KCl MgCl ₂ Glucose → pH 7.0
TAE (50x)	2 M 50 mM 1 M	Tris EDTA Acetic acid → pH 8.3
TBS(T)	25 mM 125 mM (0.05%)	Tris/HCl, pH 7.4 NaCl → pH 7.5 Tween 20)
Virus lysate solution (Iodixanol gradient)	50 mM 0.15 M	Tris/HCl pH 8.5 NaCl → pH 8.5

2.1.8 Bacteria:

Strain	Description	Source
<i>E. coli</i> MAX Efficiency DH5α TM	chemically competent	Life Technologies GmbH (Paisley, UK)
<i>E. coli</i> MegaX DH10B TM T1 ^R	electrocompetent	Life Technologies GmbH (Paisley, UK)

2.1.8.1 *Constituents of bacterial cultures*

Product	Company
Ampicillin	Roth (Karlsruhe, Germany)
Bacto™ Agar	BD (Franklin Lakes, USA)
Bacto™ Trypton	BD (Franklin Lakes, USA)
Bacto™ Yeast Extract	BD (Franklin Lakes, USA)
Gentamicin	Life Technologies GmbH (Paisley, UK)

2.1.9 **Chemicals and reagents**

All commonly used chemicals were purchased in the highest purities from the listed companies:

Product	Company
1,4-Dithiothreitol (DTT)	Roth (Karlsruhe, Germany)
TBE 10 x	Fermentas (St. Leon-Rot, Germany)
TGS (Tris/Glycine/SDS buffer) 10x	Bio-Rad (Hercules, USA)
Agarose	Biozym Scientific GmbH (Hessisch Oldendorf, Germany)
Albumin Fraktion V (BSA)	Roth (Karlsruhe, Germany)
Ammonium persulfate (APS)	GRÜSSING GmbH (Filsum, Germany)
Bromophenol blue	CHROMA (Bellows Falls, USA)
Cesium chloride	SIGMA-ALDRICH (St. Louis, USA)
Ethidium bromide	Roth (Karlsruhe, Germany)
Ethylendiamintetraacetate (EDTA)	GRÜSSING GmbH (Filsum, Germany)
HEPES	GERBU Biotechnik (Gaiberg, Germany)
Immunoselect Antifading Mounting Medium DAPI	Dianova (Hamburg, Germany)
Iodixanol (Optiprep™)	AXIS SHIELD (Dundee, UK)
Lipofectamine 2000	Life Technologies GmbH (Paisley, UK)
MOPS	Roth (Karlsruhe, Germany)
Nuclease-free water	Ambion, Life Technologies GmbH (Paisley, UK)
Paraformaldehyde	Electron Microscopy Sciences (Hatfield, UK)
Phenol red	MERCK (Darmstadt, Germany)
Polyethylene Glycol (PEG 8000)	Promega (Madison, USA)
Polyethylenimine (PEI), linear	Polysciences Inc. (Eppelheim, Germany)
PonceauS	SIGMA-ALDRICH (St. Louis, USA)
Proteinase inhibitors (Pefabloc SC (AEBSF))	Roche (Penzberg, Germany)
QIAzol	QIAGEN (Hilden, Germany)
Roti®-Aqua-Phenol/C/I	Roth (Karlsruhe, Germany)
Rotiphorese Gel 40 (19:1)	Roth (Karlsruhe, Germany)
UltraPure™ TEMED	Life Technologies GmbH (Paisley, UK)

2.1.10 Equipment

Device	Company
70Ti rotor	Beckman Coulter (Brea, USA)
Accu-jet® pro Pipette Controller	BrandTech Scientific (Essex, USA)
Agilent 2100 Bioanalyzer	Agilent Technologies (Santa Clara, US)
BANDELIN SONOREX	BANDELIN electronic (Berlin, Germany)
Beckman tube sealer	Beckman Coulter (Brea, USA)
Centrifuges:	
Allegra X-12R centrifuge	Beckman Coulter (Brea, USA)
Avanti J-26 XP centrifuge	Beckman Coulter (Brea, USA)
Benchtop centrifuge 5415R	Eppendorf (Hamburg, Germany)
Optima™ L-90K Ultracentrifuge	Beckman Coulter (Brea, USA)
Electrophoresis System:	
Mini-PROTEAN (protein gels)	Bio-Rad (Hercules, USA)
PowerPac Power Supply	Bio-Rad (Hercules, USA)
Trans-Blot® SD Semi-Dry Electrophoretic Transfer Cell	Bio-Rad (Hercules, USA)
EPS301 Power Supply (Hot lab)	GE Healthcare (München, Germany)
HOEFER™ SE 600 Ruby (Hot lab)	GE Healthcare (München, Germany)
Flow cytometer:	
Cytomics FC500MPL analyzer	Beckman Coulter (Brea, USA)
Film developing cassettes	Dr. Goos-Suprema GmbH (Heidelberg, Germany)
FlexCycler	analyticjena (Jena, Germany)
Function line incubator	Thermo Fisher Scientific (Waltham, USA)
Gel Doc XR	Bio-Rad (Hercules, USA)
Gene Pulser Xcell	Bio-Rad (Hercules, USA)
HERA cell 150 incubator	Thermo Fisher Scientific (Waltham, USA)
HERA safe sterile work bench	Thermo Fisher Scientific (Waltham, USA)
INTELLI-MIXER	neoLab (Heidelberg, Germany)
Microwave oven	Sharp Electronics (Hamburg, Germany)
Mixing block	Biozym Scientific GmbH (Hessisch Oldendorf, Germany)
MSH Basic - magnetic stirrer with steel heating plate	IKA Laboratory Equipment (Staufen, Germany)
NanoVue Spectrophotometer	Thermo Fisher Scientific (Waltham, USA)
Personal Molecular Imager	Bio-Rad (Hercules, USA)
pH meter PB-11	Sartorius (Göttingen, Germany)
Pipettes	Gilson (Middleton, Germany) / Eppendorf (Hamburg, Germany)
Refractometer	Exacta + Optech (San Prospero, Italy)
Rotor-Gene Q	QIAGEN (Hilden, Germany)
Shaker DOS-10L	neoLab (Heidelberg, Germany)
Shaker DRS-12	neoLab (Heidelberg, Germany)
Shaking Incubator Multitron	INFORS HT (Basel, Switzerland)
Tube Rotator	VWR (Radnor, USA)
Ultra Sonicator	Covaris (Woburn, MA, USA)
Vortex Genie2	Scientific Industries (Bohemia, USA)
Water bath TW12	Julabo Labortechnik (Seelbach, Germany)
X-OMAT 2000 processor (film developer)	KODAK (Rochester, USA)

2.1.11 Materials

Material	Detail	Company
Amicon® Ultra Centrifugal Filters	Ultracel - 100 K	Millipore (Billerica, USA)
Cell culture dishes	Ø 6 / 10 / 15 cm	greiner bio-one (Frickenhausen, Germany) / nunc (Roskilde, Denmark)
Cell culture flasks	75 / 175 cm ²	greiner bio-one (Frickenhausen, Germany)
Cell culture plates	6 / 12 / 96 well	greiner bio-one (Frickenhausen, Germany) / nunc (Roskilde, Denmark)
Cell lifter		Corning Incorporated (Corning, USA)
Electroporation Cuvettes	25 x 1 mm gap	peqlab (Erlangen, Germany)
illustra™ MicroSpin™ G-25 columns		GE Healthcare (München, Germany)
Microscope cover glasses	Ø 12 mm	Marienfeld GmbH (Lauda-Königshofen, Germany)
Neubauer counting chamber		Hecht Assistant (Sondheim, Germany)
Nitrocellulose membrane	PROTAN®	Whatman (Maidstone, UK)
Nylon membrane	Hybond™-N ⁺	GE Healthcare (München, Germany)
PCR tubes	0.2 ml 8-Strip	STARLAB (Hamburg, Germany)
Petri dishes	10 / 15 cm	greiner bio-one (Frickenhausen, Germany) / BD (Franklin Lakes, US)
Pipette tips	10 / 200 / 1000 µl	Sarstedt / Biozym Scientific GmbH (Hessisch Oldendorf, Germany) / Kisker / greiner bio-one (Frickenhausen, Germany)
PP tubes	14 ml	greiner bio-one (Frickenhausen, Germany)
qRT-PCR tubes	0.1 ml strip tubes	QIAGEN (Hilden, Germany)
Reaction tubes	0.5 / 1 / 2 ml	SARSTEDT (Nümbrecht, Germany)
Sephadex G-25 (fine)	Quick spin column for radiolabeled RNA purification	Roche (Penzberg, Germany)
Serological pipettes	5 / 10 / 25 ml	greiner bio-one (Frickenhausen, Germany)
Slide-A-Lyzer Dialysis Cassette	G2, 20,000 MWCO, 15 ml capacity	Thermo Fisher Scientific (Waltham, USA)
Sterile filter	0.22 µM pore size	Roth (Karlsruhe, Germany)
Tubes	15 / 50 ml	greiner bio-one (Frickenhausen, Germany)
Ultracentrifuge tubes	Quick-Seal™ (25x89 mm) Optiseal (26x77 mm) RE-SEAL (16x77 mm)	Beckman Coulter (Brea, USA) / Seton Scientific (Petaluma, USA)
Whatman paper	3 mm	Whatman (Maidstone, UK)
X-ray films	Amersham Hyperfilm™ ECL	GE Healthcare (München, Germany)

2.1.12 Software:

Software	Company
ImageJ	[269]
Quantity One	Bio-RAD (Hercules, USA)
Salanto	Developed by Christian Bender in the context of [270] and this study in close collaboration with Nina Schürmann. (https://bitbucket.org/benderc/salanto/wiki/Home)
Vector NTI	Life Technologies GmbH (Paisley, UK)

2.2 Methods

2.2.1 Standard microbiological methods

2.2.1.1 Production of bacteria

2.2.1.1.1 Chemically (CaCl₂) competent bacteria

For self-made stocks of competent bacteria, 10 ml of LB medium without antibiotics were inoculated with *E. coli* from a commercially available stock of DH5 α and grown o.n. at 37°C. 200 ml SOC medium were next inoculated with 1 ml of this o.n. culture and grown to an O.D. of 0.5-0.6 at 37°C. Bacteria were then spun down by centrifugation at 3.200 rpm for 15 min at 4°C. The supernatant was discarded, and the bacterial pellet was resuspended in TFB-I, incubated on ice for 10 min and centrifuged again at 3.200 rpm for 10 min at 4°C. The resulting pellet was resuspended in 10ml TFB-II, aliquoted on ice, frozen in liquid nitrogen and stored at -80°C.

2.2.1.1.2 Electrocompetent bacteria

Stocks of self-made electrocompetent bacteria were made from commercially available *E. coli* DH10B. Therefore, 10 ml LB medium without antibiotics were inoculated with DH10B and grown o.n. at 37°C. Next, one liter SOC medium was inoculated with 2 ml of the o.n. culture and grown to an OD of 0.5-0.6 at 37°C. The bacterial culture was cooled on ice for 30 min and centrifuged at 5.000 rpm for 15 min at 4°C. The pellet was resuspended in 30 ml ice-cold ddH₂O and dialyzed o.n. against 3 l ddH₂O at 4°C. The bacteria suspension was then centrifuged for 15 min at 5.000 rpm at 4°C, and the resulting pellet was resuspended in glycerin and adjusted to 2.5 E+10 cells/ml. Aliquots were frozen in liquid nitrogen and stored at -80°C.

2.2.1.2 Transformation of bacteria

2.2.1.2.1 Chemical transformation

Standard transformations were performed using chemically competent *E. coli* from the self-made stocks. Therefore, 8 μ l from a typical ligation reaction (see 2.2.2.4 below) were mixed with 50 μ l chemically competent bacteria and kept on ice for 30 min. The mixture was then heat-shocked at

42°C for 90 sec and immediately kept on ice again for 2 min. Depending on the resistance encoded on the plasmid, the bacteria mixture was either plated immediately (Ampicillin resistance) or incubated with 1 ml LB medium without antibiotic for 30 min (Kanamycin resistance). In the latter case, the bacteria were then pelleted through centrifugation at 4.000 rpm for 2 min, resuspended in 50-100 µl LB medium and plated. For simple re-transformation of whole plasmids, the initial 30 min incubation on ice and the heat-shock were omitted.

2.2.1.2.2 Electroporation

For higher transformation efficiencies that were required especially for plasmid library productions, electrocompetent *E. coli* were transformed by electroporation in cuvettes with 0.1 mm gaps. Per electroporation/ cuvette, 2 µl ligation mixture with a DNA concentration of 50 ng/µl were mixed with 30 µl bacteria and transferred to a pre-cooled cuvette. The electroporation pulse was performed with a constant protocol of 25 µF, 200 Ω and 2000 V. Ideally, the time constant for the pulse was close to 1 sec. Immediately after the pulse, 1 ml pre-warmed SOC medium (without antibiotics) were added to the reaction mixture, before the bacterial solution was transferred to a 1.5 ml reaction tube and incubated for 1 h at 37°C. Next, the bacteria were centrifuged and plated as described for chemical transformation. For large-scale library productions, 5-20 electroporation reactions were pooled previous to incubation and either plated on large (15 cm diameter) agar plates or grown o.n. in 1 L liquid cultures. In the latter case, the library diversity was determined by plating small aliquots on 10 cm plates and by counting colonies on the next day.

2.2.2 Standard molecular biological methods

2.2.2.1 Amplification of plasmid DNA

For amplification of plasmid DNA, bacteria were transformed with the respective plasmids, plated on agar plates and grown o.n. at 37°C. Liquid culture media (LB media) was inoculated the next day with a single colony and agitated at 37°C for 12 - 14 h. The volume of the liquid culture was chosen according to the amount of plasmid needed. Both, the agar plate and the liquid LB media contained an antibiotic for which the transformed plasmid encoded a resistance gene, to ensure that only those bacteria grew that contained the desired plasmid. Plasmid DNA was isolated from the bacteria by alkaline lysis. For larger preparations (50 ml Midi-Prep, 200 ml Maxi-Prep, and 500 ml Mega-Prep), commercially available kits were used (2.1.6), according to the manufacturer's protocol. For small 2 ml Mini-preps, plasmid DNA was isolated using self-made buffers (2.1.7) and the following protocol: 2 ml o.n cultures were spun down in a centrifuge at 13,000 rpm for 2 min. The supernatant was discarded, and the bacterial pellet was resuspended in 300 µl buffer P1. 300 µl lysis buffer were added, mixed by inversion and incubated for 5 min at RT. The lysis reaction was stopped with 300 µl neutralizing solution P3, mixed again by inversion and incubated for 5 min at RT. The solution was

cleared from cell and protein debris by centrifugation at 13,000 rpm for 10 min. Next, 800 μ l of the supernatant were taken and mixed with 600 μ l isopropanol. The suspension was mixed well by repeated inversion or vortexing, and centrifuged for 15 min at 13,000rpm. The supernatant was removed carefully to not disturb the DNA pellet. The pellet was washed with 70% ethanol (and centrifuged again at 13,000 rpm for 5 min. Ethanol was then removed completely, and the DNA pellet was air-dried and resuspended in 50 μ l DNase-free water. DNA concentration was determined with a spectrophotometer.

2.2.2.2 *Polymerase Chain Reaction (PCR)*

All PCRs were performed using either an Eppendorf Thermo cycler or Biorad Thermo cycler with a three-step protocol, unless mentioned otherwise. A typical protocol is listed below:

PCR reaction mix:

Reagent	Vol./ conc.
DNA	10-200 ng
Primer (forward)	1 μ M
Primer (reverse)	1 μ M
dNTPs	200 μ M
5x Phusion buffer	10 μ l
Phusion Hot Start II DNA polymerase	1 U
H ₂ O	add to a total volume of 50 μ l

Cycling conditions:

Step	Temperature	Time	Cycles
Initial denaturation	98°C	30 sec	1x
denaturation	98°C	10 sec	
annealing	52°C-68°C	30 sec	35x
elongation	72°C	30 sec/kb	
final elongation	72°C	10 min	1x

2.2.2.3 *Restriction digest of DNA*

Frequently used restriction enzymes are listed below.

Enzyme	Recognition site	Reaction temperature
Ascl	5'... GGCGCGCC...3' 3'... CCGCGCGG...5'	37°C
BglI	5'... GCCNNNNNGGC...3' 3'... CGGNNNNNCCG...5'	37°C
BglII	5'... AGATCT...3' 3'... TCTAGA...5'	37°C
HindIII	5'... AAGCTT...3' 3'... TTCGAA...5'	37°C
NotI	5'... GCGGCCGC...3' 3'... CGCCGGCG...5'	37°C
NsiI	5'... ATGCAT...3' 3'... TACGTA...5'	37°C
PacI	5'... TTAATTAA...3' 3'... AATTAATT...5'	37°C

PmeI	5'...GTTTAAAC...3' 3'...CAAATTTG...5'	37°C
Sall	5'...GTCGAC...3' 3'...CAGCTG...5'	37°C
SfiI	5'...GGCCNNNNNGGCC...3' 3'...CCGGNNNNNCCGG...5'	50°C
SpeI	5'...ACTAGT...3' 3'...TGATCA...5'	37°C
SwaI	5'...ATTTAAAT...3' 3'...TAAATTTA...5'	25°C

Table 2: Frequently used restriction enzymes. Shown are the recognition sites with the cutting sites indicated by black triangles. All restriction enzymes were supplied by NEB.

2.2.2.4 *Ligation of DNA*

In standard cloning procedures, fragments from restriction digests or synthesized oligomers were ligated into plasmid backbones using T4 DNA ligase. Typically, 1 µl plasmid backbone and 2-7 µl insert were ligated in a 10 µl reaction with 1 µl 10x reaction buffer and 0.5-1 µl T4 DNA ligase. The reaction was either incubated at RT for 4 h or o.n at 14°C, before an aliquot of the reaction mixture was used for bacterial transformation (2.2.2.1).

2.2.2.5 *DNA agarose gel electrophoresis*

Agarose gel electrophoresis was performed using 1-2% agarose gels at a current of 60-120 V according to the size of the gel and the expected size of the fragments. DNA samples were mixed with 10x loading dye and run together with a standard DNA length marker. DNA fragments were isolated from the gel using a commercially available kit (Gel extraction kit, Qiagen).

2.2.2.6 *Sodium dodecyl sulfate polyacrylamide gel electrophoresis (SDS-PAGE) and Western blotting*

2.2.2.6.1 SDS-PAGE

To separate proteins according to their size, samples were first denatured through 5-10 min incubation in 2x lysis buffer at 95°C. A discontinuous polyacrylamide gel was prepared as exemplified below. AAV capsid and Rep proteins were separated using 8% resolving and 5% stacking gels, respectively. Samples were run together with a standard length protein marker (PageRuler Plus Prestained Protein Ladder). Electrophoresis was performed at a constant current of 80-120 V in 1x TGS Buffer. Following gel separation, the samples were transferred to nitrocellulose membranes by Western blotting (next paragraph).

Resolving gel (5 ml)	8%	Stacking gel (3 ml)	5%
ddH ₂ O	2.6 ml	ddH ₂ O	2.2 ml
Acrylamide (19:1)	1 ml	Acrylamide (19:1)	375 µl
1.5 M Tris (pH 8.8)	1.3 ml	1.5 M Tris (pH 8.8)	375 µl
10% SDS	50 µl	10% SDS	30 µl
1% APS	50 µl	1% APS	30 µl
TEMED	3 µl	TEMED	3 µl

2.2.2.6.2 Western blotting

Transfer of separated proteins from SDS gels to nitrocellulose membranes was performed by semi-dry blotting. Therefore, the SDS gel was gently placed on top of a nitrocellulose membrane and covered with Whatman paper soaked with 1x TGS buffer containing 20% methanol. Transfer occurred at 1 mA/cm² for 1 h in a semi-dry blotter. After transfer, residual positions on the membrane not covered with the transferred proteins were blocked with 1x TBST supplemented with 6% milk powder. Transfer efficiency was validated by PonceauS staining prior to blocking. The membrane was then washed with 1x TBST buffer and incubated with primary antibody in 1x TBST with milk, either for 3 h at RT or o.n. at 4°C. Following incubation, the membrane was washed several times with 1x TBST and incubated for 1 h at RT with a secondary antibody conjugated to horseradish peroxidase. Finally, bound antibody-peroxidase conjugates were detected via chemiluminescence (Western lightning PLUS-ECL kit). Protein bands were visualized on an X-ray film that was exposed to the membrane. Antibodies used for AAV detection are listed in Table 3.

Antibody	Specificity	Dilution	References	Source
B1	VP1, VP2, VP3	1:10	[86], [147], [271], [272]	J. Kleinschmidt, DKFZ (ATV)
A1	VP1	1:10		
303.9	Rep78, 68, 52,40	1:10		

Table 3: Antibodies against AAV for Western Blot analyses. All AB were kindly provided by J. Kleinschmidt (DKFZ, Heidelberg).

2.2.3 Cell biological methods

2.2.3.1 Cultivation of eukaryotic cells

Cells were either maintained in Dulbecco's modified Eagle medium (DMEM) supplemented with 10% fetal calf serum, 100 U/ml penicillin, 100 mg/ml streptomycin, or in RPMI-1640 medium supplemented with 10% fetal calf serum, 100 U/ml penicillin, 100 mg/ml streptomycin. All cell lines were maintained in a humidified incubator with 5% CO₂ at 37°C.

2.2.3.2 *Transfection of cells with polyethyleneimine (PEI)*

Eukaryotic cells were transfected with PEI. Linear PEI was prepared by four iterative freeze-thaw cycles at -80°C and 37°C, respectively, and stored at -80°C. Adherent cells were seeded 24 h prior to transfection at a density ensuring less than 80% confluency at the time of transfection. Suspension cells were transfected directly after seeding. All reagents used for transfection (PEI and NaCl) were pre-warmed to 37°C. Plasmid DNA was adjusted to the appropriate volume (Table 4) with ddH₂O and mixed with 300 mM NaCl. A second mixture of H₂O, 300 mM NaCl and PEI was prepared, briefly mixed by inverting and added drop-wise to the DNA mixture. The combined solutions were briefly mixed by inverting, vortexed for 30 sec and incubated at RT for 10 min. The PEI/DNA mix was then slowly added to the cells. Exact volumes of DNA and reagents were adjusted to the transfection format (Table 4). Volumes are given per well or dish.

Mixture	96-well	6-well	14 cm dish
DNA	100 ng	2.6 µg	44.1 µg
DNA mix	3 µl DNA	49 µl DNA	790 µl DNA
	3 µl NaCl (300 mM)	49 µl NaCl (300 mM)	790 µl NaCl (300 mM)
PEI mix	3 µl NaCl (300 mM)	50 µl NaCl (300 mM)	790 µl NaCl (300 mM)
	1.7 µl H ₂ O	28 µl H ₂ O	438 µl H ₂ O
	1.7 µl H ₂ O	22 µl H ₂ O	352 µl H ₂ O

Table 4: PEI transfection in different formats. Volumes are given per well or dish.

2.2.4 Cloning procedures

2.2.4.1 *Fluorescence reporter constructs*

The pTR-UF3 plasmid that carries a *gfp* gene under a CMV promoter, flanked by ITRs from AAV2, was previously used to package fluorescence protein-encoding sequences into AAV capsids [273]. Self-complementary constructs for fluorescence reporter expression were generated on the basis of pBSU6 that was previously described by Dirk Grimm and colleagues [274]. The pBSU6 plasmid carries one ITR from AAV2 and another from AAV4 to avoid loss of ITRs by homologous recombination. The terminal resolution site (a short sequence adjacent to the ITR which is important during AAV replication and packaging; see also 1.2.1) in the ITR from AAV4 is mutated to allow back-folding of the self-complementary sequences to rapidly generate a double-stranded genome. The pBSU6 plasmid was digested with BglII to remove all sequences between the ITRs. The UF3 cassette in pTR-UF3 consists of a CMV promoter, IRES, *gfp* gene, a polyA site, a PO enhancer sequence, TK promoter and a neomycin resistance followed by another polyA site. It was isolated from pTR-UF3 with BglII and ligated into the pBSU6 backbone. The resulting construct was digested with NotI and Sall, leaving only the CMV promoter and a splice donor/ splice acceptor (SD/SA) sequence downstream of the

restriction site and the upstream polyA site from pTR-UF3 in the modified pBSU6 plasmid (Figure 10A). Subsequently, the fluorescent reporter genes *gfp*, *yfp*, *cfp* and *mCherry* were PCR-amplified and cloned into the newly generated pBSsds vector using the NotI and Sall restriction sites. The resulting plasmid names and the corresponding primer sequences for reporter gene amplification are listed in Table 5. In initial, comparative experiments the *yfp* reporter was found most efficient (data not shown). Thus, fluorescent data shown in this study are mainly gained with the pBSsds_YFP reporter construct (Figure 10B). Other constructs are listed for the sake of completeness.

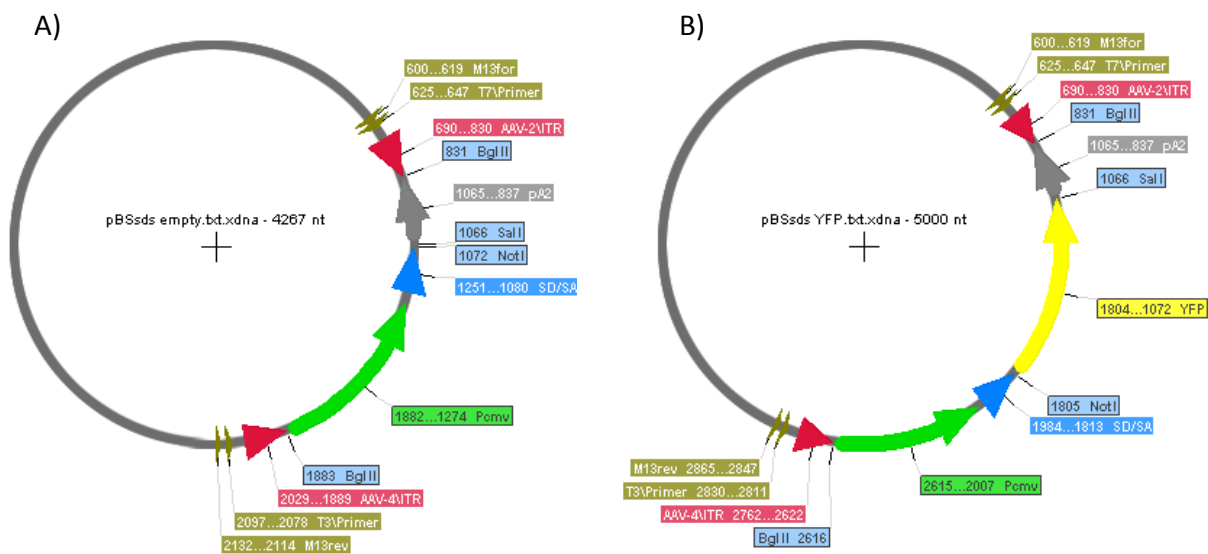


Figure 10: Fluorescence reporter plasmids. **A)** The pBSsds vector encodes a CMV promoter, a SD/SA enhancer sequence and a poly A site; all flanked by ITRs. The terminal resolution site in ITR4 is mutated to promote back-folding of the packaged sequence to directly generate a ds genome. **B)** The reporter gene of choice can be directly cloned into the pBSsds vector via NotI/Sall restriction sites. Indicated are the ITRs (red triangles), CMV promoter (green arrow), the *yfp* gene (yellow arrow in B), SD/SA sequence (blue triangle) and the polyA site (gray arrow). Commonly used primer binding sites M13 for/rev; T3/T7) are indicated by brown triangles. Restriction sites are shown in light blue boxes.

Plasmid name	#	Oligo (5' → 3')	#
pBSsdsYFP	552	5'- AAA TAT GCG GCC GCA CCG GTC GCC ACC ATG GTG AGC - 3'	118
pBSsdsGFP	553	5'- GAC TGG TCG ACG GAC CTA TCG ATT TAC TTG TAC AGC TCG TCC ATG C - 3'	119
pBSsdsCFP	558		
pBSsds mCherry	554	5'- AAA TAT GCG GCC GCA CCG GTC GCC ACC ATG GTG AGC - 3'	118
		5'- GAC TGG TCG ACG GAC CTA TCG ATT TAC TTG TAC AGC TCG TCC ATG CCG CCG GTG - 3'	120
pBSsds dsRed	557	5'- AAA TAT GCG GCC GCA CCG GTC GCC ACC ATG GCC TCC TC - 3'	116
		5'- GAC TGG TCG ACG GAC CTA TCG ATT CTA CAG GAA CAG GTG GTG GCG GCC CTC - 3'	117

Table 5: Fluorescence reporter constructs. NotI recognition sites are in bold, Sall recognition sites are in bold italics. Sequences specific to the amplified gene are underlined. # = plasmid and oligo number, respectively, in the Grimm lab plasmid database.

2.2.4.2 *AAV capsid donor plasmids*

AAV capsid sequences of twelve serotypes (AAV1 to 9, rh.10, po.1, 12) were present in the lab. In analogy to the previously described pBSAAV *cap* plasmids [212], all *cap* sequences were cloned into pBSII-KS(+) and flanked with additional restriction and primer binding sites. Initially, the AAV6 *cap* gene was PCR-amplified as follows (serotype-specific sequence is shown in italics and underlined). The forward primer 5'-GGA CTC **AAG CTT** GTC TGA GTG ACT AGC ATT CGT TAA TTA ACAG GTA TGG CTG CCG ATG GTT ATC TTC CAG-3' introduced a *PacI* restriction site (bold italics), a binding site for primer CUF (light gray background) and a *HindIII* site (bold). The reverse primer 5'-CGT GAG **ACT AGT** GCT TAC TGA AGC TCA CTG AGG GCG CGC CTT ACA GGG GAC GGG TGA GGT AAC GG-3' contained an *AscI* site (bold italics), a binding site for primer CUR (light gray background) and a *SpeI* site (bold). The resulting fragment was cloned into pBSII-KS(+) via *HindIII* and *SpeI*. The newly introduced primer binding sites allowed efficient amplification of the *cap* gene and shuffled chimeras (2.2.5), and the *PacI* and *AscI* sites facilitated later cloning. The remaining eleven *cap* genes were cloned analogously. Integrity of all *cap* genes was confirmed by sequencing. In the course of this work, *cap*-containing pBSII-KS(+) vectors were further modified. To enable iterative PCR amplification of shuffled *cap* sequences by nested PCR (2.2.5), additional primer binding sites were introduced upstream (SAfor) and downstream (SArev) of the *cap* genes. The *cap* sequence and flanking restriction and primer binding sites were removed by *NotI* and *SalI* double-digestion. An oligonucleotide that contained *NotI/SalI*-corresponding overhangs, the additional primer binding sites and *HindIII* and *SpeI* restriction sites was cloned into the pBS donor backbone. The resulting plasmid that was designed for nested PCR was named pBSnst_cx, where x denotes the serotype. All *cap* genes were then transferred from pBS donor vectors to the newly generated plasmid pBSnst_cx via *HindIII* and *SpeI*. An example with the AAV *cap2* gene is shown in Figure 11. Primer sequences are listed in Table 6.

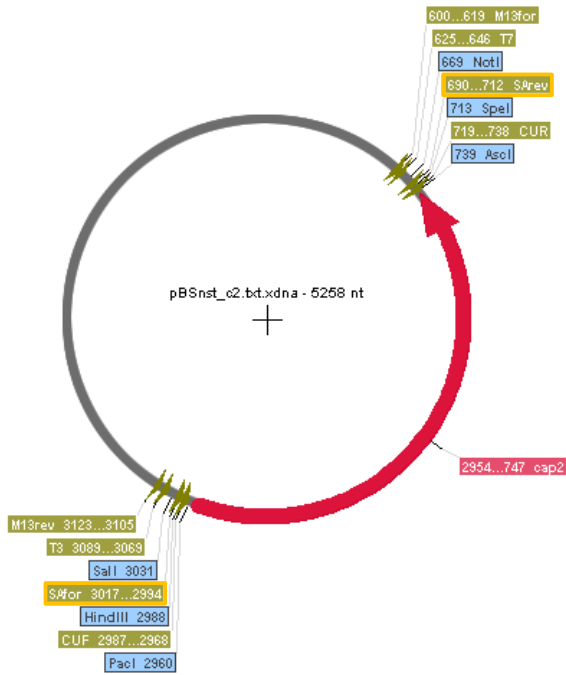


Figure 11: pBSnst_c2 capsid donor plasmid. The pBS based vector encodes AAV capsid genes (exemplified here by AAV cap2). The *cap* sequence is flanked by several primer binding sites indicated by light brown triangles and boxes. The pBSnst construct shown here differs from the pBS construct by two additional primer binding sites (SA for/rev) highlighted by orange framed boxes. Commonly used restriction sites are indicated by light blue boxes.

Plasmid name	#	Oligo (5' → 3')	#
pBSc1/ pBSnstc1	1452	5'-GGA CTC AAG CTT GTC TGA GTG ACT AGC ATT CGT TAA TTA ACAG GTA TGG CTG CCG ATG GTT ATC TTC CAG -3'	34
	1464	5'-CGT GAG ACT AGT GCT TAC TGA AGC TCA CTG AGG GCG CGC CTT ACA GGG GAC GGG TGA GGT AAC GG -3'	35
pBSc2/ pBSnstc2	1453	5'-GAC TCT TAA TTA ACA GGT ATG GCT GCC GAT GGT TAT CTT CC - 3'	121
	1465	5'-GTG AGG GCG CGC CTT ACA GAT TAC GAG TCA GGT ATC - 3'	1166
pBSc3/ pBSnstc3	1454	5'-GAC TCT TAA TTA ACA GGT ATG GCT GCT GAC GGT TAT CTT CC - 3'	123
	1466	5'-GTG AGG GCG CGC CTT ACA AGT TTC GTG TGA GAT ACC - 3'	1167
pBSc4/ pBSnstc4	1455	5'-GAC TCT TAA TTA ACA GGT ATG ACT GAC GGT TAC CTT CCA GA - 3'	1168
	1467	5'-GTG AGG GCG CGC CTT ACA GGT GGT GGG TGA GGT AGC -3'	1169
pBSc5/ pBSnstc5	1456	5'-GAC TCT TAA TTA ACA GGT ATG TCT TTT GTT GAT CAC CCT CC -3'	1170
	1468	5'-GTG AGG GCG CGC CTT AAA GGG GTC GGG TAA GGT ATC - 3'	1171
pBSc6/ pBSnstc6	1457	5'-GGA CTC AAG CTT GTC TGA GTG ACT AGC ATT CGT TAA TTA ACAG GTA TGG CTG CCG ATG GTT ATC TTC CAG -3'	34
	1469	5'-CGT GAG ACT AGT GCT TAC TGA AGC TCA CTG AGG GCG CGC CTT ACA GGG GAC GGG TGA GGT AAC GG -3'	35
pBSc7/ pBSnstc7	1458	5'-GAC TCT TAA TTA ACA GGT ATG GCT GCC GAT GGT TAT CTT CC - 3'	121
	1470	5'-GTG AGG GCG CGC CTT ACA GAT TAC GGG TGA GGT AAC -3'	122
pBSc8/ pBSnstc8	1459	5'-GAC TCT TAA TTA ACA GGT ATG GCT GCC GAT GGT TAT CTT CC - 3'	121
	1471	5'-GTG AGG GCG CGC CTT ACA GAT TAC GGG TGA GGT AAC - 3'	122
pBSc9/ pBSnstc9	1460	5'-GAC TCT TAA TTA ACA GGT ATG GCT GCC GAT GGT TAT CTT CC - 3'	121
	1472	5'-GTG AGG GCG CGC CTT ACA GAT TAC GAG TCA GGT ATC -3'	1166
pBScrh10/ pBSnstcrh10	1461	5'-GAC TCT TAA TTA ACA GGT ATG GCT GCC GAT GGT TAT CTT CC -3'	121
	1473	5'-GTG AGG GCG CGC CTT ACA GAT TAC GGG TGA GGT AAC - 3'	122

pBScpo.1/ pBSnstcpo.1	1462	5'-GAC TCT TAA TTA ACA GGT <u>ATG TCG TTT GTT GAT CAC CCT CC</u> -3'	125
	1474	5'-GTG AGG GCG CGC CTT ACA <u>GGG GTC GGG TAA GGT AAC</u> - 3'	126
pBSc12/ pBSnstc12	1463	5'-GAC TCT TAA TTA ACA GGT <u>ATG GCT GCT GAC GGT TAT CTT CC</u> - 3'	123
	1475	5'-GTG AGG GCG CGC CTT ACA <u>AGT GGT GGG TGA GGA AAC</u> -3'	124
Nested (nst) oligos	-	5'- TCG ACT GTA CAT GCA GTA GAC TAC AAG GAC GAC GAT GAC AAG AAG CTT CGT TGC ACT AGT CTT CGC CTG ATG AGA ATT CAG TGG GAA CTC GCT AGC GC - 3'	1172
	-	5'- GGC CGC GCT AGC GAG TTC CCA CTG AAT TCT CAT CAG GCG AAG ACT AGT GCA ACG AAG CTT CTT GTC ATC GTC GTC CTT GTA GTC TAC TGC ATG TAC AG - 3'	1173
SAfor	-	5'- GAC TAC AAG GAC GAC GAT GAC AAG - 3'	459
SArev	-	5'- CAC TGA ATT CTC ATC AGG CGA AG - 3'	460

Table 6: AAV capsid donor constructs. Listed are the oligos used for capsid amplification for cloning into pBS and pBSnst capsid donor vectors. HindIII and SpeI sites are shown in bold. PacI and AscI sites are in bold italics. Bold/ italics/ underlined are the NotI and Sall corresponding overhangs in the nst oligos. Primer binding sites for later amplification have a light gray background. Capsid gene-specific sequences are underlined. # = plasmid and oligo number, respectively, in the Grimm lab plasmid database.

2.2.4.3 AAV helper constructs

AAV helper constructs without ITRs that provide AAV2 Rep proteins in conjunction with *cap* genes from different serotypes have been described previously. These vectors express the viral capsid into which the ITR-flanked transgene is packaged. Here, we modified a construct that was originally used by Grimm and colleagues [212]. The previous cloning strategy relied on a Swal/ PmeI digest for *cap* gene transfer, using long 3' primers specific for each *cap* gene and containing a PmeI restriction site downstream of the polyA site. To facilitate *cap* gene cloning with shorter reverse primers, we introduced a SpeI site directly behind the *cap* stop codon (Figure 12). To this end, a reverse primer (5'-CAG GTT TAA ACG CCC TTC GCA GAG ACC AAA GTT CAA CTG AAA CGA ATC AAC CGG TTT ATT GAT TAA CAC TAG TTT ACA GAT TAC GAG TCA GGT ATC-3') was designed that contained a PmeI site (underlined/ bold/ italics) followed by a longer stretch including a minimal poly A signal, the newly introduced SpeI site (bold italics) and the last 23 nucleotides of the *cap* gene from AAV2 (underlined). Together with a forward primer comprising a Swal site, the AAV2 capsid sequence was amplified from the previously generated pBS donor plasmid and cloned into the existing, previously described AAV helper plasmid via Swal and PmeI. The remaining eleven AAV *cap* sequences were PCR-amplified and cloned in a similar manner, utilizing the newly introduced SpeI site instead of the PmeI site. Integrity of the *cap* genes was verified by sequencing. There was no influence of the newly introduced SpeI site on the expression of the *cap* genes as detected by Western blot analyses. Oligos used for capsid gene amplification are listed in Table 7.

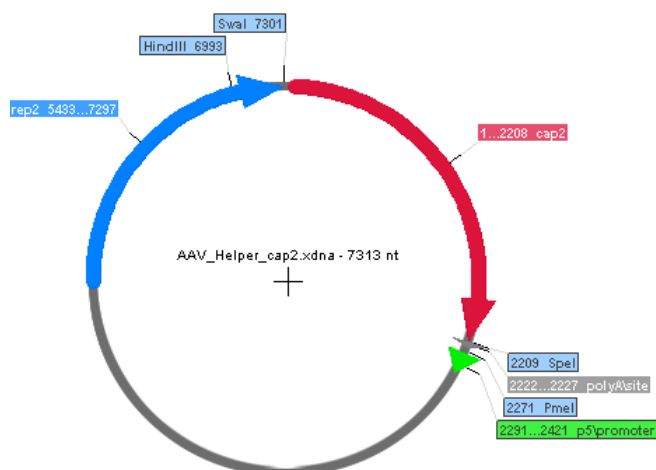


Figure 12: AAV helper construct. The AAV helper plasmids encode an AAV2 *rep* gene, followed by an AAV *cap* sequence (exemplified here for AAV cap2). *Cap* sequences were cloned via Swal/Spel digestion. *Rep* and *cap* can be provided *in trans* to form a AAV capsid. The sequences are not flanked by ITRs and are therefore not packaged in the newly generated capsid. Note that the p5 promoter is located downstream of the actual *rep* and *cap* sequence. This orientation was found favorable for AAV production [65], [88]. Restriction sites are indicated by light blue boxes.

Plasmid name	#	Oligo (5' → 3')	#
WHc1	182	5'- TGG AGA TTT AAA TCA GGT <u>ATG GCT GCC GAT GGT TAT CTT CCA G</u> -3'	129
		5'- GAC AAC ACT AGT <u>TTA CAG GGG ACG GGT GAG GTA ACG G</u> -3'	169
WHc2	183	5'- TGG AGA TTT AAA TCA GGT <u>ATG GCT GCC GAT GGT TAT CTT CCA G</u> -3'	129
		5'- CAG GTT TAAA CGC CCT TCG CAG AGA CCA AAG TTC AAC TGA AAC GAA TCA ACC GGT TTA TTG ATT AAC ACT AGT <u>TTA CAG ATT ACG AGT CAG GTA TC</u> -3'	130
WHc3	1194	5'- TGG AGA TTT AAA TCA GGT <u>ATG GCT GCT GAC GGT TAT CTT CCA G</u> -3'	163
		5'- GAC AAC ACT AGT <u>TTA CAA GTT TCG TGT GAG ATA CCG G</u> -3'	173
WHc4	184	5'- TGG AGA TTT AAA TCA GGT <u>ATG ACT GAC GGT TAC CTT CCA GAT T</u> -3'	165
		5'- GAC AAC ACT AGT <u>TTA CAG GTG GTG GGT GAG GTA GCG G</u> -3'	174
WHc5	185	5'-TGG AGA TTT AAA TCA GGT <u>ATG TCT TTT GTT GAT CAC CCT CCA G</u> -3'	166
		5'- GAC AAC ACT AGT <u>TTA AAG GGG TCG GGT AAG GTA TCG G</u> -3'	175
WHc6	186	5'- TGG AGA TTT AAA TCA GGT <u>ATG GCT GCC GAT GGT TAT CTT CCA G</u> -3'	129
		5'- GAC AAC ACT AGT <u>TTA CAG GGG ACG GGT GAG GTA ACG G</u> -3'	169
WHc7	187	5'- TGG AGA TTT AAA TCA GGT <u>ATG GCT GCC GAT GGT TAT CTT CCA G</u> -3'	129
		5'- GAC AAC ACT AGT <u>TTA CAG ATT ACG GGT GAG GTA ACG</u> -3'	171
WHc8	188	5'- TGG AGA TTT AAA TCA GGT <u>ATG GCT GCC GAT GGT TAT CTT CCA G</u> -3'	129
		5'- GAC AAC ACT AGT <u>TTA CAG ATT ACG GGT GAG GTA ACG</u> -3'	171
WHc9	189	5'- TGG AGA TTT AAA TCA GGT <u>ATG GCT GCC GAT GGT TAT CTT CCA G</u> -3'	129
		5'- GAC AAC ACT AGT <u>TTA CAG ATT ACG AGT CAG GTA TC</u> -3'	829
WHcrh10	190	5'- TGG AGA TTT AAA TCA GGT <u>ATG GCT GCC GAT GGT TAT CTT CCA G</u> -3'	129
		5'- GAC AAC ACT AGT <u>TTA CAG ATT ACG GGT GAG GTA ACG</u> -3'	171
WHcpo.1	191	5'-TGG AGA TTT AAA TCA GGT <u>ATG TCG TTT GTT GAT CAC CCT CCA G</u> -3'	164
		5'- GAC AAC ACT AGT <u>TTA CAG GGG TCG GGT AAG GTA A</u> -3'	172
WHc12	192	5'- TGG AGA TTT AAA TCA GGT <u>ATG GCT GCT GAC GGT TAT CTT CCA G</u> -3'	163
		5'- GAC AAC ACT AGT <u>TTA CAA GTG GTG GGT GAG GAA ACG G</u> -3'	170

Table 7: AAV helper constructs. Listed are the oligos used for capsid gene amplification for cloning into AAV helper plasmids. The SpeI site is indicated by bold italics. The Swal site is shown in bold, and the PmeI site is in underlined bold italics. Capsid specific-sequences are underlined. # = plasmid and oligo number, respectively, in the Grimm lab plasmid database.

2.2.4.4 Peptide insertion sites

To introduce oligonucleotides encoding specific peptides into the 12 available capsid genes, we engineered unique restriction sites into the corresponding AAV helper constructs and then used the two-fragment cloning strategy depicted in Figure 37 (chapter 3.2.1). Therefore, the first approximately 1.8 kb of every capsid gene were PCR-amplified using a suitable forward primer (Table 7) together with a reverse primer that contained SfiI and NsiI sites at its very 3' end (Table 8). In a second PCR, the residual approximately 400 bp of each capsid gene were amplified with a forward primer that contained the same sites in a reverse order - *i.e.*, NsiI at the 5' end followed by SfiI - and with a reverse primer comprising a SpeI site (Table 7 and Table 8). Both PCR fragments were digested with NsiI and either SmaI (5' *cap* fragment) or SpeI (3' *cap* fragment) and ligated into the SmaI / SpeI double-cut helper plasmid backbone. For details about the helper constructs and the respective SmaI and SpeI restriction site, see Figure 13 below or chapter 2.2.4.3 and Table 7. This resulted in a full-length *cap* gene containing two new SfiI sites for later insertion of the peptide-encoding oligonucleotides. Correct sequence composition and the presence of the two SfiI sites were confirmed by sequencing. From the AAV helper constructs, capsid genes with insertion sites were additionally transferred to the pBS donor plasmids that provide a source of capsid genes for further cloning procedures. Of note, the SfiI-based insertion sites were designed such that they introduced a frameshift into the capsid genes. Only upon correct oligonucleotide insertion, the reading frame is shifted back to the original. Annealed peptide-encoding oligonucleotides contained two overhangs matching the SfiI sites and were ligated directly into the SfiI-digested backbone (protocol chapter 2.2.2.4). Oligo sequences for peptides are listed in Table 9. Correct insertion was controlled by sequencing.

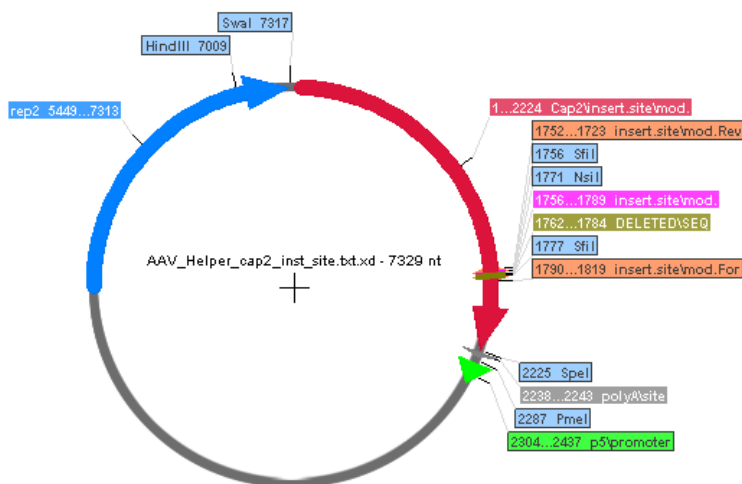


Figure 13: Peptide insertion sites. Using a PCR-based approach (chapter 3.2.1, Figure 37), we introduced insertion sites for peptide sequences into the AAV capsid genes (shown here in the context of AAV helper plasmids and exemplified for AAV cap2). The insertion sites consist of two SfiI sites and were generated via ligation of a NsiI site. Restriction sites are indicated by light blue boxes. Using the AAV helper plasmids, AAVs were produced that display a single distinct peptide and can package a reporter gene (chapter 2.2.4.1, Figure 10). Modified capsid sequences were also transferred into the pBS/pBSnst capsid donor plasmids (chapter 2.2.4.2, Figure 11) and the pTRAAVwt constructs described below (chapter 2.2.4.5, Figure 14).

Primer name	#	Oligos (5' → 3') forward and reverse
modAAV1	279	5'-CCA TGC <i>ATG CAT</i> <u>GGC C</u> CAG GCG <u>GCC</u> GGA GAT GTG CAT GCT ATG GGA GC-3'
	280	5'-CCA TGC <i>ATG CAT</i> <u>TTG GCC</u> TCT CTG <u>GCC</u> GCT GCT CTG GAA ATT GAC TGC CAC- 3'
modAAV2	132	5'-CCA TGC <i>ATG CAT</i> <u>GGC C</u> CAG GCG <u>GCC</u> ACC GCA GAT GTC AAC ACA CAA GGC GTT CTT- 3'
	133	5'-CCA TGC <i>ATG CAT</i> <u>TTG GCC</u> TCT CTG <u>GCC</u> TTG CTG GAG GTT GGT AGA TAC AGA ACC ATA CTG- 3'
modAAV3	281	5'-CCA TGC <i>ATG CAT</i> <u>GGC C</u> CAG GCG <u>GCC</u> GCT CCC ACG ACT AGA ACT GTC AAT G- 3'
	282	5'-CCA TGC <i>ATG CAT</i> <u>TTG GCC</u> TCT CTG <u>GCC</u> GTT ATT TGC CAC AGT TCC ATA CTG- 3'
modAAV4	283	5'-CCA TGC <i>ATG CAT</i> <u>GGC C</u> CAG GCG <u>GCC</u> CTG CCG ACC GTG GAC AGA CTG ACA G- 3'
	284	5'-CCA TGC <i>ATG CAT</i> <u>TTG GCC</u> TCT CTG <u>GCC</u> ACC GCC AGG TAG GTT GCC CCA CAT G- 3'
modAAV5	285	5'-CCA TGC <i>ATG CAT</i> <u>GGC C</u> CAG GCG <u>GCC</u> GCC CCC GCG ACC GGC ACG TAC AAC- 3'
	286	5'-CCA TGC <i>ATG CAT</i> <u>TTG GCC</u> TCT CTG <u>GCC</u> GTT GGT GGC CAT CTG CCC GCC GAC G- 3'
modAAV6	287	5'-CCA TGC <i>ATG CAT</i> <u>GGC C</u> CAG GCG <u>GCC</u> GGA GAT GTG CAT GTT ATG GGA GCC- 3'
	288	5'-CCA TGC <i>ATG CAT</i> <u>TTG GCC</u> TCT CTG <u>GCC</u> GCT GCT CTG GAG ATT GAC TGC CAC- 3'
modAAV7	289	5'-CCA TGC <i>ATG CAT</i> <u>GGC C</u> CAG GCG <u>GCC</u> CAG ACA CAA GTT GTC AAC AAC CAG- 3'
	290	5'-CCA TGC <i>ATG CAT</i> <u>TTG GCC</u> TCT CTG <u>GCC</u> TTG TAA GTT GCT GCT GAC TAT CCC G- 3'
modAAV8	291	5'-CCA TGC <i>ATG CAT</i> <u>GGC C</u> CAG GCG <u>GCC</u> CAA ATT GGA ACT GTC AAC AGC CAG- 3'
	292	5'-CCA TGC <i>ATG CAT</i> <u>TTG GCC</u> TCT CTG <u>GCC</u> CTG CAA GTT ATC TGC CAC GAT ACC- 3'
modAAV9	293	5'-CCA TGC <i>ATG CAT</i> <u>GGC C</u> CAG GCG <u>GCC</u> CAG ACC GGC TGG GTT CAA AAC CAA GG- 3'
	294	5'-CCA TGC <i>ATG CAT</i> <u>TTG GCC</u> TCT CTG <u>GCC</u> CTG GTG GTT TGT GGC CAC TTG TCC- 3'
modAAVrh10	295	5'-CCA TGC <i>ATG CAT</i> <u>GGC C</u> CAG GCG <u>GCC</u> ATT GTA GGG GCC GTC AAC AGT CAA G- 3'
	296	5'-CCA TGC <i>ATG CAT</i> <u>TTG GCC</u> TCT CTG <u>GCC</u> TTG CAG GTT ATC GGC CAC CAC GCC- 3'
modAAVPo1	297	5'-CCA TGC <i>ATG CAT</i> <u>GGC C</u> CAG GCG <u>GCC</u> CAT CCT ACG GTC GGA GTA TAC AAT C- 3'
	298	5'-CCA TGC <i>ATG CAT</i> <u>TTG GCC</u> TCT CTG <u>GCC</u> GTT GTT TGA TAC CTG ACC ACC GGT G- 3'
modAAV12	299	5'-CCA TGC <i>ATG CAT</i> <u>GGC C</u> CAG GCG <u>GCC</u> GCC CCT CAC ATC GCT AAC CTG GAC- 3'
	300	5'-CCA TGC <i>ATG CAT</i> <u>TTG GCC</u> TCT CTG <u>GCC</u> ATT ATC TGC AAT CTG TCC AAA CAT G- 3'
modAAV2 TG with R585	132	5'-CCA TGC <i>ATG CAT</i> <u>GGC C</u> CAG GCG <u>GCC</u> ACC GCA GAT GTC AAC ACA CAA GGC GTT CTT- 3'
	-	5'- CC TGC <i>ATG CAT</i> <u>TTG GCC</u> <i>AGT</i> CTG <u>GCC</u> <i>TCT</i> CTG GAG GTT GGT AGA TAC AGA ACC ATA CTG - 3'
modAAV2 TG w/o R585	132	5'-CCA TGC <i>ATG CAT</i> <u>GGC C</u> CAG GCG <u>GCC</u> ACC GCA GAT GTC AAC ACA CAA GGC GTT CTT- 3'
	-	5'- CC TGC <i>ATG CAT</i> <u>TTG GCC</u> <i>AGT</i> CTG <u>GCC</u> TTG CTG GAG GTT GGT AGA TAC AGA ACC ATA CTG -3'

Table 8: Oligos for capsid insertion site modification. Shown are the forward primer (top) and reverse primer (bottom) for each AAV serotype that was modified. Note that the reverse primer generates the 5' end of the insertion site, while the forward primer creates the 3' part. Both oligos (forward and reverse) contain a NsiI recognition site (bold italics) and a SfiI recognition site (underlined). For the oligos modAAV2TG with and w/o R585, the modified triplet that introduces a Thr (T) and the triplet that restores the Arg (R) are indicated by a light gray background. Compare also to Figure 32 in chapter 4.2.1. # = oligo number in the Grimm lab oligo database.

Table 9: Oligos for peptide insertion (next page). Sequences encoding the actual peptide are in bold underlined. Modified triplets for the alanine walk are in underlined bold italics. Forward and reverse oligos form overhangs that are complementary to the SfiI restriction sites in the modified plasmids. Restriction sites for BglI within the peptide library oligo are underlined; the actual recognition site is shown in underlined italics. # = oligo number in the Grimm lab oligo database.

Oligo name	#	Oligo (5' → 3')
Peptide1 (P1)	1174	5'- T GGC <u>CGC GGC GAT CTG GGC CTG AGC</u> GCC CAG G -3'
	1175	5'- G GGC <u>GCT CAG GCC CAG ATC GCC GCG</u> GCC ACT C -3'
Peptide2 (P2)	1176	5'- T GGC <u>TGC GAT TGC CGC GGC GAT TGC TTT TGC</u> GCC CAG G -3'
	1177	5'- G GGC <u>GCA AAA GCA ATC GCC GCG GCA ATC GCA</u> GCC ACT C -3'
Peptide3 (P3)	1178	5'- T GGC <u>CGC GGC GAT GCG GTG GGC GTG</u> GCC CAG G -3'
	1179	5'- G GGC <u>CAC GCCAC CGC ATC GCC GCG</u> GCC ACT C -3'
Peptide4 (P4)	1180	5'- T GGC <u>AAC GAT GTG CGC AGC GCG AAC</u> GCC CAG G -3'
	1181	5'- G GGC <u>GTT CGC GCT GCG CAC ATC GTT</u> GCC ACT C -3'
Peptide5 (P5)	1182	5'- T GGC <u>AAC GAT GTG CGC GCG GTG AGC</u> GCC CAG G -3'
	1183	5'- G GGC <u>GCT CAC CGC GCG CAC ATC GTT</u> GCC ACT C -3'
Peptide6 (P6)	1184	5'- T GGC <u>TGC AAC CAT CGC TAT ATG CAG ATG TGC</u> GCC CAG G -3'
	1185	5'- G GGC <u>GCA CAT CTG CAT ATA GCG ATG GTT GCA</u> GCC ACT C -3'
Peptide7 (P7)	1186	5'- T GGC <u>AGC CCG GGC GCG CGC GCG TTT</u> GCC CAG G -3'
	1187	5'- G GGC <u>AAA CGC GCG CGC GCC CGG GCT</u> GCC ACT C -3'
Peptide8 (P8)	1188	5'- T GGC <u>GAT GGC CCG TGG CGC AAA ATG</u> GCC CAG G -3'
	1189	5'- G GGC <u>CAT TTT GCG CCA CGG GCC ATC</u> GCC ACT C -3'
Peptide9 (P9)	1190	5'- T GGC <u>TTT GGC CAG AAA GCG AGC AGC</u> GCC CAG G -3'
	1191	5'- G GGC <u>GCT GCT CGC TTT CTG GCC AAA</u> GCC ACT C -3'
P4 'Alanine walk' (A at position 1)	1192	5'- T GGC <u>GCG GAT GTG CGC AGC GCG AAC</u> GCC CAG G -3'
	1193	5'- G GGC <u>GTT CGC GCT GCG CAC ATC CGC</u> GCC ACT C -3'
P4 'Alanine walk' (A at position 2)	1194	5'- T GGC <u>AAC GCG GTG CGC AGC GCG AAC</u> GCC CAG G -3'
	1195	5'- G GGC <u>GTT CGC GCT GCG CAC CGC GTT</u> GCC ACT C -3'
P4 'Alanine walk' (A at position 3)	1196	5'- T GGC <u>AAC GAT GCG CGC AGC GCG AAC</u> GCC CAG G -3'
	1197	5'- G GGC <u>GTT CGC GCT GCG CGC ATC GTT</u> GCC ACT C -3'
P4 'Alanine walk' (A at position 4)	1198	5'- T GGC <u>AAC GAT GTG GCG AGC GCG AAC</u> GCC CAG G -3'
	1199	5'- G GGC <u>GTT CGC GCT CGC CAC ATC GTT</u> GCC ACT C -3'
P4 'Alanine walk' (A at position 5)	1200	5'- T GGC <u>AAC GAT GTG CGC GCG GCG AAC</u> GCC CAG G -3'
	1201	5'- G GGC <u>GTT CGC CGC GCG CAC ATC GTT</u> GCC ACT C -3'
P4 'Alanine walk' (A at position 7)	1202	5'- T GGC <u>AAC GAT GTG CGC AGC GCG GCG</u> GCC CAG G -3'
	1203	5'- G GGC <u>CGC CGC GCT GCG CAC ATC GTT</u> GCC ACT C -3'
P4 'Alanine walk' (3xA at position 5 to 7)	1204	5'- T GGC <u>AAC GAT GTG CGC GCG GCG GCG</u> GCC CAG G -3'
	1205	5'- G GGC <u>CGC CGC CGC GCG CAC ATC GTT</u> GCC ACT C -3'
Peptide Library	1206	5'-CAG TCG <u>GCC</u> AGA GTG GC -NNB x7- G CCC AGG CGG <u>CTG</u> ACG AG -3'
	1207	5'- CTC GTC <u>AGC</u> CGC CTG G -3'

2.2.4.5 AAV wildtype constructs

An AAV wt vector that contains the AAV2 *rep* gene flanked by AAV2 ITRs was previously generated by D. Grimm and colleagues [212]. The vector is based on pTR-UF3 [273] and was designed such that it allows the direct cloning of AAV *cap* genes downstream of the *rep* sequence via *PacI* and *AscI* restriction sites. In the resulting construct, the *rep2* gene and the *cap* gene of choice are flanked by ITRs and enable the production of replication-competent viral particles (Figure 14). Such replication-competent vectors were needed for selection approaches of capsid libraries where a tight genotype-phenotype linkage was necessary, *i.e.*, in DNA shuffling reactions (chapter 3.1) or for the preparation of peptide display libraries (chapter 3.2). In the first case, the AAV wildtype vector served as recipient for *PacI*/*AscI*-digested chimeric capsids. For the latter case, previously described AAV capsid genes with peptide insertion sites (2.2.4.4) were first transferred from the pBS donor plasmids (2.2.4.2). Subsequently, a peptide library was inserted into the modified capsids. Peptide sequences were generated with reverse oligonucleotides that contained randomized nucleotides and a corresponding forward primer (Table 9). In contrast to the defined peptide sequences (2.2.4.4, Table 9) that form the required overhangs for direct ligation upon annealing, the newly generated peptide library had to be digested. Therefore, the random peptide oligos contain two *BglII* restriction sites that flank the actual peptide sequence. These restriction sites create overhangs that match those of the *SfiI*-digested backbone. Upon ligation, both the *BglII* and the *SfiI* restriction sites are destroyed. Further primer sequences used for capsid gene amplification from the pTR_AAVwt constructs are listed in Table 10.

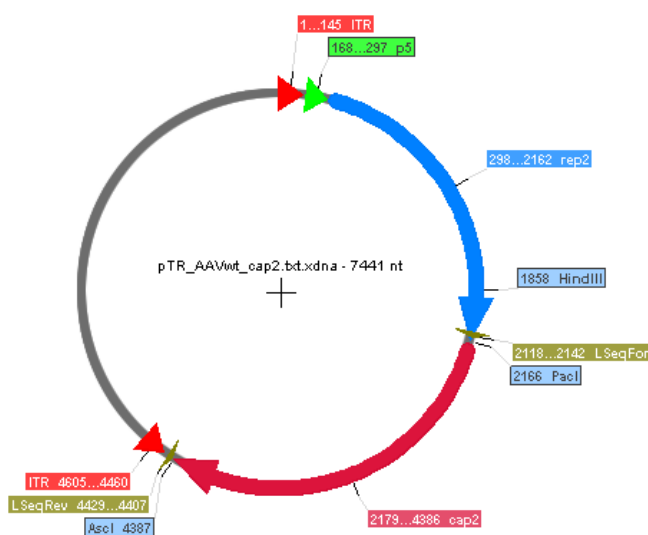


Figure 14: AAV wt constructs. The pTRAAVwt plasmids encode AAV2 *rep* genes and capsid genes (exemplified here by *cap2*) under a p5 promoter and flanked by ITRs. From these plasmids, replication-competent AAVs were produced that can package the AAV genome into the respective capsid. These plasmids were used for shuffled capsid and peptide display libraries production. In analogy to the pBS/pBSnst plasmids, different capsid genes were cloned via *PacI*/*AscI*. ITRs are shown as red triangles, commonly used primer binding sites are shown in light brown and restriction sites are indicated by light blue boxes.

Oligo name	#	Oligo (5' → 3')
LseqF	822	5'- GATCTGGTCAATGTGGATTG -3'
LseqR	823	5'- GACCGCAGCCTTTGAATGTC -3'
Lseq_nstF	824	5'- ACTGCATCTTTGAACAATAAAT -3'
Lseq_nstR	825	5'- GTTTATTGATTAGGCGCGCC -3'

Table 10: Oligos for capsid gene amplification. # = oligo number in the Grimm lab oligo database.

2.2.5 DNA family shuffling

The method of DNA family shuffling allows for the recombination of partially homologous genes into chimeric sequences using a PCR-based approach. As illustrated in more detail in chapter 3.1, it relies on the initial fragmentation of the parental genes, followed by reassembly based on partial homology and amplification of full-length sequences via flanking regions common to all input sequences. Here, this method was applied to AAV *cap* genes from multiple serotypes to create diverse libraries of AAV capsid chimeras.

2.2.5.1 Capsid PCR

In order to generate sufficient amounts of *cap* DNA for subsequent fragmentation, *cap* genes of interest were PCR-amplified from the pBScap and pBSnst donor plasmids (Figure 11, chapter 2.2.4.2 and Table 6) with the M13 primer pair, binding to sites in the standard pBSII-KS(+) backbone adjacent to all *cap* variants. In the resulting PCR fragments, *cap* sequences were flanked by sites for the T3/T7 primer pair, the CUF/CUR primer pair and - in the case of pBSnst-derived sequences - the SA primer pair (Figure 11). All fragments further contained restriction sites for HindIII and PacI (5'), as well as for SpeI and AclI (3'). These conserved regions were used for later rescue PCR of the chimeric sequences (chapter 3.1) and subsequent cloning. To obtain sufficient amounts of *cap* sequences in that first PCR, two 50 µl reactions per serotype were performed with the HotStar Hifidelity Polymerase (Qiagen). Cycling conditions are listed below. PCR products were run on a 1% agarose gel and purified with the Qiagen gel extraction kit according to the manufacturer's protocol.

PCR reaction mix:

Reagent	Vol./ conc.
DNA	200 ng
M13For	1 µM
M13Rev	1 µM
5x HiFi buffer	10 µl
HiFi polymerase	5 U
H ₂ O	add to a total volume of 50 µl

Cycling conditions:

Step	Temperature	Time	Cycles
initial denaturation	95°C	5 min	1x
denaturation	94°C	15 sec	
annealing	57°C	30 sec	40x
elongation	68°C	3 min	
final elongation	72°C	10 min	1x

2.2.5.2 DNA fragmentation

A controlled DNase digest was used to generate DNA fragments of a defined size range that efficiently re-assemble into chimeric *cap* sequences. Because the DNase digest is a crucial step in DNA family shuffling, it had to be carefully controlled. The reaction was set up as listed below, with DNase added last, flicked three times and spun down briefly. Incubation at 25°C for 1 min resulted in fragments between 100 and 1000 bp, whereas incubation of up to 2 min gave 100-500 bp fragments. Typically a reaction time of 1.5 min was sufficient for an appropriate fragment size of 100-800 bp. The reaction was stopped by adding 6 µl 25mM EDTA, brief vortexing and incubating at 75°C for 10 min. DNA fragments were separated in a 1% agarose gel and purified with the Qiagen gel extraction kit according to the manufacturer's protocol. Isopropanol was added to the sample prior to purification to enhance DNA yields. Purified fragments were eluted in 30 µl ddH₂O.

DNase digestion:

Reagent	Vol./ conc.
DNA (total amount of DNA consists of equal amounts of capsid DNA)	4 µg
10x DNase buffer	6 µl
DNase I (undiluted)	0.3 µl
H ₂ O	add to a total volume of 60 µl

2.2.5.3 Re-assembly PCR (1st PCR)

Following DNA fragmentation, the *cap* fragments were re-assembled in a first PCR reaction in which they self-prime each other based on their partial homology. Phusion Hot Start II DNA Polymerase (Finnzymes) was used in this first PCR. To foster self-priming and hence formation of chimeric sequences, DMSO was added and annealing was performed at a low temperature of only 42°C. Precise reaction conditions are indicated below. PCR products from this first shuffling PCR were not purified, but rather used directly as templates for the subsequent second PCR (see next paragraph).

PCR reaction mix:

Reagent	Vol./ conc.
DNA (from purified DNase digest)	500 ng
5x Phusion HF buffer	10 µl
DMSO	1.5 µl
dNTPs	1 µl
Phusion polymerase	0.5 µl
H ₂ O	add to a total volume of 50 µl

Cycling conditions:

Step	Temperature	Time	Cycles
initial denaturation	98°C	30 sec	1x
denaturation	98°C	10 sec	
annealing	42°C	30 sec	40x
elongation	72°C	45 sec	
final elongation	72°C	10 min	1x

2.2.5.4 **Rescue PCR (2nd PCR)**

In an ensuing second PCR, chimeric full-length sequences were amplified or ‘rescued’ from the 1st PCR with primers binding to the conserved regions that flank each capsid gene. Reaction conditions are shown below. PCR products were run on a 1% agarose gel, purified with the Qiagen gel extraction kit and eluted in 30 µl ddH₂O. The complete eluate was digested with PaeI and AseI, and then cloned into a wtAAV recipient plasmid. After ligation, *E. coli* were electroporated (see chapter 2.2.1.2.2) to ensure maximal transformation efficiency and diversity of the resulting plasmid library.

PCR reaction mix:		Cycling conditions:			
Reagent	Vol./ conc.	Step	Temperature	Time	Cycles
DNA (from 1 st PCR)	2 µl	initial denaturation	95°C	5 min	1x
SAFor	1 µM	denaturation	94°C	15 sec	40x
SARev	1 µM	annealing/ elongation	68°C	3 min	
5x HiFi buffer	10 µl	final elongation	72°C	10 min	1x
MgSO ₄	0.5 µl				
HiFi polymerase	5 U				
H ₂ O	add to a total volume of 50 µl				

2.2.6 **AAV virus production**

AAV virions were either produced as wildtype vectors containing the cognate AAV genome or as rAAV carrying a reporter construct in a specific capsid. To generate wildtype genome-containing viruses, Hek293T cells were transfected with two plasmids at equal amounts - an AAV plasmid encoding the AAV *rep* and *cap* genes flanked by ITRs, and an Adeno helper plasmid carrying the necessary adenoviral helper functions [275]. To produce reporter rAAVs, three plasmids were transfected, again at equal amounts. The first plasmid encoded the recombinant AAV vector genome comprising the reporter expression cassette, flanked by ITRs. The second plasmid provided the *rep* and *cap* genes, while the third plasmid was again the Adeno helper construct. Transfection was performed according to the PEI protocol (2.2.3.2).

2.2.6.1 **AAV small-scale production (crude lysates)**

In cases where only small amounts of virus were needed or where a large set of different viruses had to be generated in parallel (as for the AAV peptide screen, chapter 3.2.3), AAV was produced in small scale in a 6-well format. Therefore, one well of a 6-well plate of Hek293T cells was triple-transfected with 1) an AAV vector plasmid typically encoding a *yfp* reporter gene, 2) an AAV helper plasmid expressing the desired capsid proteins, and 3) the adenoviral helper construct. Seventy-two h post-transfection, the cells were harvested together with the media and transferred to a 2 ml reaction

tube. After centrifugation for 10 min at 4000 rpm to pellet cells containing virus, the supernatant was discarded. The cell pellet was washed twice with 1x PBS and centrifuged again. The final pellet was resuspended in 500 µl 1x PBS and subjected to five freeze-thaw cycles in liquid nitrogen and a 37°C water bath, respectively. The lysed cells were then additionally sonicated for 1 min at 48 W and centrifuged at 13.000 rpm for 10 min. Finally, 450 µl of the supernatant were carefully transferred to a new reaction tube. These crude lysates were either directly used for further analysis or infection, or stored at -80°C for later use.

2.2.6.2 ***AAV large-scale production***

AAV vectors were produced to the highest grade in 10 to 40 14 cm culture dishes. Per dish, 5×10^5 Hek293T cells were seeded, grown for 24 h at 37°C and transfected with the required plasmids (see 2.2.6.1) according to the PEI protocol (chapter 2.2.3.2). Seventy-two h post-transfection, the cells were harvested, scraped off the plates, centrifuged at 1.500 rpm at 4°C for 5 min and washed twice with 1x PBS. The cell pellets were then either frozen at -80°C for later processing, or virus was directly purified by iodixanol or cesium chloride density gradient centrifugation (chapters 2.2.6.2.1 & 2.2.6.2.2 below).

2.2.6.2.1 Iodixanol purification

AAV vectors produced in 10-20 14 cm dishes were typically purified by iodixanol gradient centrifugation. Therefore, the cell pellets were initially resuspended in 20 ml virus lysis solution. After five freeze-thaw cycles in liquid nitrogen and a 37°C water bath followed by sonication for 1 min at 48 W, 50 U/ml benzonase was added to degrade free nucleic acids. The mixture was incubated at 37°C for 1 h and vortexed every 10 min. Afterwards, virus lysis solution was added to a total volume of 22 ml, and samples were centrifuged at 5.000 rpm for 15 min at 4°C. The supernatant was transferred to a new reaction tube, and the centrifugation step was repeated once. The cleared lysate was carefully transferred into an ultracentrifuge tube by pipetting through a Pasteur pipette that was placed into the tube. To set up the density gradient, 7 ml 15% iodixanol solution were pipetted through the same Pasteur pipette, followed by 5 ml 25%, 4 ml 40% and 4 ml 60% iodixanol solution. The Pasteur pipette was finally carefully removed from the tube to avoid air bubbles and to not disturb the gradient. The ultracentrifugation tube was filled up with virus lysis solution, and any remaining air bubbles were carefully removed with a needle. The tubes were sealed with a tube sealer (Beckman) and centrifuged at 50.000 rpm for 2 h at 4°C in an ultracentrifuge with the 70Ti rotor. The 40% iodixanol phase containing full virus particles (*i.e.*, capsids containing viral genomes) was pulled and frozen at -80°C.

2.2.6.2.2 AAV purification by cesium chloride density gradient

In cases where the highest possible particle purity was desired, AAV stocks were purified by cesium chloride density gradient centrifugation. To this end, cell pellets from 20-40 14 cm dishes were resuspended in 15 ml benzonase buffer, subjected to five freeze-thaw cycles and sonicated for 1 min at 48 W. Next, 200 U/ml benzonase were added, and the solution was incubated for 1 h at 37°C and vortexed every 10 min during incubation. The samples were then centrifuged for 15 min at 2,500 x g at 4°C, and the supernatant was transferred to a new reaction tube. Low molecular weight proteins were removed from the samples by adding 1/39 of the total volume of CaCl₂. After incubation on ice for 1 h, the lysates were centrifuged for 15 min at 10,000 rpm. The supernatant was again transferred to a new tube and mixed with ¼ volume of 40% PEG8000/2.5 M NaCl. The samples were incubated o.n. on ice and then centrifuged at 2,500 x g for 30 min at 4°C. The supernatant was discarded, and the pellet was thoroughly resuspended in 10 ml Na-Hepes resuspension buffer. The total volume was adjusted to 24 ml using the same buffer, before 0.55 g/ml CsCl was added. Once the samples had recovered from the resulting temperature drop back to RT, their refractive index was measured using a refractometer and adjusted to 1.370 with Na-HEPES resuspension buffer to decrease, or with CsCl to increase values, respectively. The samples were transferred to ultracentrifuge tubes which were filled up with topping solution, and remaining air bubbles were carefully removed. The samples were centrifuged in an ultracentrifuge at 45,000 rpm for 24 h at 21°C in a 70Ti rotor. Afterwards, the gradient was fractionated as follows: 3, 3, 0.5, 0.5, 0.5, 5, 0.5, 0.5, 0.5, 3 ml. The refractive index of all fractions was determined, and those with an index between 1.3711 and 1.3766, containing full AAV particles, were pooled and dialyzed o.n. against 1x PBS using Slide-A-Lyzer dialysis cassettes. Resulting virus in PBS was further concentrated using Amicon-Ultra-15 centrifugal filters to a final volume of 1.5-2 ml and frozen at -80°C.

2.2.6.2.3 AAV titration

Titers of virus stocks purified via Iodixanol or CsCl density gradient centrifugation (see above) were determined by quantitative RT-PCR, using the specific primer/probe sets shown in Table 11 and plasmid standards. The latter ranged from 5x10³ to 5x10⁹ vg/ml. Samples were prepared as follows: 10 µl of virus sample and controls were lysed with 10 µl TE and 20 µl NaOH (2 M) for 30 min at 56°C. The reaction was stopped with 38 µl HCl (1 M), and the total volume was adjusted to 1 ml with ddH₂O. Iodixanol-purified samples were further diluted to avoid interference with the RT-PCR reagents. Reaction mixtures were then set up which contained 1.48 µl sample, 0.4 µM primer, 0.1 µM probe and 1 µl SensiMixII in a total volume of 10 µl. All qRT-PCRs were run on a Rotor-Gene-Q thermo cycler. Cycling conditions and primer probe sets are listed in Table 11 and Table 12.

Cycling conditions: qRT-PCR

Step	Temperature	Time	Cycles
initial denaturation	95°C	10 min	1x
denaturation	95°C	10 sec	40x
annealing/ elongation	60°C	30 sec	
final elongation	72°C	10 min	1x

Table 11: Cycling conditions for qRT-PCR.

Plasmid name	Oligo (5' → 3')
CMV primer	TGCCCAGTACATGACCTTATGG
	GAAATCCCCGTGAGTCAAACC
CMV probe	FAM-ATGCATCGCTATTACCATGG-BHQ1
GFP primer	GAGCGACCATCTTCTTCAAG
	TGTCGCCCTCGAACTTAC
GFP probe	FAM-ACGACGGCAACTACA-BHQ1
Rep2 primer	AAGTCCTCGCCCAGATAGAC
	CAATCACGGCGCACATGT
Rep2 probe	FAM-TGATCGTCACCTCCAACA-BHQ1

Table 12: Primer-probe combinations used in qRT-PCR for rAAV titrations. Probes are dually labeled with the reporter dye (FAM) 5' and the quencher molecule (BHQ1) 3'.**2.2.6.3 Infection and transduction of cultured cells**

Eukaryotic cells were infected with AAV vectors at multiple MOIs. Typically, adherent cells were seeded 24 h prior to infection at a confluency of 70-80%. In contrast, suspension cells were infected directly after seeding. Because crude lysates cannot be titered properly (qRT-PCR yields inaccurate results due to various interfering lysate ingredients), equal volumes rather than defined particle numbers were used for infection. Accordingly, adherent cells in a 96-well plate were infected with 5 µl/well and suspension cells with 10 µl/well, respectively. Purified vectors or crude lysates were added directly to the cells in complete culture medium. In cases where super-infection with Ad5 was required, such as for viral library amplification (see chapter 2.2.7.1), the medium was removed, the cells were washed with PBS and medium with a reduced amount of FCS of 2% was added. Unless otherwise mentioned, infected cells were analyzed 72 h post-infection.

2.2.6.3.1 Heparin assay

Soluble heparin is an analog of HSPG and inhibits HSPG-dependent AAV binding, allowing its use to study the role of HSPG for binding of wildtype AAVs and of mutants with peptide insertions. Therefore, 10 µl virus were incubated at 37°C for 1 h with 90 µl full medium supplemented with 50 µg/ml heparin. Virus incubated with medium without heparin served as control. After the incubation,

the medium was removed, and the cells were washed twice with 1x PBS before the virus/medium mix was added. The cells were then incubated for 24 h before the virus-containing medium was removed. The cells were washed again twice with 1x PBS, before normal medium was added. After another 48h incubation at 37°C, infection rates were determined by FACS.

2.2.6.3.2 Neuraminidase assay

Sialic acid-dependent AAV binding can be inhibited by Neuraminidase III from *Vibrio cholera* that removes sialic acid from the cell surface. To measure dependency of virus binding on sialic acid, cells were seeded and grown for 24 h at 37°C in normal medium. The medium was then removed, and the cells were washed twice with 1x PBS and incubated for 2 h at 37°C with medium without FCS, supplemented with 50 U/ml Neuraminidase III. Afterwards, the treated cells were washed twice with 1x PBS before virus in complete medium was added. After a 1 h incubation time, virus-containing medium was removed, and the cells were again washed twice with 1x PBS prior to addition of full medium. The short virus incubation time of only 1 h was chosen to avoid virus binding to restored sialic acid residues. The cells were grown for another 48 h, and infection rates were determined by flow cytometry.

2.2.7 Selection procedures

AAV capsid libraries were subjected to different selection schemes in order to identify clones with desired properties. Typically, five amplification rounds were performed per selection scheme, either in the presence of Adenovirus that promotes AAV replication, or in the absence of helper functions.

2.2.7.1 Iterative AAV library amplification in Huh7 cells

AAV library selection was conducted by iterative amplification in cultured cells. To assure a high phenotype-genotype linkage, infections were performed under minimal conditions. First, cells in a 6-well format were infected with 2×10^8 to 2×10^{10} virus particles in complete medium. The cells were incubated for 4 h at 37°C and then washed twice with 1x PBS. The full medium was then replaced with medium supplemented with only 2% FCS, and the cells were superinfected with Ad5 at an MOI of 10 to 50. The Ad5 MOI was varied so that cell lysis was ideally induced 48-72 h post-infection. After up to 72 h incubation, the cells were harvested and crude lysates were prepared. AAV protein expression was assessed by Western blotting, and only those samples which gave minimal signals were passaged (assuming that this should foster a tight phenotype-genotype linkage). In the second and in the following amplification rounds, the exact viral titer of the crude lysates was not known. Hence three different volumes (typically 0.5 μ l, 1 μ l and 10 μ l) of crude lysates that gave minimal signal in the Western blot were used for infection. Incubation times and conditions for Ad5 co-infection were adjusted as described for the first infection round. After five selection rounds, viral DNA was isolated, cloned into the wt recipient plasmid and sequenced. Individual capsid genes were

additionally transferred to the AAV helper plasmid for production and titration of vectors encoding a *yfp* reporter.

2.2.7.2 **IVIG selection**

For library selection in the presence of increasing amounts of intravenous IgG (IVIG), purified virus (first selection round) or crude lysates (subsequent rounds) were incubated for 1 h with either a 'starting concentration' of Gamunex[®], Octagam[®] and Kiovig[®] or a 'final concentration' of Gamunex[®] prior to infection. 'Starting' concentrations of IVIG ranged from 1 µg/µl in the first round, to up to 10 µg/µl in the last selection round. 'Final' concentrations of IVIG ranged from 0.1 µg/µl to 1 µg/µl. The cells were incubated for 4 h with the IVIG-treated virus, then thoroughly washed three times with 1x PBS to remove all remaining IVIG and finally co-infected with Ad5. Conditions for Ad5 co-infection were adjusted according to the protocol described for iterative amplification of AAV on Huh7 cells (previous passage 2.2.7.1). Because IVIG also contains neutralizing antibodies against Adenovirus, the Ad5 MOI had to be empirically adjusted to a level that would mediate cell lysis after 72 h. As for the amplification without IVIG (previous passage), viral DNA was isolated after five selection rounds, cloned into the wt recipient plasmid and sequenced. Individual capsid genes were also transferred to the AAV helper plasmid for production and titration of vectors encoding a *yfp* reporter.

2.2.7.3 **Selection without Ad5**

To select AAV in the absence of Ad5 and hence without AAV replication, AAV capsid genes were isolated from infected cells 48 h post-infection after each round using the virus spin kit (Qiagen) according to the manufacturer's protocol. Capsid genes were digested with *PacI* and *Ascl* and ligated into the wt recipient plasmids. According to the protocol described in more detail in 2.2.1.2.2, 2 µl ligation mixture with a DNA concentration of 50 ng/µl were transformed per electroporation reaction. Based on a plasmid library obtained from ten such electroporation reactions, virus libraries were produced. As described in 2.2.3.2 and shown in Table 4, 44.1 µg of total DNA were transfected in a double-transfection reaction together with Adeno helper plasmids according to the PEI protocol for 14 cm dishes. Purification by Iodixanol gradient centrifugation from ten such 14 cm dishes was performed as described in chapter 2.2.6.2.1. Viral titers were determined after each production round (Table 14), and 2×10^8 viral particles were used in the next infection round. In *in vivo* selection assays that were performed by our collaboration partners, AAV infection was also performed without Ad5 co-infection. AAV capsid genomes were amplified from total DNA, and viral libraries were produced, according to the protocol described above.

2.2.8 Flow Cytometry

2.2.8.1 Measurement setup

Infection rates and expression intensities of YFP- or GFP-expressing viruses were measured by flow cytometry. The size and granularity of the cells were determined by forward and sideward scatter. 'Alive cells' were defined according to these parameters and gated for measurement of fluorescence expression. YFP and GFP expression was detected in the yellow and green channel, respectively, and plotted against red fluorescence. Background fluorescence that is caused by auto-fluorescence of *e.g.* dying cells was determined with uninfected samples, and the threshold for fluorescence-positive cells was set according to this value. Infection rates were determined as percentage of positive cells out of at least 10.000 events in the 'alive cells' gate. Mean intensities that reflect the expression intensity were calculated from the total of fluorescence-positive cells. For comparison of infection rates and intensities between different cells, forward and sideward scatter as well as the definition of 'alive cells' were adjusted to the properties (size and density) of the respective cell type. Detector intensities were kept constant for all measurements to allow for comprehensive comparisons. All data were acquired with a Cytomics FC500MPL analyzer flow cytometer in a 96-well format.

2.2.8.2 Cell preparation

Eukaryotic cells in a 96-well format were prepared as follows for flow cytometry: Adherent cells were washed twice with 1x PBS 72 h post-infection and incubated with 30 μ l 0.25% trypsin for 10 min at 37°C. Next, 170 μ l PBS supplemented with 1% BSA were added and repeatedly pipetted up and down to separate cell clusters. For suspension cells, the volume of the medium was adjusted to 200 μ l. Measurement was conducted directly from the 96-well culture plates.

2.2.9 Bioinformatic analysis of shuffled sequences

Sequences from shuffled AAV clones were analyzed using the Salanto program. The program was developed by Christian Bender in cooperation with the group of Dr. Dirk Grimm to specifically suit the needs of chimeric sequence analysis [270]. Based on a sequence alignment created with other programs, *e.g.* vector NTI, Salanto assigns amino acids or nucleotides in any chimeric sequences to their corresponding parental origin. These assignments can be either position-wise, or the program allocates whole stretches to a certain serotype. Crossover frequencies and distribution of reference sequences are also indicated, which allows for a determination of the efficiency of the shuffling process itself. The program is accessible free-of-charge and is available together with a detailed manual describing the different applications and the algorithm at the following website: <https://bitbucket.org/benderc/salanto/wiki/Home>.

3 Results

3.1 AAV DNA Family Shuffling

The first part of the work in this thesis focused on the method of DFS as a potent and versatile means for molecular AAV vector evolution. The following Figure 15 again summarizes the main steps in the protocol as indicated in chapter 1.3.1 above and as originally established by Grimm and colleagues in 2008 [212], from initial *cap* gene isolation and shuffling, followed by subcloning and library production, to selection either in cultured cells or in animals (*in vivo* biopanning).

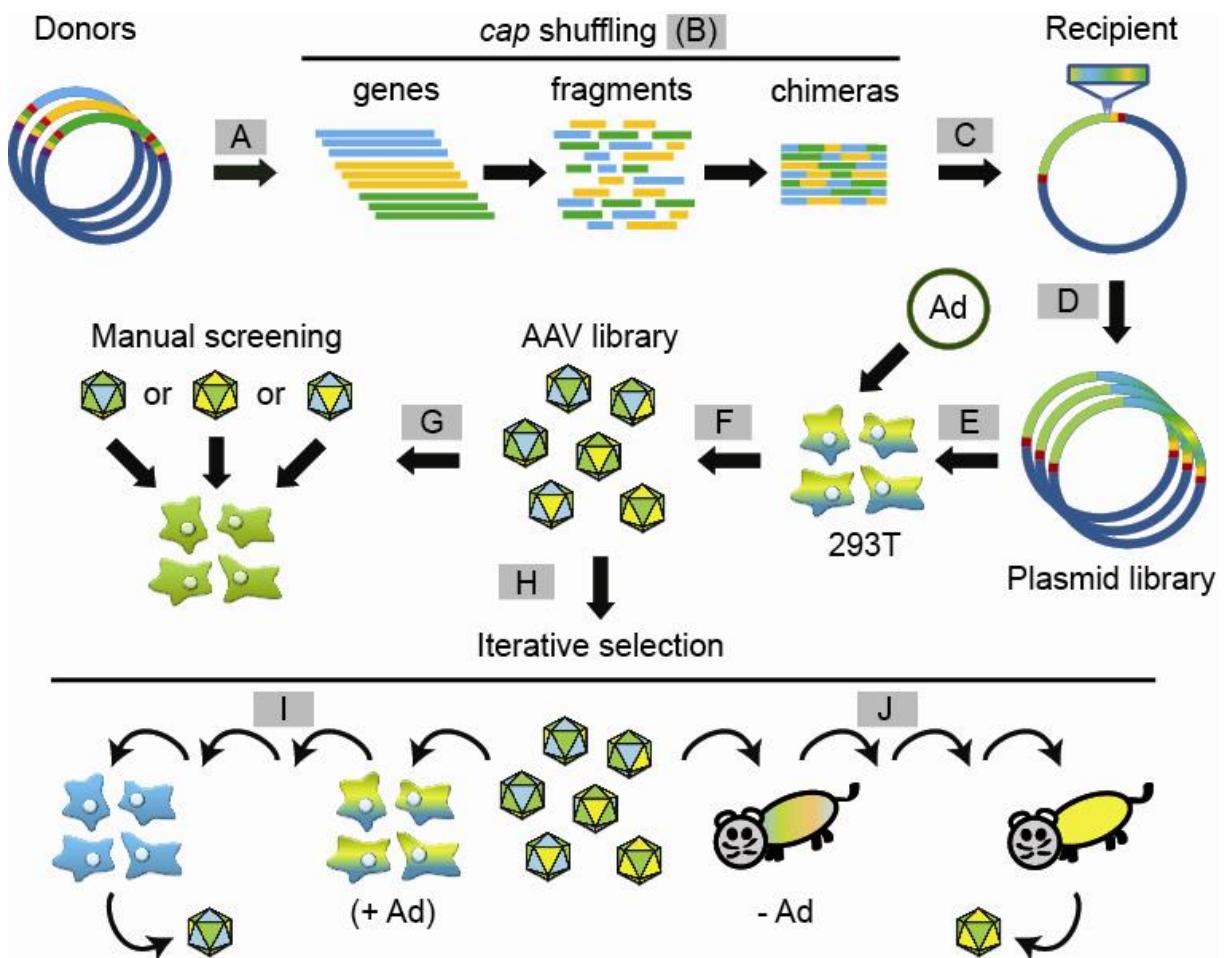


Figure 15: Overview over the DFS process. Capsid genes are amplified from donor plasmids (A), fragmented and re-assembled using two iterative PCRs (B). Resulting chimeric *cap* gene sequences are ligated into wt recipient plasmids that encode the *rep* gene of AAV2 and that carry flanking ITRs (C). After ligation, plasmids are transformed to generate a diverse plasmid library (D) from which a viral library is produced (E-F). Individual chimeric capsids of interest are selected from this library through either manual screening (G) or iterative amplification under specific selection pressures, including the presence or absence of helper Adenovirus (Ad) (H-J). (Figure adapted from [276]).

In this protocol, two processes are particularly critical:

1. The initial production of the shuffled library (steps A-D), as it a) ultimately determines the success of isolating a desired clone that combines the assets of the parental viruses in a single capsid, and b) has not yet been standardized between different labs and thus relies on personal experience and specific *cap* plasmids, hampering the wide use of this technology
2. The exact conditions for final selection in cells or animals (steps H-J), as the success of this step may depend on a variety of further parameters in addition to the target cells, especially the presence of a helper virus, as well as the combination of positive and negative pressures

Accordingly, three specific aims in the first part of this thesis were to:

1. improve and standardize the technology for AAV DFS
2. study critical parameters for AAV library selection - Adenovirus helper and IVIG pressure
3. apply the optimized tools and protocols for *in vitro* and *in vivo* AAV selection schemes

3.1.1 Optimization of the protocol for generation of shuffled AAV libraries

As shown in Figure 15 above, a prerequisite for AAV DFS is the initial isolation and then fragmentation of the *cap* genes of choice. In the original protocol by Grimm and co-workers, 8 different *cap* sequences were isolated from respective plasmids by restriction digestion, using enzyme binding sites that had been engineered into each of the *cap* plasmids. While feasible and efficient, a drawback of this strategy is that it may not be applicable to all present or future *cap* genes because some of them may inherently contain binding sites for the enzymes originally used (HindIII/SpeI). Moreover, since the DNase digestion step may have to be repeated until desired fragments are produced (see below), it can become necessary to digest large amounts of *cap* plasmid with restriction enzymes which is time-, work- and cost-intensive. Finally, since many labs have set up their own plasmids and restriction strategies, it is very difficult to share and use constructs between individual groups which hampers a broader evaluation and application of the whole technology.

To overcome these problems and to standardize the complete protocol, we decided to refine the original strategy and switched to a PCR-based approach for *cap* gene amplification rather than enzymatic digestion. Therefore, we generated an entirely new set of AAV donor plasmids in which the *cap* genes of 12 different AAV serotypes - 1 to 9, rh10, po1 and 12 - are flanked by a collection of PCR primer binding sites (Figure 16). These serotypes were chosen because they have been studied extensively in our and other labs, and because they differ substantially in their tropisms and efficiencies, making them interesting templates for DFS. The primer binding sites were identical to

those used for shuffled *cap* gene amplification in the 2008 Grimm study (CUF/R); in addition, we included the SAF/R primer binding sites (see Materials and Methods 2.2.4.2, Figure 11) that another PhD student in our lab (Nina Schürmann) had concurrently found to work well for shuffling of other genes (encoding human Argonaute proteins) [270]. As the plasmids were based on pBlueScript, they additionally contained binding sites for the standard M13 and T3/T7 primers. Finally, in our eventual constructs, each *cap* fragment is flanked by recognition sites for the restriction enzymes *PacI* (5') or *Ascl* (3') which allowed a) the initial cloning of all *cap* sequences into the new plasmids, and b) the final subcloning of shuffled sequences into an appropriately modified AAV recipient plasmid, *i.e.*, a replication-competent construct containing the AAV2 ITRs and the AAV2 *rep* gene followed by *PacI/Ascl* sites. While this strategy again introduces a need for a restriction digestion, it is important to point out that both *PacI* and *Ascl* recognize an 8 bp target sequence (in contrast to most other enzymes which bind only 6 bp, including *HindIII/Spel*) and thus cut very infrequently; indeed, there are no *PacI* or *Ascl* sites in any of the 12 AAV *cap* genes used here. Figure 16 schematically depicts the composition of the new modular AAV donor and recipient plasmids described above.

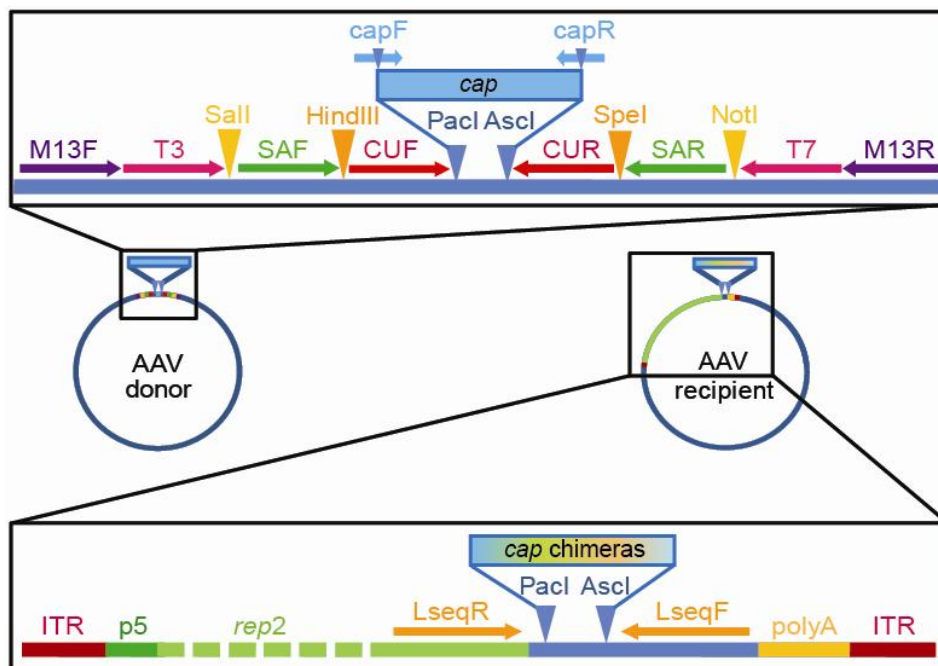


Figure 16: New AAV *cap* gene donor and recipient plasmids for standardized AAV DNA family shuffling. Top: AAV *cap* donor plasmids containing binding sites for 4 different primer pairs on each side of the *cap* gene. Also shown schematically are binding sites for the *capF* and *capR* primers used to initially amplify the capsid genes for subcloning into these plasmids, as well as the location of several restriction sites. Bottom: Similar depiction of the new AAV *cap* gene recipient plasmids, containing AAV2 ITRs and *rep* gene, followed by *PacI/Ascl* sites for *cap* subcloning. Also shown are binding sites for two primers (*LseqR/F*) that were used for sequencing of the shuffled and cloned *cap* genes.

Using these plasmids, we next assessed which primer pairs would give the best results, as measured by the strength of the band after the second PCR (for amplification of shuffled fragments, see Figure 15 above). For this proof-of-concept work, we DNase-fragmented and then re-assembled AAV serotypes 2, 8 and 9. The M13 primers (Figure 16, top) were used to amplify all *cap* genes prior to DNase digestion. According to the original protocol [212], we first tested the CUF/R primer pair and found that while it worked, the yields of the final *cap* chimera band were relatively weak which hampered subsequent large-scale cloning (data not shown). The same was observed for a nested PCR with the T7/T3 primers in a first reaction, followed by amplification with CUF/R; moreover, this primer combination produced multiple non-specific bands (Figure 17A MTC). In fact, the only setting which produced satisfactory results were “nested” PCRs in which the T3/T7 primers were re-used (Figure 17A, MTT). Interestingly, a single PCR with the SAF/R primers alone was equally efficient and specific, especially at higher annealing temperatures of up to 67°C (Figure 17B). We therefore continued to use this simple two-step PCR (including the first primerless PCR) with these two primers in the second PCR step in all subsequent shuffling reactions in this thesis.

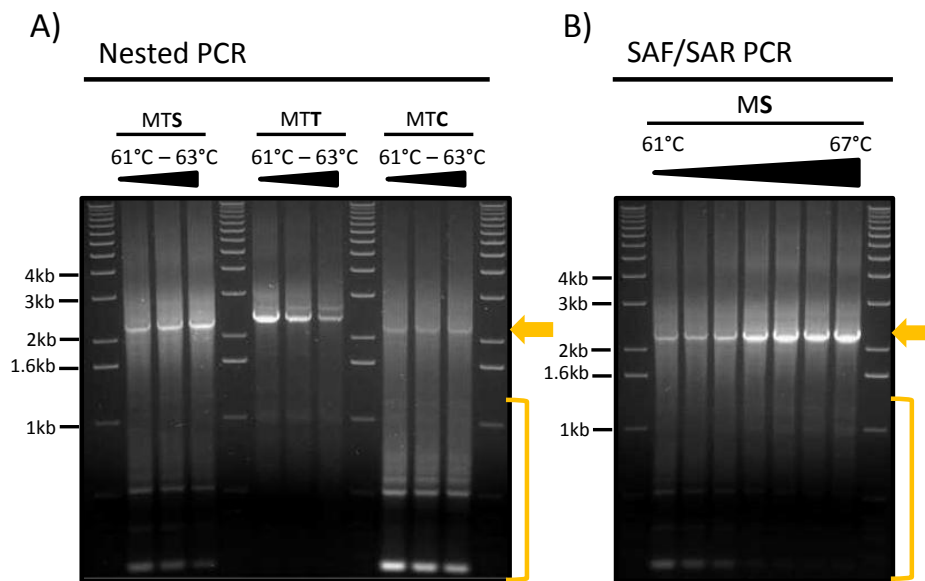


Figure 17: Comparison of experimental setups for the AAV DNA shuffling re-assembly PCR. A) Nested PCR with different primer combinations at increasing annealing temperatures. M refers to the M13 primer pair that was used in the first PCR from the donor plasmids and is hence part of all PCRs. T, C and S refer to the T3/T7 primers, the CUF/CUR primers and SAF and SAR, respectively. **B)** Single PCR to re-assemble capsid genes with the newly introduced primer pair SAF and SAR. Yellow arrows mark the desired bands, while yellow brackets indicate the area with unspecific bands.

Having optimized the PCR conditions, we next aimed to also improve the initial step of *cap* gene fragmentation via DNase I digestion. An inherent problem with this step is that the reaction is hard to standardize, due to the fact that DNase I is an extremely potent enzyme that rapidly degrades input DNA. The representative gel in Figure 18 demonstrates that even small variations in the length of the

reaction can already induce substantial differences regarding the size range of the fragments that are produced. The same variation was found when slightly different pre-dilutions of DNase I enzyme were used (data not shown).

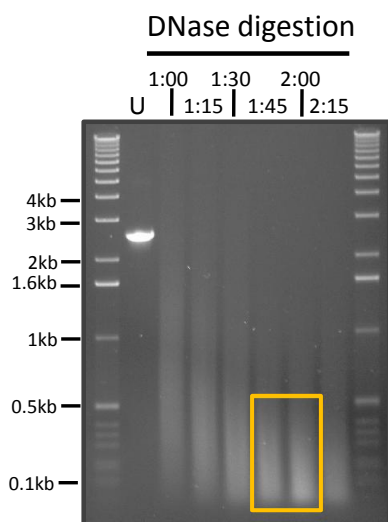


Figure 18: Example for DNase I digestion of *cap* genes (AAV2, 8 and 9). Shown is an agarose gel electrophoresis analysis of the products of *cap* gene digestion using the indicated different incubation times (in minutes:seconds). Lane U shows the undigested input *cap* fragment pool as control. In this example, ideal digests were obtained with incubation times of 1:45 or 2:00 min, which yielded the preferred predominant peak of fragments around 100 to 500 bp (yellow box).

As a result of this high and hard-to-control activity, it can be difficult to avoid complete DNA degradation and to instead generate sufficient *cap* fragments of a desired size range. In addition, the latter is typically rather broad (roughly 100 to 500 bp gives good results) since a large gel piece has to be isolated (yellow square in Figure 18), which further complicates standardization between different labs. We thus asked whether a more controlled fragmentation by physical means rather than enzymatic digestion could improve this essential step. Specifically, we tested DNA ultrasonification via “Adaptive Focused Acoustic” technology (Covaris, Woburn, USA) and compared it with conventional DNase I digestion. The Covaris system offers the possibility to generate very defined fragment sizes, allowing us to create sheared AAV *cap* fragments with a peak size of either 150, 300 or 800 bp. Their correct length distribution was confirmed by analysis on an Agilent Bioanalyzer 2100 (Figure 19A). As expected, the fragments generated through DNase I digestion showed a much broader distribution over the entire size range, with a slight accumulation of fragments of around 100 bp (Figure 19B).

For further analysis *cap* genes from AAV serotypes 1,7-9 and rh10 were fragmented, using either the DNase digestion technique or the previously determined Covaris protocols for 150bp, 300bp and 800bp fragments, respectively. The serotypes were chosen because they are representative for libraries made of several AAV parents (five in this case) with roughly 85% homology to each other. Covaris- and DNase-digested fragments were used in parallel to produce the respective shuffled

libraries. If successful, the first and second PCRs of the shuffling protocol should result in a distinct gel band of around 2.2 kb, corresponding to full-length chimeric *cap* genes. Notably, as depicted in a representative gel in Figure 19C, the re-assembly reaction did not work for Covaris fragments with an average size of 150 bp, and the PCRs with the 300 bp fragments gave only a weak band of the correct size. In fact, the Covaris conditions that produced a defined fragment size of 800 bp were the only ones that resulted in a full-length *cap* gene band that was comparable in intensity to that from the conventional DNase I digestion.

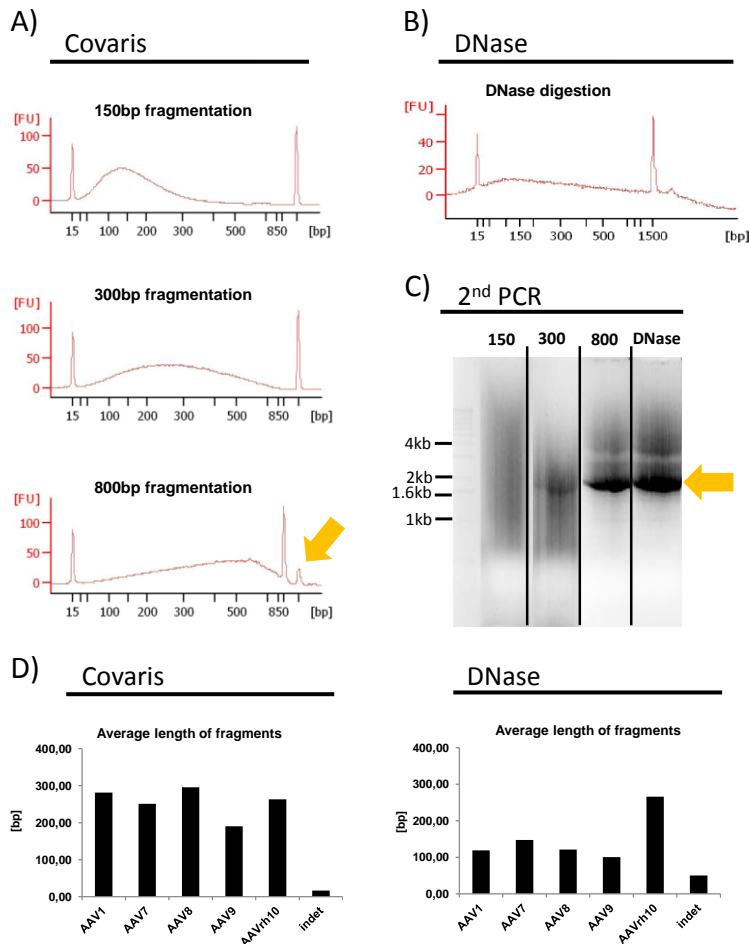


Figure 19: Fragmentation of AAV capsid genes. **A)** A pool of different capsid genes was fragmented to different average fragment lengths by ultrasonification and analyzed on a Bioanalyzer. Plotted are fragment lengths (in bp, X axis) versus fluorescence units (FU, Y axis) from which the amount of DNA is calculated, compared to standard peaks, visible at 15 and 1500bp. The small peak at 2kb in the 800bp fragmentation indicates remaining full-length *cap* genes (yellow arrow). **B)** DNA fragmented with DNase I and purified on an agarose gel was analyzed the same way. **C)** Agarose gel of PCR products from the re-assembly PCR that amplifies full-length genes. Using the Covaris fragmentation, only fragments with an average length of 800 bp resulted in comparable amounts of PCR product. Desired bands are indicated by the yellow arrow. **D)** Average length of fragments (in bp) in assembled capsid genes from a 1,7-9,rh10 library. In sequences that were generated with DNase I, digested DNA fragments are shorter and therefore the crossover frequency is higher. The 1,7-9,rh10 library was produced, sequenced and analyzed with Salanto by Stefanie Große. (C) and D) courtesy of Stefanie Große. (Indet= indetermined; sequence parts for which an exact allocation to a certain serotype is not possible.)

From both reactions, 800 bp Covaris and DNase I digestion, Stefanie Große (PhD student in the lab) produced a plasmid library, sequenced 20 clones and used the Salanto program that Christian Bender had developed together with our lab (chapter 2.1.12) to determine the average length of fragments according to the parental serotypes. Interestingly, with the exception of AAVrh10 (for reasons unknown), the average fragment length in the DNase I-derived library was about half the size of the

800 bp Covaris library (Figure 19D). The fragment length directly correlates with the number of crossovers per clone, with shorter fragments meaning more crossovers, which is beneficial for the library diversity. We therefore decided to continue using the conventional DNase I digestion rather than physical fragmentation for the remaining work in this thesis.

We finally also analyzed whether we could further improve the efficiency of the two PCRs by altering the annealing temperature in the first PCR where the partially homologous fragments are supposed to self-prime. However, we found that 42°C as used in the original Grimm *et al.* paper [212] as well as in the experiments above gave best results that were not enhanced by lowering or raising the temperature over a 20 degree range (data not shown). We accordingly concluded that 42°C is already an ideal temperature to allow annealing of different *cap* gene fragments and thus efficient shuffling.

In summary, the final optimized protocol for AAV capsid gene shuffling consists of:

1. PCR amplification of the desired *cap* genes from our new donor plasmids using M13 primers
2. DNase I-based fragmentation (aiming for fragments of 100-500 bp)
3. a primer-less recombination (shuffling) and re-assembly PCR at 42°C annealing temperature
4. a second single-step PCR (*i.e.*, combined annealing/extension at 68°C) using SAF/R primers

Important to note, this protocol has not only been used successfully for all further library productions in this thesis, but also independently by Stefanie Große in the lab for generation of >10 additional libraries based on various AAV serotype combinations (Große *et al.*, manuscript in preparation).

3.1.1.1 **Combination of AAV capsid shuffling and peptide display**

As will be described in more detail in a later chapter (3.2), we also engineered all 12 *cap* genes to contain unique restriction enzyme sites for cloning of short oligonucleotides encoding re-targeting peptides for display on the viral surface. Because the combination of this viral peptide display with DFS should theoretically create the largest possible diversity (of all currently available molecular AAV evolution techniques), we tested whether the two methods were truly compatible. Therefore, all 12 insertion site-modified *cap* genes were transferred into the new donor plasmid described above and then used in shuffling reactions, using the optimized protocol. The shuffled reaction products were then used as templates for cloning of a randomized peptide library on top. Two factors were particularly important to guarantee the success of this strategy: first, the insertion sites for peptide display were located at comparable positions across all the different serotypes, reducing the risk that one is lost upon recombination. Second, because the peptide insertion site initially creates a frameshift (see chapter 3.2.), VP protein expression and virus production are only possible with a successfully inserted oligonucleotide that corrects this frameshift.

We then produced eight different shuffled AAV libraries, with or without additional peptide library insertion, as listed in the following Table 13. As can be seen, all eight libraries were produced to decent titers, albeit we noted a 5- to 50-fold reduction in the titers of the peptide-containing libraries as compared to their direct counterparts without peptide insertion. Most likely, this difference is due to the fact that a proportion of the plasmid clones in the shuffling-display libraries has not taken up the oligonucleotide which corrects the frameshift and allows viral library production. Moreover, a fraction of the peptide-encoding oligonucleotides will comprise stop codons, which will further reduce the number of viable sequences in such a complex library. These assumptions are in fact supported by the observation that library diversities on the plasmid level were comparable between the shuffled and corresponding shuffling-display libraries (with minor variations in both directions).

Library	Diversity [whole library]	Viral titer [vg/ml]
289	3.5×10^6	2.00×10^{12}
289+PL	1.3×10^6	4.40×10^{11}
789	2.2×10^6	1.78×10^{13}
789+PL	8.9×10^5	1.54×10^{12}
1689	1.1×10^6	1.60×10^{13}
1689+PL	1.1×10^6	2.50×10^{12}
15689	1.5×10^5	6.00×10^{12}
15689+PL	5.0×10^5	1.20×10^{11}

Table 13: Comparison of AAV libraries.

Libraries based on the indicated serotypes were either generated by DNA family shuffling alone, or by combining shuffling with insertion of a peptide library (+PL). The diversity of the respective library was estimated by the number of bacterial colonies after transformation, assuming that each colony carries a distinct clone. Viral libraries were produced in Hek293T cells and purified by iodixanol density gradient centrifugation. Viral titers were determined by RT-PCR.

Notably, sequencing of 5 clones from each of the four different shuffling-peptide libraries confirmed that all clones had indeed taken up peptide-encoding oligonucleotides (representative examples in Figure 20A-C). While these libraries were not further used for selection schemes in the context of this thesis, they represent an essential proof-of-concept that our new protocol and plasmids allow for the juxtaposition of two powerful AAV evolution methods and thus provide a novel avenue that can be exploited in the future (Discussed in more detail in chapter 4.3)

A)

AAV2mod.	GTATCTACCAACCTCCAGCAA GCC CAG AGT GCC NNNNNNNNNNNNNNNNNNNN GCC CA--G GCC G CC ACC GC CAGATGT CAAC CA
AAV2	GTATCTACCAACCTCCAGAGAGGCCAACAGA -----CA-AGCAGCTACC GC CAGATGT CAAC CA
AAV8	GTGGCAGATAA CTT GC AGC-AGCAAAAC-----ACGGCTCCTCAAATT GGAACTGTCAAC CA
AAV9	GTGGCCACAAACCACCA GA-- GTGCCCAA -----GCACAG GC GCAGAC CCGGCTGGGT TCAAA
289PL#1	GTGGCCACAAACCACCA GG--GC CAG AGT GCC CAGCAGAGGGGTAG CCTCGT GCC CAG GCC G CC CAAAT GGAACTGTCAAC CA
289PL#2	GTATCTACCAACCTCCAGCAA G CC CAG AGT GCC CGTGCAGGTGGAGT TTTGT GCC CA--G GCC G CC ACC GC CAGATGT CAAC CA
289PL#3	GTGGCAGATAA CTT GC AGC G-- GC CAG AGT GCC TCCATCAGCGTGAGCG TTCC GCC CA--G GCC G CC ACC GC CAGATGT CAAC CA

B)

AAV2mod.	GTATCTACC-AACCTCCAGCAA GCC CAG AGT GCC NNNNNNNNNNNNNNNNNNNN GCC CAG GCC G CC ACC GC CAGAT--GTCAA
AAV7	GT CAGCAGC -AACTT ACAA --GCGGCTAAAT-----ACTGCAG CC CAGACAC-AA GGT GTCAA
AAV8	GTG -GCAGATAA CTTGC AG- CAGCAAAAC -----ACGGCTCCTCAAATT GGAACT -GTCAA
AAV9	GTGGCCACA -AAC CCAC AG-- AGTGCCCAA -----GCACAG GC GCAGAC CCGGCTGGGT TCAA
789PL#1	GTG -GCAGATAA CTTGC AG-- GCC CAG AGT GCC GGTCCGTCTGACT AGTAGT GC - GCC CAG GCC G CC CAAAT GGAACT -GTCAA
789PL#2	GTGGCCACA -AAC CCAC AG-- GCC CAG AGT GCC ATCCAGCGTAGCC CTCC CGC - GCC CAG GCC G CC CAGAC CCGGCTGGGT TCAA
789PL#3	GT CAGCAGC -AACTT ACAA -- GCC CAG AGT GCC GAGGC GGCA-CGT C GAC GTGC - GCC CAG GCC G CC CAGACAC-AA GT GTCAA

C)

AAV2mod.	GTATCTACCAACCTCCAGCAA GCC CAG AGT GCC NNNNNNNNNNNNNNNNNNNN GCC CAG GCC G CC ACC GC CAGATGT CAAC ACACA
AAV1	GTGGCAGTCAATTTCCAGAGCAGCAGCAG C -----CCTGCGACCGGAGATGTGCATGCTAT
AAV5	ATGGCCACCAACAACCA CCAG AGCTCCACC ACTGCC -----CCCGCAGCCGGC ACGTACA ACCTCCA
AAV6	GTGGCAGTCAATCTCCAGAGCAGCAGCAGCAGCAGC -----CCTGCGACCGGAGATGTGCATGTTAT
AAV8	GTGGCAGATAA CTT GC AGCAGCAAAAC-----ACGGCTCCTCAAATT GGAACTGTCAAC AGCCA
AAV9	GTGGCCACAAACCACCA GA GTGCCCAA -----GCACAG GC GCAGAC CCGGCTGGGT TCAAA CCCA
15689PL#1	GTGGCAGTCAATTTCCAGAGCAG C GCC CAG AGT GCC CGCCGGATGTGGTGTGT CGGG GCC CAG GCC GGAGATGTGCATGTTAT
15689PL#2	GTGGCAGTCAATTTCCAGAGCAG C GCC CAG AGT GCC GCGATTGGGTTCTGGC TTAC GCC CAG GCC G CC GGAGATGTGCATGTTAT
1689PL#1	GTGGCCACAAACCACCA GG C CAG AGT GCC GATCTGCTACGGCGAGGCT G GCC CAG GCC G CC CAAAT GGAACTGTCAAC AGCCA
1689PL#2	GTGGCAGTCAATTTCCAGAGCAGC GCC CAG AGT GCC AGTGGGTCCCGGTCGGCGC GCC CAG GCC G CC GGAGATGTGCATGCTAT

Figure 20: Comparison of chimeric sequences from different shuffled AAV libraries that harbor additional peptide insertions. A) Clones from the library 289 plus peptide insertion. B) Clones from the library 789 plus peptide insertion. C) Clones from the libraries 15689 and 1689 plus peptide insertion. Chimeric sequences are shown in alignment to their parental serotypes and compared to a modeled AAV2 sequence, where peptide insertion is indicated by 21 ‘N’ (AAV2mod.). Chimeric sequences are coded with colors that refer to the parental sequences. Note that the chimeric character of the shuffled clones is not always visible within the short area shown around the peptide insertion site, but was always confirmed by further sequencing. Modified sequences flanking the peptide insertion are boxed as triplets. Additional nucleotides are shown in bold, peptide sequences are bold underlined. For details about peptide insertions please refer to chapter 3.2.1, Figure 37 and Figure 39.

3.1.2 Analysis of parameters influencing AAV library selection

As described in introductory chapter 1.3.1, the first chimeric AAV that was reported in the literature to have emerged from DNA family shuffling was AAV-DJ [212]. To obtain this clone, the authors had shuffled eight AAV serotypes (2, 4, 5, 8, 9, avian, bovine, caprine) and then selected their library in human hepatocytes in the presence of IVIG (pooled human antisera) and Adenovirus. Curiously, this led to elimination of five of the eight parental serotypes and yielded the DJ clone, which is solely composed of AAV2, AAV8 and AAV9 and which combines their assets - high efficiency both *in vitro* and *in vivo* - in a single capsid.

Here, we considered it interesting to test whether it was possible to recapitulate the isolation of AAV-DJ or similar clones through selection of a new library that would only contain the three leading serotypes - 2, 8 and 9 - to begin with. Ideally, this would then help to better understand the unique features - capsid parts and combinations thereof - of the DJ clone and AAV vector transduction in

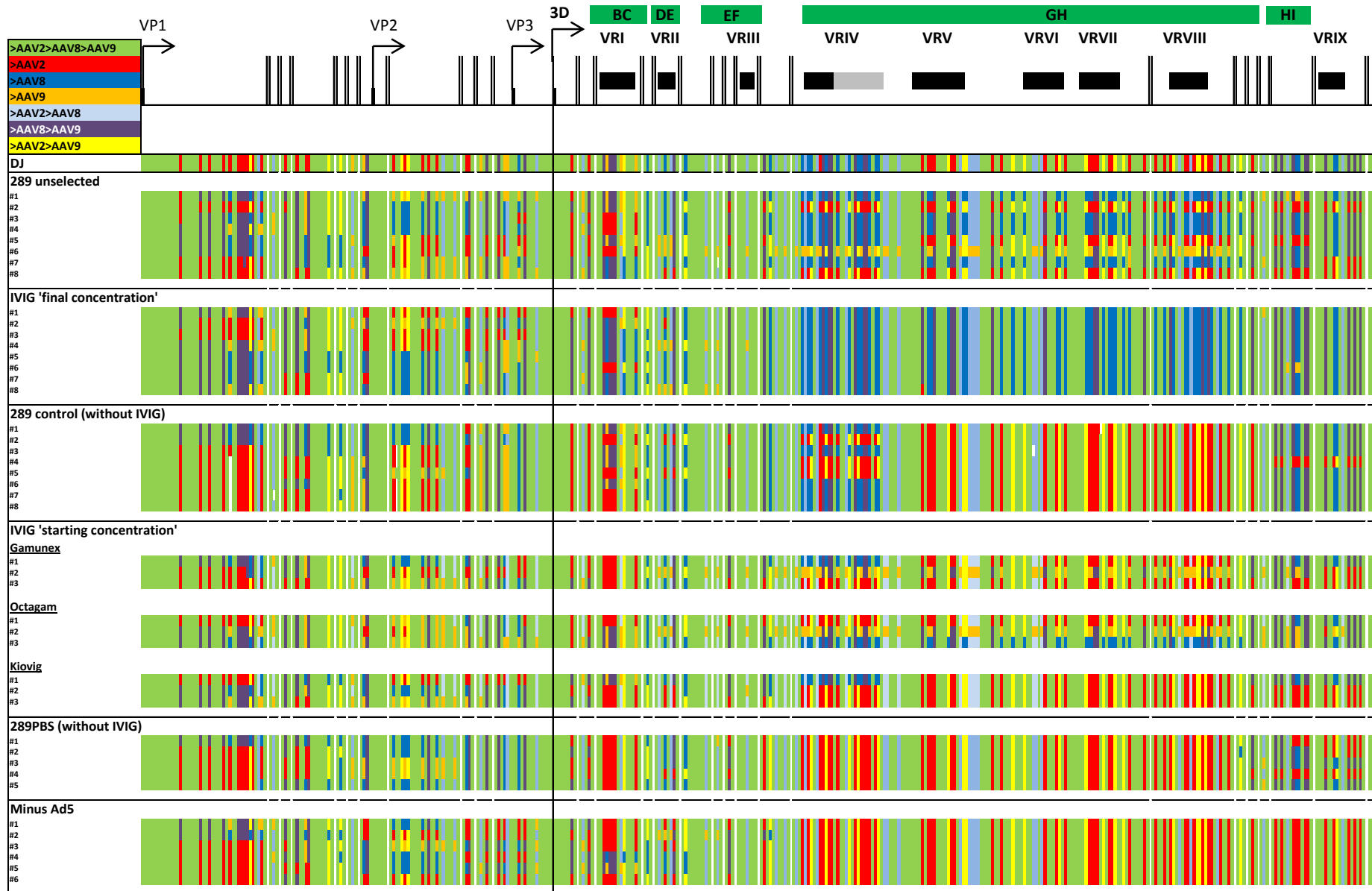
general. Moreover, such a new selection would permit to experimentally dissect the role of two critical parameters that likely influence the outcome of this process, namely, the type and dose of IVIG, and the presence or absence of helper Adenovirus.

We therefore produced the 289 library listed in Table 13 above, using our optimized protocol and plasmids also described in the previous chapter. As shown in the table, this library had a diversity of 3.5×10^6 (calculated from bacterial colony numbers), and virus was produced to a titer of 2×10^{12} particles per ml. Prior to applying different selection pressures, we first sequenced 8 randomly selected clones to verify the presence of all three serotypes in the library, and to ensure that the clones were diverse. DNA and protein sequence alignments were performed using the Salanto program (chapter 2.1.12) [270].

As hoped for, we found that the three parental sequences were all present in the 8 clones, without a dominance of one or two serotype(s) in a certain part of the capsid sequence (Figure 21-23) (see also Appendix for full sequences). Still, the percentage of AAV9 on both the nucleotide and protein level was slightly decreased as compared to AAV2 and AAV8 throughout the entire capsid (Figure 22). While a few clones contained single point mutations (that are frequently found in shuffled libraries [212] and originate from errors during the PCRs), none of the 8 randomly chosen clones had a stop codon. Moreover obvious was a decrease of crossover frequencies starting from the EF-loop that is readily explained by a lower homology of AAV serotypes in the C-terminal part which hampers recombination (Figure 22). Nonetheless, the numbers of crossovers from one serotype to the other were comparable, as were the average fragment lengths (Figure 23).

Figure 21: (next page) Amino acid sequence of analyzed AAV clones with chimeric capsids from the original 289 shuffled library before and after different selection schemes. Amino acids are indicated by colors according to the parental AAV serotypes from which they originate. In cases where they could be assigned unambiguously to a single serotype, red was used for AAV2, blue for AAV8 and orange for AAV9. Amino acids that originate from either AAV2 or AAV8 are drawn in light blue, those from either AAV2 or AAV9 are yellow, and those that could be allocated to either AAV8 or AAV9 are colored in purple. Light green areas mark amino acids that could originate from any of the three parental serotypes. The top panel shows starting points for the three capsid proteins (VP1-VP3) as well as the beginning of the outer part of the capsid that could be crystallized and for which a 3D structure is available. Black bars mark variable regions and green bars the respective loops. For space reasons, not the entire sequence is shown. Larger parts where sequences are identical to all parental serotypes are cut out as indicated by light gray vertical lines in the top panel and white lines in the sequences. Note that due to shortening of the sequences, some loops are not shown.

Results



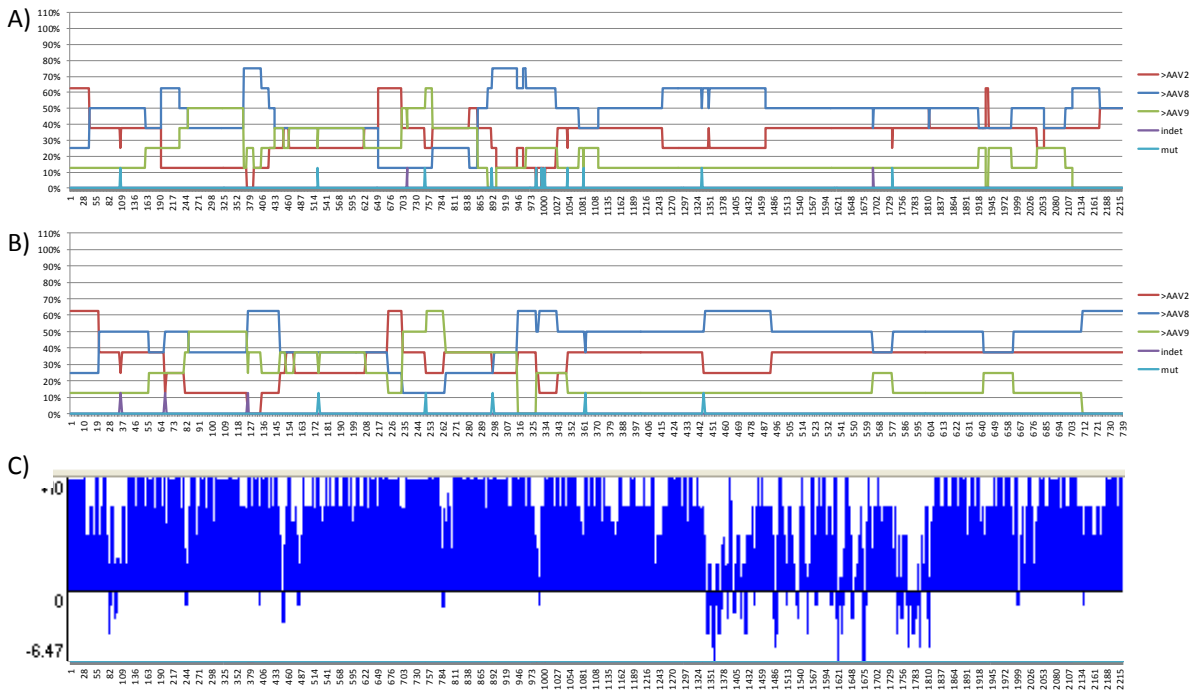


Figure 22: Clonal composition of shuffled AAVs derived from serotypes 2, 8 and 9. **A)** Position-wise nucleotide distribution of the parental serotypes (in percent) in the capsid genes of 8 shuffled clones from the unselected AAV289 library. **B)** Position-wise amino acid distribution of the parental serotypes (in percent) in the capsid protein sequence of 8 shuffled clones from the unselected AAV289 library. Parental serotype AAV2 is shown in red, AAV8 in blue and AAV9 in green. Mutations and positions that could not be allocated to a certain serotype are shown in light blue and purple, respectively. **C)** Absolute complexity of the aligned parental serotypes AAV2, 8 and 9 (nucleotide level). The graph was derived by calculating a sum of all pair-wise substitution scores at a given alignment position, divided by the number of pairs in the alignment. The scores are taken from the residue substitution matrix used for alignment calculation in AlignX, VectorNTI (Invitrogen). For more details, please refer to the VectorNTI manual (available online at <http://www.lifetechnologies.com>) and the Salanto online manual (<https://bitbucket.org/benderc/salanto/wiki/Home>). A lower complexity implies a higher variability between the sequences. As can be seen from the comparison of graph C) with A) crossover numbers in the C-terminal half decrease around an area where the variability between the parental sequences increases (nt1300 to nt1900).

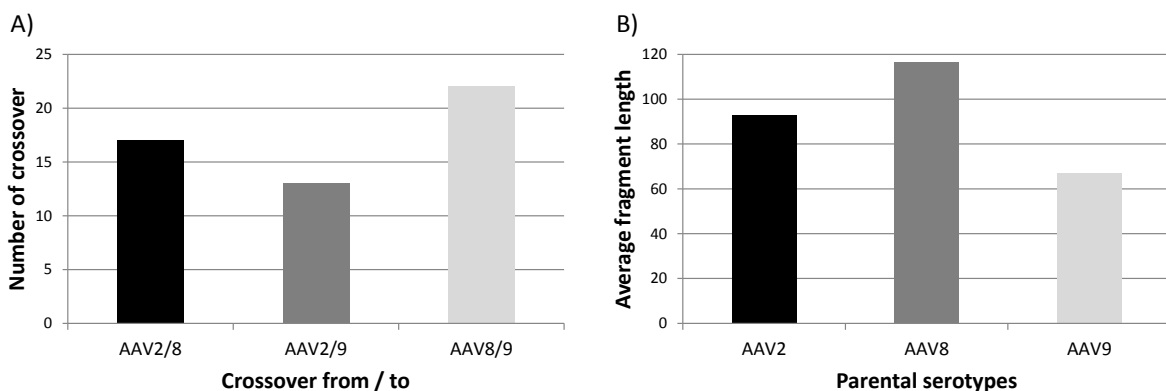


Figure 23: Crossover analysis of the shuffled AAV289 library. **A)** Shown are the numbers of crossovers from one serotype to another within a pool of 8 randomly picked clones. **B)** Depiction of the variations in average length (in bp) of the combined fragments, calculated from the length of fragments derived from a distinct serotype and the number of fragments of that size present in the entire capsid sequence.

Finally important was to demonstrate that the AAV289 library not only contained all parental serotypes on the DNA and protein level, but that the individual clones were also functional. We therefore transferred the capsid genes from the 8 randomly picked clones into an AAV helper plasmid and then produced YFP reporter-expressing vectors in small scale, in parallel to vectors with the parental AAV2, 8 or 9 capsids, or the chimeric vector DJ. The resulting crude vector lysates were next titered on Huh7 cells, and the results are depicted in the form of a heatmap in the following Figure 24. As expected, the 8 clones exhibited a large variety of transduction efficiencies, from clones that were nearly inert (akin to AAV8 and 9) or that showed intermediate reporter expression, to one clone (#2) approaching the potencies of AAV2/DJ. Notably, this clone #2 shares a large portion of the C terminus with AAV2/DJ (Figure 21 above), supporting prior conclusions that this region of the capsid is particularly important for potent transduction in cultured cells [212].

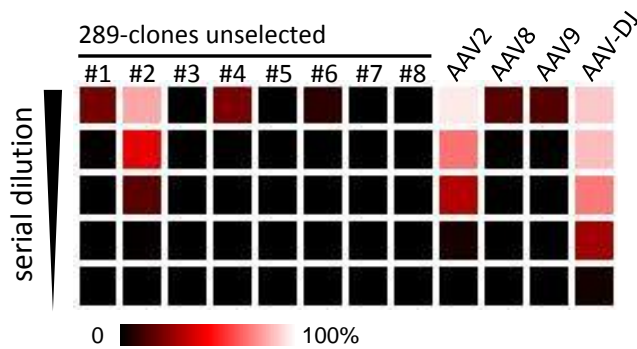


Figure 24: Titration of chimeric clones from the AAV289 shuffled library. Virus encoding a YFP reporter construct was produced in small scale (6-well format). From crude lysates, 10 μ l were applied to the first well of a 96-well plate of Huh7 cells and diluted serially (ten-fold). Shown are infection rates in percent as determined by FACS. The data are shown as heatmaps where the percentage of YFP-expressing cells is color-coded, starting from zero in black to the maximum in white. Here and in the following heatmaps, the overall maximum for each heatmap is indicated by the color: yellow = 25%; green = 50%; blue = 75% and red = 100%.

3.1.2.1 *IVIG selection*

Knowing that our AAV289 library contained all parental serotypes and was diverse and functional, we next exploited this library to gain more insight into the role of neutralizing anti-AAV antibodies as a negative selection pressure that eventually shapes the composition and structure of AAV libraries during selection. In the original 2008 study by Grimm *et al.*, the AAV-DJ capsid was isolated after five rounds of library amplification on Huh7 hepatoma cells in the presence of increasing amounts of IVIG, *i.e.*, pooled human antisera containing neutralizing anti-AAV-antibodies. Because this former study had applied a specific IVIG brand available in the US (GamimmuneN, [212]), it was now interesting to repeat the selection procedure with our new AAV289 library in the same cell line, but using three different IVIG variants that are available in Germany (Gamunex, Kiovig and Octagam). The underlying goal was to dissect whether the various IVIG brands with their different antibody compositions would still enrich capsids similar or identical to DJ, or whether the original result was specific for the particular IVIG batch. Either way, the results would provide important information and should guide future AAV library selection schemes. Moreover, the library was amplified

iteratively (five times) either alone or in the presence of a low ‘starting’ or a higher ‘final’ IVIG concentration. The ‘final’ concentration was higher because it was expected that the particles in the selected library would gain resistance to the antibodies present in the IVIG. At ‘starting’ IVIG concentrations, ranging from 0.1-1 $\mu\text{g}/\mu\text{l}$ human protein with a minimum of 95-98% IgG, the three different brands were used to account for the mentioned batch or donor variations. Selection at the higher ‘final’ doses from 1-10 $\mu\text{g}/\mu\text{l}$ human protein was exclusively performed with Gamunex. This was the only brand that was used for the high dose selection since this particular scheme was started late in this work, once the results from the low dose selection had been analyzed.

In the first selection round, the purified virus library was used at different concentrations, ranging from 2×10^8 to 2×10^{10} particles (corresponding to 0.1 to 10 μl , based on the original library stock with a titer of 2×10^{12} , see Table 13), and incubated for 1 h at 37°C with either 0.1 or 1 $\mu\text{g}/\mu\text{l}$ IVIG diluted in PBS, or with PBS alone as a control. Afterwards, the virus-IVIG mixture was added to Huh7 cells in a well of a 6-well plate and incubated at 37°C for 4 h. The cells were next washed twice with PBS to remove unbound virus and IVIG, and then kept in DMEM complete growth medium supplemented with 1% FCS (FCS was reduced from the normal 10% to enhance AAV transduction). Adenovirus type 5 was added to the cells at an MOI that led to cell lysis at approximately 72 h post-infection, assuming that this will allow for complete AAV replication. Because the Rep proteins of AAV (which are expressed from the viral library) as well as (residual) IVIG inhibit adenoviral growth, the ideal helper virus MOI had to be determined empirically. As exemplified in Figure 25, Adenovirus infection without AAV co-infection and in the absence of IVIG leads to the start of cell lysis after 72 h at an MOI of 20. During the selection process, a slightly higher Adenovirus MOI between 20 and 50 has been found ideal.

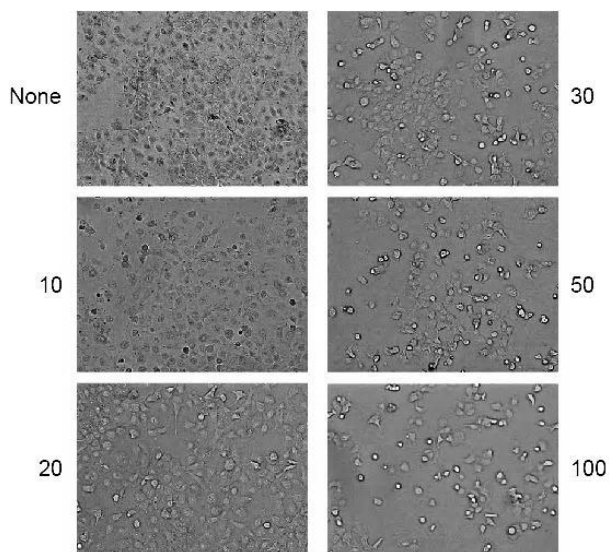


Figure 25: Cytopathic effect of Adenovirus on Huh7 cells. Microscopic images of Huh7 cells 72 h post-infection with different MOIs of Adenovirus. At an MOI of 10, cell growth is inhibited as compared to the non-infected control, but no obvious cytopathic effect is visible. In contrast, at an MOI of 100, most cells already appear dead.

The cells were then harvested into the medium, washed twice with 1x PBS and lysed in 1x PBS according to the protocol for crude lysates (chapter 2.2.6.1). After heat inactivation of the contaminating Adenovirus (30 min incubation at 56°C), these crude lysates were used for re-infection in subsequent selection rounds (#2-5). The exact AAV titers used for infection were no longer determined as this would have required virus purification and titration; instead, three different volumes of crude lysates (usually again 0.1-10 μ l) were used. Only during the selection with the higher 'final' IVIG dose, a higher volume of up to 50 μ l of crude lysates was used in the first selection rounds, to still enable detection of replicating AAV by Western blotting at an increased IVIG concentration. Still, as indicated in Figure 26 for this last selection round, infections with 1 μ l lysates were again sufficient for detection. Prior to re-infection, each of these lysates was again incubated with 0.1 or 1 μ g/ μ l IVIG for the 'starting' dose selection, or with >1 μ g/ μ l IVIG for the 'final' dose selection (up to 10 μ g/ μ l in the final round #5). The purpose of testing this multitude of parameters was always to empirically identify conditions that would result in the weakest detection of AAV capsid proteins in cell lysates amongst all samples. A minimal AAV protein expression in the Western blots was indicative of limited progeny particle production, which was in turn an indirect proof of a desired tight genotype-phenotype linkage, *i.e.*, a high probability that newly produced capsids would actually carry the corresponding capsid gene. Otherwise, if the cells had produced large amounts of particles (evidenced by strong bands in the Western blots), there would have been a high risk that the majority of these capsids carried the wrong capsid gene and that the selection would have failed.

The representative Western blots in Figure 26 show examples for different conditions (library and IVIG concentrations) and corresponding VP protein expression levels after round #1 (top), round #3 (center) or the last round #5 (bottom). Also shown is a comparison of the 'starting concentration' (panel A) and the 'final concentration' (panel B) IVIG selections. As can be seen, there were always conditions that led to the desired relatively weak VP expression. Accordingly, those were used for re-infection in the next selection round. Since the PBS control underwent no additional selection pressure, and the corresponding bands were relatively strong, crude lysates from the 0.1 μ l infection were diluted 1:10 prior to subsequent infections.

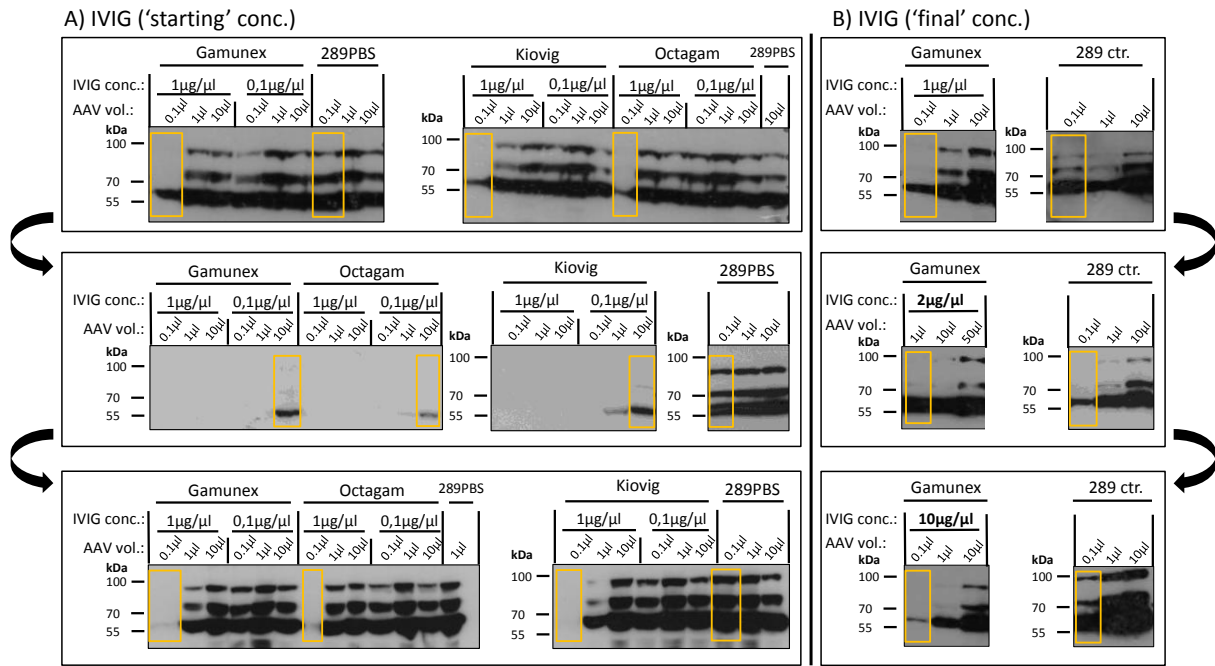


Figure 26: Monitoring of AAV library selection via Western blotting. The B1 antibody was used to detect the viral capsid proteins VP1, VP2 and VP3. Shown are results after the first (top), third (center) or fifth (bottom) round of amplification. Yellow boxes depict lanes with barely visible AAV protein expression that were considered ideal for re-infection in the next round (see main text). **A)** Selection at 'starting' doses of IVIG. Three different volumes of virus - either 0.1-10 μl or 1-50 μl - were incubated with two different concentrations - 0.1 or 1 $\mu\text{g}/\mu\text{l}$ - of IVIG of either the Gamunex, Kiovig or Octagam brand. **B)** Selection at 'final' doses of Gamunex. Starting from 1 $\mu\text{g}/\mu\text{l}$, as in the IVIG low selection, the IVIG concentration was increased to up to 10 $\mu\text{g}/\mu\text{l}$ in the last round (#5). In all cases, samples from the 0.1 μl PBS infection were used as controls and diluted 1:10 prior to further infection.

After five rounds following this scheme, we randomly picked and analyzed 6-8 individual clones from each library or from the control (where the library was amplified in the presence of 1x PBS instead of IVIG). An overview over the results from the three groups - 'starting concentration' IVIG (pooled for all three IVIG batches or subdivided according to IVIG brands), 'final concentration' IVIG and PBS control - together with a side-by-side comparison of the data from the unselected AAV289 library (see also chapter 3.1.2 and Figure 22) is shown in the following Figure 27 and Figure 28. Note that clones from the control amplification with PBS that were selected together with the IVIG 'starting conc.' are referred to as **289PBS**, while those selected with the IVIG 'final conc.' are named **289ctr**.

Results

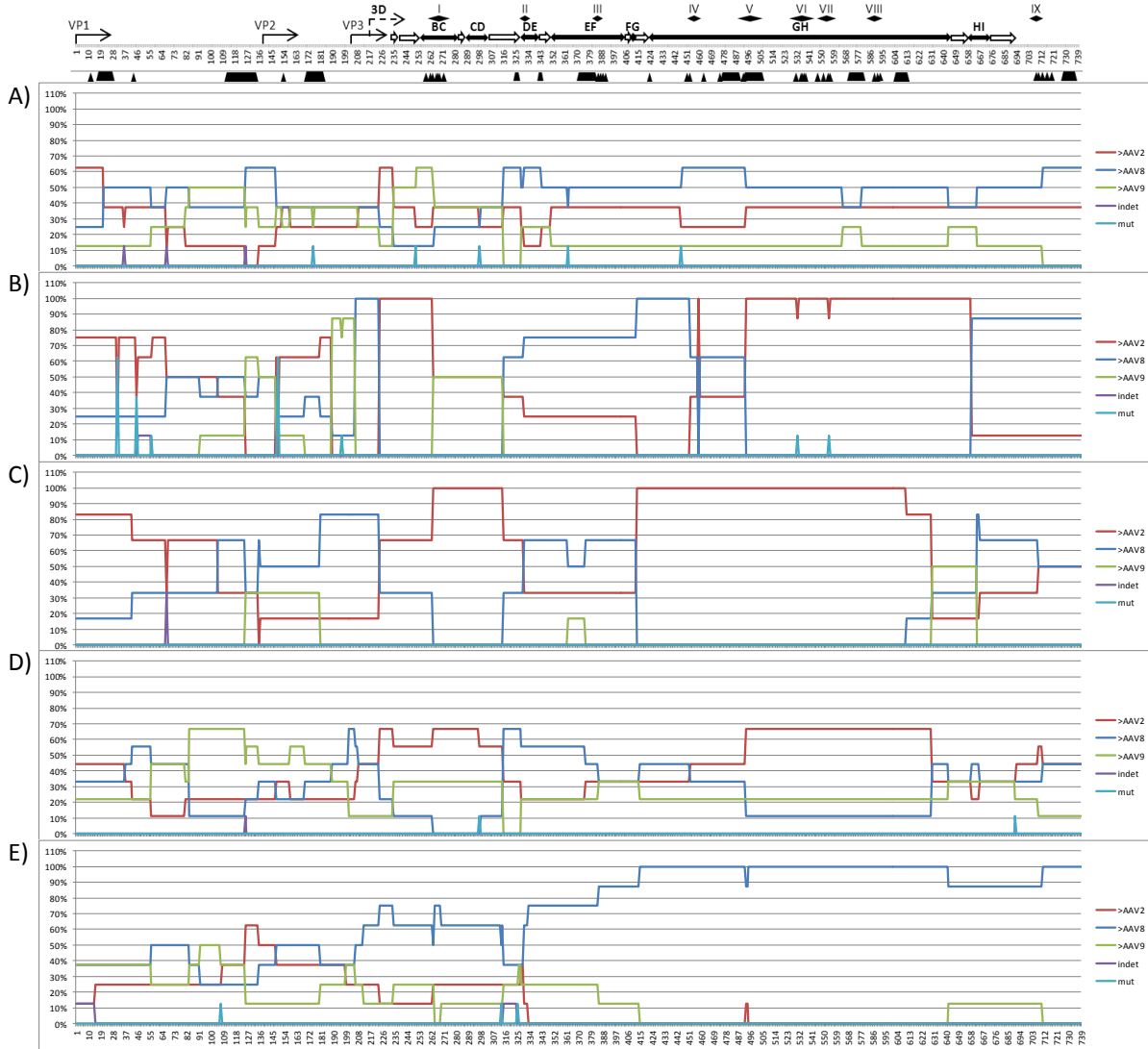


Figure 27: Overview over the capsid protein composition of the AAV289 library before and after IVIG selection. The top panel shows the linear alignment of VP amino acid residues. See Figure 4 in the Introduction for details. Colored lines in the four panels underneath indicate the percentage of clones that originate from the respective parental serotype at their position within the AAV capsid sequence. **A)** Clones from the original library, not subjected to any selection process. **B)** 289ctr clones (selected together with IVIG 'final conc.') and **C)** 289PBS clones (selected together with IVIG 'starting conc.') were iteratively amplified on Huh7 cells in the presence of PBS, but no IVIG. **D)** Selection at 'starting concentrations' of IVIG. **E)** Selection at 'final concentrations' of IVIG. 6-8 clones from each library were analyzed per graph.

Results

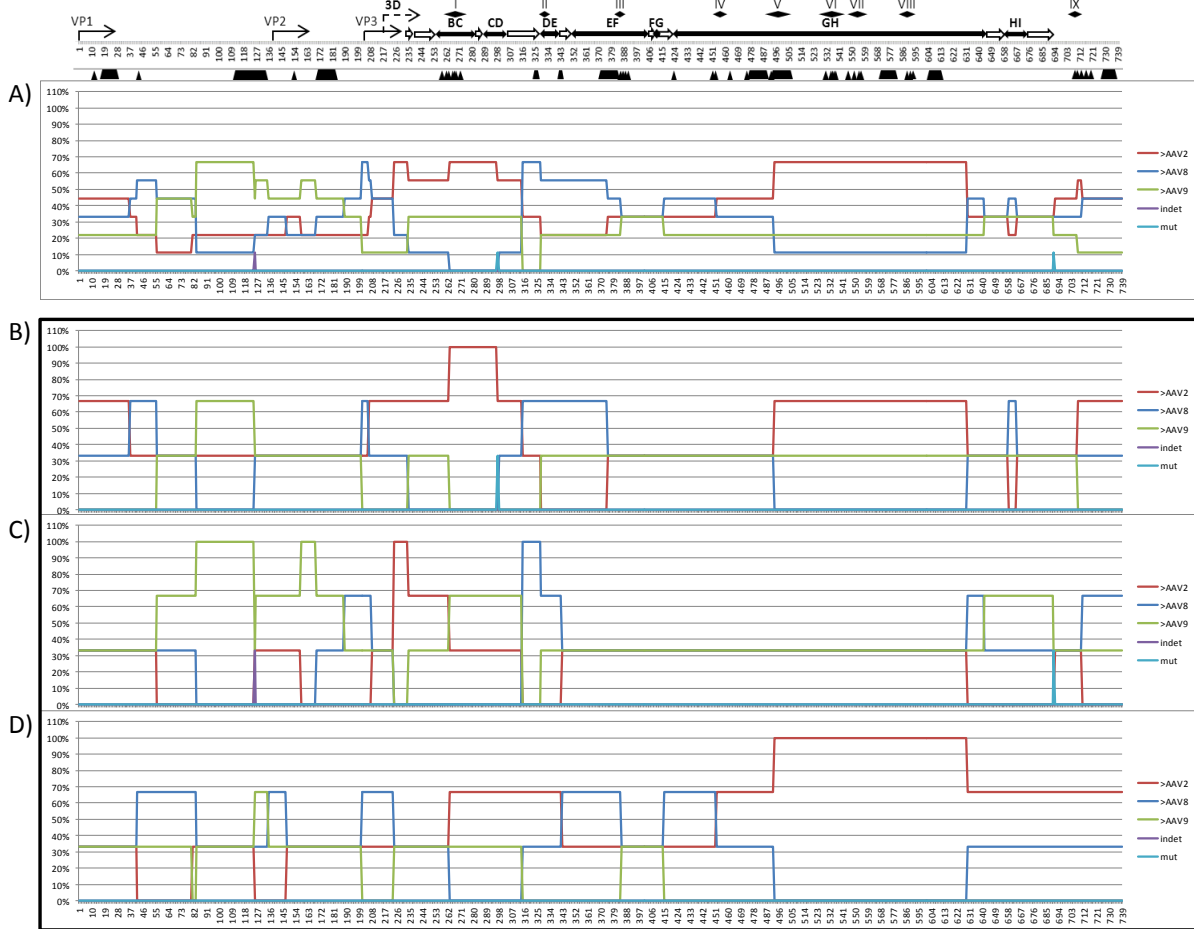


Figure 28: Overview over the capsid protein composition of the AAV289 library after IVIG selection at the 'starting' concentrations. The top panel shows the linear alignment of VP amino acid residues. See Figure 4 in the Introduction for details. Colored lines in the four panels underneath indicate the percentage of clones that originate from the respective parental serotype at any position within the AAV capsid sequence. **A)** Combined clones from IVIG selection at 'starting' concentration. The capsid protein composition of all clones is further subdivided into clones selected in the presence of **B)** Gamunex, **C)** Octagam and **D)** Kiovig, with three clones per batch.

As is evident from Figure 27 above, the sequences from these clones revealed striking differences in the overall capsid composition for each selected pool, with the clearest patterns visible in the C-terminal part that comprises the exterior of the capsid. Amplification of the library without additional IVIG selection pressure (Figure 27 panel B and C) has led to sequences that mainly consisted of AAV2 and AAV8. In particular in the area comprising the hypervariable regions IV-VIII within the GH-loop, the frequency of AAV2-like amino acids was increased as compared to the unselected library (panel A). In contrast, the HI-loop and the very C-terminal end of 88% of the clones in panel B) and 50-80% in panel C) were composed of sequences from AAV8. No such clear enrichments were noted in the N-terminal part (Figure 27B and C). Pooled results from all three IVIG batches from the selection at 'starting' concentrations showed an increase in AAV9-like amino acids throughout the entire capsid sequence compared to the PBS control (Figure 27B-D and Figure 28A). This trend was most

prominent for clones selected in the presence of Octagam (Figure 28C). On average, the increase of AAV2-like sequences in the GH-loop, especially in hypervariable regions V to VIII, was again visible, albeit less pronounced than in the PBS controls (Figure 27B-D and Figure 28A). A notable exception were again clones from the Octagam selection where AAV9 prevailed in this particular capsid area (Figure 28C). At the C-terminal end, comprising the HI-loop and the hypervariable region IX, non-AAV2-like amino acids again became more abundant, regardless of IVIG brand (Figure 27D and Figure 28A-D).

The most drastic differences were observed, however, for the selection in the presence of the 'final' concentrations of IVIG. As seen in Figure 27 panel E, these selection conditions markedly shifted the overall clonal composition towards AAV8, with the entire second protein part consisting almost exclusively of amino acids from this serotype. Accordingly, the outer part of the capsids of those clones is mostly composed of AAV8-like amino acids (Figure 27E) (see also Figure 30 below).

Based on these remarkable differences, we were interested to also compare the transduction efficiency of selected clones, to ideally link their activity to specific parts of each capsid. We therefore re-cloned eight individual capsid genes per selection scheme (nine clones for the 'starting' IVIG concentration selection) into the AAV helper plasmid, produced YFP reporter-expressing vectors as crude lysates and used them to transduce Huh7 cells in a 96-well format. Prior to infection, the vectors were incubated with increasing amounts of IVIG (Gamunex brand) or PBS as control. In parallel, we titered vectors based on wt AAV2, AAV8, AAV9 or the chimera AAV-DJ as further controls. Infection rates were determined by FACS analysis 72 h post-infection and are depicted as heatmaps in Figure 29.

Amongst the eight clones from the **unselected** library, clone #2 was by far the most efficient and resembled AAV2, as already noted during the initial characterization of the AAV289 library (chapter 3.1.2). Also notable is that it seemed more resistant to IVIG than AAV2, since the reduction in infectivity at 1 $\mu\text{g}/\mu\text{l}$ IVIG was less pronounced (as compared to the titration without IVIG, Figure 24). The same was noted for some other clones in the unselected library (#1, 4 and 6), although they were far less efficient to begin with, similar to AAV8 and 9. (For aa sequences of these clones refer to Figure 21)

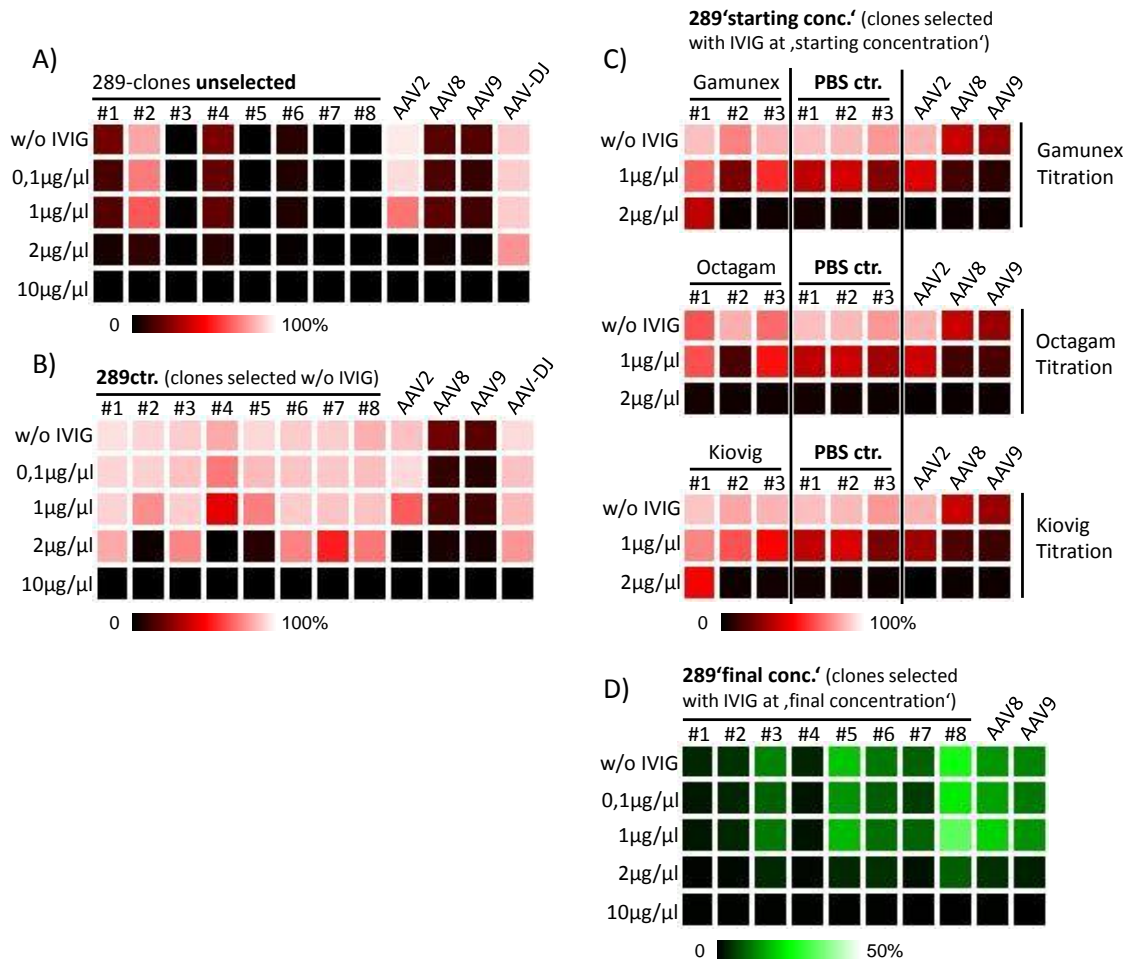


Figure 29: Titration of selected clones at increasing IVIG concentrations. Vectors were produced from individual clones from the different pools as described in the text and titered in the presence of the indicated IVIG concentrations in Huh7 cells. The data are shown as heatmaps where the percentage of YFP-expressing cells is color-coded, starting from zero in black to the maximum in white. Here and in the following heatmaps, the overall maximum for each heatmap is indicated by the color: yellow = 25%; green = 50%; blue = 75% and red = 100%. **A)** Chimeras from the original AAV289 library yielded a variety of transduction efficiencies, as expected. These are the same clones as in Figure 24 above. **B)** Clones from iterative library amplification without IVIG (289ctr.) behave similarly to AAV2 and AAV-DJ. **C)** Selection at the 'starting' IVIG concentration (shown are the three different brands Gamunex, Octagam and Kiovig). Note that these clones show no obvious improvement over the iterative amplification with the PBS control (PBSctr.) (panel B). **D)** Selection at high levels of IVIG led to AAV8-like particles with decreased infectivity but high resistance to IVIG. Titration data for AAV2 and AAV-DJ were omitted as these vectors were far superior to those shown in this panel and would thus have distorted their color-coded depiction.

Interestingly, all chimeras from the **289ctr.** scheme (amplified without IVIG) exhibited an infectivity of more than 90% when titered without IVIG (Figure 29B). Common to all these clones is a part of the GH-loop-comprising hypervariable regions (VR) IV-VIII that was derived from serotype AAV2. Within this area, at positions 585 and 588 in VR-VIII, lies the HSPG binding domain which is present in AAV2 but absent in AAV8 and AAV9. This strongly suggests that library amplification in cultured cells had led to an enrichment of clones that contained this HSPG binding site which presumably enhances infection. When incubated with IVIG prior to titration, the infectivity of some of these clones dropped comparable to that of AAV2. Still, other clones continued to transduce efficiently even at

higher amounts of IVIG, akin to AAV-DJ. Interestingly, these more efficient clones #1, #3 and #6-8 consist of sequences from AAV8 in VR-IV, indicating that this region is responsible for the increased IVIG resistance of these clones (Figure 21). Remarkably, AAV-DJ, which is also very resistant to IVIG, likewise contains VR-IV from AAV8. Together, these findings suggest that the AAV-DJ phenotype (high transduction efficiency and high IVIG resistance) is due to a combination of the first part of the GH-loop including VR-IV from serotype 8, and a second part of the GH-loop with VR-VIII from AAV2.

Considering that these clones were not exposed to human sera during the selection process, one may moreover conclude that this GH-loop combination primarily increases transduction efficiency and that the enhanced resistance to IVIG is a by-product. In this respect, clone #7 is particularly interesting. It shares this GH-loop with the other DJ-like isolates yet its efficiency at an IVIG concentration of 2 $\mu\text{g}/\mu\text{l}$ was decreased. One obvious difference between clone #7 and these other clones is in hypervariable region VR-I within the BC-loop, which is composed of amino acids from serotype 2 in clone #7, not serotype 8/9 as in AAV-DJ (Figure 21). This region is indeed involved in transduction, as well as neutralization with A20 (an antibody which recognizes and neutralizes assembled AAV2 capsids [147], [271], [272]) and IVIG [81], [86], [97], [277]. Nonetheless, this cannot be the only explanation as clone #8 is identical to clone #7 in this region yet it is more resistant to IVIG, similar to AAV-DJ.

Another interesting clone is #4 which was less efficient than AAV2 despite the fact that of all eight clones, it is most homologous to this serotype. Not only is the entire GH-loop from AAV2, but in contrast to the other seven clones in this group and to AAV-DJ, the parts from AAV2 extend to the very C terminus including the HI-loop and VR-IX. Conversely, the BC-loop and VR-I are from serotypes 8/9 in clone #4, akin to AAV-DJ (Figure 21). Taken together, this implies that the combination of VR-V to -VIII from AAV2 with an HI-loop and VR-IX from AAV8/9, as present in AAV-DJ but not in clone #4, provides a capsid composition that exhibits high transduction efficiencies. Notably, this is consistent with, and extends, the conclusions from the analysis of the clones selected in the absence of IVIG (see above).

Equally interesting were the results from the **selection at 'final' doses of IVIG** where the clones differed substantially from the other groups in terms of overall sequence composition (Figure 21, Figure 27 and Figure 30) and infection rates (Figure 29D).

Particularly obvious and consistent is that all eight clones largely resembled AAV8, especially in the second protein half including VR-IV to -IX; accordingly, none of the eight clones in this group had the GH-loop from AAV2. AAV8 was also clearly the predominant serotype in VR-I to -III of these eight clones (Figure 21). Moreover notable is that despite their overall low efficiency (as compared to the

potent AAV2 and AAV-DJ), all eight clones in this group were able to resist even high doses of IVIG during the titration, as expected from this selection scheme. Altogether, this strongly suggests that the very stringent IVIG selection in this group had shifted the bias towards chimeras that largely mimic AAV8 and that thus can evade neutralization, at the cost of alternative capsid compositions that would have mediated a higher infectivity.

Finally also noteworthy is clone #8 from this group as it mediates a slightly increased transduction rate as compared to AAV8/9 (Figure 29D). The only notable difference to these two wildtypes is in the C-terminal part where clone #8 carries a single mutation at position 493, causing a switch from threonine (T) to lysine (K) as in AAV2 (Figure 21). However, whether this single amino acid change truly contributes to the increased transduction of this peculiar clone has to be analyzed more thoroughly in future experiments.

Titration of clones from the IVIG **selection at 'starting' concentrations** showed no significant difference in transduction efficiency as compared to the pool from the selection without IVIG, consistent with their comparable capsid composition. It can be assumed that the previously described increase in AAV9-like amino acids in these clones is due to the IVIG selection pressure, but it has no obvious effect on transduction efficiency (Figure 27D, Figure 28 and Figure 29)

To summarize and better visualize the findings from all these experiments, the 3D structures of selected clones are depicted in Figure 30 on the following page. Based on their transduction efficiencies, the shown clones were clustered into DJ-, AAV2- or AAV8/9-like chimeras. As already noted above and as further exemplified by these 3D structures, it is particularly the composition and combination of the different hypervariable regions that are exposed on the capsid surface which determines capsid properties. Consequently, the pattern of these regions is largely dictated by the selection pressure that has been applied to the AAV289 library. A weak selection pressure - no IVIG or a low dose, regardless of IVIG batch - favors clones that resemble AAV2 and can therefore infect potently, but are also readily neutralized by the pre-existing antibodies present in IVIG. In contrast, a stringent selection with high IVIG produces the opposite, *i.e.*, hybrids that transduce poorly but are concurrently more resistant to neutralization. The AAV-DJ chimera and the newly selected chimeras that behave similarly combine the best of both worlds, by mediating potent transduction even in the presence of relatively high IVIG doses.

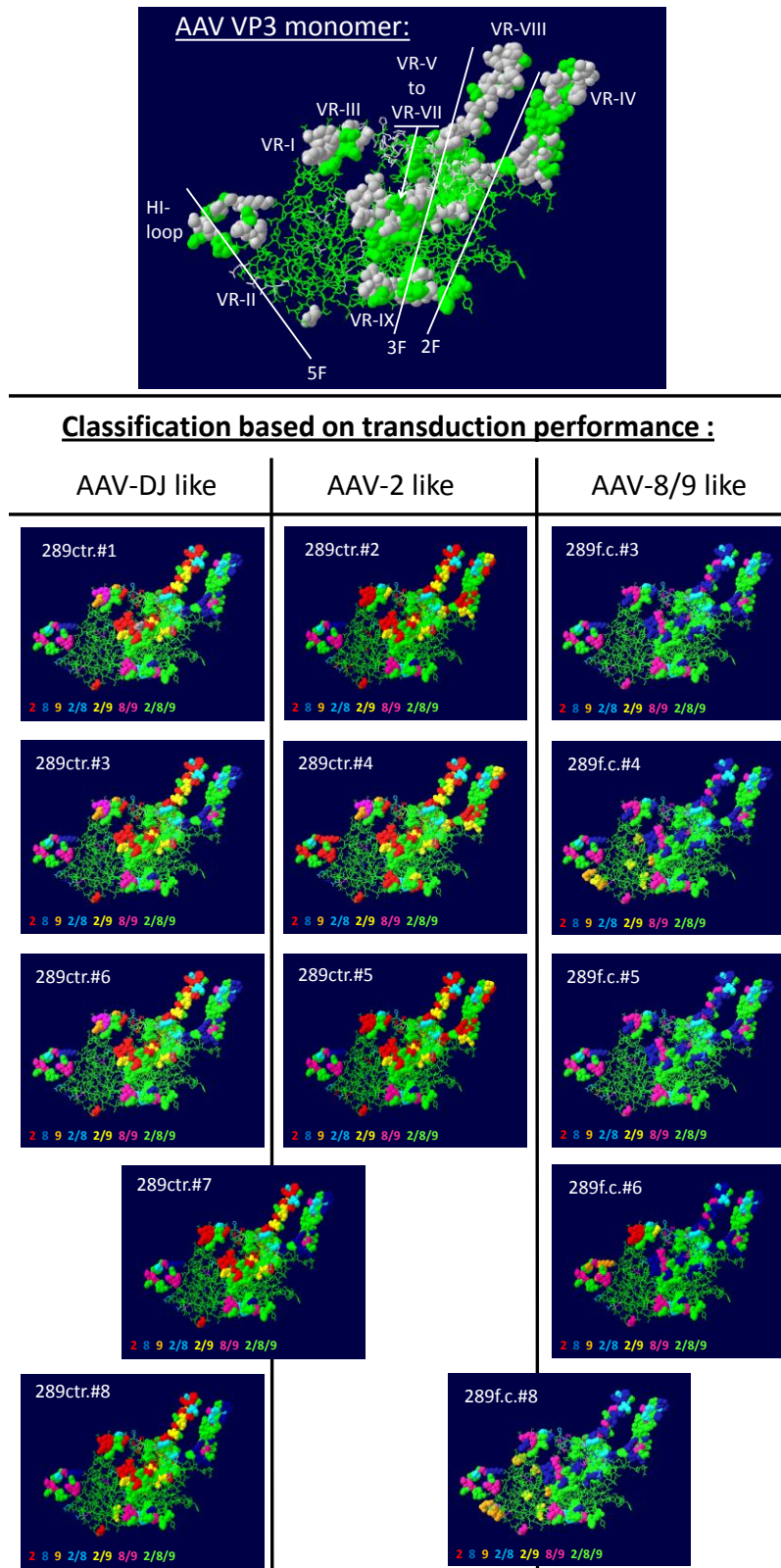


Figure 30: 3D structure of clones selected under various conditions. The top panel gives an overview of a VP3 monomer. Variable regions are named and indicated by light gray color. Thin white lines indicate the 2-fold (2F), 3-fold (3F) and 5-fold (5F) symmetry axis, respectively, of the assembled AAV capsid. Shown below are the eight clones from the 289ctr. group, selected in the absence of IVIG, as well as five of the eight clones after IVIG selection at 'final concentration' (f.c.). Also shown is how they cluster into AAV-DJ, AAV2- or AAV8/9-like chimeras, according to their transduction efficiency in Huh7 cells *per se* or with increasing concentrations of IVIG. Dark gray ribbons/balls in the lower panel indicate sites of mutation. All 3D structures were generated with PDB viewer on the basis of the structure of AAV2 (file 1LPD).

3.1.2.2 *Library selection without Adenovirus helper*

In all selections above, Adenovirus type 5 (Ad5) was used as helper virus to promote the replication of AAV particles that had entered the infected cells and to thus permit the production of progeny AAV for re-infection of fresh cells. This co-infection is necessary as AAV is a replication-deficient virus that has evolved to hijack RNA and protein functions of its helper virus for its own agenda. Hence, the vast majority of previously published protocols include this helper virus co-infection step, except for a few reports of *in vivo* biopanning where Adenovirus was omitted due to safety or toxicity concerns, or where the target tissue was resistant to helper virus infection from systemic virus inoculation [212], [216], [217]. However, also for *in vitro* selection in cultured cells, there are at least three concerns with the use of a helper Adenovirus. **First**, the inherent Ad5 tropism will limit or even prohibit the selection in cell types of interest that are not or only poorly infectable with this virus. This is equally problematic for mixed cell populations, such as peripheral blood mononuclear cells (PBMCs), where the Ad5 tropism will induce a bias for or against a cellular subpopulation. **Second**, the adenoviral helper functions act throughout the entire AAV life cycle, up to final cell lysis and hence efficient release of AAV progeny. Yet, AAV vectors are intended to only transduce target cells, *i.e.*, to deliver their genome to the nucleus for expression, but not for replication and subsequent packaging into new virions. Hence, it is conceivable that the use of helper virus during AAV library selection may enrich AAV capsids that are optimized for later steps in the productive infection which are, however, irrelevant for their use as recombinant vectors. **Third**, because the adenoviral helper is replication-competent and pathogenic in humans, its use requires the entire selection protocol to be conducted under biosafety 2 conditions (despite the fact that the AAV library *per se* is level 1) which are not available in any lab.

For all these reasons, there is a rationale and preference, at least in theory, to molecularly evolve and select AAV chimeras in the complete absence of infectious Adenovirus. We therefore asked two essential questions: 1) does AAV selection in cultured cells without helper virus lead to the isolation of AAV clones that differ substantially from those selected under standard conditions, *i.e.*, in the presence of Ad5, and 2) if so, will these clones really transduce cells more efficiently when used as vectors, or will they have some defect in transgene delivery and/or expression?

To answer these questions, we again exploited the AAV289 library that we had used for the different IVIG selections in the previous chapter. As described there, our control selection scheme represented a standard approach, where a shuffled library was amplified five times in the presence of helper Ad5 (**289PBS**, Figure 27C). Notably, the same helper virus-dependent approach, albeit with a different library and in the presence of IVIG, had also been used to enrich the AAV-DJ chimera in the original Grimm study [212]. As a second and new strategy, we now re-screened our AAV289 library by five

cycles of infection in the absence of any helper virus, followed each time by PCR amplification of viral genomes that had entered the cell, re-cloning into the ITR/*rep* plasmid, and finally production (in ten 14 cm dishes) and iodixanol gradient purification of a fresh library for the next infection round. The titers of each new library were determined by RT-PCR, and virus integrity was confirmed by Western blot analysis (Table 14). Because this selection scheme does not result in expression of AAV proteins in the infected cells, it was impossible to monitor changes in library potency over time by Western blotting, or to use these data to in turn adjust the volume for re-infection to a minimal amount promising a tight genotype-phenotype linkage (see chapter 3.1.2.1 above). Instead, we kept a constant titer of 2×10^8 particles per well of a 6-well plate for each infection round, based on our empirical observation that this virus amount permitted a robust PCR rescue (data not shown).




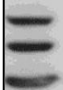
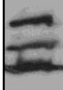
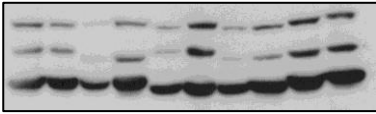
Library	Viral titer vg/ml	Western Blot
289	2.00E+12	VP1 — VP2 — VP3 — 
289-Ad5-1st	6.48E+11	VP1 — VP2 — VP3 — 
289-Ad5-2nd	7.65E+11	VP1 — VP2 — VP3 — 
289-Ad5-3rd	4.00E+12	VP1 — VP2 — VP3 — 
289-Ad5-4th	1.36E+12	VP1 — VP2 — VP3 — 
289-Ad5-5th		

Table 14: Selection of the AAV289 library in the absence of helper Adenovirus. Shown are the titers of the original library and after each round (up to #4) of infection and re-production. Also shown are Western blots made after virus production and purification. The B1 antibody was used to detect the viral capsid proteins VP1, VP2 and VP3. After five rounds of selection, the titer of the fifth library was no longer determined. Instead, ten clones of this last library were isolated, subcloned into an AAV expression plasmid and tested individually by Western blotting. The shown results confirm the integrity of the intermediate libraries as well as of the individual clones.

Results

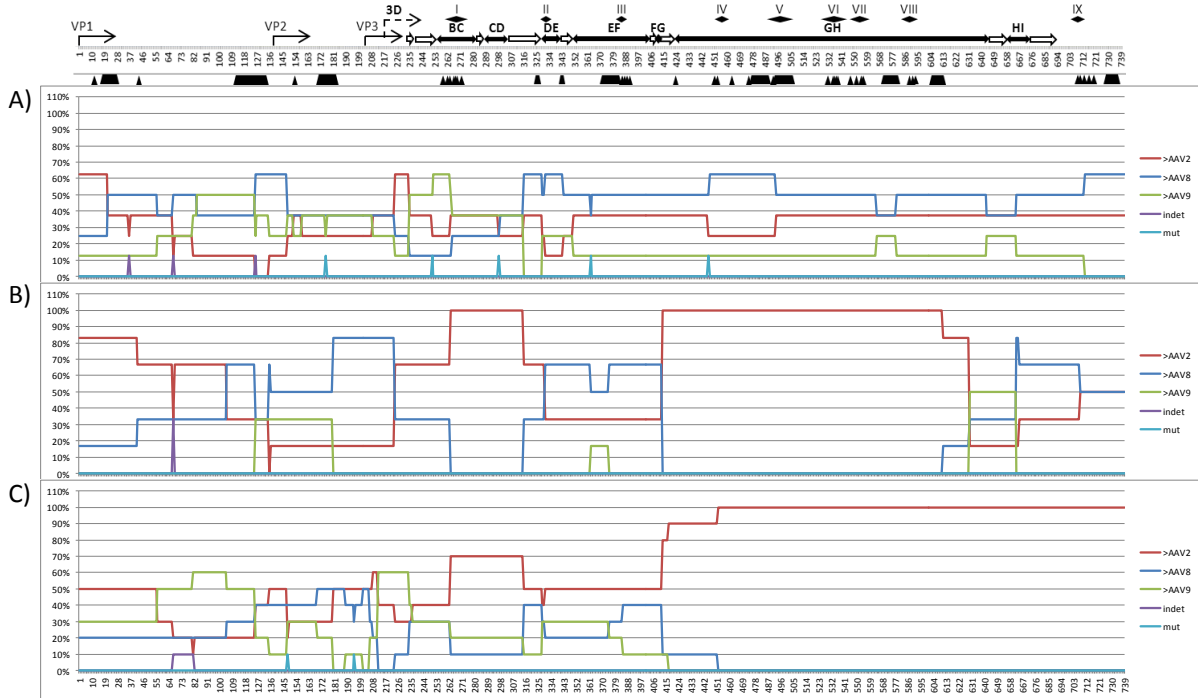


Figure 31: Clonal composition of the shuffled AAV289 library after selection with or without Adenovirus. Shown on top is the linear alignment of VP capsid residues akin to the depiction in Figure 4 and Figure 27 (see these for details). Colored lines in the three panels underneath indicate the percentage of clones that originate from the respective parental serotype at any position within the AAV capsid sequence. **A)** Data for the original unselected AAV289 library. All serotypes are equally distributed throughout the capsids. **B)** The 289 library after iterative amplification on Huh7 cells in the presence of adenoviral helper. **C)** The same AAV289 library after selection without Ad5. Note how the entire C-terminal half of all clones, starting from the beginning of the GH-loop, is composed of AAV2-like amino acids. 8 to 10 clones from each library were analyzed per graph. Graphs A) and B) have been shown before in Figure 27 and were again included here for direct comparison.

After five rounds of infection and PCR rescue, 10 individual clones were picked randomly, sequenced and analyzed in direct comparison to the clones previously isolated from the unselected library or after selection in the presence of Adenovirus, respectively (see chapter 3.1.2.1). As is evident from the graphical representations in Figure 27 and Figure 31, the most striking differences occurred again in the C terminus, which was entirely derived from AAV2 in 100% of the clones selected without Ad5 helper. This included the complete GH-loop, the HI-loop as well as VR-IX at the very end (Figure 31). Consequently, none of these new clones carried the aforementioned combination of a GH-loop from AAV2 with a C-terminal end from AAV8 that was found in clones selected in the presence of Adenovirus (Figure 27 and Figure 31).

From six of these ten clones, we next also produced vectors (after re-cloning of the corresponding *cap* genes into an AAV helper plasmid) encoding a YFP reporter and titered them in Huh7 cells along with clones from the previous 289PBS control pool that was selected in the presence of Adenovirus. Parental serotypes AAV2, AAV8 and AAV9 served as controls. As compared to previous titration experiments, we shortened the time until FACS analysis after infection to 48 instead of 72 h since we

added helper virus during the titration in some experiments and wanted to avoid excessive cell death.

Curiously, despite their differences in sequence composition, the infection rates of clones selected without Ad5 did not differ dramatically from those selected with Ad5. Instead, the infectivity of all clones, regardless of selection protocol, was between 80% and 90% (at the lowest dilution, top wells in Figure 32A). Adding Adenovirus during the titration increased the infection rate of AAV2 from 86% to 100%, yet had no effect on the chimeric AAVs (Figure 32A). Thus, despite selection of particular library clones in the presence of Adenovirus, adding this helper did not further boost the activity of the corresponding capsids once they had been transferred into an AAV vector context.

One notable general outlier was clone #2 which gave only 37-39% transduction in both assays. While it shares the complete AAV2 C terminus with all other clones in this pool (selected without Ad5), it is the only clone whose β G-sheet and beginning of GH-loop originate from AAV8, and whose VR-II in the DE-loop is from AAV9 (Figure 21) (for more detailed information about the AAV capsid loops and intermediate β -sheets, please refer to Figure 4). This C-terminal capsid composition is shared by only one other clone tested, the also less functional clone #4 from the previously selected control pool 289ctr (selected together with IVIG 'final conc.', Figure 21, Figure 27B, chapter 3.1.2.1).

Thus far, all titration experiments had used a relatively long AAV infection time of 4h. To dissect potential differences in the early kinetics of receptor binding or virus uptake between the two pools (plus/minus Ad5 during selection), we performed a time course experiment where we kept Huh7 cells on ice after AAV addition to inhibit virus uptake, followed by a switch to 37°C for 1, 5 or 20 min. The cells were then washed twice with 1x PBS supplemented with fresh medium and incubated for 48 h until FACS analysis. Again, we found no clear differences between the chimeras from both selection schemes, despite some variation between individual clones (Figure 32B).

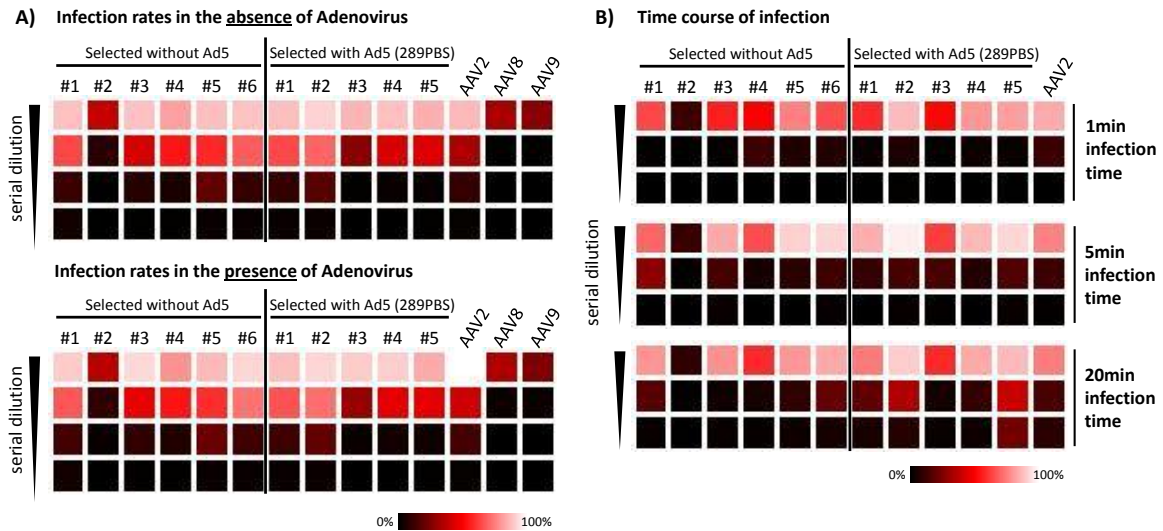


Figure 32: Infection rates of AAV chimeras selected with or without Ad5 helper. A) Infection rates 48 h post-infection either in the absence (top) or presence (bottom) of Adenovirus during the titration. **B)** Time course experiment as described in the text, also showing no clear difference between the clones (except for #2 without Ad5) from the two pools. (For color code of the heat maps refer to Figure 24 and Figure 29.)

At this point, we were surprised to find that selection with or without adenoviral helper apparently resulted in clones that differed in sequence, but were identical in transduction. This tempted us to speculate that the capsids might differ in their strength of transgene expression, a parameter not studied thus far (since we had only measured numbers of infected cells). Consequently, we re-analyzed the FACS data with a new focus on YFP expression intensities as a means for how well the virion is processed within the cell. Indeed, as shown in the following Figure 33, this now revealed striking differences between the two capsid pools.

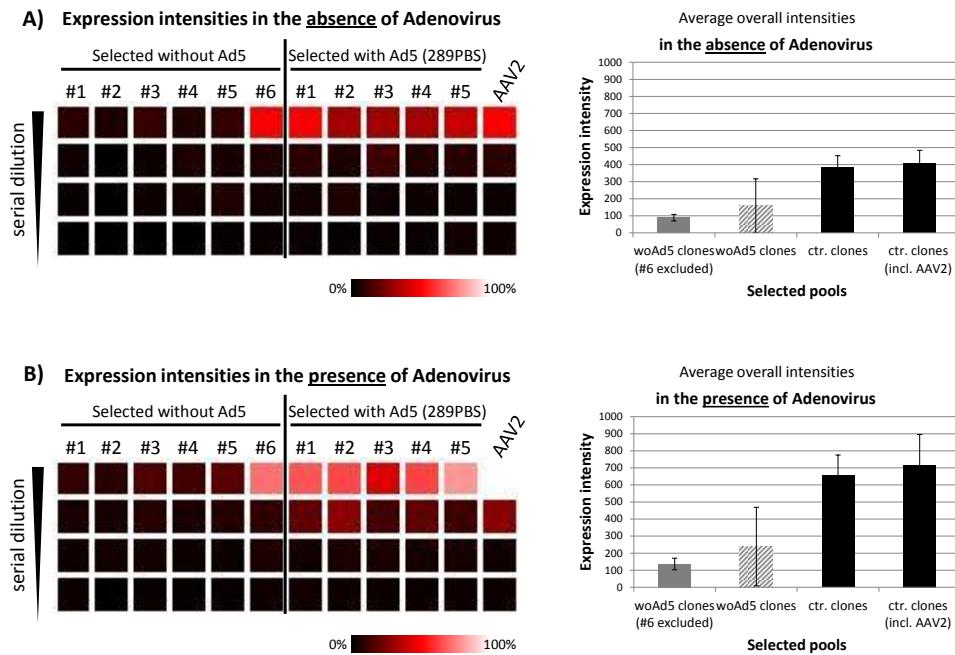


Figure 33: Mean YFP expression intensities of AAV chimeras selected with or without Adenovirus. A) Results at 48 h post-infection in the absence of Adenovirus during titration. **B)** Same as **A**, but in the presence of Adenovirus during titration. Depicted are the expression intensities of individual clones (heat maps) as well as the average overall intensities of the different pools (corresponding bar graphs on the right). Intensities in both heat maps were normalized to the highest value of AAV2 expression measured with Adenovirus (white square in panel B) and given in percent. The average overall expression intensities of the pools are shown as absolute values. Note that two bars (gray or hatched) are shown for the clones selected without Ad5 that either omitted or included clone #6, which was an obvious outlier in this group. (For color code of the heat maps refer to Figure 24 and Figure 29.)

As compared to the highest mean intensity value, measured with AAV2 in the presence of Ad5 during the titration and set to 100%, clones from the selection plus Ad5 helper gave a relative expression intensity of 30-50%. In marked contrast, clones from selection without Adenovirus gave only around 10% expression (Figure 33A). These differences were noted in the absence or presence of Adenovirus during the titration, where the average overall YFP expression intensities increased from 405 to 718 (without Ad5) or 159 to 238 (with Ad5) (Figure 33B).

The only exception in the pool of clones selected without Ad5 was clone #6 whose transduction rates as well as expression intensities are similar to those of the clones selected in the presence of helper virus. Indeed, clone #6 resembles AAV2 almost entirely except for only two amino acids in VP1 (Figure 21). Accordingly it is in all probability that all capsid mediated functions of #6 are AAV2-like. However, these two aa changes apparently led to a slightly decreased infectivity of clone #6 upon Ad5 super-infection, as compared to wtAAV2.

In summary, we can draw at least two essential conclusions from these experiments, which are again highly relevant with respect to the design and application of future selection strategies (see Discussion for more details). First, our sequence and titration data strongly support the concept that

the different properties of AAV capsids, such as transduction rates and efficiencies (or IVIG resistance, as studied before in chapter 3.1.2.1), are not determined by single residues or regions, but rather by a very complex interplay of multiple dispersed domains. This explains why we obtained several clones in all selection schemes that differed in their primary sequence yet gave comparable phenotypes. It also highlights that the original combined positive-negative pressure used to isolate the AAV-DJ clone as the only lead candidate in the Grimm *et al.* study must have been very potent and stringent [212]. Second, our data show that the presence or absence of Ad5 helper virus during library selection indeed has a profound effect on the performance of the resulting clones, as we had hypothesized originally. Surprisingly though, our results suggest that adding helper virus is actually beneficial, despite the mentioned concerns about safety and biased tropism. Clear evidence is the superior transgene expression per cell from the clones selected in the presence of Ad5, which is a feature that is very relevant for many gene therapy applications. Nonetheless, there are specific scenarios where a helper Adenovirus can or should not be used during selection, as exemplified in the next chapter and as further discussed below (Discussion chapter 4).

3.1.3 *In vivo* biopanning of an AAV15689 library

One of the capsid libraries that we had generated during the initial work when we established and validated the new plasmids for AAV shuffling was made of serotypes 1, 5, 6, 8 and 9 (Table 13 above). This AAV combination was not only picked because it represented a typical experimental setting where users wish to shuffle five different serotypes, but also because these particular candidates are interesting for a variety of *in vivo* selections and applications. AAV1 and AAV6, for instance, potently transduce smooth muscle cells and heart [110], [155]. Moreover, our own data (shown later, chapter 3.2.5.2) imply their great potential to also efficiently infect cells of neuronal origin, blood cells as well as cell lines derived from organs like spleen or pancreas (3.2.3). AAV8 and AAV9 poorly transduce *in vitro* but are very efficient *in vivo*, plus they have a broad tissue tropism and the potential to cross the blood-brain barrier [155], [212]. Finally, AAV5 was chosen for its unique capsid composition (it is the most diverse of all known AAV serotypes) and its low abundance in humans, with only 10% of the human population carrying pre-formed antibodies against AAV5 [278]. Besides, AAV5 was also recently described to mediate retrograde transport along axons [279]. Last but not least, we purposely omitted AAV2 from this library to lower the risk of neutralization by prevalent anti-AAV2 antibodies and to avoid a bias towards hepatotropic chimeras. As shown in Table 13, the final CsCl-purified library had a diversity of 1.5×10^5 colonies and a viral titer of 6×10^{12} particles per ml.

Because we had this unique library, we were able to establish a collaboration with the company Boehringer Ingelheim (BI) in which they screened this library in the pancreas of adult mice *in vivo*, with the aim to isolate chimeras that potentially transduce β -islets.

3.1.3.1 *Library selection in murine pancreas*

The β -islets, also called islets of Langerhans, are located in the pancreas and consist of approximately 75% β -cells. These cells are important for insulin regulation and are crucially involved in type 1 diabetes, making them important targets for therapeutic gene transfer and intervention. To screen our library for candidates that can infect these cells, we transferred it to our collaborators at BI who injected it intravenously into the tail vein of adult C57/BL6 mice at a dose of 3×10^{11} viral particles per mouse. Treated animals were sacrificed 3 d post-injection, and β -islets were isolated from the pancreas. Figure 34A shows a microscopic image of β -cells isolated after the first selection round.

Of note, the mice were not co-injected with Ad5 helper virus, despite our evidence described in the previous chapter 3.1.2.2 that this may foster the isolation of potent capsids. Our reasons for omitting the helper virus in the *in vivo* biopanning were that systemic Ad5 delivery is toxic in mice, and that it may additionally introduce a bias towards cells other than the desired β -cells, such as hepatocytes. As also noted before, leaving out the helper virus created the need to rescue the capsid genes of the infected AAV particles by PCR and to re-clone them for a new library production prior to re-infection.

Accordingly, we extracted whole DNA from β -cells after library infusion and then PCR-amplified the chimeric capsid genomes from the DNA samples using primers LseqF and LseqR (see Figure 16). To obtain sufficient DNA amounts for cloning into the AAV library recipient plasmids and subsequent library production, we additionally ran a second nested PCR using primers Lseq_nstF and Lseq_nstR (Figure 34C-E) (see 2.2.4.5 for primer sequences). Moreover, after each round, tissue samples from liver, heart, visceral fat and kidney were also taken to monitor the distribution of AAV capsid genomes in other organs besides β -islets. As exemplified in Figure 34B, capsid sequences could never be amplified from heart or kidney, and were only found in visceral fat after the first selection round, but no longer after the second or third injection, implying de-targeting from fat as a consequence of β -cell selection. In contrast, AAV capsid sequences were detected abundantly in the liver DNA samples especially after the second and third injection.

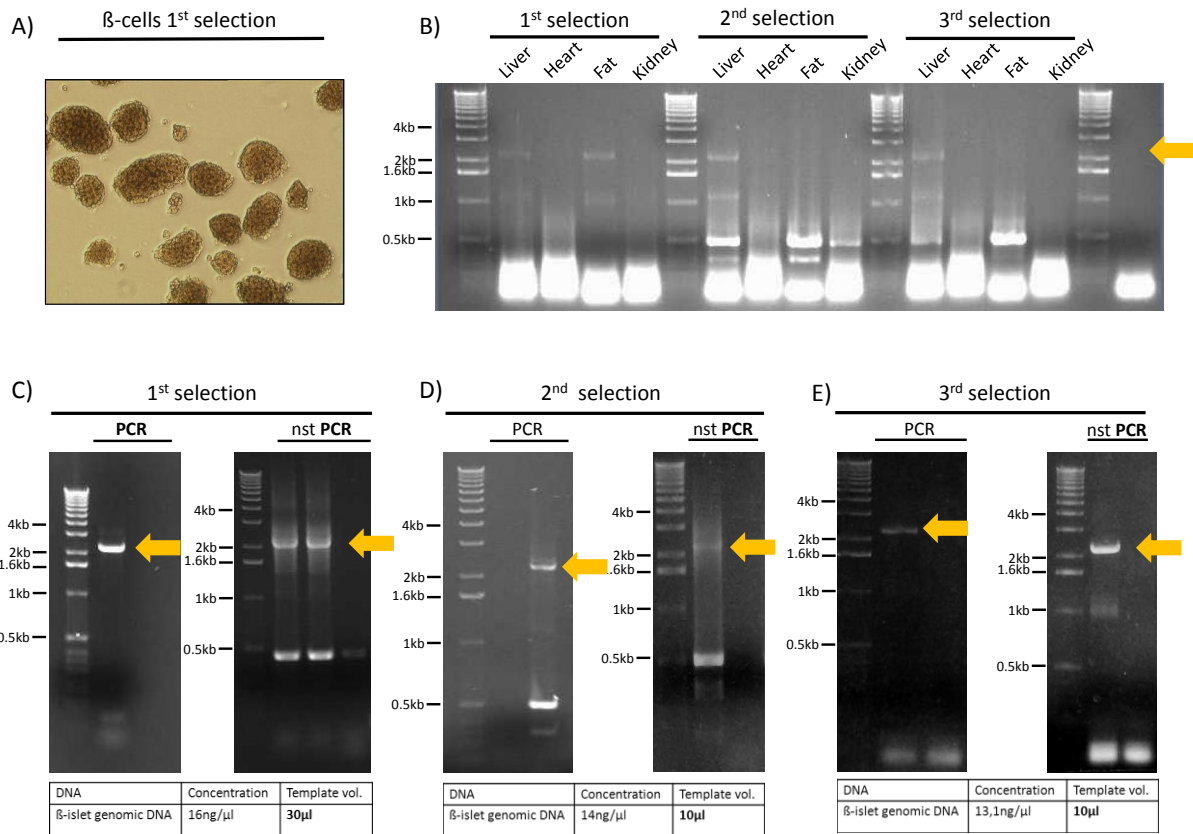


Figure 34: *In vivo* selection of an AAV15689 library in murine β -islets. A) Representative photo of β -islets isolated from mouse pancreas after the first injection with the AAV15689 library. **B)** AAV genome amplification from the shown tissue samples after the first, second and third selection round. **C-E)** AAV capsid gene amplification from β -cells by PCR and nested PCR after the first, second and third injection. Total DNA concentrations and template volumes in each round are shown at the bottom. Desired *cap* bands are indicated by yellow arrows.

From each selection round, ten clones were sequenced and analyzed for their overall composition according to the five parental genes. After the **first** injection, AAV5 was almost entirely depleted from the library, whereas the remaining four parental sequences were still present throughout the entire capsid sequence, with a slight tendency towards an AAV1/AAV6 (the two serotypes are hard to distinguish in this region) over-representation in the C-terminal part (Figure 35A). After the **second** selection round, the bias towards AAV1/AAV6 substantially increased for the entire GH- and HI-loop (Figure 35B). Three clones from the first and second selection round carried an asparagine (N) at their very C terminus that originates from serotype AAV8, while the rest of their C-terminal half was composed of sequences from AAV1/AAV6. Besides, most clones from the second selection could only be clearly distinguished according to their BC-loop.

Results

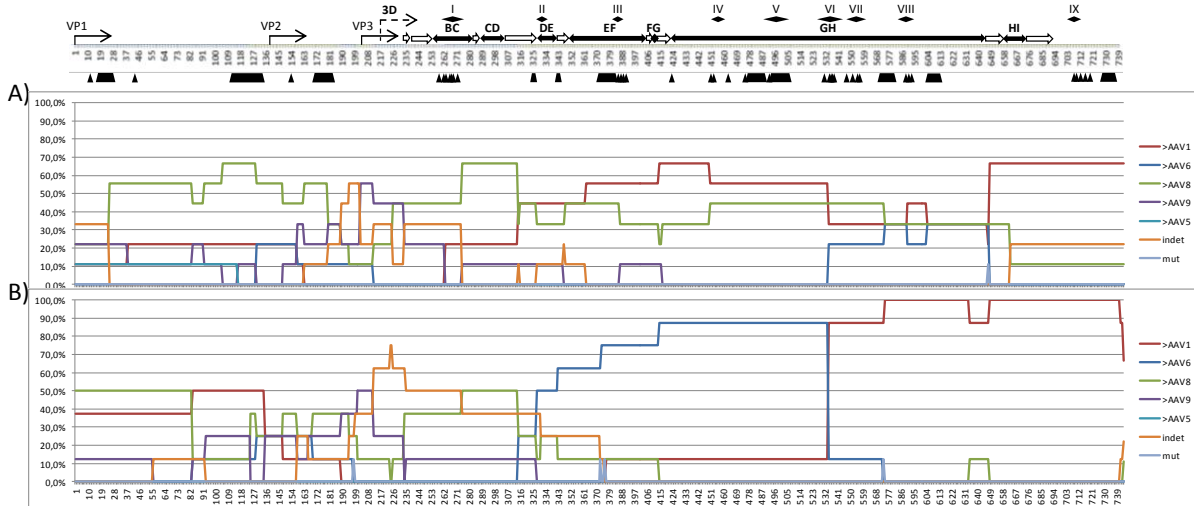


Figure 35: Overview over the clonal composition of the shuffled AAV15689 library after *in vivo* biopanning. The top panel shows the linear alignment of VP capsid residues, while colored lines indicate the percentage of clones that originate from the respective parental serotype at any position within the different AAV capsid sequences. See Figure 4 for further details. **A)** Composition of the library after the first selection round. **B)** Composition of the library after the second selection round. Ten clones per selection round were sequenced and analyzed using the Salanto program.

Surprisingly, already after the **third** selection round, we detected only a single sequence after PCR amplification (all ten clones were 100% identical). This clone, called AAV-BIEK, consists of AAV1/AAV6 in its entire VP3 sequence except for the BC-loop that came from AAV8 and the aforementioned AAV8-like asparagine at the very C terminus (Figure 36A). In fact, the combination of both these AAV8-like elements was the only obvious feature that distinguished this clone from clones from previous selection rounds.

To analyze whether this lead candidate would indeed transduce pancreas cells, we transferred its capsid sequence into our AAV helper plasmid to produce YFP-encoding vectors. As controls, we included several clones from the first and second selection round. These were picked based on their sequence that comprised AAV8- and AAV9-like amino acids in the C-terminal part, for example in clone BI1st#2. Alternatively, they combined the AAV1-/AAV6-like GH-loop with a BC-loop of a different origin, as in the case of BI1st#3, BI2nd#10 and BI2nd#12 (Figure 36B). When we tested the different purified vectors on Panc-1 cells, a human pancreatic carcinoma cell line, most gave only weak transduction as compared to AAV6. Here we chose AAV6 as a control, since it was found superior to all other wildtype and modified AAV clones in cells from pancreas and spleen (chapter 3.2.3). The only clone that transduced Panc-1 more efficiently than the other isolates, yet still less than AAV6, was clone #12 (Figure 36C). Notably, this clone was from the second selection round and consisted almost entirely of AAV1/AAV6-like amino acids.

To our surprise, our actual lead candidate AAV-BIEK not only transduced the human pancreatic cells inefficiently, but it also did not provide transgene expression in β -islets *in vivo* after intravenous injection into mice (undisclosed data from BI; not shown). Alas, our collaboration partner did not study whether the viruses had at least bound to the cells or entered the β -islets without uncoating and expressing their transgene; two possibilities that would be fully compatible with our enrichment of this clone despite its presumable inactivity in its target cells. Moreover, our experience from the *in vitro* selections with or without helper Adenovirus suggest a critical and positive role of the helper virus in the isolation of capsids that mediate robust transgene expression within the infected cell. Taken together, we can envision a number of explanations for this initially counter-intuitive result from our *in vivo* selection, as will be discussed in more detail in chapter 4 below.

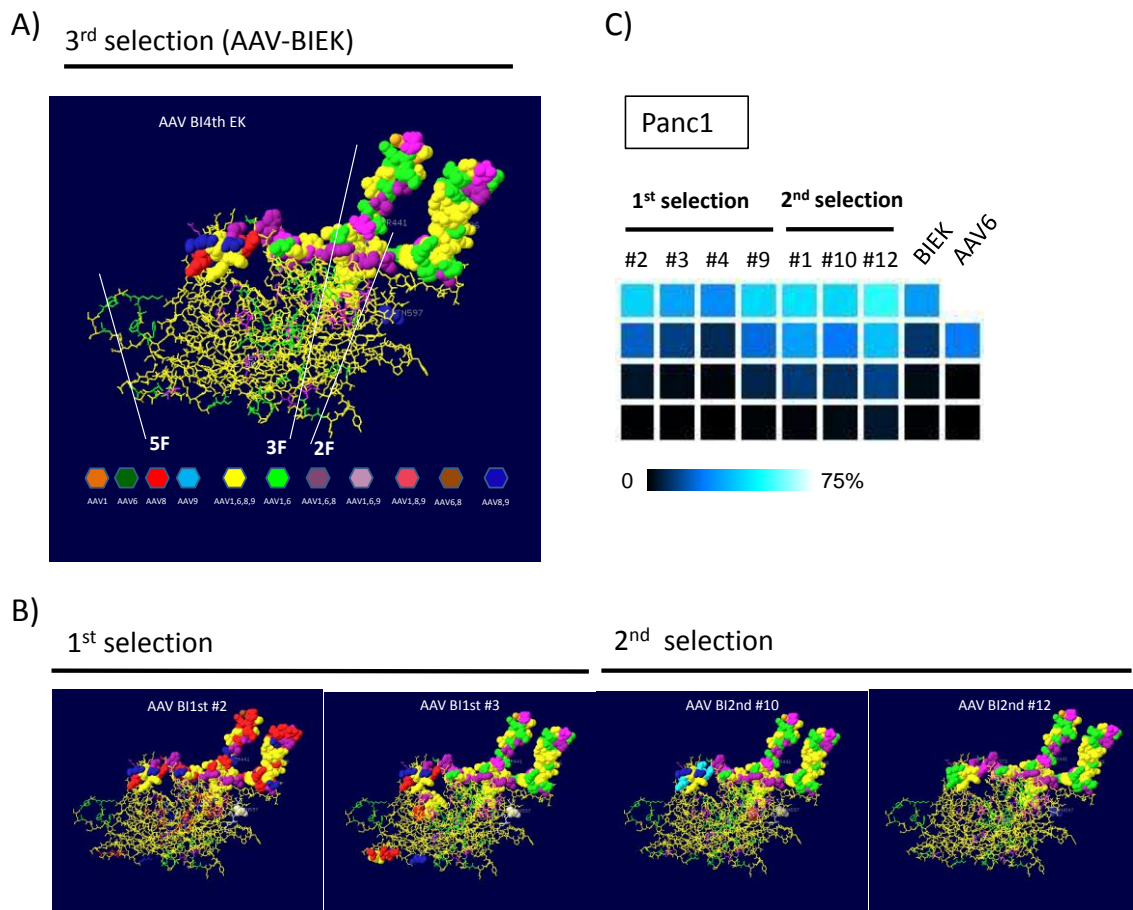


Figure 36: 3D structure of selected clones and YFP expression ratios in Panc-1 cells. **A)** 3D structure of the lead candidate AAV-BIEK after three selection rounds in murine β -cells *in vivo*. Thin white lines indicate the 2-fold (2F), 3-fold (3F) and 5-fold (5F) symmetry axis, respectively, of the assembled AAV capsid. **B)** 3D structure of two clones each from the first and second injection rounds. See panel **A)** for color code. **C)** Transduction efficiency of AAV-BIEK as compared to shuffled clones from previous selection rounds or AAV6 as control. (For color code of the heat maps refer to Figure 24 and Figure 29.)

3.2 AAV peptide display

The second part of the work in this thesis focused on viral peptide display as an alternative technique for molecular AAV vector evolution. As already described in more detail in introductory chapter 1.3.2, display of short peptide libraries on the AAV surface and subsequent selection on target cells have been used extensively over the past decade to alter AAV tropism. However, with the exception of a few recent studies, these approaches were always restricted to the capsid of AAV serotype 2, due to the fact that this has long been the best characterized isolate and that its structure had been resolved [212], [221], [224]–[226]. In the meantime, the structures of eight other serotypes have become available, yet the expansion of peptide display to isolates other than AAV2 remained challenging because of our incomplete knowledge of the receptor binding sites in these capsids. These sites would be preferred regions for peptide insertion, along the basic idea to ablate the primary tropism while concurrently adding a new specificity through the displayed peptide. Still, alternative serotypes continue to be highly interesting templates for AAV peptide display as it is very likely that the eventual particle properties are not only determined by the peptide, but rather by a complex interplay of the additional amino acids with residues and domains in the underlying capsid scaffold.

Here, our major aim was thus to comprehensively assess the potential of 11 AAV serotypes other than AAV2 to serve as templates for peptide display. Therefore, it was **first** necessary to genetically engineer these alternative capsid genes in order to allow simple and straight-forward insertion of peptide-encoding oligonucleotides. **Second**, we aimed to analyze the resulting capsid-peptide panels in a large variety of cell types, including different primary cells as well as established cell lines, in comparison to the 12 unmodified viruses. **Third**, if functional in principle, we planned to screen our new AAV panels on selected clinically relevant cell types in-house or in collaboration with other labs.

3.2.1 Engineering of alternative AAV serotypes for peptide display

The first specific aim was to modify the capsid sequences of different non-AAV2 serotypes to introduce sites for insertion of peptide-encoding oligonucleotides. This posed two challenges: 1) the technology how to engineer these sites, and 2) the selection of the precise region for modification/insertion. In the pioneering work with AAV2, the two most preferred sites were positions 587 or 588 since they are exposed on the capsid surface, tolerate peptide insertions and comprise 588 or are near 587 a residue that is critical for primary receptor binding (an arginine at position 588, R588). To insert oligonucleotides at either of these positions, the AAV2 *cap* gene has been mutated to introduce two endonuclease restriction sites that are neither present elsewhere in the AAV2 genome nor in the plasmid backbone. Moreover, these sites ideally produced two different

overhangs after cleavage, to facilitate directed cloning of the oligonucleotide (as two single-stranded DNA strands that form matching overhangs after annealing). A typical enzyme that fulfills these criteria is *SfiI* which was first used by the Kleinschmidt lab in the AAV2 context, and later also by Grimm and co-workers for the modification of AAV-DJ which is identical to AAV2 in the area surrounding R588 [212], [221]. Unlike other possible non-cutters in AAV2/-DJ that could have been used, *SfiI* has the benefit that it is a class I restriction enzyme that cuts outside its actual recognition site, allowing for the creation of individual sticky overhangs. Luckily, we found that *SfiI* is also a non-cutter in the 11 other serotypes that we had available in the lab and wanted to modify - AAV1, 3-9, rh10, po1 and 12 (the same as used in the shuffling work above). The problem that remained was how to insert two *SfiI* sites into all 11 serotypes, considering that the originally published strategy comprised a series of three work- and time-consuming iterative mutagenesis steps (Figure 37 left, top). In fact, to adopt this strategy to *e.g.* AAV9, even five mutagenesis reactions would have been required (Figure 37 left, bottom). We therefore designed a new, much simpler and faster strategy that is depicted on the right in Figure 37 and explained in detail in the next chapter.

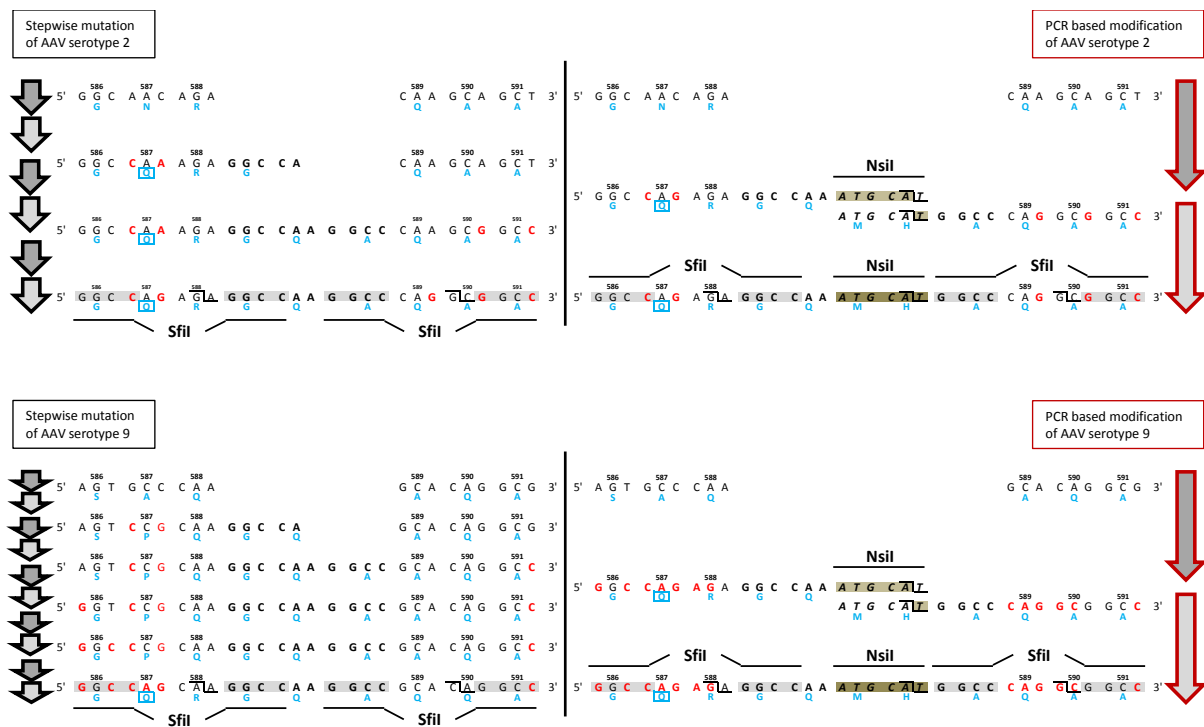


Figure 37: Strategies for insertion of peptide display sites in AAV serotypes. Shown is a comparison of the standard iterative site-directed mutagenesis approach (left) with a new PCR-based protocol (right) that was implemented in this thesis. AAV2 (upper panel) and AAV9 (bottom panel) are depicted as examples. Starting from the wt (top in each panel) to the final modified sequence (bottom in each panel), each sequence in between marks one intermediate step. Red nucleotides highlight the changes over the previous sequence, and blue letters are the corresponding amino acids. Numbers above are amino acid positions corresponding to AAV2 *cap*. After each site-directed mutagenesis step in the original protocol (left), the modified *cap* genes have to be cloned and sequenced (indicated by arrows). The number of intermediate steps necessary to introduce the two *SfiI* sites via this strategy varies largely between serotypes, from three for AAV2, to five for AAV9 and other serotypes. In contrast, the new PCR-based protocol permits the introduction of the same two *SfiI* sites in only two steps, for any serotype. It is based on *NsiI* digestion of two PCR-amplified fragments and their subsequent ligation via the resulting overhangs.

3.2.1.1 **PCR-based creation of a peptide insertion site in AAV2**

The hallmark of our new strategy is that a *cap* gene of interest is first PCR-amplified in two halves using primers that contain the two desired *SfiI* sites - one in the 3' primer for the left part of *cap*, and the other in the 5' primer for the right *cap* fragment. This is followed by a triple ligation that joins the two halves using an *NsiI* site also present in these two primers and that concurrently inserts the modified *cap* gene into a library plasmid containing AAV2 ITRs and *rep* (the same as used for the shuffled libraries above), or into an AAV2 helper plasmid (lacking the ITRs). Because both *SfiI* and *NsiI* generally cut infrequently, this strategy was fully compatible with all 12 AAV serotypes (including AAV2) that we studied here, and will most likely also work with other viral isolates in the future.

To obtain proof-of-concept, and to compare the efficiency and speed of our approach with the conventional strategy, we initially tested it with AAV2. We therefore designed appropriate PCR primers according to the rules outlined above for the amplification of a ~1.8 kb left half of AAV2 *cap* (ending with *SfiI* and *NsiI* sites) and a ~400 bp right half (starting with *NsiI* and *SfiI* sites). Following digestion with *NsiI* and further unique restriction enzymes that cut upstream of the left *cap* half (*SwaI*) or downstream of the right (*SpeI*), the two halves were gel-purified and ligated into a *SwaI*-*SpeI* double-digested AAV2 helper plasmid. Further details of the primer design and cloning procedure can be found in the Materials and Methods section (2.2.4). Notably, control digests as well as sequence analyses confirmed successful *cap* re-assembly and *SfiI* site insertion in nearly 100% of the resulting clones (Figure 38A). In contrast, the success rate of the original step-wise mutagenesis using a commercial kit (Stratagene, QuikChange Site-Directed Mutagenesis Kit) is only ~80% per mutagenesis step, according to the information provided by the manufacturer and to our own prior experience (D. Grimm, personal communication).

Analogous to the original method, our new primers were designed such that they introduced a frameshift into the modified and re-assembled *cap* genes, and that proper insertion of the peptide-encoding oligonucleotide is required to correct this shift. The purpose of this frameshift is to prevent contamination of the final viral library with capsids that have not taken up the oligonucleotide and hence do not display the re-targeting peptide(s). We verified this presumption by inserting a specific oligonucleotide, encoding the peptide NSSRDLG that was previously selected from peptide libraries in two independent studies [212], [221], into our modified AAV2 helper plasmid. The oligonucleotide was designed to introduce an additional *AvrII* restriction site that enabled us to confirm its insertion by control digestion. Moreover, after annealing of the two single DNA strands, the resulting double-stranded oligonucleotide contained two overhangs that were compatible with those from the *SfiI* digestion. As exemplified in Figure 38B, the success rate of this ligation was 100%. Importantly, Western blot analysis after small-scale virus productions validated the restoration of correct VP

protein expression after oligonucleotide insertion (Figure 38C). Titration of the recombinant AAV2 variant displaying the NSSRDLG motif showed a decreased efficiency in Huh7 cells as compared to wildtype AAV2 (Figure 38D). This result was expected since the peptide insertion destroyed the HSPG binding domain in AAV2 which is critical for efficient cell binding, and since the particular peptide had not been selected in liver cells. Together, these data confirm the feasibility and efficiency of our new PCR-based insertion site modification strategy in the context of AAV2, and thus tempted us to translate it into the other 11 serotypes as well.

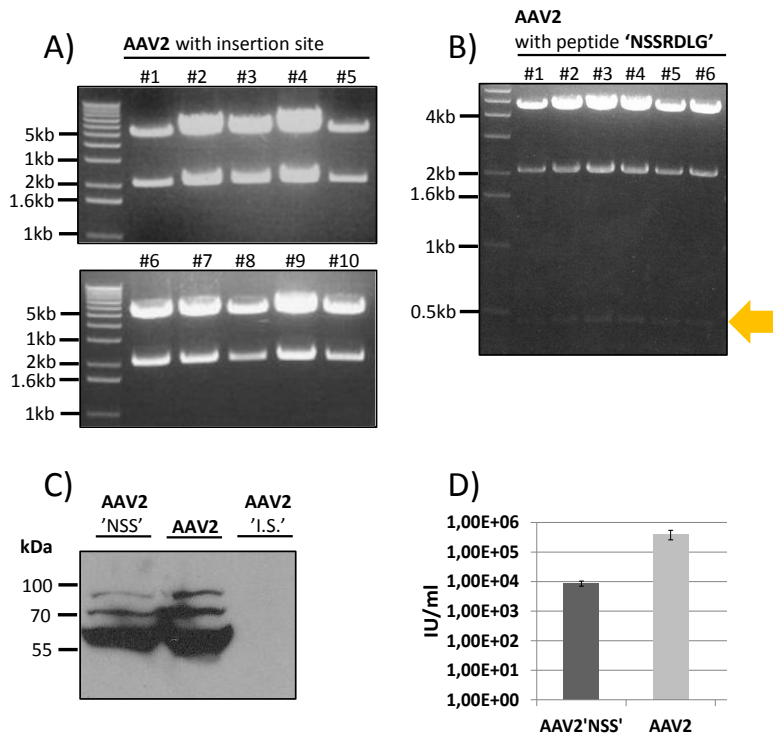


Figure 38: Validation of the new strategy for creation of peptide insertion sites in AAV2. An insertion site for peptide-encoding oligonucleotides was introduced into an AAV2 helper plasmid through the new PCR-based protocol and validated by sequencing and expression analysis. **A)** Control digestion with restriction enzymes HindIII and NsiI of 10 clones from two independent ligation reactions. All clones show the correct restriction pattern with a 5.2 kb and a 2.1 kb band. **B)** Control digestion after oligonucleotide insertion with HindIII, AvrII and SpeI. All three expected bands of 4.7 kb, 2.1 kb and 450 bp (faint and thus marked with an arrow) were detected. **C)** Western blot analysis of virus lysates. Virus was produced in a 6-well format by triple transfection of an adenoviral helper plasmid, a mCherry reporter construct and an AAV helper plasmid that encodes either the capsid of AAV2wt or AAV2 with the 'NSS' peptide or AAV2 with the insertion site ("I.S.") alone. The B1 antibody was used to detect the viral capsid proteins VP1, VP2 and VP3. AAV2 with the inserted peptide NSSRDLG ("NSS") and wt AAV2 gave clear bands. In contrast and as expected, transfection of AAV2 with only the insertion site but no peptide-encoding oligonucleotide did not lead to VP expression. **D)** Titration of crude cell extracts. Values are infectious units per ml (IU/ml). Shown are average values from three individual experiments plus SD.

3.2.1.2 *Expansion of PCR-based cap gene modification to non-AAV2 serotypes*

As noted, a major hurdle in the translation of viral peptide display to AAV serotypes other than AAV2 has long been the lack of a detailed knowledge about their three-dimensional structure and the precise location of the receptor binding sites. At the time when the work in this thesis commenced, such knowledge was exclusively available for the AAV2 prototype, despite first emerging reports on the cellular receptors for some other serotypes. Our best and only option to identify possible peptide insertion sites in the 11 alternative AAV isolates that we were interested in - AAV1-9, rh10, po1 and 12 - was therefore to align their primary protein sequences to that of AAV2. Akin to the strategy for AAV2, we aimed to place the insertion sites in variable region VIII within the GH-loop, postulating that the peptides would then also become displayed on the capsid surface. Moreover, because of the variability and exposure of this region across all serotypes, it was likely that it contained critical residues and domains for receptor binding also in the 11 alternative isolates. Table 15 shows the insertion sites (amino acid positions and actual residues) that we eventually picked based on the comparison with AAV2 (also shown in more detail in Figure 39 below).

Serotype	Insertion Site	Modified Amino Acids
AAV1	D590_P591	STD/PAT
AAV2	R588_Q589	GNR/QAA
AAV3b	S586_S587	LQS/SNT
AAV4	S584_N585	DQS/NSN
AAV5	S575_S576	NQS/STT
AAV6	D590_P591	STD/PAT
AAV7	N589_T590	AAN/TAA
AAV8	N590_T591	QQN/TAP
AAV9	Q588_A589	SAQ/AQA
AAVrh10	N590_A591	QQN/AAP
AAVpo.1	N567_S568	NQN/SNT
AAV12	N592_A593	NQN/ATT

Table 15: Features of peptide insertion sites in twelve AAV serotypes. Listed are the modified serotypes (first column), the position of each peptide insertion site (second column) and the six amino acids that flank this site in the original VP proteins (third column). Numbers in the second column refer to the amino acid position within each serotype.

We next engineered all 11 capsid sequences according to the newly established PCR strategy, using serotype-specific primers that introduced the same *SfiI* and *NsiI* restriction sites and hence also allowed *cap* modification by a single PCR and triple ligation. Notably, we designed the 11 primer pairs to introduce two further changes in all *cap* genes. First, they added two amino acids - glycine (left) and alanine (right) - that served as spacers between the inserted peptide and the surrounding capsid sequence, and that were intended to facilitate proper peptide display and folding [221]. Second, the primers further modified the three original amino acids flanking the insertion site on either side

(third column in Table 15), rendering them identical to the engineered AAV2 *cap* gene. This was done to further increase the probability that a given peptide would be displayed in a comparable manner at the tip of the GH-loop across all 12 serotypes. The changes included the introduction of a glutamine at position -2 relative to the peptide insertion site, based on the corresponding alteration in the AAV2 prototype (asparagine-to-glutamine mutation) that resulted from the engineering of the first *SfiI* site (Figure 37). A second change upstream of the insertion site (position -1) changed an arginine (R588) in AAV2 into a serine and was introduced to further ablate AAV2 binding to its primary HSPG receptor. For consistency, this serine was also maintained in the 11 other serotypes.

A comprehensive overview over these changes and other features of the insertions sites is shown in Figure 39. As is evident from the serotype-specific color code in this figure, the peptide insertion sites were located within a highly variable region of the AAV capsid (corresponding to VR-VIII in AAV2).

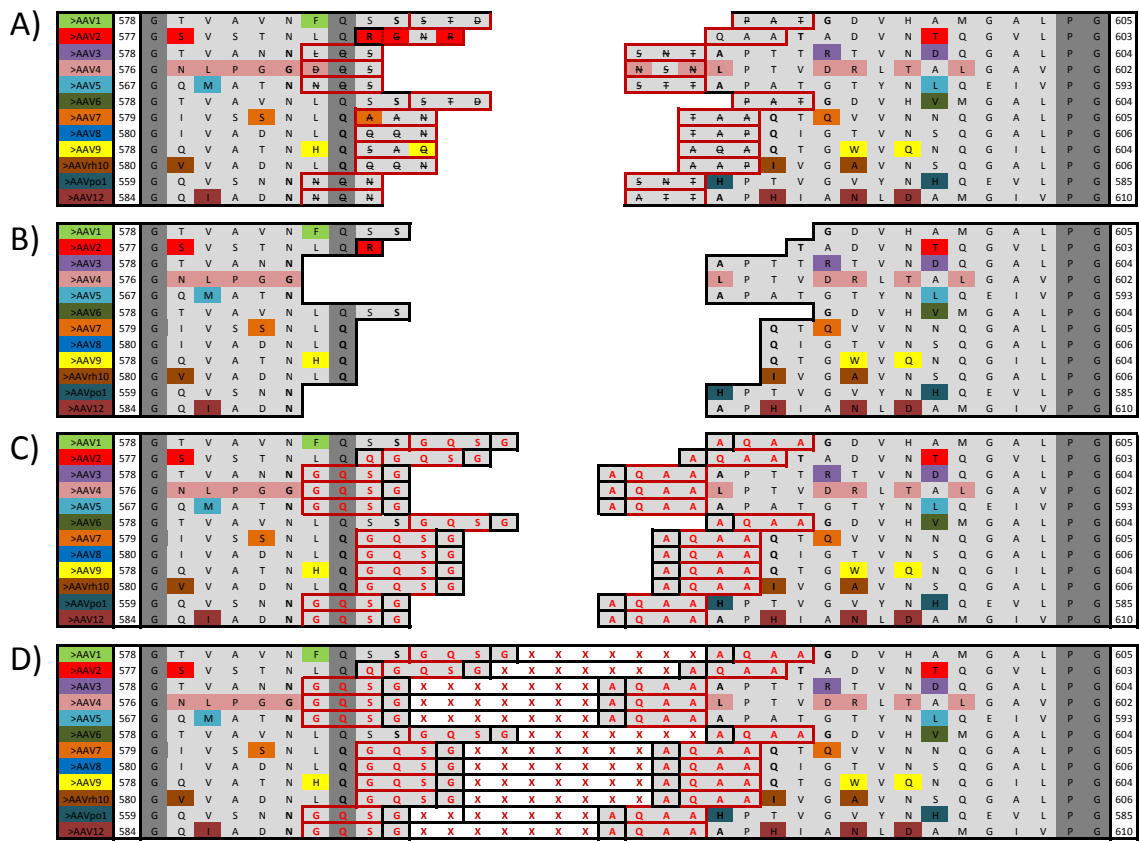


Figure 39: Comparison of the peptide insertion sites in the 12 modified AAV serotypes. The serotypes are color-coded to permit visualization of amino acids that originate from, and are specific for, one particular serotype. Amino acids with a light gray background could be assigned to more than one serotype, while dark gray shading indicates a possible origin from any of the 12 serotypes. **A)** Original sequences surrounding the peptide insertion site (depicted as gap) prior to PCR-based modification (compare to panel C). Red frames highlight the amino acids that were altered during PCR amplification. Slashed letters indicate the amino acids of the original sequence that are replaced. **B)** Sequences that were maintained regardless of the PCR or peptide insertion (*i.e.*, same as panel A, but lacking the residues in the red frames). **C)** Sequences after PCR amplification. Red frames highlight amino acids that were changed from the original wildtype sequences (compare to panel A), while residues in black frames (flanking glycine and alanine) were introduced additionally. **D)** Final sequences including an inserted peptide (red x as placeholders).

Correct insertion site modification was confirmed for all 11 serotypes again in about 90% of the analyzed clones, almost reaching success rates of that of the model serotype AAV2. Moreover, we also validated the functionality of all *cap* genes again by inserting an oligonucleotide encoding the NSSRDLG peptide, and by then producing vectors in small scale to analyze whether correct VP protein expression was restored. As shown by the Western blot analyses of the respective crude vector lysates in Figure 40, all three capsid proteins (VP1 to VP3) were indeed detected in the expected 1:1:10 ratio. These results indicate that our improved cloning strategy was successful in all cases, and that peptide insertion is compatible with all 12 AAV serotypes tested here (at least on the VP protein expression level). Together, this provided the basis for a much broader evaluation of the approach using a larger collection of peptides and cell lines, as detailed in the next chapter.

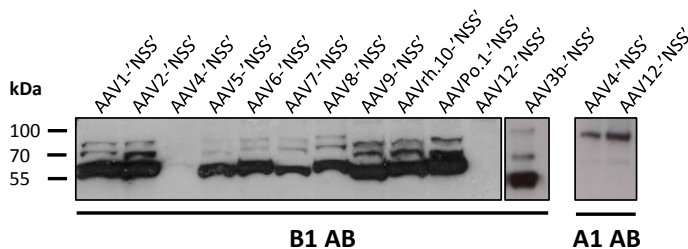


Figure 40: Western blot analysis of 12 AAV serotypes harboring peptide NSSRDLG. The peptide-modified capsid genes were used to produce vectors (encoding a YFP reporter), and crude lysates were probed with the B1 antibody (detecting VP1-3 of all serotypes except for AAV4 and AAV12) for the expression of capsid proteins. Protein expression of AAV4 and 12 was detected with antibody A1 that binds VP1 of all serotypes [86], [272]. AAV3b with peptide insertion was created later than the other clones and was visualized on a separate Western blot.

3.2.2 Characterization of AAV serotype-peptide panels

3.2.2.1 Selection of further peptide motifs

Thus far, we had verified the feasibility to insert a distinct peptide of seven aa into 12 different AAV serotypes. To provide a broader proof-of-concept for the usefulness of alternative viral isolates as scaffolds for peptide display, and to demonstrate that the inserted sequences in fact alter capsid properties, we selected a panel of six additional peptides for analysis. The candidates listed in Table 16 were chosen from the literature and had been isolated either from phage display or AAV2 display libraries. Regardless of origin, all six peptides had previously been inserted into the AAV2 capsid and then been reported to mediate vector re-targeting to certain cell types. It was thus a particularly interesting question whether and to what extent the exact same peptides would also re-target the 11 other serotypes that we tested here. In more detail, peptides P1 to P3 contain an RGD motif that is a consensus sequence for integrin binding [220], [223], [280]. P2 is believed to especially target $\alpha\beta3$ and $\alpha\beta5$ integrins and was found to mediate increased AAV2 transduction of HeLa, K562, Raji and SKOV-3 cells. In contrast, P1 and P3 were reported to re-target AAV2 to primary PymT tumor cells (P1) or to MCF-7 and M07e (P3). Peptides P4 and P5 originate from an AAV2-based selection on HsaVEC cells, and both share the NDVR sequence [226]. P6, that targets MT1-MMP [281], and P2

were both selected by phage display and consist of nine amino acids, rather than seven as all other peptides (including the NSSRDLG peptide used for initial validation, see above). For more details on the cell lines and their origin, please see 2.1.1. Accordingly, these six sequences represented a good mixture of different lengths, motifs and efficiencies in various cell types.

Peptide No.	Peptide sequence	Oligonucleotide sequence	Target	Reference
P1	RGDLGLS	5'-CGCGGCGATCTGGGCCTGAGC-3'	Primary PymT tumor cells	[223]
P2	CDCRGDCFC	5'-TGCATTGCCGCGGCGATTGCTTTTGC-3'	$\alpha\beta3$ & $\alpha\beta5$ integrins	[220]
P3	RGDAVG	5'-CGCGGCGATGCGGTGGGCGT-3'	M07e	[280]
P4	NDVRSAN	5'-AACGATGTGCGCAGCGCGAAC-3'	HSaVEC	[226]
P5	NDVRAVS	5'-AACGATGTGCGCGGTTGAGC-3'	HSaVEC	[226]
P6	CNHRYMQMC	5'-TGCAACCATCGCTATATGCAGATGTGC-3'	MT1-MMP	[281]

Table 16: Overview over peptides P1 to P6. Shown are the peptide amino acid sequences with common motifs highlighted in bold and the corresponding nucleotide sequences. Note that the actual oligonucleotides used for cloning were extended on both sides, to also encode the flanking glycine and alanine residues (see Materials and Methods chapter 2.2.4.4 for full sequences). The cells and papers in which the peptides were originally selected are also shown.

Akin to the cloning of the NSSRDLG-encoding oligonucleotide before, the sequences corresponding to the six new peptides were designed such that after annealing, they contained overhangs matching the ends from *SfiI* digestion of the 12 different *cap* genes (see Figure 37 above). Correct insertion was confirmed by sequencing of all resulting 72 peptide-serotype combinations (6 peptides in 12 serotypes). Including the 12 wildtype capsid genes, a total of 84 different vectors containing a YFP reporter for later transduction analysis were next produced in a small-scale 6-well format. The vectors were again harvested as crude lysates and analyzed by Western blotting. As shown in Figure 41, correct VP1-3 expression was found in all cases independent of peptide sequence or length. Only proteins comprising peptide P6 were never detected, irrespective of the underlying serotype (Figure 41). They were found, however, in Western blots made from whole cell pellets after transfection of the various AAVP6 plasmids, and they were likewise detected in iodixanol- or CsCl-purified virus stocks [282]. Together, this suggests that P6-containing particles can assemble, but are potentially trapped in an intracellular compartment from which they are not efficiently released during the preparation of crude lysates. Nonetheless, we included P6-expressing clones into our further analysis as it remained possible that the viral titers in crude lysates were below the detection limit for Western blotting, but still in a range that would mediate infection of certain cell types.

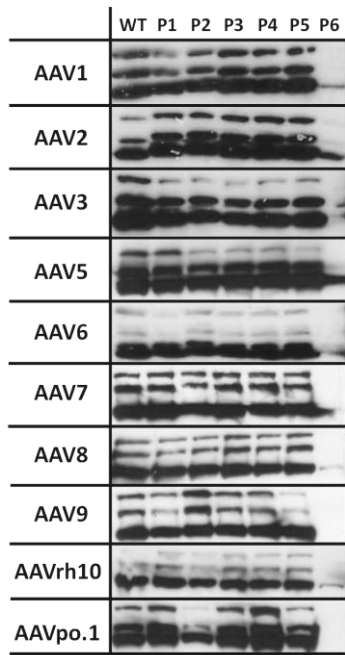


Figure 41: Western blot analysis of the complete set of 84 different AAV variants. Analyzed were crude lysates from wtAAVs (first lane) and derivatives displaying peptides P1 to P6. Except for P6, VP1-3 proteins were detected for all serotypes in the expected ratio of 1:1:10, independent of the peptide insertion. As noted in the text, vectors displaying P6 could only be detected in cell pellets or purified virus stocks (data not shown). These Western blots were performed together with Marina Bechtle, a former MSc student in our lab.

3.2.2.2 Analysis of peptide function

To evaluate the principal functionality of our new clones, we first tested them in HeLa cells which are amenable to infection with several AAV wildtype capsids. Because all vectors were produced as crude lysates (generation of 84 purified stocks was technically impossible), we could not determine exact titers; instead, we used equal volumes for the infection. Based on the Western blots shown in Figure 41, this likely resulted in the delivery of comparable vector amounts amongst all peptide-serotype combinations (with the exception of the P6 variants, see above). The infections of HeLa cells and all other cells shown below were always carried out in a 96-well format, and YFP expression was analyzed by FACS 48 h later. To determine transduction efficiencies, we measured both the percentage of infected cells (infection rate) as well as expression intensities. The results are depicted in heatmaps in which all values were color-coded, always ranging from 0% in black, to the maximal value in white. The intermediate colors denote the maximum values, with yellow corresponding to 25%, green to 50%, blue to 75% and red to 100%. The infection rate reflects the overall potential of each vector to bind, enter and functionally transduce the target cells, whereas the median intensity shows the strength of YFP expression per cell. If both are comparable between different vectors, it indicates a similar correlation between their infection rates and expression strengths. However, as observed previously (3.1.2.2), they can also differ, hinting at distinct cell attachment, uptake and/or intracellular vector processing.

The first results from the analysis of our 84 vectors in HeLa cells were already highly intriguing and promising, as they revealed a large variety of vector efficiencies depending on the capsid and peptide

(Figure 42). Differences over two orders of magnitude were found for one capsid displaying various peptides (or none at all), or, *vice versa*, for one peptide exposed on different capsids. For instance, display of P1 or P3 frequently resulted in a loss-of-function of the wildtype capsid (where detectable to begin with, *e.g.*, AAV1-3, 5 and 6). In contrast, especially peptides P4 and P5 substantially enhanced several serotypes, as was most evident for AAV1, 7-9 and rh10. The improvement was visible both on the levels of infection rate and transduction intensity. Of all capsid-peptide combinations, AAV1P5 gave the highest YFP expression per cell and was set to 100% (Figure 42B). AAV1P4 gave 89% of this maximum intensity, while wildtype AAV1 reached only 26%. Curiously, P4 and P5 had no enhancing effect on AAV6, despite that fact that it differs from AAV1 in only six amino acids [65], [89]. This result confirms our assumption that even marginal differences in capsid composition can already largely impact the performance of the displayed peptides, and thus supports our investigation of alternative AAV serotypes. Further notable are cases where peptide display not only altered the efficiency of an inherently functional wildtype capsid, but instead enabled this AAV isolate to transduce at all. Examples are the already mentioned AAV7-9 and rh10 which are nearly inert as wildtypes, but became very efficient upon display of peptides P2, P4 and P5. The infection rate of AAVrh10, for instance, was increased from merely 3% to more than 90% with P4 and P5.

Our two main conclusions from this pilot experiment with our panel of 84 vectors in HeLa cells were that 1) the function of a displayed peptide critically depends on the AAV capsid scaffold, and that 2) non-AAV2 serotypes represent intriguing scaffolds for peptide display that, when combined with certain peptides, can vastly outperform the AAV2 prototype and its peptide derivatives.

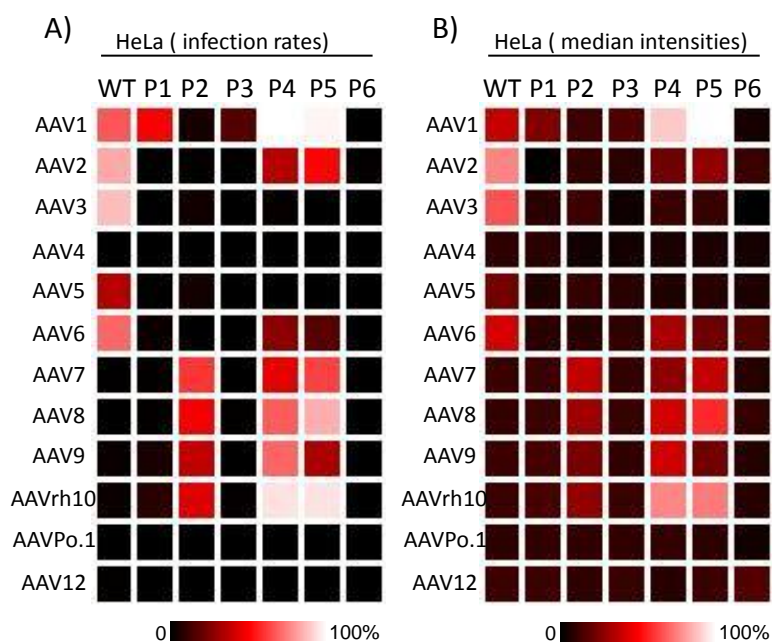


Figure 42: FACS analysis of the complete set of 84 different AAV variants. A) Infection rates of 12 wtAAVs and 72 peptide-displaying clones in HeLa cells, ranging from black (no transduction) to white (highest value). The intermediate color red indicates a maximum infection ratio of 100% (see main text for our four-color coding scheme). **B)** Mean YFP expression intensities in percent, normalized to the highest value obtained with AAV1P5 (set to 100%). (For color code of the heat maps refer to Figure 24 and Figure 29.)

3.2.3 AAV peptide display screens

The interesting and diverse results with our panel of 84 vectors in HeLa cells motivated us to expand the analysis of this panel to a large array of human or non-human cell lines or primary cells. Table 17 below summarizes the findings in 30 cell types of different origin, by showing the infection rate of the best performing wildtype serotypes and peptide derivatives. All individual data for all cell types are moreover displayed in the form of heatmaps in the Appendix. Furthermore, several selected examples will be presented and discussed in more detail in the following chapters 3.2.4 and 3.2.5.

No.	Tissue/ Cell type	Origin	Cell line	Wildtype	1st	2nd	3rd
1	cervix	H. sapiens	HeLa	wt2 96.0	1P4 99.0	1P5 99.0	rh10P4 99.0
2	ovary	H. sapiens	OVCAR-3	wt2 93.0	5P2 96.0	1P5 95.0	1P4 93.0
3	pancreas	H. sapiens	Panc-1	wt6 99.0	rh10P2 99.0	8P2 97.0	7P2 95.0
4	spleen	M. musculus	RawE	wt6 50.0	7P2 17.0	wt1 9.5	8P2 7.8
5	kidney	H. sapiens	Hek293T	wt2 98.0	wt1 97.0	wt3 97.0	wt6 91.0
6	liver	H. sapiens	Huh7	wt2 100.0	1P4 99.0	1P5 99.0	wt3 99.0
7	liver	M. musculus	H4IIE	wt1 34.0	wt6 29.0	1P4 23.0	wt2 16.0
8	liver	H. sapiens	HepG2	wt2 95.0	7P2 92.0	rh10P2 74.0	9P2 66.0
9	liver	M. musculus	Hepa1-6	wt6 88.0	1P4 69.0	1P5 56.0	8P4 39.0
10	liver	H. sapiens	pr hu hep	wt2 0.1	6P1 7.9	9P3 6.3	7P3 2.1
11	skin	H. sapiens	SK-MEL2	wt2 94.0	9P2 98.0	8P2 97.0	7P2 97.0
12	embryo/fibroblast	M. musculus	MEF	wt1 17.0	1P4 16.0	1P5 10.0	7P2 8.7
13	embryo/fibroblast	M. musculus	NIH/3T3	wt6 58.0	1P4 71.0	1P5 49.0	8P4 47.0
14	breast	H. sapiens	MCF7	wt2 100.0	1P5 88.0	1P4 86.0	7P2 86.0
15	breast	H. sapiens	MCF10A	wt6 98.0	7P2 62.0	1P1 48.0	wt2 46.0
16	breast	H. sapiens	MDA-MB-231	wt2 94.0	wt6 94.0	9P2 85.0	rh10P2 80.0
17	breast	H. sapiens	MDA-MB-436	wt2 99.0	wt6 99.0	9P2 93.0	1P4 93.0
18	bone marrow	H. sapiens	K562	wt6 78.0	rh10P2 84.0	1P5 82.0	1P4 81.0
19	blood	H. sapiens	NKL	wt6 68.0	wt4 51.0	wt5 45.0	4P3 19.0
20	blood	H. sapiens	pr n-a NK	wt6 5.4	6P2 0.5	6P5 0.5	6P3 0.5
21	blood	H. sapiens	pr a NK	wt6 0.4	6P2 0.3	6P5 0.3	6P4 0.3
22	blood	H. sapiens	SKW6.4	wt6 25.0	1P5 18.0	1P4 13.0	rh10P2 12.0
23	blood	H. sapiens	Sup-T1	wt5 9.2	1P4 59.0	1P5 51.0	8P5 45.0
24	blood	H. sapiens	Raji	wt6 47.0	wt5 18.0	3P5 8.6	wt2 7.4
25	blood	H. sapiens	Jurkat	wt1 0.7	1P5 28.0	1P4 20.0	7P5 13.0
26	brain	H. sapiens	T98G	wt6 99.0	wt5 96.0	wt2 86.0	7P2 73.0
27	brain	H. sapiens	SH-SY5Y	wt1 97.0	7P2 98.0	9P2 98.0	rh10P2 98.0
28	CNS	H. sapiens	SF-539	wt2 99.0	wt6 99.0	7P2 99.0	1P5 98.0
29	Human glioblastoma astrocytoma	H. sapiens	U373	wt2 51.0	8P1 90.0	1P1 84.0	9P1 80.0
30	astrocytes	H. sapiens	Astrocytes	wt6 15.0	9P1 57.2	1P1 52.7	9P2 48.1

Table 17: Results from cell screening with 12 wildtype AAVs and 72 peptide-displaying clones. Shown are 30 cell types and their origin. The cells are clustered according to their derivation from solid organs, or to their hematopoietic or neuronal nature. Infection rates of the best performing wildtype AAV and, in addition, the three best performing viral isolates (wt and peptide displaying clones) are indicated. Note that in some cases the best wt virus outperforms all other isolates. Wildtype (wt) viruses are always shown in light gray. Screening experiments and FACs analysis were performed together with Marina Bechtle (a former MSc student in our lab) and Dr. Kathleen Börner (Infectious Diseases/ Virology Dept.). Color code is in analogy to the heatmaps. Pr = primary; n.a.= non activated; hu = human; hep = hepatocytes.

One remarkable result was that in several cases, naturally occurring AAV capsids were already very efficient, in particular AAV1, 2 and 6 that frequently gave around 80 to >95% transduction. For instance, AAV6 was superior to all other wildtypes or peptide mutants in cells from pancreas and spleen. Its potency is particularly evident in RawE cells (spleen), where the second best performing

vector, AAV7 with peptide P2 (7P2), only gave 17% transduction as compared to 50% with AAV6. In the case of H4IIE, a hard-to-infect murine liver cell line, AAV1 and AAV6 gave comparable maximum efficiencies of 29-34%. These two wildtype serotypes were also the best in SH-SY5Y or T98G (cells from brain) which they transduced at nearly 100%, whereas wildtype AAV2 was on par in another CNS cell line, SF539. As a final example that should be highlighted, AAV6 was also superior to all other capsid variants in Raji cells, a human cell line that originates from Burkitt lymphoma and NKL, a human leukemia natural killer cell line.

Even more notable was, however, that the newly generated capsid-peptide combinations often outperformed the natural capsids. As already noted for HeLa cells (see above), we frequently found an increase in the efficiency of serotypes 1, 7-9 and rh10 when they displayed peptides P4 (NDVRSAN) or P5 (NDVRAVS). A similar pattern was observed for AAV7-9 and rh10 in combination with the P2 nonamer CDCRGDCFC. For instance, AAV1P4 and P5 matched the potency of wtAAV2 in Huh7 cells (almost 100%), and AAV1P4 was most efficient in NIH/3T3 cells (71%, outperforming wtAAV6 by more than 10%). Very striking findings were also made in some difficult-to-infect cells of hematopoietic origin, such as Sup-T1 cells which were transduced at 59, 51 and 45% by AAV1P4, AAV1P5 or AAV8P5, respectively, as compared to only 9.2% with wtAAV5 (the best wildtype). Another example are Jurkat cells that are refractory to wtAAV infection, but transduced at more than 20% with AAV1P4 and AAV1P5. Accordingly, these and other cells in Table 17 exemplify interesting cases where peptide display in non-AAV2 serotypes allows, for the first time, for efficient AAV-based transduction of cells that have previously not been accessible to this vector system.

Our results from this extended analysis confirm the conclusions from the HeLa pilot experiment, by validating that AAV transduction is not determined by the peptide alone, but rather by its embedding in a certain capsid context. In addition, it was interesting to note the recurring patterns of efficient peptide-capsid combinations, such as AAV1, 7-9 and rh10 with peptides P2, P4 and P5. Because these patterns were observed in numerous different cell types, it tempted us to study whether these combinations mediated binding to common receptors (3.2.3.1 below). Another intriguing conclusion was that specific peptide-capsid pairs mediated efficient transduction of clinically relevant cell types that were resistant to wildtype AAV serotypes, motivating us to investigate their potential in more detail for selected examples (chapter 3.2.5 below).

3.2.3.1 *Analysis of cellular binding features of capsid-peptide mutants*

3.2.3.1.1 HSPG

The first cellular receptor that we investigated were heparan sulfate proteoglycans (HSPG), as they are known to act as primary receptor for the AAV2 prototype as well as for AAV3 [93], [206]. To test

whether any of our new capsid-peptide combinations also depends on HSPG, we performed a heparin competition assay where soluble heparin is added to cells and then functions as an analog to membrane-bound HSPG that can block this receptor [93]. Previous to the infection of HeLa cells, viral isolates were incubated for one hour in complete growth medium supplemented with soluble Heparin. Virus incubated with complete growth medium alone served as control. The cells were washed twice with 1x PBS 24 h post-infection, and infection rates were determined by FACS another 48 h later in analogy to the previous analyses.

As shown in Figure 43A-B, wt serotypes AAV2 and AAV3 were profoundly inhibited by heparin, as expected. Specifically, infection rates dropped from 70% (AAV2) or 40% (AAV3) to less than 1%. Decreases were also noted for the peptide-displaying derivatives of these two viruses, but the changes were much less pronounced, implying that HSPG no longer served as (sole) primary receptor for these mutants. The majority of all other capsid-peptide combinations also remained largely unaffected, as compared to the substantial drops for wt AAV2 and AAV3. We thus concluded that none of our peptides had restored or *de novo* introduced heparin binding ability in any of our clones, although further analyses are probably required to solidify this notion (Discussion chapter 4).

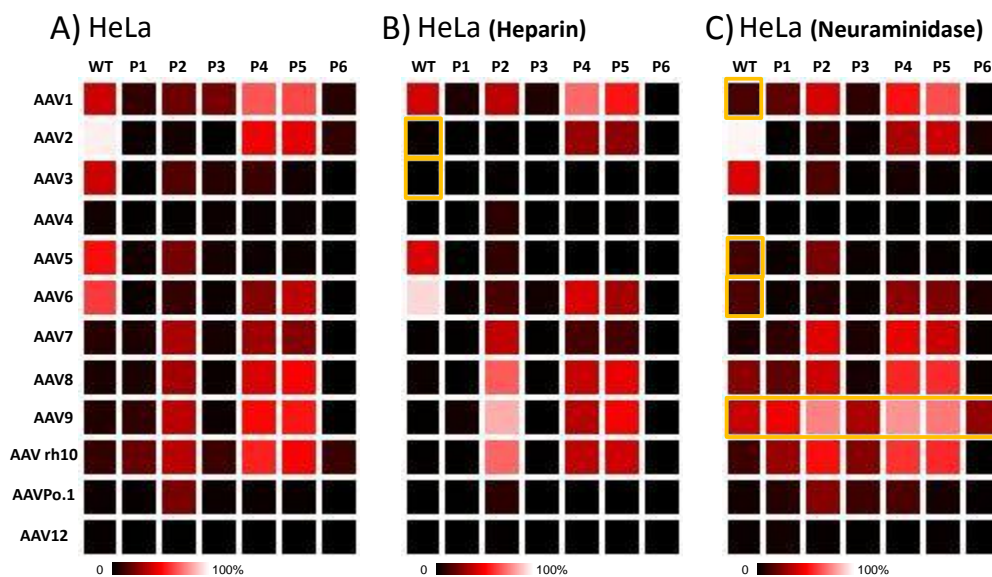


Figure 43: Influence of heparin or neuraminidase on transduction of wildtype or peptide-modified AAV vectors in HeLa cells. A) Control infection of HeLa cells without inhibitors. **B)** Infection of HeLa cells in the presence of a soluble heparin competitor. The orange boxes highlight the profound inhibition of AAV2 and AAV3 (compare to their transduction rate in panel A). **C)** Infection of neuraminidase-treated HeLa cells. The orange boxes demarcate vectors whose infectivity was affected by removal of sialic acid. Note that possible changes for AAV4, whose primary receptor is N-linked sialic acid, could not be determined due to the low infectivity of this vector in HeLa cells. Also note how neuraminidase treatment increases the transduction efficiency of AAV9 and various derivatives (see text for explanation). (The neuraminidase- and heparin assays were partially performed together with Marina Bechtle, a former MSc student in our lab.) (For color code of the heat maps refer to Figure 24 and Figure 29.)

3.2.3.1.2 Sialic acid

A second common AAV attachment receptor that we studied is sialic acid. Therefore, HeLa cells were treated with neuraminidase type III from *Vibrio cholera* for 2 h at 37°C (to remove sialic acid from the cell surface), washed twice with 1x PBS and then infected with the viral lysates. After one hour, unbound virus was removed by washing the cells again with 1x PBS, and transduction efficiencies were determined by FACS analysis 48 h post-infection as usual. Removal of unbound virus was necessary as the cells would have otherwise recovered from the neuraminidase treatment and started to produce new sialic acid, which would have blurred the analysis.

As expected, the absence of sialic acid profoundly decreased the infectivity of serotypes AAV1, AAV5 and AAV6, all of which bind O-linked sialic acid as primary receptor, by 25-45%. The infectivity of AAV4, whose main receptor is N-linked sialic acid, could not be assessed as it was already below the detection limit even without neuraminidase treatment. In general, infection rates were diminished overall as compared to previous experiments due to the shortened infection and incubation times. Notably, none of the peptide-displaying mutants were markedly affected by neuraminidase treatment, suggesting their independence of sialic acid. A striking exception was wildtype AAV9 and its derivatives whose transduction efficiency was actually increased in the treated cells. While curious at the time of this work, it was later reported that AAV9 binds N-terminal galactose which is masked by sialic acid on the cell surface, and hence becomes accessible upon neuraminidase treatment [283], [284] (see also Discussion). Accordingly, our data suggest that peptide insertion had not completely abolished primary receptor binding in AAV9 but nonetheless improved the efficiency of the capsid.

3.2.3.1.3 RGD receptors

As mentioned earlier, some of the peptides we used had previously been selected in the context of AAV2, including P2 which contained an RDG motif (known to bind to integrins) and which was reported to improve AAV2 transduction in HeLa, K562, and Raji cells [220]. However, in our own hands, these enhancements were not observed (Figure 42, Figure 44, Table 17 and Appendix). One possible explanation for this discrepancy were differences in the aa that flanked the peptide in the published or our own vectors, respectively. In our vectors, both arginines (R) at position 585 and position 588 were mutated, to completely abolish HSPG binding. In contrast, the original plasmid still contained both wildtype arginines, plus an additional threonine/glycine (TG) linker downstream of the peptide insertion. To reproduce the original conditions, we generated a new set of peptide mutants based on AAV2 that carried the described TG linker, and in which either both arginines were mutated (AAV2-TG-P2_ΔR585/ΔR588) or only arginine 588 alone (AAV2-TG-P2_ΔR588). Vectors were produced as usual and then titered in HeLa cells in direct comparison to wildtype AAV2 and our unmodified AAV2P2 (ΔR585/ΔR588) (Figure 44A).

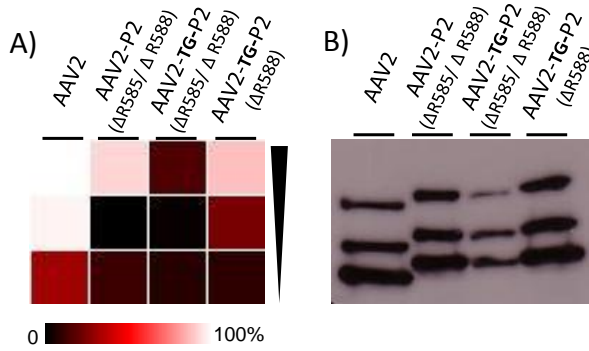


Figure 44: Comparison of different variants of AAV2P2. Three distinct versions of AAV2P2 were analyzed in which (i) R585 was either mutated (AAV2-P2 Δ R585/ Δ R588), (ii) mutated and juxtaposed with a linker sequence (AAV2-TG-P2 Δ R585/ Δ R588), or (iii) kept together with this linker (AAV2-TG-P2 Δ R588). The third variant should resemble the construct in the original paper that identified P2 [220]. **A)** Titration of these three variants together with wildtype AAV2 in HeLa cells. **B)** Confirmation of virus integrity by Western blotting (using B1 antibody for VP1-3 detection). Note the slightly weaker signals for AAV2-TG-P2 Δ R585/ Δ R588 which could explain the reduced infectivity of this mutant (as compared to the other two) in panel A). (Experiments were done together with Marina Bechtle a former MSc student in our lab.) (For color code of the heat maps refer to Figure 24 and Figure 29.)

In line with our prior data, the transduction efficiency of our own AAV2P2 construct but also that of the new AAV2-TG-P2_ Δ R588 mutant was reduced by more than one order of magnitude as compared to wildtype AAV2. Infectivity dropped even further with AAV2-TG-P2_ Δ R585/ Δ R588 which could hardly transfect HeLa cells anymore, albeit this may correlate with the reduced levels of viral protein in the respective supernatant (Figure 44B). Even taking this into consideration, our data clearly show that none of the different P2 contexts reproduced the described gain-of-function with our clone AAV2P2. Of course, it remains possible that there were further differences between our own and the published construct, especially since the information given in the original report was incomplete. Potentially unique modifications on our side include the upstream linker amino acid alanine (part of the *SfiI* site) or a glutamine instead of an asparagine at position 587 (chosen for steric reasons in the original design by the Kleinschmidt lab on which our own approach is based). Generally, this reaffirms our conclusion that not only the peptides or capsids themselves, but also even minor changes within the sequences surrounding the peptide can substantially impact the performance of the whole particle.

3.2.4 Consensus sequence NXXRXXX

A remarkable observation we made during many titrations was how frequently peptides P4 (NDVRSAN) and P5 (NDVRAVS) improved the transduction efficiency of a set of different serotypes, especially AAV1, 7-9 and rh10. Intriguingly, both peptides share the motif NDVR as the first four amino acids of the heptamer, suggesting that it might be critical for peptide function. Of the remaining three amino acids, two more are identical (S and A) but arranged in a different order, whereas only one residue is truly diverse (N at position 7 in P4 or V at position 6 in P5).

In order to further dissect the relevance of the seven single residues, we performed an alanine walk whereby we individually mutated each aa within peptide P4 into alanine (using GCG as triplet). Furthermore, we made another construct in which we altered all three aa at the C-terminal peptide end simultaneously, since this part comprises the actual differences between P4 and P5. All new peptides were displayed in the AAV1 context, and the corresponding particles were titered in HeLa cells in comparison to wildtype AAV1 or AAV1 displaying the unmodified P4 peptide. The results as shown in Figure 45 confirm our hypothesis, that the first four aa are most important for peptide function, while mutation of the last three aa has no clear effect on transduction. Most crucial aa are the asparagine (N) at position one, arginine (R) at position four as well as valine (V) at position three. Substitution of each of these three aa led to a reduction in transduction efficiency of one (V) or even two orders (N/R) of magnitude. Hence, we concluded that NX(V)RXXX represents a new peptide consensus sequence that frequently improves transduction with AAV1 (and likely other serotypes as well, especially AAV7-9 and rh10).

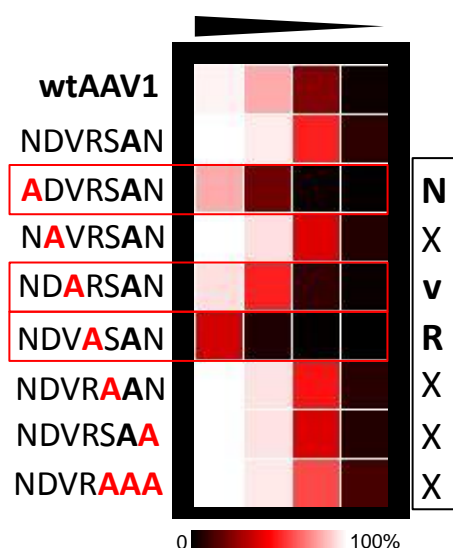


Figure 45: Alanine walk to dissect the function of the NDVRSAN peptide. Shown on the left are the new peptides that were derived by stepwise mutation of the original P4 sequence. All peptides were displayed on AAV1, and resulting vectors were compared to wildtype AAV1 (shown on top). Therefore, vector supernatants were titered in HeLa cells in 10-fold dilutions (from left to right, indicated by the black caret on top). Displayed are transduction efficiencies. Note the substantial drops after point mutation of N or R at positions 1 or 4, respectively. (Heatmap is partially based on results that were acquired together with Marina Bechtle, a former MSc student in our lab.) (For color code of the heat maps refer to Figure 24 and Figure 29.)

Of note, further verification of these findings and conclusions was obtained through a collaboration with Anna Sacher from the group of Martin Müller (German Cancer Research Center). They used our 12 new constructs for display of another array of peptides named A1 to A6 (from their own initial screening of an AAV2 peptide library in dendritic cells), and confirmed that many of their candidates worked particularly well with our AAV1, 7-9 and rh10 scaffolds, akin to our own data [285]. Interestingly, two of their six peptides were highly similar to peptides P4 and P5, namely, **NYSRGVD** (A2) and **NEARVRE** (A6). Strikingly, screening of A2 and A6 in the context of our modified viral capsid backbones, in a multitude of different cells, revealed a general improvement similar to that with peptides P4 and P5. As noted above, our two peptides NDVRSAN (P4) and NDVRAVS (P5) led us to

hypothesize that amino acids **NX(V)RXXX** are most important. The comparison with the two new candidates A2 and A6 now solidified that the crucial features are actually mediated by the amino acids N and R at positions 1 and 4, respectively, that are shared by all four peptides. This refined hypothesis is fully congruent with our mutation analysis as it had shown a stronger influence of these two residues as compared to V at position three (Figure 45 above). We thus finally identified the sequence **NXXRXXX** as a consensus motif that frequently enhances at least the serotypes AAV1, 7-9 and rh10 in a large variety of cell types, by interacting with an as-of-yet unknown receptor or by improving any other step during vector transduction (see Discussion for possible mechanisms).

3.2.5 Specific applications of AAV peptide display

The work described in the previous chapters showed the great potential of serotypes other than AAV2 as templates for peptide display, in particular their ability to transduce cells that are refractory to infection with wt viruses and that were hence not considered as targets for AAV-mediated gene transfer in the past. Encouraged by these results, we initiated a number of collaborations with other groups on Heidelberg campus in order to more thoroughly investigate the usefulness of our capsid-peptide panel in clinically relevant cell types. Specifically, as detailed in the following three chapters, we studied blood cells (including T-cells, collaboration with Dr. Kathleen Börner, Infectious Diseases/Virology Dept.), myeloma cells (collaboration with Dr. Anja Seckinger, Medizinische Klinik V) and neuronal cells (collaboration with Prof. Armin Blesch, Orthopedics Dept.). Note that only selected representative examples will be shown in each case below, while the complete data set (all cell types and titration data) can be found in the Appendix of this thesis.

3.2.5.1 Blood cells

Figure 46 below shows exemplary results from the titration of our panel in three human cell lines of lymphoid origin, K562 (chronic myelogenous leukemia cell line), SupT1 (T-lymphoid cell line) and SKW6.4 (B-lymphoid cell line). In particular for SupT1 and SKW6.4, it is again evident that these cells were largely refractory to infection with any of the 12 wildtype capsids, but that potent transduction could be achieved with some of our new peptide-displaying vectors. The most impressive results were obtained for SupT1, which were almost completely resistant to AAV wildtype infection. However, when transduced with AAV1P4 or AAV1P5, more than 70% of the cells became YFP-positive (Figure 46B). Similarly remarkable observations were made in SKW6.4 cells; albeit they were generally less infectable, display of P4 or P5 on AAV1 resulted in a five-fold and six-fold increase in efficiency, respectively, over the best wildtype capsid (AAV6, 2.81%) (Figure 46C).

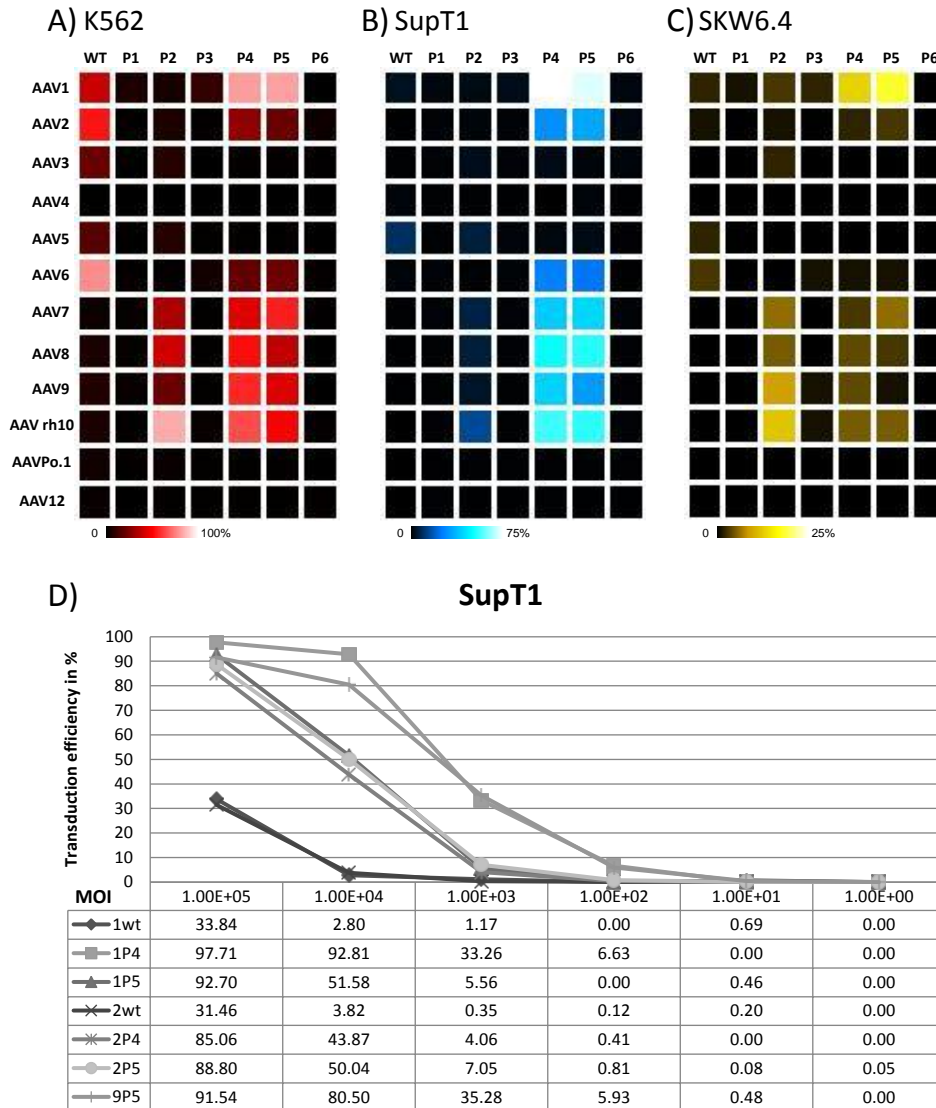


Figure 46: Transduction of cells of lymphoid origin. The three cell lines shown in **A-C**) were transduced with our panel of 12 wildtype and 72 peptide-modified AAV vectors (all encoding a YFP reporter). **D**) Titration of SupT1 cells with purified vectors (abbreviated labels on the left). Numbers in the table next to the capsids represent % transduction efficiency (same data as in the graph above). (For color code of the heat maps refer to Figure 24 and Figure 29.)

In view of the notable results in SupT1 cells, and because they are frequently used in HIV research in our Department, we decided to perform a more thorough analysis of vector dose responses in these cells. Towards this end, we picked the two best vectors, AAV1P4 and AAV1P5, and also included wildtype AAV1 for direct comparison. Moreover, we chose the equivalent set for AAV2 (*i.e.*, the wt and the two peptide derivatives), as well as AAV9P5 as a representative of the other serotypes that were also improved by the P4/P5 peptides. All vectors were produced as purified high-titer stocks and then used to infect SupT1 cells at doses over a range of six orders of magnitude (Figure 46D). Importantly, the results confirm the pattern observed with the crude lysates (Figure 46B); only the absolute numbers were higher, as could be expected from the use of purified stocks. The two

wildtypes gave ~30% transduction at the highest dose, and then showed a linear decline to ~3% at a ten-fold lower dose and to undetectable levels at all subsequent vector dilutions. Interestingly, these dose responses were markedly different for the peptide derivatives. For AAV1P5, AAV2P4 and AAV2P5, transduction decreased from 85-90% at the highest concentration, to still ~50% at an MOI of 1×10^4 , *i.e.*, only a two-fold drop. However, the next ten-fold vector dilution yielded a ten-fold drop in transduction, *i.e.*, again a linear response akin to the wildtype viruses. Unique results were also noted for AAV1P4, the overall most efficient capsid in these cells. Starting with nearly complete transduction (~98%) at the highest vector dose, the number of positive cells dropped by only ~5% at a ten-fold lower vector dilution. Even at a further 100-fold dilution, still ~6% of the cells were transduced, while all the other capsids had already become inert. Of note, the high robustness and efficiency of AAV1P4 (and AAV1P5) in human T-cell lines was also observed and extensively validated by others (especially Dr. Kathleen Börner; manuscript in preparation), verifying the findings in this thesis.

In general, these additional comprehensive data further highlight the potential of peptides with the consensus sequence NXXRXXX to substantially increase the infectivity of different serotypes in many cell types. Moreover, as can be seen in Figure 46A-C, also peptide P2 (CDCRGDCFC) gave a robust improvement of selected wildtypes in the three blood cell lines and likewise in several others (see Appendix). We therefore designated a “Master panel” in which we juxtaposed our three best peptides - P2, P4 and P5 - with the three lead candidates from our collaboration partner Dr. Anna Sacher, A1, A2 and A6. All six peptides were displayed in all 12 serotypes, again resulting in a total set of 84 vectors (12 wildtypes and 72 peptide variants). To date, this Master panel has been screened in ~80 different cell types (cell lines and primary cells of different species origins) and has in all cases led to the isolation of potent capsids (manuscript in preparation). It was also used for the screening of myeloma cells as described in the next chapter.

3.2.5.1.1 Myeloma cells

Multiple myeloma is a cancer of plasma cells of lymphoid origin. As is typical for B-lymphocytes, most myeloma cell lines and primary cells are difficult to transduce, hampering advances in myeloma analysis and treatment. Together with our collaboration partner Dr. Anja Seckinger (Medizinische Klinik V), we therefore screened our Master panel in different myeloma cell lines and primary cells (Figure 47).

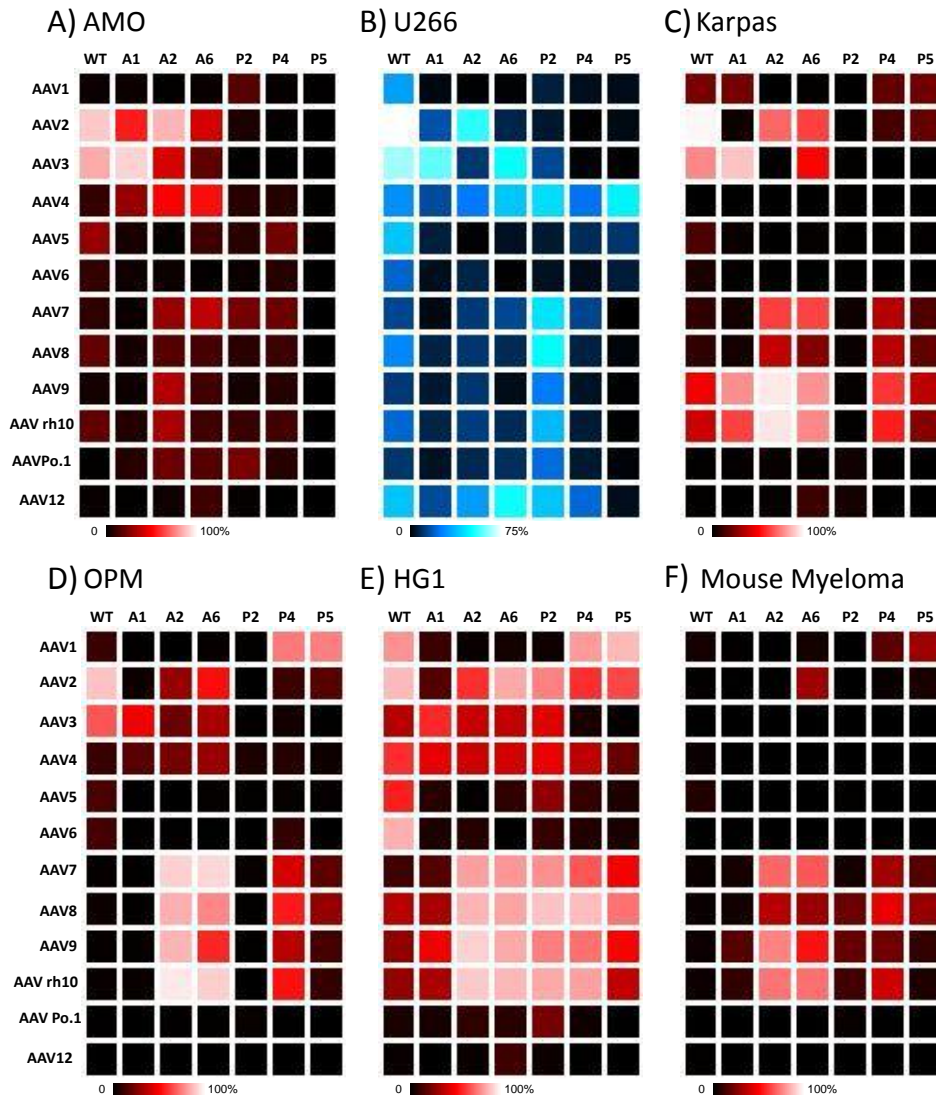


Figure 47: Transduction of human or murine myeloma cells with the AAV peptide Master panel. Shown in A-F) are representative examples of the unique transduction patterns that were obtained. (For color code of the heat maps refer to Figure 24 and Figure 29.)

The six examples shown above exemplify the different transduction patterns that were observed and that were cell line- and species-specific. For instance, AMO (Figure 47A) cells were most potently infected by wildtype AAV2 and AAV3, as well as by their derivatives, displaying peptides A1, A2, and A6 (maximum was 93% with AAV3p1). Decent transduction was also obtained with AAV4 displaying these three peptides, which was remarkable as AAV4 and its descendants frequently remained inconspicuous in other screens. In contrast, the other NXXRXXX peptides P4 and P5 did not enhance transduction of any serotype, which was also unusual (in view of our prior data in other cells, see above). As compared to the other five cell lines, transduction of U266 cells was less efficient, but wtAAV2 and AAV3 remained most potent with up to 75% positive cells (Figure 47B). In addition, peptide P2 improved the efficiency of several serotypes in these cells, AAV7-9, rh10, po1 and 12.

Further interesting was that AAV4 and AAV12 were both able to transduce U266 cells, independent of the displayed peptides. The two serotypes are close relatives but distinct from most other AAV isolates [108], suggesting that a common, as-of-yet unknown shared capsid feature is responsible for their efficacy in these specific cells. In Karpas cells (Figure 47C), AAV2 and AAV3 with A1, A2 and A6 were again most efficient, with AAV2 peaking with an almost 100% infection rate. While AAV9 and AAVrh10 were also enhanced by A1 (to up to 78%), even more notable was the increase to 95% observed with the same serotypes displaying peptide A2. Contrary to AMO and U266 cells, P4/P5 display also resulted in improved transduction for a few serotypes (e.g., AAV7-8), albeit the increase was marginal. OPM cells (Figure 47D) gave a comparable pattern as Karpas cells, with the exception of AAV1 which was improved by P4 and P5, but became less potent by A1 display. HG1 cells (Figure 47E) were also unique as they were efficiently infected by more than half of all clones in the Master panel, including the whole set of serotypes AAV7 to rh10 displaying all six peptides (especially with A2, A6, P2, P4 and P5). The final examples were primary mouse myeloma cells and hence the only non-human cell type (Figure 47F). Strikingly, none of the 12 wildtypes could infect the cells, not even AAV2 or AAV3 which worked on all five human specimens (see above). Instead, robust transduction was observed with AAV7 to rh10 displaying peptides A2 and A6, as well as, to a lesser extent, P4 and P6. The difference in efficiency between A2/A6 and P4/P5 was, however, not as pronounced as in Karpas or OPM cells (compare Figure 47 panel F to panels C/D).

As noted above, it was interesting that AAV2 and AAV3 were efficient in all five human cell lines. The fact that both serotypes use HSPG as primary receptor tempted us to study the role of this receptor in human myeloma transduction. We therefore performed a heparin competition assay in the human myeloid cell line L363 that gave a comparable transduction pattern as OPM cells (Appendix). The assay was essentially conducted as described before (3.2.3.1.1), and infection rates were again determined by FACS 48 h after virus addition. As expected, wildtype AAV2 and AAV3 transduction dropped from 70% to less than 1% in the presence of heparin. Also AAV3A1 infection was completely abolished after heparin incubation. Remarkably, the ~90% transduction efficiency of AAV7 to rh10 with A2 and A6 decreased to that of the same serotypes displaying P4 and P5. In contrast, the potency of all serotypes displaying P4 and P5 (including AAV1P4 and AAV1P5) remained unaffected by heparin treatment (Figure 48).

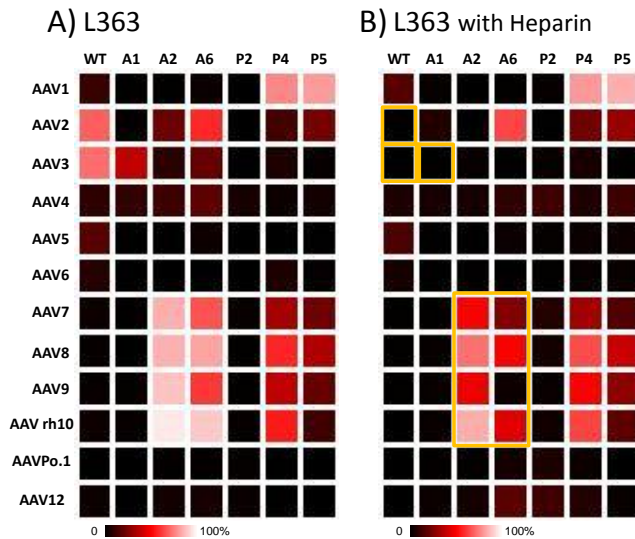


Figure 48: Transduction of L363 cells with the peptide Master panel. A) Titration in the absence of heparin. **B)** Titration of vectors previously incubated with heparin. Main differences between the two data sets (see main text) are highlighted by orange frames. (For color code of the heat maps refer to Figure 24 and Figure 29.)

Based on these results, we hypothesized that the higher infectivity achieved with the NXXRXXX peptides A2 and A6 is least partially due to a heparin-dependent effect. However, as the A1-displaying vector was also inhibited by soluble heparin we further speculated that the ability to bind heparin might be related to a unique feature of the oligonucleotides from the “A” series, located most likely in the flanking sequences of the three peptides (see also Discussion, chapter 4.2). As a whole, these results thereby once again demonstrate the enormous potential of AAV peptide modification to create novel properties and to further dissect AAV biology.

Finally, towards the application of our new vectors, we assessed their potential in primary human myeloma cells from different patients. These cells were isolated from fresh blood samples, grown for 48 h and then transduced. Representative FACS results for three donors are shown in Figure 49. The overall infection rates in these primary cells were lower than those in cell lines, but the basic pattern was recapitulated. We also observed donor-dependent differences in infectivity. Notably, ~12% of the cells from the donor with the weakest infectivity were transduced with AAV3A1, and even up to 43% from the donor with the highest overall transduction (Figure 49C). Serotypes displaying the A2 or A6 peptides were again amongst the most efficient, suggesting that their partial heparin binding might also facilitate primary cell transduction. Consequently, these capsids will now be studied further by our collaboration partner and used for RNAi-mediated regulation of myeloma-associated factors (Dr. Anja Seckinger, personal communication).

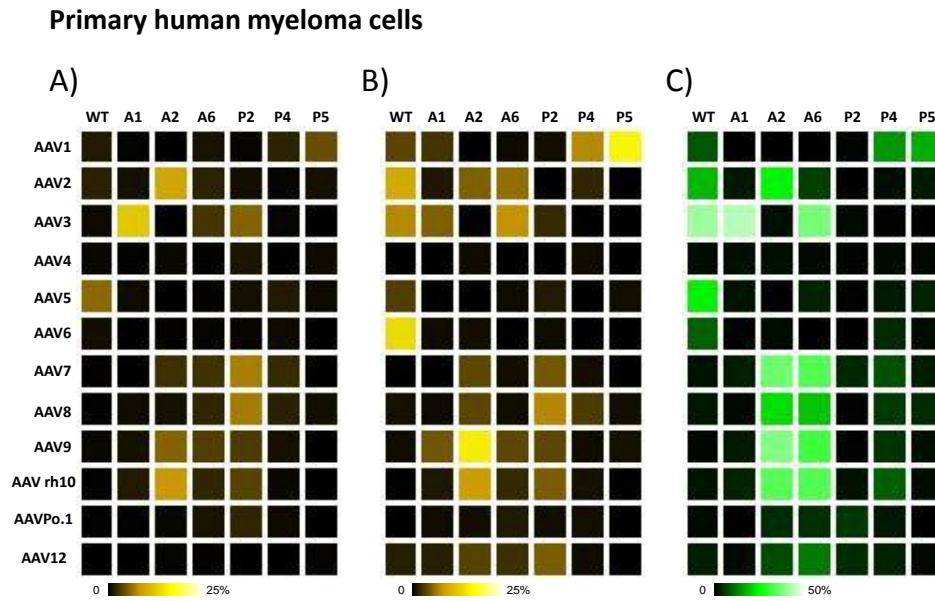


Figure 49: Transduction of primary human myeloma cells from three different donors (A-C). Transduction efficiencies were determined by FACS. (For color code of the heat maps refer to Figure 24 and Figure 29.)

3.2.5.2 Neuronal cells

Our initial screen of different cells and cell lines had revealed the potential of several AAV peptide-display clones to transduce difficult-to-infect cells of neuronal origin (chapter 3.2.3, Table 17 and Appendix). Notably, P1 in conjunction with AAV1, AAV2, as well as AAV7-9 and AAVrh10 gave the highest infection rates. Hence, we decided to utilize the original peptide panel P1-P6 rather than the Master panel for screenings in additional neuronal cell types. A first example was U373, a cell line derived from human glioblastoma/astrocytoma that could be transduced to 89% with AAV8P1. P1 also increased the infectivity of AAV1, AAV2 and the set of AAV7 to AAVrh10 to more than 80%. For AAV1, display of P1-P3, all of which contain the ‘RGD’ motif, led to a gain-of-function. In contrast, display of peptides P4 and P5 had no effect on U373 transduction, independent of the underlying AAV serotype (Figure 50A). Second, we tested a subset of the P1-P6 panel on human neuronal stem cells (HNSC-100, provided by Christine Kammel, Helmholtz Zentrum München) (The complete panel could not be evaluated due to a limited number of available cells). AAV9P1 peaked with a transduction efficiency of 50%, and AAV9P2, AAV1P1, AAV8P1 and AAV8P2 infection rates were also remarkably high (Figure 50B). Our third example were astrocytes derived from HNSC-100. For those AAV serotype/peptide combinations that were already tested in HNSC-100, infectivity in astrocytes basically mirrored the infection pattern of their progenitor cells, except for a decrease in wtAAV2 infection and an increase for AAV2P1 (Figure 50B and C). Astrocyte transduction was further increased again for the set of AAV7 to AAVrh10 in conjunction with P1 and P2. However, while P4 and P5 increased AAV1 infectivity in HNSC-100 as well as in astrocytes, display of the same peptides

in other AAV serotypes was not beneficial in these cells. Altogether, our results thus suggest that the RGD-containing peptides P1 and P2 are most suitable to improve neuronal cell transduction with AAV.

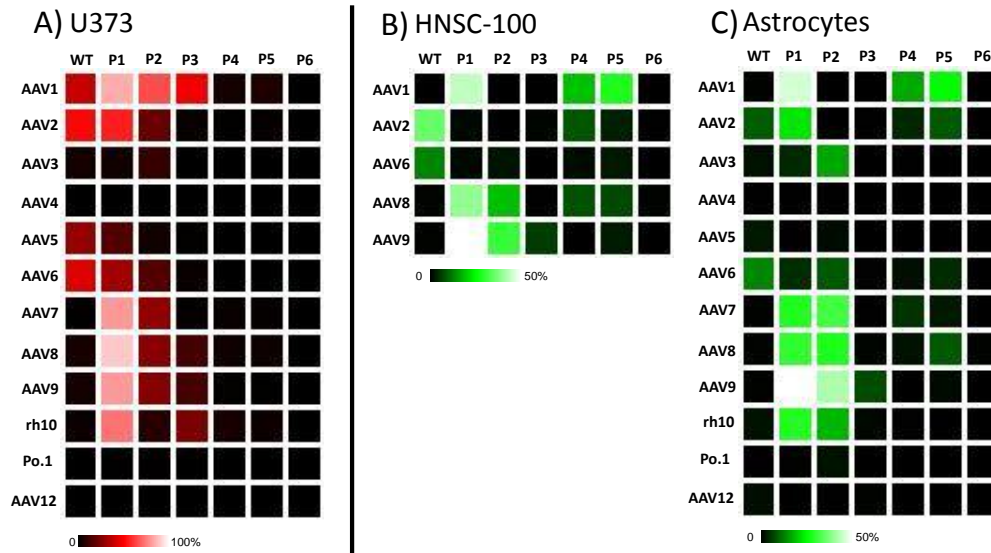


Figure 50: Transduction efficiencies of wtAAVs and AAVs displaying the peptide panel P1-P6 on cells of neuronal origin. A) U373 cells. B) Human neuronal stem cells, HNSC-100. C) Astrocytes, derived from HNSC-100 cells, provided by Christine Kammel, Helmholtz Zentrum München. (For color code of the heat maps refer to Figure 24 and Figure 29.)

3.2.5.2.1 Peptide-serotype combinations with DRG-targeting peptides

Neuronal cells of the dorsal root ganglion (DRG) are sensory neurons of the periphery that possess two axonal branches: one that innervates a peripheral sensory organ and another, central branch, which projects into the spinal cord. While the peripheral branch possesses the ability to repair upon injury, the capability of the central branch to regenerate is limited, just like for other neurons of the CNS. Due to these divergent assets of two branches of a single cell, DRGs serve as excellent models to study cell-autonomous mechanisms upon injury and their influence on cell regeneration in the CNS (For details refer to [286]). However, most experimental and therapeutic approaches towards nerve regeneration rely on effective gene delivery techniques. Together with our collaboration partners Prof. Dr. Armin Blesch and Julianne McCall (Orthopedics Dept., Klinik Heidelberg), we aimed at the development of a more effective AAV-based *in vivo* gene delivery system for adult DRG neurons.

We first tested our set of clones displaying peptides P1-P6 in DRG neurons. Our results confirmed the potential of AAV wt serotypes AAV1 and AAV6 to transduce DRG neurons [287], yet we could not further increase wildtype infection with the peptide motifs we had used so far (data not shown). We therefore investigated additional peptides that were previously reported to specifically target DRG neurons [288]. In particular, we chose three motifs that were isolated in the context of Adenovirus

[289] and inserted these peptides into our 12 AAV serotypes according to our scheme (identical insertion sites and peptide flanking regions as for all other peptide insertions from the 'P' series of peptides, see above). The sequences of these three additional peptides P7-P9 are shown in Table 18.

Peptide	Sequence	Oligonucleotide sequence	Reference
P7 (SPG)	SPGARAF	5'- AGCCCGGGCGCGCGCGTTC -3'	[288], [289]
P8 (DGP)	DGPWRKM	5'- GATGGCCCGTGGCGCAAAATG -3'	
P9 (FGQ)	FGQKASS	5'- TTTGGCCAGAAAGCGAGCAGC -3'	

Table 18: Peptides P7 to P9. Shown are the peptide amino acid sequences selected for DRG targeting and the corresponding nucleotide sequences. Not shown are the flanking spacer amino acids. Letters in bold refer to the abbreviation used in the following text instead of the entire peptide sequence.

Correct peptide insertion and AAV capsid protein expression were confirmed by sequencing and Western blot analysis (data not shown). We then again produced vectors with *yfp* transgenes and analyzed transduction efficiency by FACS in analogy to previous experiments. In a first approach, we confirmed the ability of these newly displayed peptides to alter AAV tropism in general. We therefore tested our set of DRG-targeting peptides along with wtAAVs in cell lines that were already part of our previous AAV peptide screen (Table 17 and appendix). We found that display of P7-P9 mainly affected the infectivity of serotypes AAV1, AAV6 and AAV8 to AAVrh10 (Figure 51). In most of the cells derived from solid organs, infection rates of AAV8 and especially of AAV9 were increased. For instance, in Huh7 cells, display of P8 in the context of AAV9 boosted infectivity from 30% to 89%. In contrast, AAV7 was not further enhanced by P7-P9. Except for the lymphoblast cell line K562, DRG-targeting peptide display had no effect on transduction of lymphoid cells, regardless of the serotype. Surprisingly, with only a few exceptions display of P7-P9 also had no clear effect on infection of cells of neuronal origin. However, AAV1P9 and AAV9P8 in U373 as well as AAV6P7 and AAVrh10P7 in SHSY5Y, exhibited increased infectivity over the respective wt serotypes. Still, in most other cells tested, independent of their origin, DRG-displaying clones could not outperform transduction by the corresponding wildtype. Instead, maximum transduction efficiencies were mostly achieved with wt AAVs. Nonetheless, it was important to find that our new peptide clones are functional in principal, since these peptides were never before displayed in any AAV context, neither in AAV2 nor in other serotypes. These first results thereby again confirm the validity and versatility of our peptide display approach.

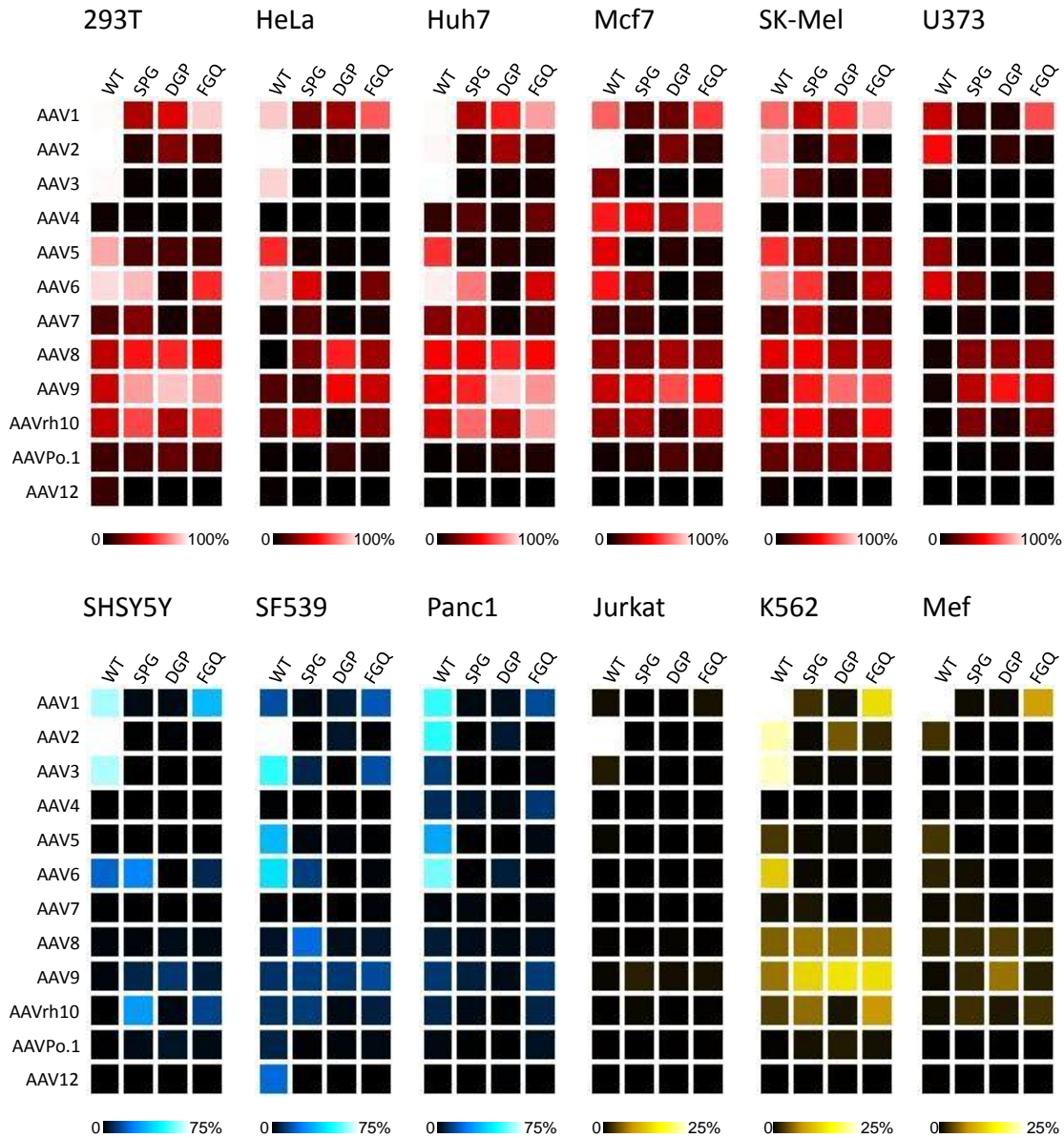


Figure 51: Titration of cells of disparate origin with AAV serotype / DRG-targeting peptide combinations. Shown are infection rates of 12 wtAAVs and the respective clones displaying peptides SPG, DGP and FGQ (complete peptide sequences are listed in Table 18) (For color code of the heat maps refer to Figure 24 and Figure 29.)

In an attempt to study transduction on DRGs we directly targeted these cells with AAVs displaying the DRG-peptide panel in a neurite outgrowth assay that was optimized by Prof. Dr. Armin Blesch and Julianne McCall (Orthopedics Dept., Klinik Heidelberg), allowing for observation of viral transduction rates in murine DRGs *ex vivo*. Briefly, DRGs were isolated from the spinal column of adult Fischer 344 rats (10–14 weeks) and dissociated mechanically and by enzymatic treatment. From one animal, between 1.25 and 1.75×10^6 cells including neurons and glia cells were typically obtained. Isolated cells were plated at a density of 1.8×10^3 cells per well in 2 ml complete medium. At 24 h post-plating, 10 μ L of rAAV crude lysate was added to the culture medium (0.5 ml total

volume), and cells, were analyzed by microscopy 72 h post-infection. Due to their morphology and since these cells are rather sensitive, a FACS-based analysis was not possible. For detailed analyses, the general DRG population was determined by labeling with an AB against Beta-III-tubulin, including all DRG subpopulations. Amongst all Beta-III-tubulin-positive (BIII-Tub) neurons, the highest transduction efficiency of 23% positive cells was achieved with wildtype AAV6. The second best infection rate of 19% positive cells was noted for AAV9P9, outperforming wtAAV7 and wtAAV5 with about 10% infectivity each. In contrast, AAV9 wildtype -together with other wtAAVs and the remaining viral clones - hardly transduced these neurons at all (Figure 52).

Isolated DRGs could be further subdivided based on expression of neuropeptides. Of special interest among the DRGs subtypes were the proprioceptive sensory neurons, the largest sensory neurons that provide information regarding body position, muscle length and tension. From the general BIII-Tub-positive neuron population, proprioceptive neurons were further distinguished by NF200 antibody labeling. Interestingly, in this NF200-positive neuron population, the overall infectivity of our DRG-targeting panel was higher. Display of peptides P8 and P9 in the context of AAV7 to AAVrh10 increased transduction efficiency over that of the respective wtAAVs. In fact, AAV9P9 showed the highest rate of infection with 65% positive cells. In contrast to the Beta-III-tubulin-positive neurons, AAV9P9 slightly outperformed wtAAV6 which exhibited an infectivity of 63%. Also interesting was the gain-of-function for AAV1 together with P9, from 20% of the wt virus to 40% YFP-positive neurons with the modified clone. As compared to the BIII-Tub-positive general DRG population, wtAAV5 and wtAAV7 transduction rates were not further increased for NF200-positive cells. Since NF200-positive proprioceptive neurons are a subpopulation of BIII-Tub-positive DRGs, the overall higher efficiencies of the AAV-DRG panel on NF200-positive cells hint at their increased specificity for proprioceptive neurons.

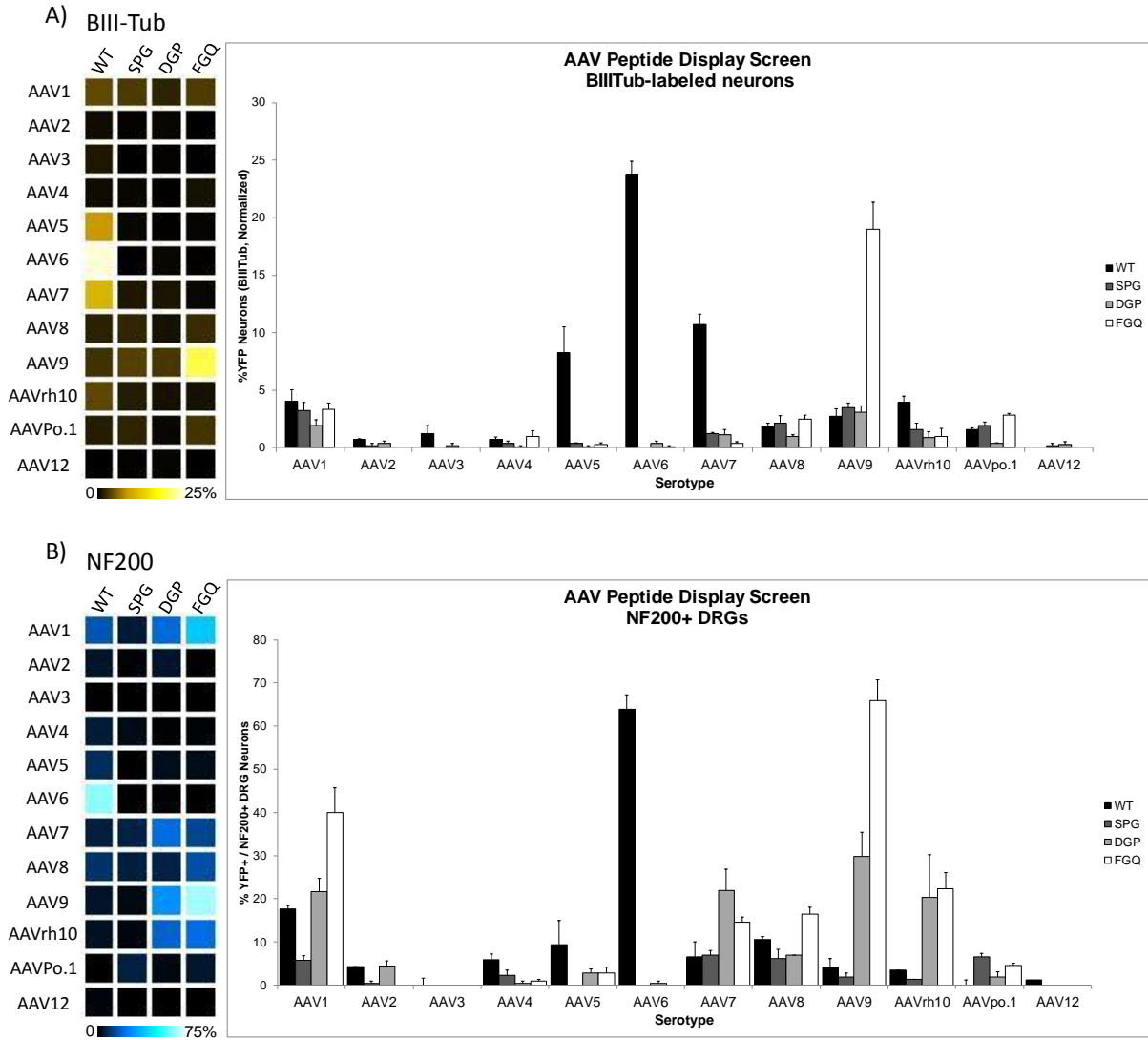


Figure 52: Transduction efficiencies of wtAAVs and AAVs displaying the DRG-targeting peptide panel P7-P9. A) Transduction of Beta-III-tubulin-positive neurons. **B)** Transduction of NF200-positive proprioceptive neurons. Infection rates were visualized through heatmaps and bar charts. Note that the maximum value of the x-axis is at 30% in the BIII-Tub graph versus 80% in the NF200 graph. (For color code of the heat maps refer to Figure 24 and Figure 29.)

4 Discussion

Advances in gene therapy rely to a large extent on improvements of available vector systems. High safety, specificity and efficiency are the key features that have to congregate to define a clinically useful gene therapy vector. Remarkably, AAV vectors inherently possess most of these properties as their parental viruses are apathogenic in humans, and as the vectors themselves are gutless (*i.e.*, devoid of any viral genes) and non-integrative. Furthermore, the wealth of natural AAV serotypes and isolates, coupled with techniques for molecular capsid evolution and engineering, offers a wide range of possibilities to find or create an AAV vector that meets specific demands. The approval of an AAV1-based gene therapeutic in Europe (EMA/H/C/002145, 2012, European Medicines Agency London) and >70 clinical trials to date using AAV vectors, including several derived from serotypes other than the AAV2 prototype [15], clearly emphasize the potential of rAAVs for therapeutic applications.

Nonetheless, there is room for further improvement as specificity after systemic application and particle immunogenicity remain critical issues with respect to clinical use of AAV. In the recent past, a variety of strategies have been proposed to partially overcome these concerns, such as the use of endogenous cell-specific miRNAs as regulators of AAV vector specificity on the post-transcriptional level [290]–[293]. Others have started to clinically evaluate the use of immunosuppressants to block humoral or cellular immune responses against the AAV capsid, or have proposed co-delivery of empty AAV particles that act as decoys which bind and sequester neutralizing anti-AAV capsid antibodies [199], [294]–[296]. A common disadvantage of these and other related strategies is that they complicate the clinical protocol since they require additional agents and regimes. Especially in the case of immunosuppression, these supplementary treatments can invoke extra physical and mental burdens on the treated individual and may ultimately interfere with patient compliance.

Here, we therefore decided to focus on engineering of the AAV capsid as a straight-forward strategy to improve vector efficiency and specificity without a need for either exogenous modulation of the patient's immune system, or for recrafting of pre-existing vector genomes. In particular, we concentrated on two powerful methods, (i) DNA family shuffling (DFS), *i.e.*, fragmentation and subsequent reassembly of capsid genes from different AAV serotypes, and (ii) peptide display, *i.e.*, insertion of short amino acid sequences into the AAV capsid to mediate vector de- and retargeting. In both cases, we pursued two goals: (i) to further optimize the technology *per se*, from the creation of synthetic AAV capsids to their selection *in vitro* or *in vivo*, and (ii) to concurrently exploit these methods as a unique opportunity to improve our understanding of fundamental AAV biology.

4.1 AAV capsid shuffling

4.1.1 An optimized shuffling protocol is key to generation of diverse AAV libraries

The generation of AAV capsid chimeras through the technique of DFS is a multistep process that comprises **first** the fragmentation of sufficient amounts of parental genes; **second** the reassembly of capsid sequences from these fragments in a primerless PCR, based on their partial homology; **third**, the amplification ('rescue') of chimeric full-length capsid genes; and **finally**, cloning and virus production in order to generate a diverse plasmid or viral library, respectively. Because of the complexity of this workflow, only a few groups in the world have thus far been able to establish this technology, which is unfortunate as it continues to hamper its wider application. Therefore, the first specific aim in this thesis was to develop a robust protocol for AAV *cap* gene shuffling that only requires standard laboratory expertise and equipment, and that can be easily adapted to custom needs including different types and numbers of parental AAV serotypes. In particular, we attempted to streamline and simplify the following aspects of the general workflow:

cap plasmids: A limitation of the original protocol as first reported by Grimm and colleagues [212] and subsequently later used by others [6], [214]–[217], [219], [297]–[301] is the need to isolate desired capsid genes from plasmids via restriction digests. While relatively simple, there may be a need to amplify and then extensively digest large amounts of plasmid DNA since the subsequent DNase I reaction can consume substantial input DNA (see also next paragraph). Here, we improved this step by introducing a new set of standardized and modular plasmids that contain the *cap* genes of 12 important AAV serotypes flanked by multiple restriction and primer binding sites. As demonstrated, these plasmids allow to isolate any desired *cap* gene in sufficient amounts in a very efficient and rapid PCR reaction. Accordingly, they help to save significant material and time, and permit to proceed to the DNA fragmentation step within less than two hours (see Figure 53 below).

DNA fragmentation: This step is highly critical for the success of DFS because the *cap* DNA fragment size or rather the range of sizes determines the crossover rate and hence the degree of shuffling. Larger fragments will increase the chances of recombination and thus improve the yields of full-length genes, but this comes at the cost of reduced diversity. *Vice versa*, shorter fragments pose less opportunity for homologous recombination, but where it occurs, it results in highly diverse progeny. Alas, DNA fragmentation via DNase I is very difficult to control due to the high inherent activity of the enzyme. We therefore studied whether physical shearing (Covaris ultra-sonication) of *cap* DNA could be more reliable and reproducible, and produce more defined fragment sizes. Interestingly, while we found that the latter is indeed the case, we concomitantly noted a drop in shuffling efficiency, as evidenced by low yields of reassembled full-length capsid genes and fewer crossovers. In fact, even

the best Covaris condition (Fig. 19, 800 bp fragments) which resulted in yields comparable to those from DNase I-based digestion produced clones that were less diverse. Notably, these findings were confirmed independently by another PhD student in the lab (Stefanie Große) who likewise achieved better results for various AAV *cap* gene combinations with DNase I digestion rather than with Covaris (Große *et al.*, manuscript in preparation). Curiously though, yet another PhD student in our group, Nina Schürmann, successfully applied the Covaris system to create libraries from the four human Argonaute proteins [270], using conditions comparable to those here. Taken together, these three independent observations suggest that the success of library generation through chemical versus physical fragmentation depends on numerous parameters, especially the primary sequences of the parental genes. We thus refrain from generally recommending one method versus the other, but conclude that at least for AAV library production, *cap* gene fragmentation via DNase I digestion is the preferred approach.

Reassembly & amplification PCRs: Equally important as optimizing the conditions for *cap* gene fragmentation was to streamline the subsequent steps of reassembly and amplification of chimeric full-length sequences. This was a very challenging endeavor for two major reasons: (i) the success of the first reassembly PCR can only be visualized through a robust second amplification PCR, since the first PCR itself does not yield a detectable product; hence the two PCRs are closely interrelated and had to be optimized simultaneously. Moreover, (ii) the goal of the first PCR (and the preceding DNA fragmentation step, see above) is to create maximum diversity, whereas the second PCR rather focuses on producing high yields; it was accordingly important to strike a balance between these two aims when optimizing the individual PCR conditions. In the end, we indeed found conditions that fulfill the last requirement and that not only improve but also simplify the original protocol. This is because we eliminated the need for a nested PCR by establishing an experimental setup that allows for robust production of full-length and diverse *cap* genes via a simple and rapid two-step PCR. The efficiency of this improved PCR is in fact so high that it also permits to skip the intermediate TOPO cloning step that was necessary in the original protocol to increase the amount of *cap* genes [212]. This is again an essential advance in the present work as it minimizes the risk of a loss of sequence diversity due to suboptimal TOPO ligation and/or subsequent transformation.

Collectively, the improvements implemented in this work substantially streamline the AAV DNA shuffling protocol and now permit the routine production of highly diverse capsid libraries derived from various serotype combinations within less than one week. Figure 53 on the next page illustrates the entire workflow and the individual reactions required to create a typical small-scale AAV library.

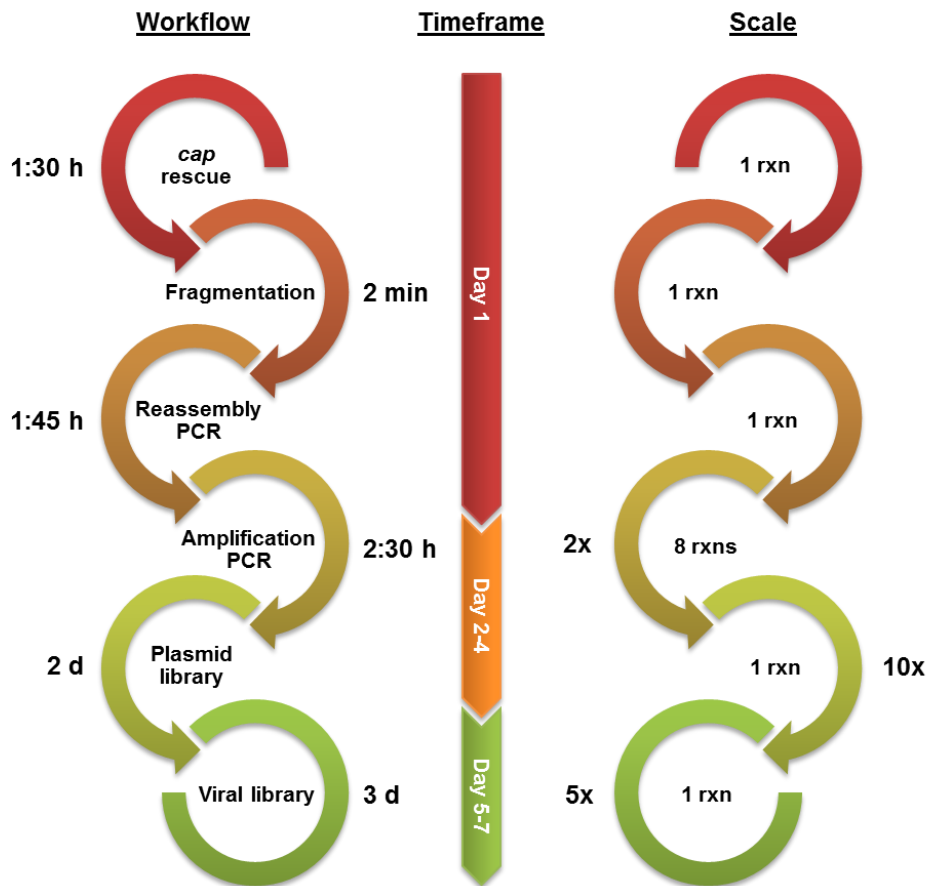


Figure 53: Schematic depiction of the streamlined protocol for AAV library production established in this work. Shown on the left are the individual steps with estimated times, while the corresponding numbers of reactions (“rxn/s”) are depicted on the right. Numbers outside the circles indicate options for up-scaling. Center arrows denote the required time in days.

4.1.2 The selection process is equally decisive for the success of the shuffling approach

The power of AAV capsid shuffling is that it creates highly diverse and versatile libraries of chimeric clones that ideally combine multiple assets of their parental serotypes. However, as an isolated step, library generation is insufficient to yield new vector candidates, for two reasons: (i) the size of these libraries typically vastly exceeds the number of natural AAV isolates, which is already too large for rational screening of individual capsids; hence, it would appear counter-intuitive to only up-scale the wealth of capsids to choose from without any additional measures. Second, (ii) large numbers of capsids in a newly produced library are in fact rather inefficient or even completely non-functional, further highlighting the need for subsequent steps to identify lead candidates. This second concern was well exemplified in the present thesis with the analysis of eight randomly picked clones from an AAV289 library, all of which showed relatively poor efficiencies as compared to various wildtype AAVs (3.1.2, Figure 24). We can envision a variety of possible explanations for this phenomenon:

First, the high diversity of typical libraries (3.5E+6 clones for the present AAV289 library) makes it unlikely that randomly chosen clones are already suitable for a certain application. **Second**, one can also expect to find clones that are completely inert due to adverse recombination of distinct capsid parts from different serotypes. This is particularly likely when AAV serotypes such as AAV4 or AAV5 are included in a library, because the isolates are only remotely related to the majority of other AAVs, as reflected by the unique length and sequence of their *cap* genes as well as numerous further differences in genome structure and regulation [56], [65], [74], [98], [105], [106], [155], [302]. Consequently, shuffling of such distinct serotypes with others increases the risk of adverse changes and shifts in the *cap* open reading frame, including nucleotide “deletions” or “additions”. Even if a frame shift is quickly corrected by a subsequent second recombination event, the resulting short aberrant sequence can already suffice to disrupt AAV capsid functionality. Moreover, a shift to an alternative reading frame can result in premature termination of translation due to the presence of out-of-frame stop codons. In fact, although such an event is unlikely for closely related serotypes, it was found in one of the clones of the AAV289 library (data not shown).

Third, it is also conceivable that *cap* gene shuffling unintentionally disrupts the ORF of the assembly activating protein (AAP). This protein, which has been discovered recently by the lab of Jürgen Kleinschmidt [55], [56], [303], is believed to (i) interact with AAV VP proteins and (ii) aid in capsid assembly. Notably, work from our own lab (Stefanie Große, PhD student) moreover shows that AAP is also important for the maintenance of high steady-state levels of AAV VP proteins, and that AAP is a rate-limiting factor during AAV virus/vector production since its over-expression boosts particle yields. Still, the exact molecular mechanisms remain unknown to date, including potential sites in the VP proteins with which AAP might interact. Accordingly, it is well possible that shuffling affects AAP protein function in at least two ways, both of which could readily explain the high percentage of non-functional clones in AAV libraries: (i) since the AAP ORF is located within the *cap* gene (more specifically, AAV is encoded by the second ORF and largely overlaps with the VP2 N terminus), it is also shuffled and probably disrupted in the majority of clones in a library. In addition, (ii) it is likewise possible that the binding sites for AAV within the VP proteins are perturbed as a result of shuffling, hence preventing proper AAP-VP interaction and thus hampering the putative roles of AAP for VP stabilization and assembly.

Altogether, it is clear from the combination of these two major considerations - (i) shuffling creates far more capsids that can be screened individually, and (ii) many of these capsids are likely non-functional, for various reasons - that libraries have to be subjected to a selection process, in order to concurrently purge inert capsids and to enrich desired candidates.

4.1.2.1 *Interplay of different capsid parts contributes to efficient cell transduction*

The most basic selection routine is amplification of an AAV library in target cells in the presence of helper virus. This is also one half of the selection scheme that was used in the original shuffling paper by Grimm and colleagues to enrich the AAV-DJ chimera (the other half was IVIG selection) [212]. As outlined in chapter 3.1.2, it was thus interesting to recapitulate this particular selection with a new library solely based on AAV serotypes 2, 8 and 9, *i.e.*, the DJ parents. We accordingly iteratively amplified this AAV289 library in the hepatic cell line Huh7 in the presence of Ad5 and different IVIG batches. Notably, we had moreover included a selection in the absence of IVIG to study whether the withdrawal of negative pressure would alter the composition and function of the enriched capsids, as compared to Ad5/IVIG co-selection. Intriguingly, this is indeed what we found, as briefly summarized and discussed in the following.

A **first** remarkable observation was that in all selected clones, a large portion of the GH-loop, ranging from VR-V to VR-VIII, consists of AAV2-like sequences. These aa are located around the 3-fold symmetry axis of the AAV capsid, where VR-V to -VII form the depression while VR-VIII contributes to the spike-like protrusion. As in AAV2, we noted the presence of the HSPG binding domain at the very tip of the spike in all enriched clones, indicating an AAV2-like cell binding.

An interesting **second** notion was that in most of the clones, there was a shift to AAV8 mainly in the HI-loop, in VR-IX and also at the very C-terminal end. Both VR-IX and the C terminus are part of the invading loop that mediates interaction of VP3 monomers at the 2-fold axis and are essential for capsid assembly, likely by mediating VP interaction with AAP [79], [97], [304]. A similar function was proposed for the β I-sheet proximate to the HI-loop [303], where a single point mutation (I682S) disrupts AAP interaction. The HI-loop contributes to most of the interactions at the 5-fold axis and was also found essential for capsid formation and genome packaging [79], [305].

A **third** striking finding was that the DE-loop, which together with the HI-loop forms the 5-fold pore, was also derived from AAV8 in most of the chimeric virions. In particular these areas around the 5-fold axis were described to undergo conformational changes upon uncoating and genome release. It was further reported that the first aa of VP3 are located within the capsid at the base of the 5-fold channel that connects the inside and the outside of the capsid [72], [80], [306]. Correspondingly, these aa near the site of PLA2 and NLS externalization also originate from AAV8 in all clones from the plus Ad5 / minus IVIG selection.

Finally, in some chimeras, VR-IV in the GH-loop was composed of AAV8-like sequences. This part lies in close proximity to the 2-fold axis and contributes to the interactions of VP monomers at the 3-fold

symmetry axis. It seems to be even more salient than the rest of the GH-loop and crucially influences AAV transduction [64], [79], [211].

Overall, we realized that those chimeras were most efficient which combined all the aforementioned aspects in a single capsid, *i.e.*, which exhibited a specific juxtaposition of sequences from AAV2, in particular in protruded parts of the capsid, with others from AAV8. We thus conclude that selection in Huh7 cells in the presence of helper virus (positive pressure) but absence of IVIG (negative pressure) favors AAV capsids that contain at least the primary receptor binding site from AAV2 (two adjacent arginines at position 585 and 588). This is reasonable since Huh7 express HSPG, the primary AAV2 receptor. At the same time, capsid parts which are associated with VP monomer interaction exhibit a preference for AAV8. These parts that contribute to capsid stability, together with AAV8 parts that function in the externalization of PLA2 and NLS domains, might play a role in endosomal escape and uncoating [58], [72], [79], [80]. It is indeed believed that AAV8 uncoating is superior to AAV2 and that the uncoating step rate-limits AAV transduction [142], [154], [307], [308]. Our own data corroborate previous data that correlated the increased transduction and rapid onset of AAV8 expression with VR-IV and -IX located at the 2-fold axis of the AAV capsid [211], [309]. Besides, Nam and co-workers described a pH-induced destabilization at the 2-fold symmetry axis of AAV8 that promotes uncoating, and that was not observed for AAV2 [125].

Altogether, we conclude that selection of an AAV289 library in Huh7 cells in the presence of helper virus results in clones merging AAV2-like cell binding with potent AAV8-like uncoating and rapid onset of expression/replication. This particular combination most likely provides these clones with a growth advantage over the individual parental viruses or over other chimeras, permitting them to outgrow their competitors and to become enriched after multiple selection rounds.

4.1.2.2 ***Immune tolerance versus transduction efficiency***

As noted, an ideal AAV capsid or a gene therapy vector in general should not only be able to potently and specifically infect a target cell, but it should also do so in the presence of neutralizing antibodies that are either already circulating in a patient, or that arise after the first vector treatment. This is particularly true for cases where the vector is applied systemically and is hence highly prone to making contact with such antibodies. Indeed, there is ample evidence from pre-clinical studies in mice and other animals that humoral immunity against AAV capsids - but typically not against the encoded transgene product - can readily block *in vivo* transduction [87], [110], [199], [277], [295], [310]–[313]. As also mentioned before, AAV-DJ combines high transduction efficiency with the capability to at least partially escape antibody (IVIG) neutralization [212]. Curiously, we observed some similarities to AAV-DJ with respect to the combination of domains from AAV2, AAV8 and AAV9 in our clones selected in the absence of IVIG (see paragraph 4.1.2.1 above). In particular the GH-loop

was shared between AAV-DJ and most of our clones, indicating that it is primarily important for high transduction efficiency rather than for antibody escape. Many other regions and subdomains were different, however, suggesting that these are indeed critical determinants of cell transduction versus antibody recognition.

This hypothesis tempted us to further experimentally delineate these properties, by again selecting the shuffled AAV289 library but now with additional IVIG pressure comparable to that which had originally led to AAV-DJ. To account for possible donor- or batch-specific effects, we applied three distinct IVIG brands - Gamunex, Octagam and Kiovig – at lower doses and used two different ranges of concentrations for Gamunex. Interestingly, the analysis of our clones selected with the three IVIG brands did not imply a major effect of the IVIG source, as the only notable difference was a slight increase of AAV9-like amino acids in the clones selected with Octagam. This notion is further supported by a cross-titration study, where clones selected at high concentrations of Gamunex were titered with Octagam or Kiovig, and where we again saw no major influence of a specific IVIG brand (data not shown). We thus conclude that the exact source of IVIG is not critical for this particular selection scheme, which is an important information for future attempts at evolution of antibody-resistant AAV capsids.

While the three IVIG batches gave similar results when compared to each other at lower concentrations, we could draw a number of interesting conclusions from their comparison to clones selected in the absence of any IVIG (see also paragraph 4.1.2.1 above). Basically, we can distinguish two categories of clones that emerged: (i) capsids that mediate efficient transduction and closely resemble those obtained in the absence of IVIG, versus (ii) poor transducers that are, however, more resistant to IVIG. Clones in category (ii) are obviously what we expected from selection in the presence of IVIG, at least regarding their higher antibody resistance. Congruent with our knowledge on the seroprevalence of wildtype AAV serotypes [278], we found an increase of AAV8- and AAV9-like amino acids in these clones, especially within the protruded parts of the GH-loop. This observation is in line with a substantial accumulation of AAV8-like amino acids after selection in the presence of high amounts of IVIG (Gamunex). In fact, all clones from the high dose selection resemble AAV8 in most of their entire extrinsic capsid part, starting from the EF-loop, including the complete GH- and HI-loop, up to the very C-terminal end. Again, these clones gave relatively poor transduction, but were still infectious even when titered in the presence of high IVIG doses, where all other clones were already fully neutralized. In this respect, chimeras from the IVIG high dose selection not only resemble the structure but also the function of their parental serotype AAV8 which likewise hardly infects cells *in vitro* but readily escapes IVIG neutralization.

Taking our results from the selection without IVIG into account as well, we propose that the block that hampers AAV8 transduction *in vitro* lies in VR-V to -VIII and is located around the 3-fold axis of the capsid. In turn, this implies the block to be linked to receptor binding rather than intracellular processing. Along this line, data by Shen *et al.* who swapped domains between AAV2 and AAV8 indicate a role of VR-V in cell transduction that is not related to the onset of transgene expression [211]. Furthermore, a most recent study using a comparable experimental setup described an influence of VR-VII (either alone or in conjunction with VR-IX) on transduction efficiency [309]. Intriguingly, in both reports, swapping of VR-VIII from AAV2 to AAV8 and *vice versa* resulted in a substantial decrease in transgene expression. Moreover, mutation of two amino acids in VR-VIII of AAV8 into arginines that are essential for HSPG binding in AAV2 recapitulated AAV2-like HSPG affinity but did not increase AAV8 transduction *in vitro* [212]. Thus, sheer physical binding of a single cellular receptor seems insufficient to mediate potent transduction.

In the future, one option to circumvent natural cell binding and to thus permit the further dissection of intracellular processing of our AAV8-like clones could be their coating with PEG8000, as it was found to enhance wildtype AAV8 transduction *in vitro* (personal communication, Dr. S. Urban; Molecular Virology; University Hospital Heidelberg). It will moreover be interesting to evaluate our AAV8-like chimeras in mice as well, hoping that this will help to further delineate the capsid features that determine AAV(8) transduction *in vitro* versus *in vivo*.

Generally, it was intriguing to note in these experiments how the IVIG dose and hence the strength of the negative selection pressure can shift the balance between two opposing capsid features - transduction efficiency versus antibody resistance. Both features are mainly mediated by protruded capsid areas and influenced by the serotype origin - AAV2 contributes to a better cellular binding and uptake (at least *in vitro*), while AAV8 and AAV9 are superior at escaping neutralizing antibodies. (For an overview over AAV tropism and immunogenic epitopes, please refer to the introductory chapter 1.2.3, as well as to reference [110], [111], [314].) Under mild selection pressure at moderate IVIG doses, there appears to be a bias towards receptor binding and internalization. This explains why in AAV-DJ as well as in some of our new clones selected at the low IVIG dose, the most exposed regions of the capsid around the 3-fold axis still originate from AAV2 despite its high reactivity with IVIG. It likewise explains why following a more stringent IVIG selection, different capsids emerge which have gained resistance to neutralizing antibodies, even if it comes at the cost of diminished infectivity. Notably, this distinct bias between potent transduction versus antibody escape that we observed after selection in cultured cells may not necessarily reflect the *in vivo* situation. This is because in our *in vitro* selection approach, we had incubated the viral libraries with IVIG prior to infection in a confined space and in the absence of target cells. Accordingly, neutralizing antibodies had a high

chance of finding, binding and occupying a matching AAV capsid. This is in stark contrast to the typical *in vivo* situation where AAV particles can escape from such antibodies through rapid binding to, and entry into, cells. We thus postulate that a more relevant selection scheme is *in vivo* biopanning in animals that are passively immunized with IVIG (which is feasible in principle, [212]), as it would more closely mimic the actual situation in human patients. However, as shown and as will be discussed below, such an *in vivo* selection is challenging for other reasons and also requires further optimization in the future.

4.1.2.3 ***Helper virus-supported AAV replication alters the outcome of selection***

All selection schemes discussed so far, with or without IVIG, included the addition of helper virus as a means to support a complete AAV replication cycle and to thus enhance the recovery of desired clones [43], [315]. Yet, as outlined in chapter 3.1.2.2 and as briefly recapitulated here, there are at least four possible arguments against the use of a helper virus for AAV selection: (i) it could create a bias towards chimeric AAVs that more potently complete steps in the life cycle after transduction, such as assembly of progeny capsids; these are, however, irrelevant for their use as vectors; (ii) it will favor AAV amplification in cells that are also highly infectable by the helper virus, which may not be the proper targets, especially in mixed cell populations or *in vivo*; (iii) Adenovirus needs to be handled under special biosafety conditions which are not available everywhere; and (iv) its use is questionable in whole animals since it may cause severe toxicity [212] and it may not infect the majority of interesting target cells (as noted in (ii) above).

To investigate in particular the first concern and to study which effects, if any, the helper virus would exert on the structure and function of enriched AAV capsids, we performed an additional selection of the AAV289 library in the absence of helper virus. Owing to the lack of AAV replication, we had to isolate viral DNA from infected cells, clone the *cap* genes back into AAV *rep*- and ITR-containing plasmids and then produce new virus for the next round. The results from analysis of clones enriched after five such selection rounds and from their comparison to capsids selected in the presence of Adenovirus were intriguing and surprising on numerous levels, as discussed in the following.

A **first** observation was that after selection without Ad5, the entire GH-loop, the proximate HI-loop and the C-terminal end of all analyzed clones consisted of AAV2-like amino acids. In addition, the BC- and DE-loops were also comprised of AAV2-like sequences in several clones, so that the complete extrinsic part of their capsid resembles AAV2. This capsid composition is in sharp contrast to that of clones from the other selection schemes discussed above that included adenoviral co-infection. There, the HI-loop and the very C-terminal region were typically derived from AAV8, as was VR-IV within the GH-loop. As noted, we believe that these regions contribute to uncoating and intracellular processing and hence to AAV infectivity when juxtaposed with AAV2 elements that mediate potent

cell attachment and entry. Nonetheless, this particular AAV2-AAV8 combination, as it is also present in AAV-DJ [212], was no longer found after selection in the absence of Ad5.

Second, capsids selected without helper virus also display distinct transduction patterns. While their infection rates - defined as numbers of cells expressing a vector-encoded YFP reporter - matched those of capsids selected with helper virus, YFP intensities per cell were far weaker. Moreover, in contrast to the AAV2 wildtype [316], this moderate expression was not enhanced upon Ad5 superinfection. It seems unlikely that the lower intensities per cell were due to overall fewer infection events considering that this should have also resulted in decreased infection rates; this, however, was not observed. Instead, we hypothesize that these capsids selected in the absence of Ad5 were defect at an as-of-yet unknown intracellular step that is ultimately critical for transduction.

Originally, we had expected that selection without helper virus would predominantly yield capsids that perform well as vectors, since such a helper virus-free selection scheme most closely mimics vector transduction. Nonetheless, we found the opposite, which raises the question how and at which point Adenovirus benefits the outcome of AAV vector evolution. It is generally known that Ad5 helper functions (E1, E2 and E4 proteins, as well as VA RNAs) act mainly on the level of AAV gene expression and replication [45]. Briefly, E1A is a transcriptional activator and drives the host cell into the S-phase of the cell cycle [317]. E2A encodes a DNA-binding protein that functions in promoter regulation, mRNA maturation and DNA replication [318]–[320]. E1B55K and E4orf6 promote the export of AAV mRNA from the nucleus, and E4orf6 further functions in second strand synthesis of viral DNA [144], [145], [321], [322]. Finally, VA RNA further enhances translation [323]. Besides its role in AAV gene expression and replication, helper Adenovirus provides yet another function that is interesting in the context of this study. In fact, Ad5 co-infection facilitates nuclear translocation of AAV particles and thus further enhances transduction [119]. The early onset of enhanced AAV translocation upon Ad5 co-infection suggests a role of proteins of the Ad5 particle rather than expressed gene products [119]. Still, there is evidence that *e.g.* the Ad5 protein E4orf1 localizes to clathrin-coated vesicles [324]. Regardless of exact mechanism, it is clear that this particular adenoviral helper function could support both wildtype and recombinant AAV.

At this point, we hypothesize that capsids selected with or without helper virus enter the cell with similar efficiencies, provided they share sequences from AAV2 which are critical for potent cell binding and entry. However, in the presence of Ad5, those that can also robustly complete the following steps, *i.e.*, trafficking through the endosome, nuclear entry, uncoating, gene expression and genome replication, will have an advantage over others that are defect at any of these steps; hence these fully functional capsids will outgrow all defunct particles. Conversely, in selection schemes without adenoviral help which exclusively rely on PCR rescue; it is very difficult to distinguish fully

functional capsids from those that might be arrested at any step during the viral life cycle. In fact, it is likely that the majorities of capsids in a shuffled library at least possess the ability to enter a cell, but then get stuck during trafficking or other complex processing steps. Based on our rescue strategy in the adenoviral-free selection scheme which relies on PCR from total cellular DNA, it is thus well possible that we inadvertently created or rather reflected an inherent bias for capsids that have some form of processing deficiency in the cytosol. One possibility to overcome this problem in the future would be to segregate cytosolic and nuclear fractions from cells after infection with an AAV library, and to then only perform PCR rescues on the nuclei. While this may still amplify capsids that remained intact in the nucleus and are thus defect (at uncoating), it should at least substantially increase the chances to eliminate all other capsids that are arrested at earlier steps in the cytosol.

Altogether, the direct comparison of the results from our selections with or without helper virus supports our hypothesis that AAV8-like capsid parts act in intracellular steps of the AAV life cycle. This is also clearly in line with the previously mentioned seminal study by Thomas *et al.* who showed that AAV8 uncoats much more rapidly than AAV2, and hence leads to a higher amount of single-stranded AAV DNA genomes which can become double-stranded and express their genes [142]. Other reports confirmed the importance of uncoating during transduction of various AAV serotypes but also correlated the limited transduction efficiency of AAV2 with impaired nuclear translocation [307], [325], [326]. Curiously, the most efficient AAV2/8 capsid chimera described by Tenney *et al.* not only uncoated efficiently but also showed higher nuclear translocation exceeding that of AAV2 and rather resembling AAV8. The improved performance of this clone is most likely mediated by the combination of two AAV8-like domains VR-VII and -IX that are replaced in a clone that otherwise consists of AAV2-like sequences [309].

In conclusion, our work suggests that efficient transduction is the result of a very complex interplay of multiple domains that are dispersed throughout the entire AAV capsid. Additional support comes from a clone described by Hauck *et al.* in which domains VR-I to -III were replaced in AAV2 with the corresponding sequence from AAV1. Due to the sequence homology between AAV1 and AAV2 this 'domain swapping' in this less protruded capsid area actually comprised nine aa changes. These nine aa in the AAV2 based clone were found already sufficient to increase its transduction efficiency in muscle cells equaling that of wtAAV1. At the same time the clone retained the HSPG domain of wtAAV2 [209]. The requirement for complex interactions is further exemplified by our own clone #2 selected without Adenovirus, which poorly transduces despite the fact that its capsid is largely derived from AAV2, except for an area around the DE-loop that originates from AAV9 and an AAV8 like N-terminal VP1 part. This implies that potent transduction does not exclusively depend on the outer or most protruded part of the AAV capsid, but rather on its conjunction with other domains

and their orchestrated interplay with other factors (cellular and/or viral). To identify these domains and to further unravel their interactions within the AAV capsid along with possible cellular or helperviral interaction partners remains an important goal for future work, and fortunately one that can be readily addressed using shuffling technology.

4.1.2.4 *Ad5-free in vivo biopanning supports results from Ad5-free in vitro selection*

As described in chapter 3.1.3.1, the availability of a library composed of AAV serotypes 1, 5, 6, 8 and 9 allowed us to collaborate with Boehringer Ingelheim and to select this library in pancreatic β -cells in adult mice. At this point in the work, we were already aware of the possible role of Adenovirus for AAV selection (see above). Still, we decided to omit Ad5 co-infection for safety reasons and to avoid an inadvertent bias towards helper virus target cells outside the pancreas. Consequently, the purified AAV library was injected intravenously into mice, and total DNA was isolated from pancreatic β -cells (and other organs) to PCR-amplify viral capsid DNA and to produce a new viral library for re-injection.

During the total of three selection rounds, we obtained early evidence - including a detargeting from fatty tissue after round #1 - that the library composition was changing, as one would predict for a functional selection. AAV5-like sequences disappeared almost completely from the library after the first selection round, and while AAV8- and AAV9-like sequences were still found, the entire C-terminal half of all clones (starting from the EF-loop) originated from AAV1 or AAV6 after the second infection cycle. As expected, we continued to detect AAV in the liver through all selection rounds, in line with the high susceptibility of this organ for AAV transduction. We were then pleased to find that three infection rounds already sufficed to enrich a single clone in our actual target cells, considering that most previous selection schemes required four to five or even up to seven rounds [212], [218], [219], [297], [300]. Still, there are also a few examples where functional AAV chimeras were isolated after only three or even two selection rounds [6], [215]–[217].

Even more surprising was of course the subsequent realization that despite being the only survivor, this capsid failed to functionally transduce pancreatic cells *in vitro* or *in vivo* when produced as vector. Interestingly, this clone consists of AAV1 or AAV6 in almost its entire outer capsid part, except for an AAV8-like VR-I in the BC-loop and an asparagine at the very C-terminus (also akin to AAV8). Likewise, another chimera which actually worked in pancreatic cells and which was isolated after the second round, also nearly exclusively consists of sequences from AAV1 and AAV6. This is noteworthy since wildtype AAV6 is very efficient in pancreatic cells, suggesting that the selection was essentially successful and enriched AAV6-like capsid variants. In this respect, it is reminiscent of our selections of the AAV289 library where the best candidates also resembled the most potent parental serotype, AAV2. We speculate that the striking inertness of our lead capsid from the pancreas selection may be explained analogously to our hypothesis that emerged from the comparison of *in vitro* selections

with or without helper virus. Accordingly, we believe that the capsid isolated from total β -cell DNA may possess the ability to very efficiently bind and enter these cells (explaining why it was enriched by PCR), but is then trapped in an intracellular compartment and fails to uncoat in the nucleus and to hence mediate gene expression (explaining the lack of functional transduction). It is thus important for future work to dissect the biology of this capsid in more detail, to understand the putative block in transduction and to ideally learn lessons that can be used to improve looming selection strategies.

In this respect, despite our belief that supporting AAV replication with Adenovirus can help to enrich functional capsids, we clearly refrain from drawing the opposite conclusion that *in vivo* biopanning in the absence of helper virus is inefficient. In fact, several reports have already described successful *in vivo* AAV selections before [216], [217], [327]. In one study, Yang *et al.* isolated a chimeric clone after two infection rounds in the absence of helper virus that gave increased expression in the heart. Concurrent with our hypothesis that Ad5 helper functions during selection mainly support the ability of chimeric AAVs for efficient intracellular processing, a comparison of vector uptake and transgene expression of this clone revealed that enhancement is rather mediated by better cell binding than increased gene expression [216]. Another notable study exemplified an original hybrid *in/ex vivo* approach that could also be used to improve the odds for selection of a functional capsid in murine pancreas in a potential repeat experiment. In this study, Ying *et al.* injected an AAV2 peptide library into mice with the aim to target the heart. Three days post-infection, organotypic heart slices were super-infected with Ad5, to *ex vivo* amplify AAV clones that possessed the ability to replicate. Thereby, the authors eventually enriched two peptide motifs that preferentially target heart tissue. In addition, these motifs differed substantially in sequence and performance from two other sequences that were isolated in parallel from an *in vitro* selection in cardiomyocytes, again highlighting the importance of physiological selection conditions [327].

In analogy to this work, we suggest the following new workflow for a future repeat experiment: (i) inject the AAV15689 library without Ad5, as before; (ii) isolate target β -cells; (iii) culture them *ex vivo* and super-infect with Ad5; and (iv) subclone replicated AAV *cap* DNA to produce a new library for another selection round. The key modification is the *ex vivo* culture and helper virus super-infection, which we propose to include as we expect this step to trigger amplification of particles with capsids that have efficiently entered the nucleus and released their DNA for expression and replication. In turn, they should outgrow inferior particles or capsids, respectively, and thus enhance the success of selection. As an alternative, akin to our suggestions for the *in vitro* selections (see above), one could distinguish between particles that have entered the nucleus and those that have only attached to the cell or are trapped in cytoplasmic compartments. The success of this second strategy will depend,

however, on the feasibility to enrich sufficient nuclei from isolated murine β -cells and to then PCR-amplify the probably miniscule (at least after the first library injection) amounts of AAV DNA.

4.2 Peptide display

AAV peptide display was one of the first methods that was used to create libraries of modified AAV capsids and remains one of the most powerful strategies to date. While it is similar to DFS in that it can yield entirely novel AAV properties, it does so by adding exogenous aa to an otherwise full-length capsid sequence. The fact that this requires profound knowledge on at least the primary sequence of the underlying wildtype virus explains why the overwhelming majority of previous studies which applied this technology, including the original 2003 report by Müller and colleagues [221], used the well characterized AAV2 prototype. In fact, there are only a handful of papers which described peptide display in non-AAV2 serotypes, in particular [224], [225], [298], [328]. In this thesis, we therefore thoroughly explored the feasibility to further expand peptide display to eleven alternative serotypes other than AAV2 for which at least the protein sequence was known. Our key findings were that (i) it is the combination of peptide and capsid which determines vector specificity and efficiency, not the peptide alone; and (ii) the “right” combination can drastically boost even inherently inefficient capsids and ultimately permit transduction of very difficult cell types. These results, as discussed in more detail in the following, were highly surprising since they illustrate a previously unanticipated tremendous potential of different AAV serotypes as scaffolds for peptide display and thereby further expand the breadth of AAV vectors as one of our most promising gene transfer systems.

4.2.1 Expansion of peptide display to 11 AAV serotypes other than AAV2

In order to extend peptide display to non-AAV2 serotypes, we initially chose positions for peptide insertion in each serotype according to sequence alignments and available 3D structures. While the exact receptor binding sites were unknown for most serotypes at the time, comparative studies of AAV capsid structures suggested that they are located in comparable regions [79]. Still, we could not be sure that mutation and insertion at these sites would truly disrupt the primary tropism of the underlying serotype. Nonetheless, we hypothesized that this may not even be a prerequisite for efficient AAV re- or de-targeting. This is because it was also reasonable to expect an additive effect of the peptide even if the original receptor binding site remained intact, in analogy to the natural interplay of primary and secondary receptor functions (discussed in more detail below; for a recent overview over AAV receptors see [111]).

4.2.1.1 ***Rationale of capsid engineering and peptide design***

A first challenge we had to overcome concerned the cloning of peptide-encoding oligonucleotides. We did not want to adapt the previously reported iterative point mutation strategy [221] to create insertion sites in all 11 serotypes since it would have required excessive mutation, cloning and sequencing. Instead, we introduced these insertion sites through a combination of two PCRs and one triple-ligation, as detailed in chapters 3.2.1 and 3.2.2 above. This provided several important advantages over the original approach: (i) our strategy is substantially faster as insertion sites can be created in only two steps, in contrast to up to five with the point mutagenesis protocol; (ii) as a consequence of its simplicity, it also reduces costs for reagents and sequencing reactions; (iii) it can easily be adapted to other serotypes in the future since it only requires two primer pairs to amplify the two halves of a *cap* gene, as opposed to a much larger set of customized primers that are needed for the original protocol (which is especially complicated since the insertion sites lie within hypervariable regions, requiring numerous individual primers for each serotype); and (iv) our method concurrently changes the three flanking amino acids on each side of the inserted peptide to those from AAV2, which likely provides a much greater comparability between results obtained in different serotypes as it reduces effects from adjacent capsid-specific residues.

A second critical step was to select peptides for display and comparison in the 12 different AAV serotypes. In principle, there were three major possibilities: sequences that have been (i) published previously in the context of AAV2, (ii) identified in own screens, or (iii) designed *de novo* for AAV display. While we eventually exploited all three options in the context of this thesis, we decided to select candidates from the literature for initial construct validation. Our rationale was that these would provide ideal reference points, as they all had in common that they were pre-selected and characterized in an AAV2 scaffold in certain cell types, despite variations in peptide sequence and length [220], [226], [280], [281], [329]. We altered the amino acids that flanked this initial peptide set into AAV2-like sequences, except for the arginine corresponding to position 588 in AAV2 in the vicinity of the peptide sequence which was replaced after oligonucleotide insertion (see also Figure 54 below). This arginine was part of a motif that is important for HSPG binding in the context of AAV2 [95]. In view of results of Perabo and colleagues [330] who demonstrated that certain peptides can restore a HSPG binding phenotype, we wanted to ensure that none of our initial peptide-displaying variants has developed HSPG affinity *de novo*. In the course of our work, we then expanded our approach to the second class of peptides, identified through a 7mer peptide library *in vitro* selection in the AAV2 context by our collaboration partner Dr. Anna Sacher [285]. Notably, oligonucleotides used in this screen differed slightly in their design and restored the peptide-flanking arginine, which affected the performance of the respective clones, as discussed in detail in 4.2.3. Finally, we found our peptide display approach also suitable for *de novo* designed peptides, as exemplified with three

motifs that target neuronal cells of the DRG [288], [289] and that were never expressed in the context of AAV before.

In all cases, the peptides were either 7 or 9 aa in length (plus 2 flanking aa that served as spacers) and hence well in the range of 5 to 12 aa that were found optimal for peptide display in a study by Naumer and colleagues [331]. In accordance with this report, almost all our AAV/peptide combinations could be produced efficiently, with the single exception of peptide P6 (CNHRYMQMC) from the initial peptide set. Irrespective of the underlying serotype, clones displaying this particular peptide were never detected in cell lysates, but were rather found associated with the remaining cell debris. Interestingly, P6 was originally identified in an *in vivo* phage display screen in atherosclerotic lesions and later displayed in the context of AAV2 to target endothelial cells for atherosclerosis treatment [281], [332]. Due to its sequence homology to tissue inhibitor of matrix metalloproteinase 2 (TIMP2), it binds membrane type-1 matrix metalloproteinase MT1-MMP with high affinity. We thus speculate that P6 mediates interaction of modified AAV capsids with cell surface fragments of Hek293T cells after cell lysis via MT1-MMP and thus hampers virion release. However, capsid formation seems not perturbed as P6-displaying AAV particles could, in principle, be produced and purified to high titers.

4.2.2 Implications of peptide display on AAV transduction

Our collection of 12 wildtype and 72 peptide-modified capsids allowed us to perform comprehensive vector screenings in a large variety of cell lines and primary cells. Amongst the unmodified wildtypes, it was notable that AAV1, AAV2, AAV3 and AAV6 frequently performed best. In contrast, AAV5, AAV8 and AAV9 transduced fewer cell types and only to a medium degree, and AAV4, AAV7, AAVrh10, AAVpo.1 and AAV12 hardly infected any of the tested cells (3.2.3, Appendix). These results, especially the striking *in vitro* inertness of serotypes that are highly potent *in vivo*, such as AAV7-9, are consistent with previous reports, including a comparative study of AAV1 to AAV9 [155], [212], [302], [329], [333].

4.2.2.1 *Interplay of capsid backbone and peptide insert determines vector properties*

Interestingly, the transduction patterns of the wildtype capsids changed dramatically upon peptide display. Basically, one can distinguish gain- from loss-of-function phenotypes. With respect to AAV applications, the first category is obviously more relevant and will thus be discussed in more detail below. Here, suffice it to point out one example for a loss-of-function phenotype, namely, display of the P2 peptide in AAV2. This case is interesting because P2 was one of the first peptides for which an increase in AAV2 infectivity was reported and concurrently linked to a potential receptor [220]. In particular, an RGD motif as present in P2 mediates $\alpha V\beta 3$ and $\alpha V\beta 5$ integrin binding during Adenovirus infection [38], [220], [280], [329], [334]. Although AAV2 lacks a specific RGD motif, $\alpha V\beta 5$

integrin was described as one of its co-receptors [104], [304]. It was thus postulated that the RGD-containing P2 mediates binding to abundant integrins on target cells and thereby boosts vector transduction [220]. In our hands, however, this improvement was not observed; instead the P2-modified AAV2 was inferior to its parental wildtype. One possible explanation are subtle differences in the sequences surrounding the peptide insertion, which would be well in line with most recent data from our lab that alterations of the two arginines which constitute the AAV2 HSPG binding domain can significantly impact infectivity of a given AAV2-peptide combination (D. Grimm, personal communication). We can, however, rule out that the peptide *per se* was non-functional since it substantially enhanced the infectivity of several other AAV isolates in numerous cell types. In fact, the increase was so pronounced that P2 eventually became part of our Master panel.

Together, these findings exemplify a crucial lesson from the analysis of our peptide-serotype combinations: the peptide alone does not determine specificity, but it is rather its embedding in a certain capsid scaffold that dictates the AAV phenotype. While this may appear obvious in view of the bulk data in this thesis, it must be pointed out again that over the past decade, peptide display has been performed almost exclusively in the context of AAV2. The ensuing lack of comparison to other serotypes may have blurred the actual contribution of the underlying AAV2 capsid - positive or negative - and tempted the authors of numerous studies to conclude that it is indeed the peptide which is solely responsible for the observed specificities and efficiencies. In contrast, our new findings that the same peptide can enhance a subset of serotypes (frequently including the inherently weak transducers AAV7-9 and AAVrh10, but also AAV1) while having no or even a detrimental effect on others (such as AAV2, as mentioned) clearly implies that the peptide and the capsid mutually influence each other and together shape the properties of the resulting virion.

4.2.2.2 ***A peptide consensus sequence that frequently enhances cell transduction***

As just noted, one observation was that serotypes AAV1, AAV7-9 or AAVrh10 were frequently enhanced by various peptides, suggesting a common underlying mechanism. We then realized that the two peptides P4 and P5, which typically mediated this effect and which were originally described to improve AAV2 infection of HSaVEC [226], shared the first four amino acids of their sequence (NDVR). This motif is remarkably similar to NGR, a sequence found close to VR-V within the GH-loop and conserved in most AAV serotypes, except for AAV4, AAV5 and AAV11. NGR was described to mediate $\alpha 5\beta 1$ integrin binding and to thereby be essential for viral entry of AAV2 [100]. Moreover, mutation of either the arginine (R) or the glycine (G) in NGR was found to block endocytic uptake of AAV2, while leaving cell binding largely unaffected [81], [100]. This is partially congruent with our own mutational analysis of P4 which illustrated an essential role of the N and R residues. Notably, after we had initiated a collaboration with Dr. Anna Sacher from the DKFZ, we found additional

NGR/NDVR-like sequences in peptides isolated from a library screen in the context of AAV2. Furthermore, one more NDVR-like peptide was recovered from an own preliminary peptide library screen in AAV1 (Appendix). Last but not least, motifs similar to NGR were observed before and discussed by Dirk Grimm and colleagues in the context of their potent AAV-DJ chimera [212].

From the sum of all these independent findings, we eventually identified the consensus sequence NxxR as a common motif in most of our efficient peptides. The similarity to the NGR motif implies that our lead peptides comprising NxxR might likewise bind to $\alpha 5\beta 1$ integrin, a known co-receptor of AAV2. This hypothesis is in line with the current model for AAV infection which assumes that the virion first binds to cells via attachment to a primary receptor, often glycosaminoglycans, followed by interactions with secondary receptors that mediate internalization and intra-cellular processing [111]. Congruent with this, Asokan *et al.* described a 'click-to-fit' mechanism whereby initial HSPG attachment facilitates repeated binding to the same receptor and finally to integrin as a co-receptor via the NGR motif, ultimately resulting in viral uptake [100]. Also consistent with this model, Levy *et al.* reported a conformational change in AAV2 upon HSPG binding in an area close to the NGR motif, causing a transition that was postulated to expose co-receptor binding motifs [71]. Consequently, we hypothesize that insertion of NxxR and hence a potential co-receptor binding motif into VR-VIII, one of the most protruded capsid areas, may exhibit a synergistic or additive effect with virion binding to the primary receptor and thereby boost infection.

4.2.2.3 *Interdependency of natural and synthetic receptor functions*

During our studies, we noted that serotype AAV1 seems more receptive than AAV6 to peptide-mediated gain-of-function, especially in conjunction with the supposed $\alpha 5\beta 1$ integrin-binding peptides P4 and P5. In contrast, wtAAV6 more frequently transduced cells from disparate origin than AAV1. These observations are interesting, since AAV1 and AAV6 differ in only six aa from each other, yet these minor differences cause remarkably altered tropisms for the two wildtype viruses as well as peptide-displaying mutants derived thereof. AAV1 and AAV6 use N-linked sialic acid as glycan receptor, but AAV6 (thought to be a cell culture-derived chimera of AAV1 and AAV2) additionally binds HSPG, due to an AAV2-like lysine at position 531 [89], [94]. Results from our heparin competition assay with AAV6 now suggest that saturation of the HSPG receptor can enhance N-linked sialic acid binding as well as P4-mediated integrin binding, albeit to a lesser extent. Removal of sialic acid from the cell surface, however, almost completely abolishes AAV6 infection, indicating that the weak interaction with heparin alone [335] is insufficient for virus transduction. Taken together, we hypothesize that the ability of AAV6 to bind heparin broadens its natural tropism, but hampers its amenability for peptide-mediated effects. More generally, this points out the complex interdependency of different receptors and receptor binding sites.

Interestingly, neuraminidase treatment of cells prior to AAV infection abolished sialic acid-dependent transduction but increased AAV9 infectivity. This was initially curious until it was reported later that N-terminal galactose, AAV9's primary receptor, becomes accessible once sialic acid is removed from the cell surface [283], [284]. Notably, we found this increase in infectivity not only for wildtype AAV9 but also for its peptide-displaying derivatives. One likely interpretation is that albeit AAV9 primary receptor binding was not fully disrupted, peptide insertion improved transduction efficiency. This further supports our conclusion that the success of peptide display strategies does not necessarily require ablation of the primary tropism of the underlying AAV serotype.

4.2.3 AAV peptide mutants can be readily exploited for specific applications

A major advantage of our pre-arrayed panel of peptide-modified vectors is that it allows for much faster identification of potent mutants in a given cell type, as compared to conventional iterative screening of shuffled or peptide display AAV libraries. One example where we applied this feature in the present thesis are cells of hematopoietic origin which are relevant targets *e.g.* in HIV research, but which are largely refractory to wtAAV infection. Importantly, we here identified a number of capsid variants that could transduce these cells very efficiently, especially the combinations of peptides P2, P4 and P5 with serotypes AAV1, AAV7-9 and AAVrh10. For instance, our best efficiencies reached 81% in K562 or 76% in SupT1. Moreover, by exploiting our peptide display strategy and parental serotypes, our collaboration partner Dr. Sacher reached high infection rates in macrophages and dendritic cells, comparable to those that we obtained for other cells of myeloid and lymphoid origin. Based on these and other results, we combined our best six peptides - P2, P4, P5, A1, A2 and A6 - in a Master panel (MP; 84 vectors: 12 wildtypes and 72 peptide display mutants). Notably, four of these peptides - P4, P5, A2 and A6 - contained the previously discussed consensus sequence NxxR.

In one specific application, we applied this MP to a set of myeloma-derived cell lines and primary cells to evaluate its potential to target multiple myeloma, a cancer of plasma cells of lymphoid origin. As shown in chapter 3.2.5.1.1, we achieved remarkable transduction efficiencies of up to 95% in cell lines and 43% in primary human myeloma cells. Not surprisingly, transduction rates in primary cells were found to be donor-dependent. To our best knowledge, no other vector system has achieved comparably high infection rates on such a variety of myeloma-derived cells as our AAV variants.

Interestingly, we observed distinct infection patterns among the myeloid cells. First, we frequently found potent transduction with serotypes AAV1, AAV7-9 and AAVrh10 displaying the NGR/NxxR-like peptides P4, P5, A2 and A6, in line with our prior observations in other cell types. Second, we further noted a slight advantage of peptides A2 and A6 ("A-panel") versus P4 and P5 ("P-panel"). Considering that wildtype AAV2 and AAV3 also worked well in these cells and that both bind HSPG, we speculated that cell binding with capsids displaying A-peptides is at least partially associated with HSPG. Indeed,

we found evidence for HSPG-dependent cell binding of the A-panel in a heparin competition assay. It was thus an interesting question what caused this potential effect that was presumably common to different A-peptides regardless of their primary sequence.

To answer this question, we examined possible differences in the capsid sequences after insertion of A- versus P-peptides. As noted previously, our PCR strategy for the creation of the oligonucleotide insertion sites changed the three upstream amino acids into GQS in all serotypes. The nucleotide sequence encoding the third residue (the S in GQS) is in fact determined by the design of the inserted oligonucleotide duplex, as the respective triplet is part of its 5' end. Notably, the oligonucleotides used by our collaboration partner Dr. Sacher to create the A peptide variants slightly differ from ours at their 5' end, resulting in replacement of the serine in GQS with an arginine (Figure 54).

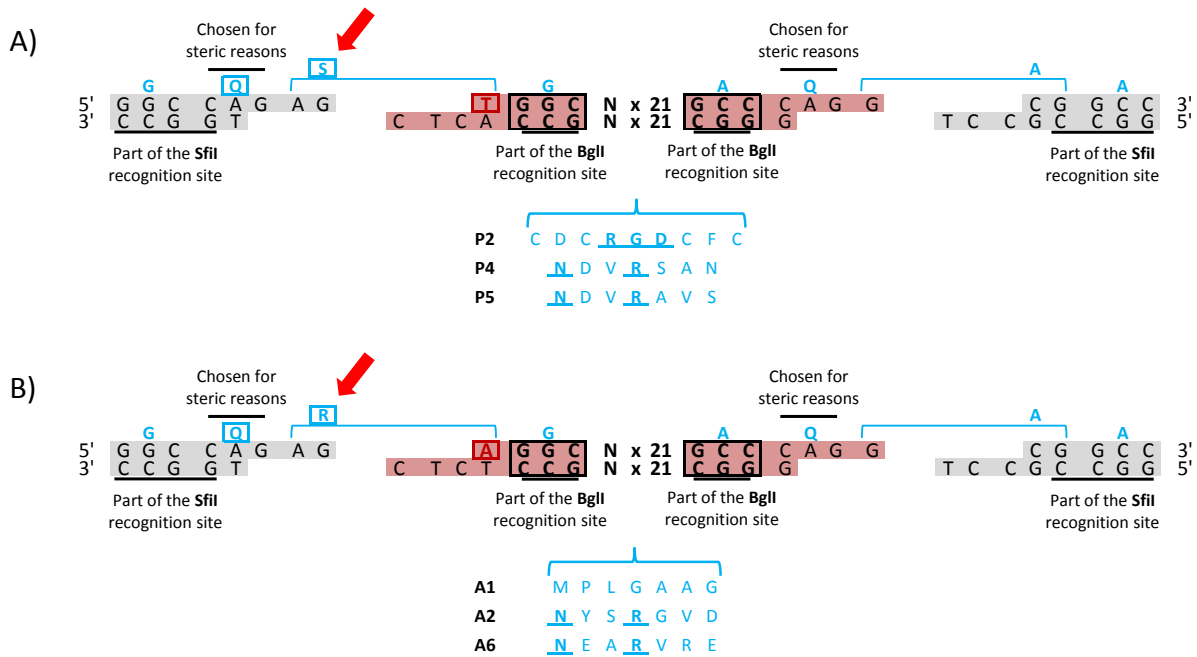


Figure 54: Comparison of “P” and “A” peptide insertion variants. A) “P” peptide insertions - as created by our group - are flanked by a serine (red arrow) downstream of the peptide due to the threonine in the 5' overhang of the oligonucleotide (red letter in bold and red box). **B)** “A” peptide insertions create an arginine instead of the serine (red arrow) because of the alanine in the 5' overhang of the oligonucleotide (red letter in bold and red box). This arginine, which is common to all “A” peptide variants, might contribute to heparin binding. Shown are nucleotide sequences as well as the corresponding amino acids (blue letters) of the flanking regions of the peptide insertions. Sequences determined by the peptide-encoding oligonucleotide are highlighted in red; those common to all serotypes with the insertion site modification are highlighted in light gray. Peptide sequences of the “P” and “A” series that were used in the Master Panel are shown in blue.

Accordingly, it is well possible that this additional R residue in combination with the R present in peptides A2 and A6 partially restored heparin binding, congruent with our observations and also with a previous report in the AAV2 context [330]. Nonetheless, the fact that AAV1, AAV7-9 and AAVrh10

displaying A2 and A6 still transduced even in the presence of heparin and thus behaved differently than AAV2 or AAV3 suggests that these particles use NxxR-bound integrins or other molecules as additional receptor next to HSPG for transduction. Thereby, our results with the myeloma cells once again imply that AAV is able to concurrently exploit different receptor-binding motifs (even artificial sequences) and thus highlight the plasticity and versatility of this virus.

Beyond the value of our data for AAV vector applications, our observations of recurring transduction patterns in a set of well characterized cells of the same origin, such as myeloma cell lines, can also provide important insights into AAV biology. For instance, it was interesting to note that AAV4 and AAV12 were both able to transduce U266 cells, while they hardly worked in any other cells during our screens. The ability of both serotypes to specifically infect myeloma U266 cells, independent of displayed peptides, suggests that a common, as-of-yet unknown shared capsid feature is responsible for their efficacy in these particular cells. To date, little is known about AAV4 and AAV12 other than that these two serotypes are close relatives to each other, but distinct from most other AAV isolates [108]. AAV12 transduction is independent from sialic acid, but alternative receptors have not yet been identified [92], [110], [335]. Serotype AAV4 binds sialic acid as a glycan receptor, like AAV1, AAV5 and AAV6, but differs in its sialic acid linkage specificity (O-linked for AAV4 versus N-linked for other serotypes) [73], [94], [98], [99]. However, recent results obtained by Mietzsch *et al.* question the described binding properties of AAV4 [335]. Ideally, our findings from the present work that both AAV4 and AAV12 efficiently and specifically transduce U266 cells may help to further unravel the cellular factors that these two serotypes interact with, and thereby aid in completing our picture of AAV biology.

4.3 Advantages, challenges and perspectives of AAV evolution technology

Any method aimed at improving the AAV vector system (including AAV capsid shuffling and peptide display) has to tackle the challenge that viral transduction is a highly complex process where different parts of the AAV capsid are involved at each of the multiple steps, from vector attachment to nuclear uncoating [111]. Accordingly, an ideal method for vector evolution has to be able to concurrently improve all these various steps and associated capsid parts. The difficulty of achieving this goal is exemplified by several studies that have assessed the contribution to transduction of single amino acids within the AAV capsid, next to those that form primary receptor binding sites [95], [96], [328], [336]. For instance, a mutational analysis of the AAV2 capsid identified 19 aa whose individual mutation decreased transduction despite the fact that heparin binding ability was retained. These aa are scattered in the C-terminal half of the linear capsid sequence but cluster in the assembled capsid, mostly in an area that was termed 'dead zone' [81] (see also Figure 55). The same report described aa that are important for capsid formation or whose mutation increased resistance

to nAB. A most recent study confirms these observations with AAV9, by identifying individual aa associated with primary receptor binding, virion formation, resistance to human AB, liver tropism or slower clearance from the blood [337]. Again these aa were found to be dispersed throughout the entire capsid sequence, although some important aa cluster in areas which are largely consistent with the VR [66] (Figure 55). Together, these and other studies yielded important information on the diverse functions of certain aa, and they also consistently highlight how these functions are determined by aa that are often located in distant capsid parts. This, in turn, explains why the direct and rational translation of the findings from these studies into a more efficient and/or more specific AAV vector is very challenging. This is because a single point mutation frequently suffices to abolish functions such as receptor binding, whereas gain-of-functions usually require several simultaneous aa changes. This is further exemplified by reported difficulties to transfer an AAV9-like galactose binding ability into AAV2 [336], [337] or to create a HSPG binding domain in AAV8 [212], using site-directed mutagenesis of selected individual residues.

In fact, the only method available to date that can comprehensively dissect functions that are dispersed throughout the AAV capsid, and that can concurrently exploit this potential to create new gain-of-function phenotypes, is DNA family shuffling. As compared to conventional mutagenesis strategies, it yields a far higher diversity and has the unique potential to combine most desirable aspects of different capsids in a single chimeric particle. Still, at first glance, it seems counter-intuitive that the rearrangement of conserved capsid domains could lead to an increase in transduction efficiency and/or specificity, considering that these features have developed during long evolutionary processes. Nonetheless, there is ample evidence that the juxtaposition of specialized properties from different serotypes in a single capsid can produce entirely novel phenotypes not found in nature. For example, it is the combination of different features in AAV-DJ that is assumed to be the reason for its superior performance, namely, AAV2-like cell binding and AAV8-like uncoating [212]. Congruent with this, our best chimeras from the AAV289 library selection also display a distinct combination of motifs from AAV2 and AAV8. This tempts us to speculate that akin to AAV-DJ, these capsids likewise combine the ability to partially escape neutralizing antibodies with improved intracellular processing; a likely hypothesis that should be interesting to study in more detail in future work.

Despite its enormous power and potential to improve capsid features related to dispersed aa, a remaining limitation of DNA family shuffling is that it relies on motifs that are already present in at least one of the parental serotypes. In particular for attempts to target cells that are completely refractory to all the known wildtype AAVs, it may be beneficial to be able to introduce entirely novel sequences and properties into an AAV capsid. This possibility is provided by the alternative AAV evolution method that was studied in this thesis, *i.e.*, AAV peptide display [221], [338]. This technique

often yields capsids that exhibit increased, but not always specific transduction [226], [327], [329], [339]. As opposed to capsid shuffling, display of peptides at defined positions within the capsid represents a spatially restricted modification of an exposed capsid part. This explains why first attempts at peptide display mainly aimed at modulating receptor binding, considering that this initial step of infection is mostly controlled by exterior capsid parts. Interestingly though, receptor binding can in turn determine the mechanisms of virus internalization and consequently control intracellular particle fate, thereby allowing displayed peptides to also affect other steps in vector transduction beyond cell attachment. However, data obtained by Ying *et al.* indicates that their AAV2-based peptide-displaying clone enters heart tissue better than wtAAV9 (shown by increased genome numbers in the cells) while its genome expression is limited by intracellular processing [327].

In the future, a possible way to further expand the power of peptide display could be the insertion at alternative regions within the capsid; either alone or in juxtaposition with validated insertion sites. As previously discussed (chapter 4.2), peptides in this thesis were mainly inserted at the tip of the HI-loop in VR-VIII of AAV2, corresponding to the position of its HSPG binding domain (Figure 55). Concurrent with our own results from the shuffling approach that identified VR-IV as being important for AAV infection, Naumer *et al.* [331] chose position 453 in AAV2 to display a heptamer peptide library (see also Figure 55). They confirmed the ability of this region to harbor peptides of different sequence and then showed how subsequent selection on human coronary artery endothelial cells (HCAEC) led to a slight enrichment of particular sequences. Amongst those, two sequences that contained an RGD motif significantly improved target cell transduction. Interestingly, a parallel selection on HCAEC cells with a peptide library displayed at position 588 yielded completely different sequences. The lack of RGD-containing motifs in this alternative selection indicates that the site of insertion also influences the sequence of the selected peptides and thus supports our suggestion to explore further alternative positions in the future. However, as not every position within the capsid sequence is suitable for peptide insertion [340], peptide display will probably remain restricted to only a few domains.

Meanwhile, our expansion of peptide display to non-AAV2 serotypes significantly broadens the prospects of this method. It was a central finding of this work that a given capsid scaffold and a specific peptide sequence can largely and mutually influence each other. This finding is not only important from a biological point of view, but by inserting defined peptides into the context of different serotypes previously not utilized for alternative receptor targeting, we also obtained vectors with new assets that should prove highly useful in the future. Nonetheless, it remains an intriguing question why certain peptides behaved completely unique in the context of different serotypes. One explanation could be that a displayed peptide in conjunction with the AAV backbone

forms a new set of primary and secondary receptors (as discussed in 4.2). Another explanation is indicated by 3D modeling of peptide-containing AAV capsids from different serotypes, performed in the lab of Mavis Agbandje McKenna (University of Florida, USA). Their data generated with selected capsid-peptide combinations from our collection suggest that it is not necessarily the peptide itself that alters the properties of the modified vector. Instead, it is possible that peptide insertion leads to regional or global changes in capsid conformation, which in turn alter the features of the entire particle (personal communication). This alternative explanation is very exciting and will be studied further in collaboration with this group, as it questions the previous hypothesis that displayed peptides primarily act as an entity and directly mediate specific effects.

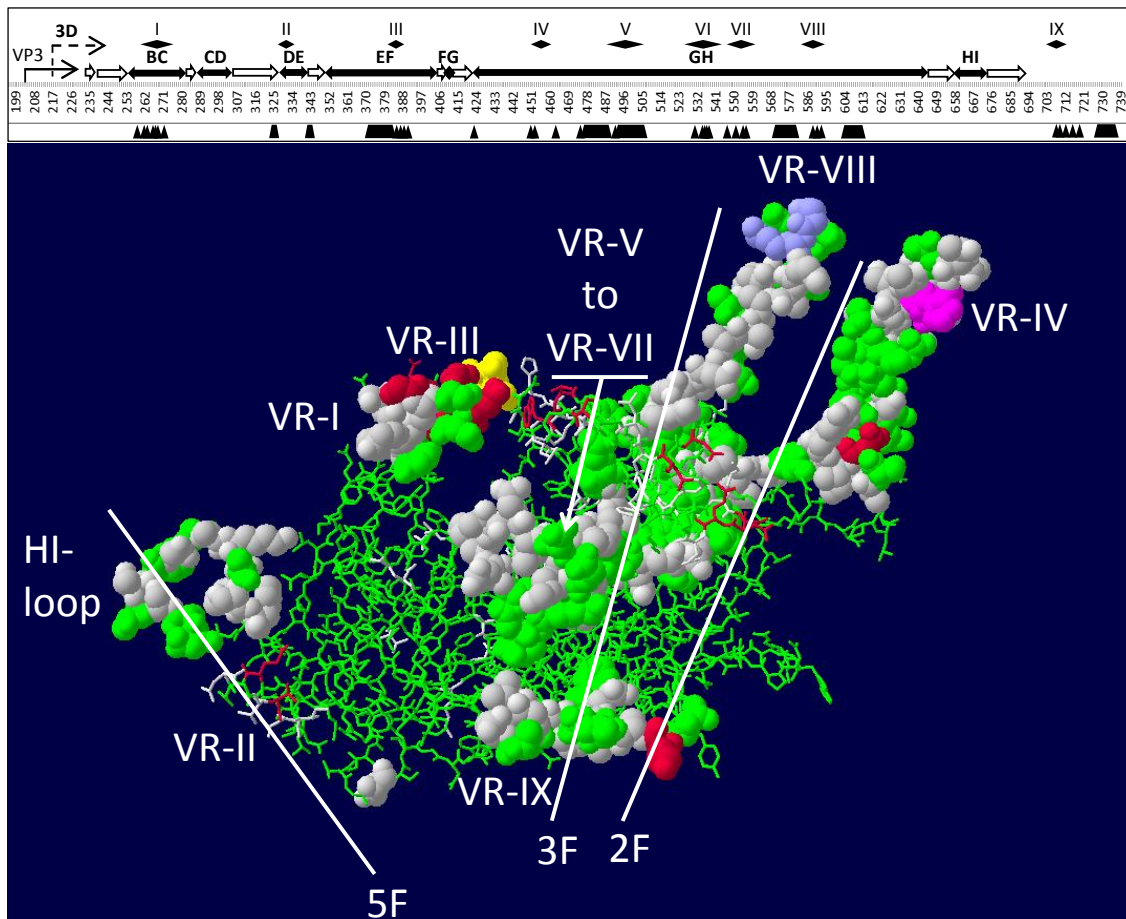


Figure 55: Structure of the AAV VP3 protein. The top panel shows a linear alignment of the C-terminal aa that are shared by all three VP proteins in analogy to **Figure 4** in the introductory chapter. The lower part gives an overview over a VP3 monomer. Variable regions are named and indicated by light gray color. Thin white lines indicate the 2-fold (2F), 3-fold (3F) and 5-fold (5F) symmetry axis, respectively, of the assembled AAV capsid. Colored residues show aa that contribute to the 'Dead Zone' (red) [81], peptide insertion sites at position 453 (purple) [331] and 588 (blue) [221] and the 'NGR' motif (yellow) [100].

Importantly, albeit the methods of capsid shuffling and peptide display are fundamentally different, they are also highly complementary. For example, our approach to display DRG-targeting peptides aimed at improving transduction of sensory and motor neurons upon direct application, but could not account for retrograde transport. Therefore, very recently, we have started to screen the AAV15689 chimeric library in analogy to the selection on β -cells (chapter 3.1.3) for chimeric AAV vectors that allow efficient transduction of DRG neurons by retrograde transport upon sciatic nerve injection *in vivo*. Preliminary data from the analysis of some of the enriched chimeras revealed that they were mostly composed of sequences from serotypes AAV1 and AAV6 (data are shown in the Appendix). These results are in accordance with our observed high efficiency of wtAAV6 on neurons and DRGs (Figure 52). Considering now also the further increase of AAV1 transduction by display of peptide P9 (FGQ) (3.2.5.2.1), it might be possible to boost the efficiency of the selected AAV chimeras that are already capable of effective retrograde transport. Hence, the combination of the results from both approaches may yield a vector suitable for DRG transduction upon peripheral vector administration.

In the course of our work, we finally provided first evidence that AAV capsid shuffling can indeed be combined with peptide display. Therefore, we shuffled capsid sequences that already contain insertion sites for peptide display, which allows to merge both methods for subsequent capsid selection from the resulting, highly complex library. Considering the observed mutual influence of capsid backbone and peptide sequence, the feasibility to screen a peptide library within a shuffled capsid scaffold has important implications for AAV capsid engineering and evolution. In fact, by inserting a distinct peptide with a known binding ability into a shuffled capsid library, it should be possible to evolve a capsid backbone whose composition ideally supports display and activity of the given peptide. Thereby, such a combinatorial library has potential to merge the best of both worlds, *i.e.*, the global effects of DNA family shuffling on capsid structure and function, with the local refinements introduced by peptide display.

In the future, an important next step is the *in vivo* evaluation of our peptide displaying AAV panels as well as of our lead candidates from the multiple shuffling approaches. To maximize the efficiency of this process, it should be beneficial to adapt a recently described method for high-throughput screening termed AAV barcode sequencing that relies on reporter constructs that additionally contain short, specific sequences. These 'DNA barcodes' allow to determine the biodistribution of different individual AAVs or of whole libraries *in vivo* in a single animal [337]. With such approaches and together with the ever increasing structural information on AAV serotypes, our results, our methodological improvements and our new tools should help to significantly advance the field of AAV vector evolution and thereby foster the clinical implementation of human gene therapy.

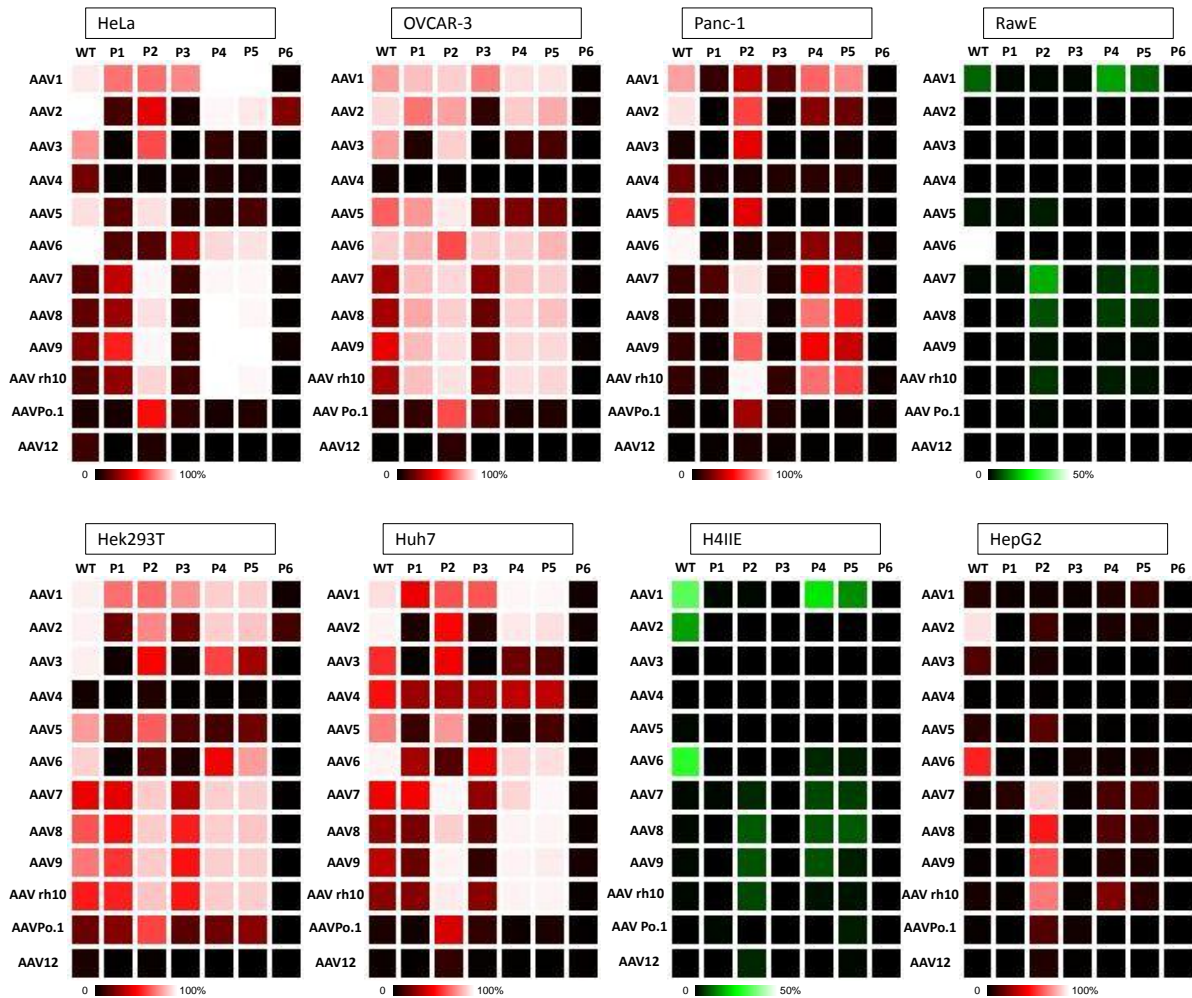
5 Appendix

5.1 Supplementary heatmaps

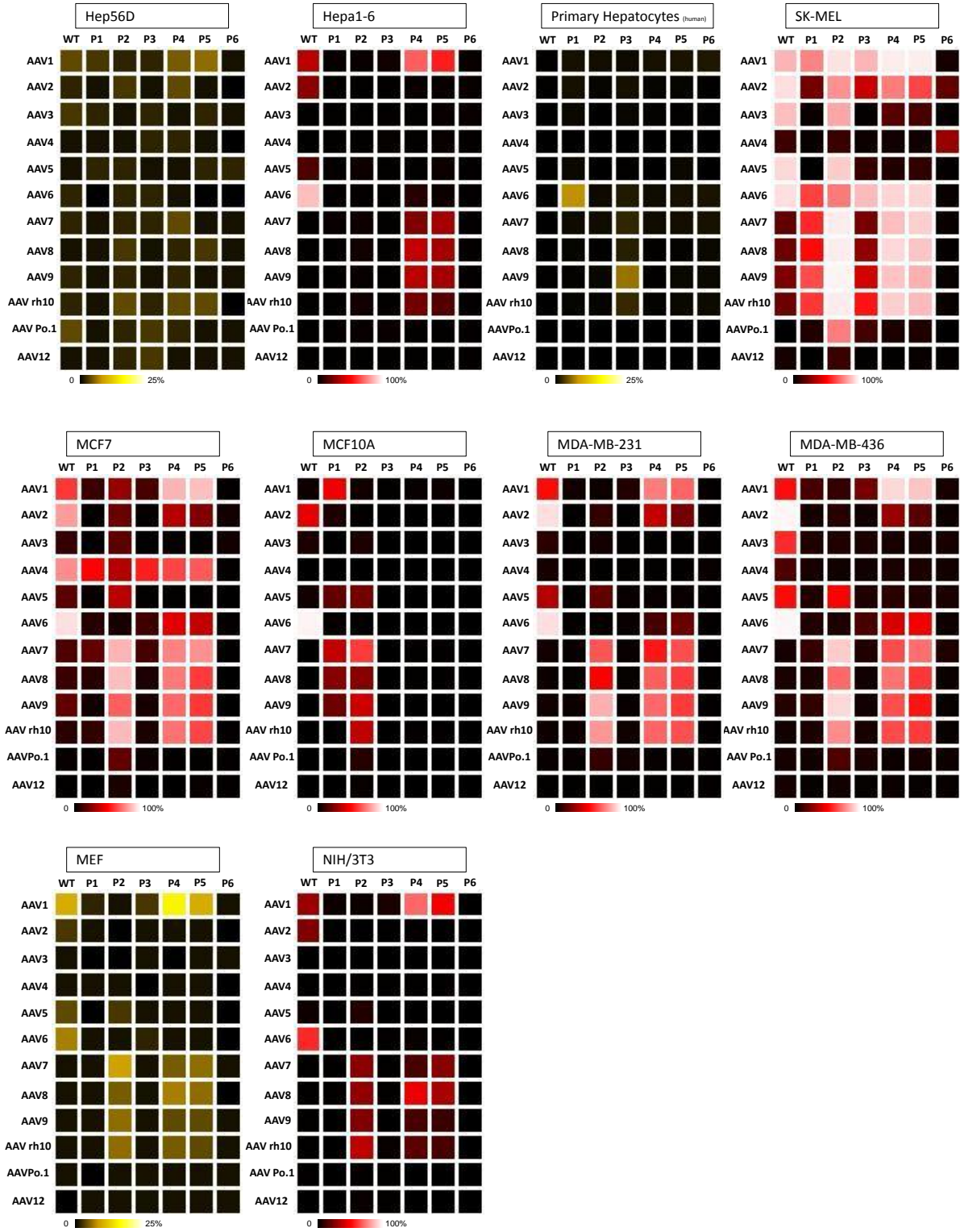
5.1.1 Transduction pattern of AAV1-12 with peptides P1-P6

The following heatmaps provide additional information on the peptide display screens conducted with peptides P1 to P6, described in detail in 3.2.3. Screening experiments and FACS analysis were performed together with Marina Bechtle, a former MSc student in our lab.

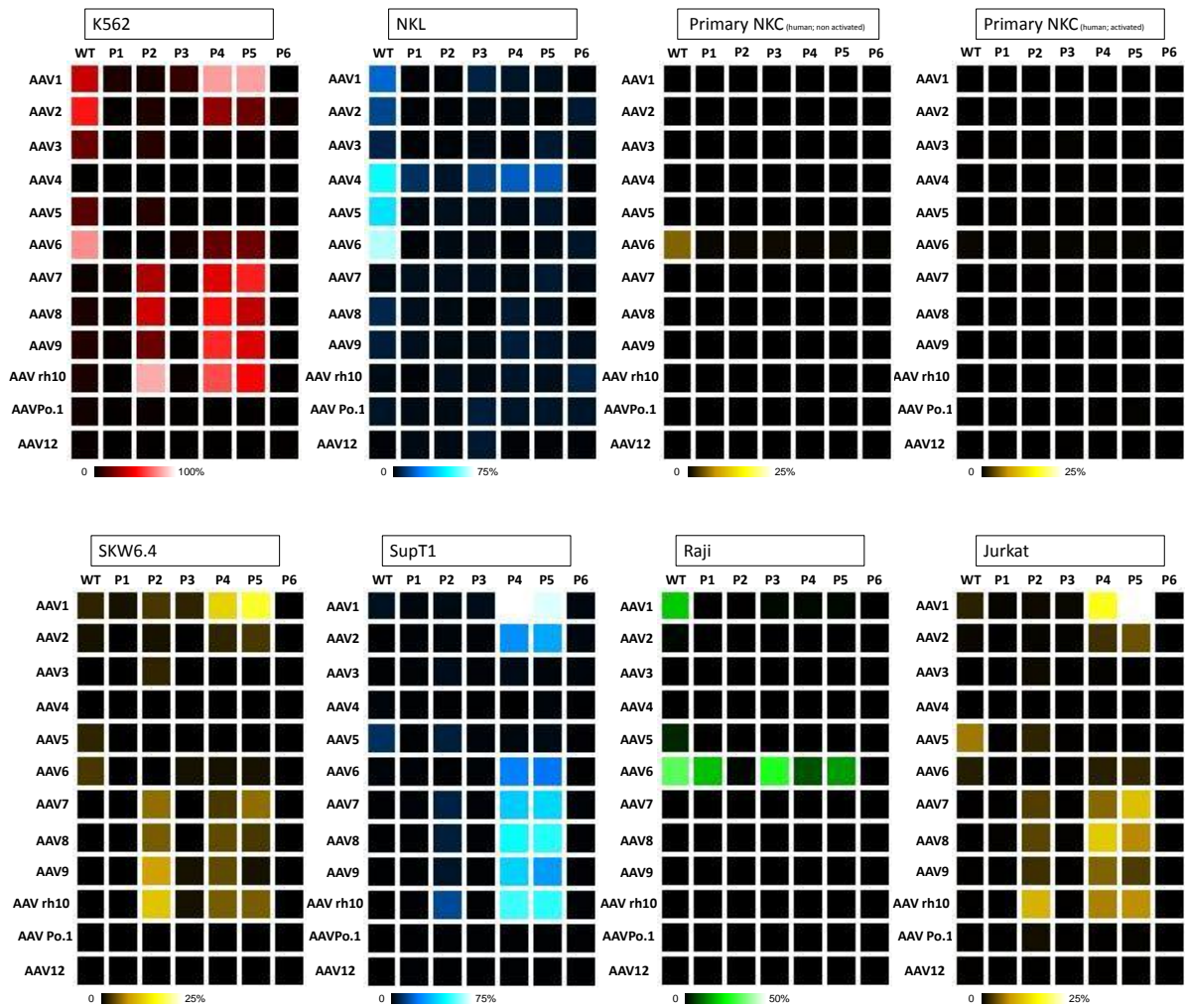
5.1.1.1 Transduction of cells from solid organs:



Appendix

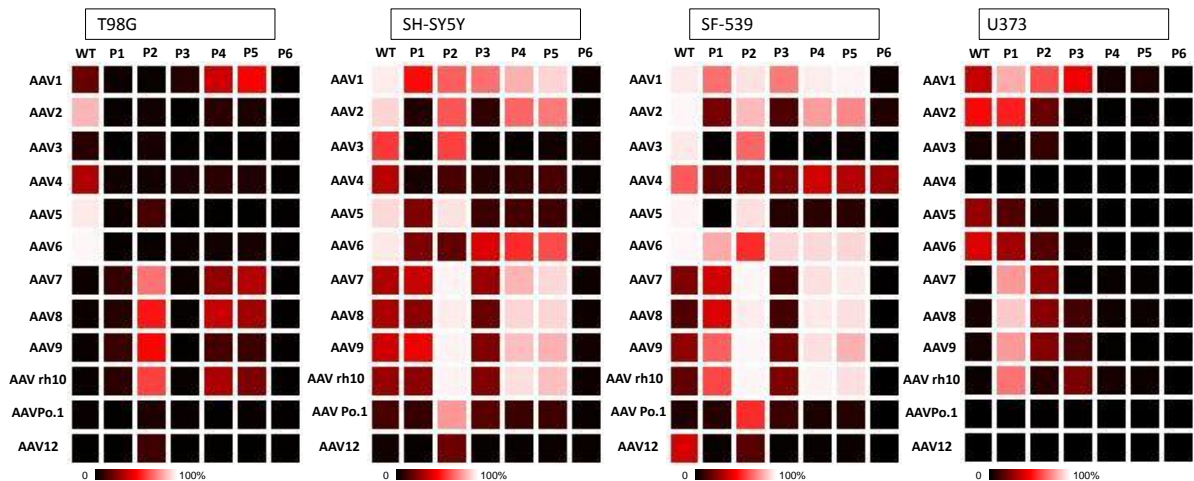


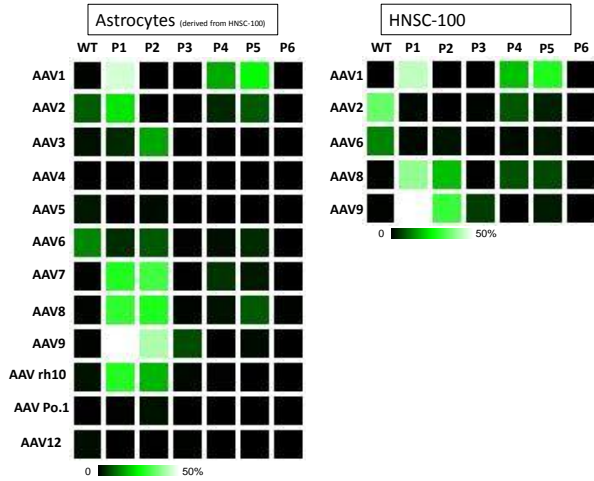
5.1.1.2 Transduction of cells from bone marrow and of hematopoietic origin:



Heat maps with P1-P6 are partially based on data obtained by Marina Bechtle, a former MSc student in our lab. Heat maps of primary NKC (activated and non-activated) are courtesy of Marina Bechtle. Cells of hematopoietic origin were provided by Dr. Kathleen Börner (Infectious Diseases/ Virology Dept.).

5.1.1.3 Transduction of cells of neuronal origin:



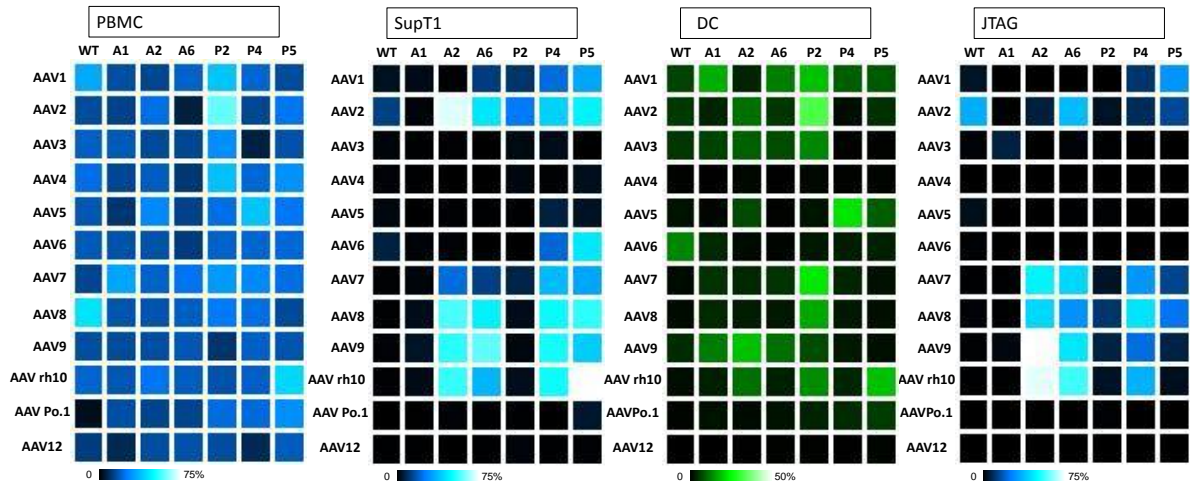


HNSC-100 were provided by Christine Kammel, Helmholtz Zentrum München. Astrocytes were derived from HNSC-100 by Christine Kammel.

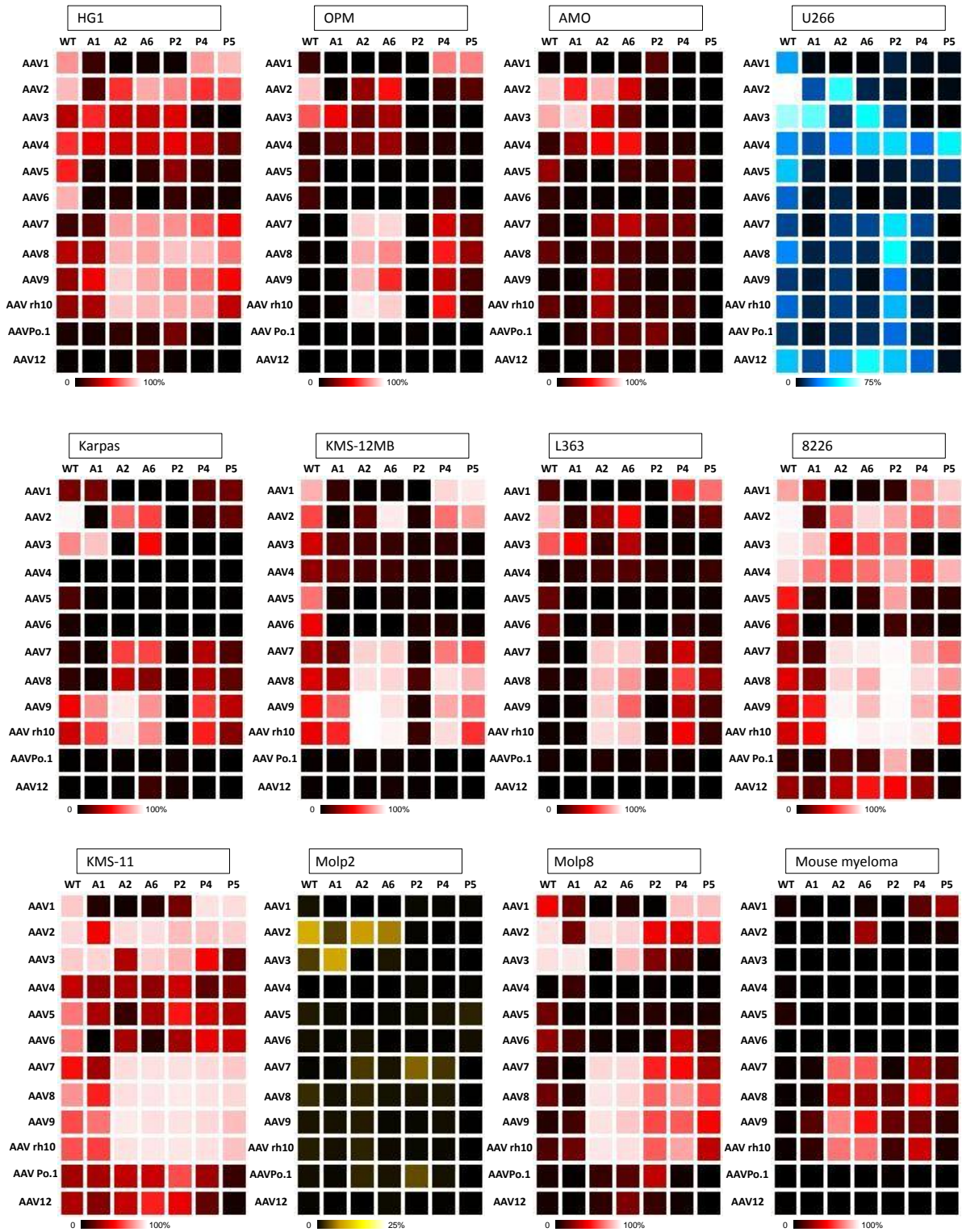
5.1.2 Transduction pattern of AAV1-12 with peptides of the MP

The following heatmaps provide additional information on the peptide display screens conducted with the MP that includes peptides A1, A2 and A6 as well as P2, P4 and P5. Screening experiments and FACs analysis were performed together with Dr. Kathleen Börner (Infectious Diseases/ Virology Dept).

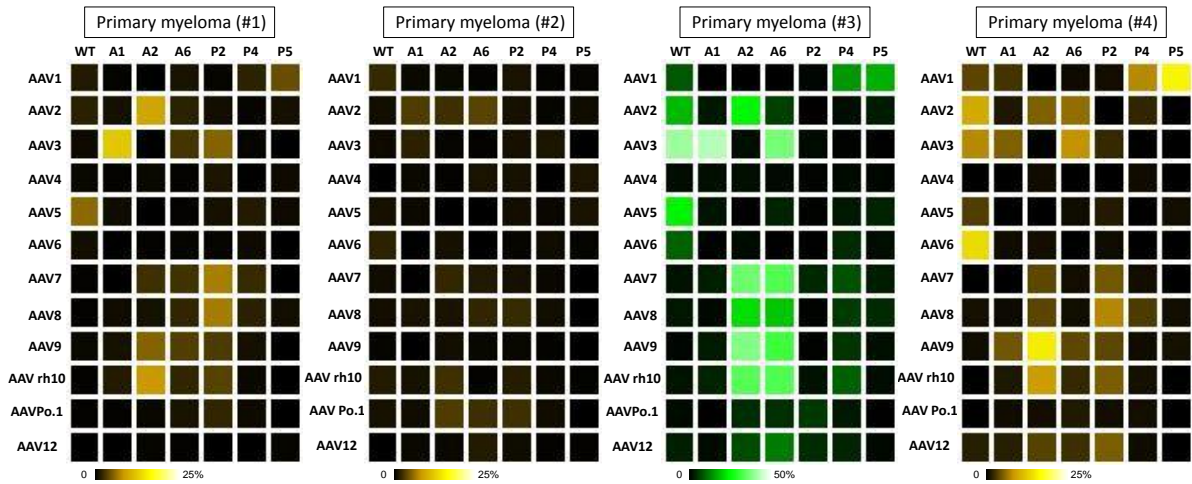
5.1.2.1 Transduction of cells of hematopoietic origin:



5.1.2.2 *Transduction of myeloid cells:*

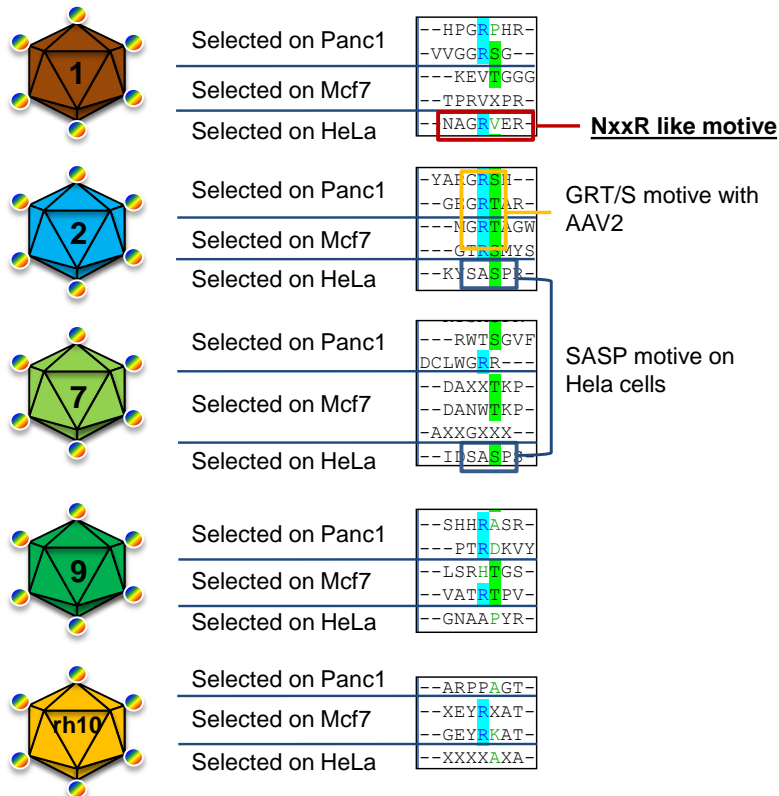


5.1.2.3 Transduction of primary human myeloma cells:

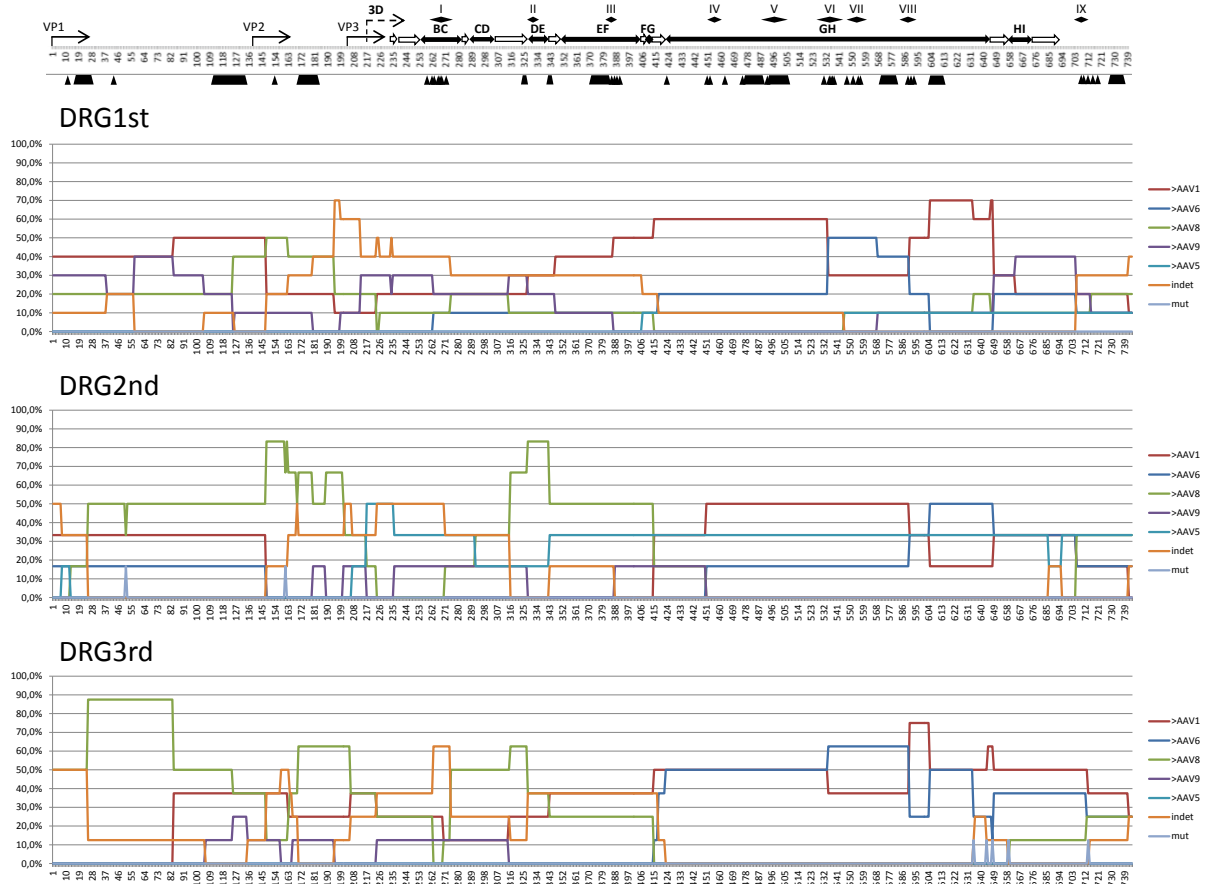


Peptide sequences A1, A2 and A6 of the MP were provided by Dr. Anna Sacher from the group of Prof. Dr. Martin Müller, German Cancer Research Center. Cells of hematopoietic origin were provided by Dr. Kathleen Börner (Infectious Diseases/ Virology Dept.). Myeloid cell lines and primary myeloma cells were provided by Dr. Anja Seckinger (Medizinische Klinik V, Heidelberg).

5.2 Supplementary data on AAV library selection schemes



Supplementary Figure 1: Peptide library screen in selected AAV serotypes. Shown are serotypes with peptide libraries indicated and cell lines on which the libraries were selected. Single clones were sequenced after two rounds of selection to generally control the functionality of the approach. Peptide sequences that emerged are shown on the right and possible pattern are indicated by colored boxes. 'X' marks positions where sequencing could not determine an exact nucleotide or aa, respectively. Note that due to the limited number of selection rounds and analyzed clones, these data are preliminary and only show tendencies.



Supplementary Figure 2: Overview over the capsid protein composition of the AAV15689 library selected *in vivo*. Shown are results after the first (DRG1st), second (DRG2nd) and third (DRG3rd) injection. The top panel shows the linear alignment of VP amino acid residues. See Figure 4 in the Introduction for details. Colored lines in the three panels underneath indicate the percentage of clones that originate from the respective parental serotype at any position within the AAV capsid sequence. Experiments were performed together with Julianne McCall (Orthopedics Dept., Klinik Heidelberg, group of Prof. Dr. Armin Blesch)

5.3 Supplementary electronic Data

Together with the printed dissertation, a CD is provided that contains additional sequence information on clones selected from the AAV289 and AAV15689 capsid shuffled libraries. These files (Excel) show complete capsid amino acid sequences of selected chimeras in a sequence alignment with their parental serotypes.

6 References

- [1] R. C. Lee, R. L. Feinbaum, and V. Ambros, "The *C. elegans* heterochronic gene *lin-4* encodes small RNAs with antisense complementarity to *lin-14*," *Cell*, vol. 75, no. 5, pp. 843–54, Dec. 1993.
- [2] A. Fire, S. Xu, M. K. Montgomery, S. A. Kostas, S. E. Driver, and C. C. Mello, "Potent and specific genetic interference by double-stranded RNA in *Caenorhabditis elegans*," *Nature*, vol. 391, no. 6669, pp. 806–11, Feb. 1998.
- [3] R. C. Lee and V. Ambros, "An extensive class of small RNAs in *Caenorhabditis elegans*," *Science*, vol. 294, no. 5543, pp. 862–4, Oct. 2001.
- [4] D. Grimm and M. A. Kay, "Therapeutic application of RNAi: is mRNA targeting finally ready for prime time?," *J. Clin. Invest.*, vol. 117, no. 12, pp. 3633–41, Dec. 2007.
- [5] K. Tiemann and J. J. Rossi, "RNAi-based therapeutics-current status, challenges and prospects," *EMBO Mol. Med.*, vol. 1, no. 3, pp. 142–51, Jun. 2009.
- [6] P. Asuri, M. a Bartel, T. Vazin, J.-H. Jang, T. B. Wong, and D. V Schaffer, "Directed evolution of adeno-associated virus for enhanced gene delivery and gene targeting in human pluripotent stem cells," *Mol. Ther.*, vol. 20, no. 2, pp. 329–38, Feb. 2012.
- [7] S. Misra, "Human gene therapy: a brief overview of the genetic revolution.," *J. Assoc. Physicians India*, vol. 61, no. 2, pp. 127–33, Feb. 2013.
- [8] S. L. Ginn, I. E. Alexander, M. L. Edelstein, M. R. Abedi, and J. Wixon, "Gene therapy clinical trials worldwide to 2012 - an update.," *J. Gene Med.*, vol. 15, no. 2, pp. 65–77, Feb. 2013.
- [9] E. Marshall, "Gene therapy death prompts review of adenovirus vector.," *Science*, vol. 286, no. 5448, pp. 2244–5, Dec. 1999.
- [10] S. Lehrman, "Virus treatment questioned after gene therapy death.," *Nature*, vol. 401, no. 6753, pp. 517–8, Oct. 1999.
- [11] R. SoRelle, "Human gene therapy: science under fire.," *Circulation*, vol. 101, no. 12, pp. E9023–4, Mar. 2000.
- [12] E. Marshall, "Gene therapy on trial.," *Science*, vol. 288, no. 5468, pp. 951–7, May 2000.
- [13] S. Hacein-Bey-Abina, C. von Kalle, M. Schmidt, F. Le Deist, N. Wulffraat, E. McIntyre, I. Radford, J.-L. Villeval, C. C. Fraser, M. Cavazzana-Calvo, and A. Fischer, "A serious adverse event after successful gene therapy for X-linked severe combined immunodeficiency.," *N. Engl. J. Med.*, vol. 348, no. 3, pp. 255–6, Jan. 2003.
- [14] A. J. Thrasher, H. B. Gaspar, C. Baum, U. Modlich, A. Schambach, F. Candotti, M. Otsu, B. Sorrentino, L. Scobie, E. Cameron, K. Blyth, J. Neil, S. H.-B. Abina, M. Cavazzana-Calvo, and A. Fischer, "Gene therapy: X-SCID transgene leukaemogenicity.," *Nature*, vol. 443, no. 7109, pp. E5–6; discussion E6–7, Sep. 2006.

- [15] A. C. Nathwani, E. G. D. Tuddenham, S. Rangarajan, C. Rosales, J. McIntosh, D. C. Linch, P. Chowdary, A. Riddell, A. J. Pie, C. Harrington, J. O'Beirne, K. Smith, J. Pasi, B. Glader, P. Rustagi, C. Y. C. Ng, M. A. Kay, J. Zhou, Y. Spence, C. L. Morton, J. Allay, J. Coleman, S. Sleep, J. M. Cunningham, D. Srivastava, E. Basner-Tschakarjan, F. Mingozzi, K. A. High, J. T. Gray, U. M. Reiss, A. W. Nienhuis, and A. M. Davidoff, "Adenovirus-associated virus vector-mediated gene transfer in hemophilia B.," *N. Engl. J. Med.*, vol. 365, no. 25, pp. 2357–65, Dec. 2011.
- [16] J. Bennett, M. Ashtari, J. Wellman, K. A. Marshall, L. L. Cyckowski, D. C. Chung, S. McCague, E. A. Pierce, Y. Chen, J. L. Bennicelli, X. Zhu, G.-S. Ying, J. Sun, J. F. Wright, A. Auricchio, F. Simonelli, K. S. Shindler, F. Mingozzi, K. A. High, and A. M. Maguire, "AAV2 gene therapy readministration in three adults with congenital blindness.," *Sci. Transl. Med.*, vol. 4, no. 120, p. 120ra15, Feb. 2012.
- [17] M. Ashtari, L. L. Cyckowski, J. F. Monroe, K. A. Marshall, D. C. Chung, A. Auricchio, F. Simonelli, B. P. Leroy, A. M. Maguire, K. S. Shindler, and J. Bennett, "The human visual cortex responds to gene therapy-mediated recovery of retinal function.," *J. Clin. Invest.*, vol. 121, no. 6, pp. 2160–8, Jun. 2011.
- [18] F. Simonelli, A. M. Maguire, F. Testa, E. A. Pierce, F. Mingozzi, J. L. Bennicelli, S. Rossi, K. Marshall, S. Banfi, E. M. Surace, J. Sun, T. M. Redmond, X. Zhu, K. S. Shindler, G.-S. Ying, C. Ziviello, C. Acerra, J. F. Wright, J. W. McDonnell, K. A. High, J. Bennett, and A. Auricchio, "Gene therapy for Leber's congenital amaurosis is safe and effective through 1.5 years after vector administration.," *Mol. Ther.*, vol. 18, no. 3, pp. 643–50, Mar. 2010.
- [19] A. Biffi, E. Montini, L. Lorioli, M. Cesani, F. Fumagalli, T. Plati, C. Baldoli, S. Martino, A. Calabria, S. Canale, F. Benedicenti, G. Vallanti, L. Biasco, S. Leo, N. Kabbara, G. Zanetti, W. B. Rizzo, N. A. L. Mehta, M. P. Cicalese, M. Casiraghi, J. J. Boelens, U. Del Carro, D. J. Dow, M. Schmidt, A. Assanelli, V. Neduva, C. Di Serio, E. Stupka, J. Gardner, C. von Kalle, C. Bordignon, F. Ciceri, A. Rovelli, M. G. Roncarolo, A. Aiuti, M. Sessa, and L. Naldini, "Lentiviral hematopoietic stem cell gene therapy benefits metachromatic leukodystrophy.," *Science*, vol. 341, no. 6148, p. 1233158, Aug. 2013.
- [20] A. Aiuti, L. Biasco, S. Scaramuzza, F. Ferrua, M. P. Cicalese, C. Baricordi, F. Dionisio, A. Calabria, S. Giannelli, M. C. Castiello, M. Bosticardo, C. Evangelio, A. Assanelli, M. Casiraghi, S. Di Nunzio, L. Callegaro, C. Benati, P. Rizzardi, D. Pellin, C. Di Serio, M. Schmidt, C. Von Kalle, J. Gardner, N. Mehta, V. Neduva, D. J. Dow, A. Galy, R. Miniero, A. Finocchi, A. Metin, P. P. Banerjee, J. S. Orange, S. Galimberti, M. G. Valsecchi, A. Biffi, E. Montini, A. Villa, F. Ciceri, M. G. Roncarolo, and L. Naldini, "Lentiviral hematopoietic stem cell gene therapy in patients with Wiskott-Aldrich syndrome.," *Science*, vol. 341, no. 6148, p. 1233151, Aug. 2013.
- [21] D. Pezzoli, A. Kajaste-Rudnitski, R. Chiesa, and G. Candiani, "Lipid-based nanoparticles as nonviral gene delivery vectors.," *Methods Mol. Biol.*, vol. 1025, pp. 269–79, Jan. 2013.
- [22] D. Zhi, S. Zhang, B. Wang, Y. Zhao, B. Yang, and S. Yu, "Transfection efficiency of cationic lipids with different hydrophobic domains in gene delivery.," *Bioconjug. Chem.*, vol. 21, no. 4, pp. 563–77, Apr. 2010.
- [23] S. Bhattacharya and A. Bajaj, "Advances in gene delivery through molecular design of cationic lipids.," *Chem. Commun. (Camb.)*, no. 31, pp. 4632–56, Aug. 2009.

- [24] W.-B. Li, W. Yuan, F.-J. Xu, C. Zhao, J. Ma, and Q.-M. Zhan, "Functional study of dextran-graft-poly((2-dimethyl amino)ethyl methacrylate) gene delivery vector for tumor therapy.," *J. Biomater. Appl.*, vol. 28, no. 1, pp. 125–35, Jul. 2013.
- [25] Y.-Q. Wang, J. Su, F. Wu, P. Lu, L.-F. Yuan, W.-E. Yuan, J. Sheng, and T. Jin, "Biscarbamate cross-linked polyethylenimine derivative with low molecular weight, low cytotoxicity, and high efficiency for gene delivery.," *Int. J. Nanomedicine*, vol. 7, pp. 693–704, Jan. 2012.
- [26] J. Zhou, J. Liu, C. J. Cheng, T. R. Patel, C. E. Weller, J. M. Piepmeier, Z. Jiang, and W. M. Saltzman, "Biodegradable poly(amine-co-ester) terpolymers for targeted gene delivery.," *Nat. Mater.*, vol. 11, no. 1, pp. 82–90, Jan. 2012.
- [27] L. Jin, X. Zeng, M. Liu, Y. Deng, and N. He, "Current Progress in Gene Delivery Technology Based on Chemical Methods and Nano-carriers.," *Theranostics*, vol. 4, no. 3, pp. 240–55, Jan. 2014.
- [28] Y. Xu and F. C. Szoka, "Mechanism of DNA release from cationic liposome/DNA complexes used in cell transfection.," *Biochemistry*, vol. 35, no. 18, pp. 5616–23, May 1996.
- [29] O. Boussif, F. Lezoualc'h, M. A. Zanta, M. D. Mergny, D. Scherman, B. Demeneix, and J. P. Behr, "A versatile vector for gene and oligonucleotide transfer into cells in culture and in vivo: polyethylenimine.," *Proc. Natl. Acad. Sci. U. S. A.*, vol. 92, no. 16, pp. 7297–301, Aug. 1995.
- [30] P. Kreiss, B. Cameron, R. Rangara, P. Mailhe, O. Aguerre-Charriol, M. Airiau, D. Scherman, J. Crouzet, and B. Pitard, "Plasmid DNA size does not affect the physicochemical properties of lipoplexes but modulates gene transfer efficiency.," *Nucleic Acids Res.*, vol. 27, no. 19, pp. 3792–8, Oct. 1999.
- [31] D. V Schaffer, J. T. Koerber, and K. Lim, "Molecular engineering of viral gene delivery vehicles.," *Annu. Rev. Biomed. Eng.*, vol. 10, pp. 169–94, Jan. 2008.
- [32] R. Waehler, S. J. Russell, and D. T. Curiel, "Engineering targeted viral vectors for gene therapy.," *Nat. Rev. Genet.*, vol. 8, no. 8, pp. 573–87, Aug. 2007.
- [33] R. D. Sloan, B. D. Kuhl, T. Mesplède, J. Münch, D. A. Donahue, and M. A. Wainberg, "Productive entry of HIV-1 during cell-to-cell transmission via dynamin-dependent endocytosis.," *J. Virol.*, vol. 87, no. 14, pp. 8110–23, Jul. 2013.
- [34] K. Miyauchi, Y. Kim, O. Latinovic, V. Morozov, and G. B. Melikyan, "HIV enters cells via endocytosis and dynamin-dependent fusion with endosomes.," *Cell*, vol. 137, no. 3, pp. 433–44, May 2009.
- [35] C. J. Buchholz, M. D. Mühlbach, and K. Cichutek, "Lentiviral vectors with measles virus glycoproteins - dream team for gene transfer?," *Trends Biotechnol.*, vol. 27, no. 5, pp. 259–65, May 2009.
- [36] J. Cronin, X.-Y. Zhang, and J. Reiser, "Altering the tropism of lentiviral vectors through pseudotyping.," *Curr. Gene Ther.*, vol. 5, no. 4, pp. 387–98, Aug. 2005.
- [37] M. Havenga and A. Lemckert, "Exploiting the natural diversity in adenovirus tropism for therapy and prevention of disease.," *J. Virol.*, vol. 76, no. 9, pp. 4612–20, May 2002.

- [38] A. Sharma, X. Li, D. S. Bangari, and S. K. Mittal, "Adenovirus receptors and their implications in gene delivery.," *Virus Res.*, vol. 143, no. 2, pp. 184–94, Aug. 2009.
- [39] G. T. Mercier, J. A. Campbell, J. D. Chappell, T. Stehle, T. S. Dermody, and M. A. Barry, "A chimeric adenovirus vector encoding reovirus attachment protein sigma1 targets cells expressing junctional adhesion molecule 1.," *Proc. Natl. Acad. Sci. U. S. A.*, vol. 101, no. 16, pp. 6188–93, Apr. 2004.
- [40] S. C. Nouredini, A. Krendelshchikov, V. Simonenko, S. J. Hedley, J. T. Douglas, D. T. Curiel, and N. Korokhov, "Generation and selection of targeted adenoviruses embodying optimized vector properties.," *Virus Res.*, vol. 116, no. 1–2, pp. 185–95, Mar. 2006.
- [41] V. Krasnykh, N. Belousova, N. Korokhov, G. Mikheeva, and D. T. Curiel, "Genetic targeting of an adenovirus vector via replacement of the fiber protein with the phage T4 fibritin.," *J. Virol.*, vol. 75, no. 9, pp. 4176–83, May 2001.
- [42] K. I. Berns and C. Giraud, "Biology of adeno-associated virus.," *Curr. Top. Microbiol. Immunol.*, vol. 218, pp. 1–23, Jan. 1996.
- [43] R. W. Atchison, B. C. Casto, and W. M. Hammon, "Adenovirus-Associated Defective Virus Particles.," *Science*, vol. 149, no. 3685, pp. 754–6, Aug. 1965.
- [44] M. D. Hoggan, N. R. Blacklow, and W. P. Rowe, "Studies of small DNA viruses found in various adenovirus preparations: physical, biological, and immunological characteristics.," *Proc. Natl. Acad. Sci. U. S. A.*, vol. 55, no. 6, pp. 1467–74, Jun. 1966.
- [45] M.-C. Geoffroy and A. Salvetti, "Helper functions required for wild type and recombinant adeno-associated virus growth.," *Curr. Gene Ther.*, vol. 5, no. 3, pp. 265–71, Jun. 2005.
- [46] L. Mishra and J. A. Rose, "Adeno-associated virus DNA replication is induced by genes that are essential for HSV-1 DNA synthesis.," *Virology*, vol. 179, no. 2, pp. 632–9, Dec. 1990.
- [47] N. Alazard-Dany, A. Nicolas, A. Ploquin, R. Strasser, A. Greco, A. L. Epstein, C. Fraefel, and A. Salvetti, "Definition of herpes simplex virus type 1 helper activities for adeno-associated virus early replication events.," *PLoS Pathog.*, vol. 5, no. 3, p. e1000340, Mar. 2009.
- [48] R. M. Linden, E. Winocour, and K. I. Berns, "The recombination signals for adeno-associated virus site-specific integration.," *Proc. Natl. Acad. Sci. U. S. A.*, vol. 93, no. 15, pp. 7966–72, Jul. 1996.
- [49] D. M. McCarty, S. M. Young, and R. J. Samulski, "Integration of adeno-associated virus (AAV) and recombinant AAV vectors.," *Annu. Rev. Genet.*, vol. 38, pp. 819–45, Jan. 2004.
- [50] J. A. King, R. Dubielzig, D. Grimm, and J. A. Kleinschmidt, "DNA helicase-mediated packaging of adeno-associated virus type 2 genomes into preformed capsids.," *EMBO J.*, vol. 20, no. 12, pp. 3282–91, Jun. 2001.
- [51] R. Dubielzig, J. A. King, S. Weger, A. Kern, and J. A. Kleinschmidt, "Adeno-associated virus type 2 protein interactions: formation of pre-encapsidation complexes.," *J. Virol.*, vol. 73, no. 11, pp. 8989–98, Nov. 1999.

- [52] S. R. Kyöstiö, R. A. Owens, M. D. Weitzman, B. A. Antoni, N. Chejanovsky, and B. J. Carter, "Analysis of adeno-associated virus (AAV) wild-type and mutant Rep proteins for their abilities to negatively regulate AAV p5 and p19 mRNA levels.," *J. Virol.*, vol. 68, no. 5, pp. 2947–57, May 1994.
- [53] M. D. Weitzman, S. R. Kyöstiö, R. M. Kotin, and R. A. Owens, "Adeno-associated virus (AAV) Rep proteins mediate complex formation between AAV DNA and its integration site in human DNA.," *Proc. Natl. Acad. Sci. U. S. A.*, vol. 91, no. 13, pp. 5808–12, Jun. 1994.
- [54] R. H. Smith and R. M. Kotin, "The Rep52 gene product of adeno-associated virus is a DNA helicase with 3'-to-5' polarity.," *J. Virol.*, vol. 72, no. 6, pp. 4874–81, Jun. 1998.
- [55] F. Sonntag, K. Schmidt, and J. A. Kleinschmidt, "A viral assembly factor promotes AAV2 capsid formation in the nucleolus.," *Proc. Natl. Acad. Sci. U. S. A.*, vol. 107, no. 22, pp. 10220–5, Jun. 2010.
- [56] F. Sonntag, K. Köther, K. Schmidt, M. Weghofer, C. Raupp, K. Nieto, a Kuck, B. Gerlach, B. Böttcher, O. J. Müller, K. Lux, M. Hörer, and J. a Kleinschmidt, "The assembly-activating protein promotes capsid assembly of different adeno-associated virus serotypes.," *J. Virol.*, vol. 85, no. 23, pp. 12686–97, Dec. 2011.
- [57] A. Girod, C. E. Wobus, Z. Zádori, M. Ried, K. Leike, P. Tijssen, J. a Kleinschmidt, and M. Hallek, "The VP1 capsid protein of adeno-associated virus type 2 is carrying a phospholipase A2 domain required for virus infectivity.," *J. Gen. Virol.*, vol. 83, no. Pt 5, pp. 973–8, May 2002.
- [58] F. Sonntag, S. Bleker, B. Leuchs, R. Fischer, and J. a Kleinschmidt, "Adeno-associated virus type 2 capsids with externalized VP1/VP2 trafficking domains are generated prior to passage through the cytoplasm and are maintained until uncoating occurs in the nucleus.," *J. Virol.*, vol. 80, no. 22, pp. 11040–54, Nov. 2006.
- [59] J. C. Grieger, J. S. Johnson, B. Gurda-Whitaker, M. Agbandje-McKenna, and R. J. Samulski, "Surface-exposed adeno-associated virus Vp1-NLS capsid fusion protein rescues infectivity of noninfectious wild-type Vp2/Vp3 and Vp3-only capsids but not that of fivefold pore mutant virions.," *J. Virol.*, vol. 81, no. 15, pp. 7833–43, Aug. 2007.
- [60] J. S. Johnson, C. Li, N. DiPrimio, M. S. Weinberg, T. J. McCown, and R. J. Samulski, "Mutagenesis of adeno-associated virus type 2 capsid protein VP1 uncovers new roles for basic amino acids in trafficking and cell-specific transduction.," *J. Virol.*, vol. 84, no. 17, pp. 8888–902, Sep. 2010.
- [61] K. H. W. Jr, O. S. Gorbatyuk, K. Jeffrey, S. R. Opie, S. Zolotukhin, K. H. Warrington, J. K. Harrison, and N. Muzyczka, "Adeno-associated virus type 2 VP2 capsid protein is nonessential and can tolerate large peptide insertions at its N terminus.," *J. Virol.*, vol. 78, no. 12, pp. 6595–609, Jun. 2004.
- [62] R. Popa-Wagner, M. Porwal, M. Kann, M. Reuss, M. Weimer, L. Florin, and J. A. Kleinschmidt, "Impact of VP1-specific protein sequence motifs on adeno-associated virus type 2 intracellular trafficking and nuclear entry.," *J. Virol.*, vol. 86, no. 17, pp. 9163–74, Sep. 2012.
- [63] R. Popa-Wagner, F. Sonntag, K. Schmidt, J. King, and J. A. Kleinschmidt, "Nuclear translocation of adeno-associated virus type 2 capsid proteins for virion assembly.," *J. Gen. Virol.*, vol. 93, no. Pt 9, pp. 1887–98, Sep. 2012.

- [64] Q. Xie, W. Bu, S. Bhatia, J. Hare, T. Somasundaram, A. Azzi, and M. S. Chapman, "The atomic structure of adeno-associated virus (AAV-2), a vector for human gene therapy.," *Proc. Natl. Acad. Sci. U. S. A.*, vol. 99, no. 16, pp. 10405–10, Aug. 2002.
- [65] G. Gao, L. H. Vandenberghe, M. R. Alvira, Y. Lu, R. Calcedo, X. Zhou, and J. M. Wilson, "Clades of Adeno-associated viruses are widely disseminated in human tissues.," *J. Virol.*, vol. 78, no. 12, pp. 6381–8, Jun. 2004.
- [66] E. Padron, V. Bowman, N. Kaludov, H. Levy, P. Nick, R. McKenna, N. Muzyczka, J. A. Chiorini, T. S. Baker, M. Agbandje-McKenna, and L. Govindasamy, "Structure of adeno-associated virus type 4.," *J. Virol.*, vol. 79, no. 8, pp. 5047–58, Apr. 2005.
- [67] L. Govindasamy, E. Padron, R. McKenna, N. Muzyczka, N. Kaludov, J. a Chiorini, and M. Agbandje-McKenna, "Structurally mapping the diverse phenotype of adeno-associated virus serotype 4.," *J. Virol.*, vol. 80, no. 23, pp. 11556–70, Dec. 2006.
- [68] H.-J. Nam, M. D. Lane, E. Padron, B. Gurda, R. McKenna, E. Kohlbrenner, G. Aslanidi, B. Byrne, N. Muzyczka, S. Zolotukhin, and M. Agbandje-McKenna, "Structure of adeno-associated virus serotype 8, a gene therapy vector.," *J. Virol.*, vol. 81, no. 22, pp. 12260–71, Nov. 2007.
- [69] T. F. Lerch, Q. Xie, and M. S. Chapman, "The structure of adeno-associated virus serotype 3B (AAV-3B): insights into receptor binding and immune evasion.," *Virology*, vol. 403, no. 1, pp. 26–36, Jul. 2010.
- [70] R. W. Walters, M. Agbandje-McKenna, V. D. Bowman, T. O. Moninger, N. H. Olson, M. Seiler, J. A. Chiorini, T. S. Baker, and J. Zabner, "Structure of adeno-associated virus serotype 5.," *J. Virol.*, vol. 78, no. 7, pp. 3361–71, Apr. 2004.
- [71] H. C. Levy, V. D. Bowman, L. Govindasamy, R. McKenna, K. Warrington, W. Chen, N. Muzyczka, X. Yan, S. Baker, and M. Agbandje-mckenna, "Heparin binding induces conformational changes in Adenoassociated virus serotype 2," *J. Struct. Biol*, vol. 165, no. 3, pp. 146–56, Mar. 2009.
- [72] S. Kronenberg, B. Böttcher, C. W. Von Der, S. Bleker, J. A. Kleinschmidt, B. Bo, and C. W. Von Der Lieth, "A Conformational Change in the Adeno-Associated Virus Type 2 Capsid Leads to the Exposure of Hidden VP1 N Termini," *J. Virol.*, vol. 79, no. 9, pp. 5296–303, May 2005.
- [73] R. Ng, L. Govindasamy, B. L. Gurda, R. McKenna, O. G. Kozyreva, R. J. Samulski, K. N. Parent, T. S. Baker, and M. Agbandje-McKenna, "Structural characterization of the dual glycan binding adeno-associated virus serotype 6.," *J. Virol.*, vol. 84, no. 24, pp. 12945–57, Dec. 2010.
- [74] M. DiMattia, L. Govindasamy, H. C. Levy, B. Gurda-Whitaker, A. Kalina, E. Kohlbrenner, J. A. Chiorini, R. McKenna, N. Muzyczka, S. Zolotukhin, and M. Agbandje-McKenna, "Production, purification, crystallization and preliminary X-ray structural studies of adeno-associated virus serotype 5.," *Acta Crystallogr. Sect. F. Struct. Biol. Cryst. Commun.*, vol. 61, no. Pt 10, pp. 917–21, Oct. 2005.
- [75] M. D. Lane, H. J. Nam, E. Padron, B. Gurda-Whitaker, E. Kohlbrenner, G. Aslanidi, B. Byrne, R. McKenna, N. Muzyczka, S. Zolotukhin, and M. Agbandje-McKenna, "Production, purification, crystallization and preliminary X-ray analysis of adeno-associated virus serotype 8.," *Acta Crystallogr. Sect. F. Struct. Biol. Cryst. Commun.*, vol. 61, no. Pt 6, pp. 558–61, Jun. 2005.

- [76] J. O'Donnell, K. A. Taylor, and M. S. Chapman, "Adeno-associated virus-2 and its primary cellular receptor--Cryo-EM structure of a heparin complex.," *Virology*, vol. 385, no. 2, pp. 434–443, Mar. 2009.
- [77] T. F. Lerch, Q. Xie, H. M. Ongley, J. Hare, and M. S. Chapman, "Twinned crystals of adeno-associated virus serotype 3b prove suitable for structural studies.," *Acta Crystallogr. Sect. F. Struct. Biol. Cryst. Commun.*, vol. 65, no. Pt 2, pp. 177–83, Feb. 2009.
- [78] Q. Xie, H. M. Ongley, J. Hare, and M. S. Chapman, "Crystallization and preliminary X-ray structural studies of adeno-associated virus serotype 6.," *Acta Crystallogr. Sect. F. Struct. Biol. Cryst. Commun.*, vol. 64, no. Pt 11, pp. 1074–8, Nov. 2008.
- [79] M. Agbandje-McKenna and J. Kleinschmidt, "AAV capsid structure and cell interactions.," *Methods Mol. Biol.*, vol. 807, pp. 47–92, Jan. 2011.
- [80] S. Bleker, F. Sonntag, and J. A. Kleinschmidt, "Mutational analysis of narrow pores at the fivefold symmetry axes of adeno-associated virus type 2 capsids reveals a dual role in genome packaging and activation of phospholipase A2 activity.," *J. Virol.*, vol. 79, no. 4, pp. 2528–40, Feb. 2005.
- [81] M. A. Lochrie, G. P. Tatsuno, B. Christie, J. W. McDonnell, S. Zhou, G. F. Pierce, P. Colosi, and R. Suroskey, "Mutations on the External Surfaces of Adeno-Associated Virus Type 2 Capsids That Affect Transduction and Neutralization," *J. Virol.*, vol. 80, no. 2, pp. 821–34, Jan. 2006.
- [82] N. Maheshri, J. T. Koerber, B. K. Kaspar, and D. V Schaffer, "Directed evolution of adeno-associated virus yields enhanced gene delivery vectors.," *Nat. Biotechnol.*, vol. 24, no. 2, pp. 198–204, Feb. 2006.
- [83] L. Perabo, J. Endell, S. King, K. Lux, D. Goldnau, M. Hallek, and H. Büning, "Combinatorial engineering of a gene therapy vector: directed evolution of adeno-associated virus.," *J. Gene Med.*, vol. 8, no. 2, pp. 155–62, Feb. 2006.
- [84] a Girod, M. Ried, C. Wobus, H. Lahm, K. Leike, J. Kleinschmidt, G. Deléage, and M. Hallek, "Genetic capsid modifications allow efficient re-targeting of adeno-associated virus type 2.," *Nat. Med.*, vol. 5, no. 12, p. 1438, Dec. 1999.
- [85] N. a Huttner, a Girod, L. Perabo, D. Edbauer, J. a Kleinschmidt, H. Büning, and M. Hallek, "Genetic modifications of the adeno-associated virus type 2 capsid reduce the affinity and the neutralizing effects of human serum antibodies.," *Gene Ther.*, vol. 10, no. 26, pp. 2139–47, Dec. 2003.
- [86] C. E. Wobus, B. Hügler-dörr, A. Girod, G. Petersen, M. Hallek, A. Jürgen, and B. Hu, "Monoclonal Antibodies against the Adeno-Associated Virus Type 2 (AAV-2) Capsid : Epitope Mapping and Identification of Capsid Domains Involved in AAV-2 – Cell Interaction and Neutralization of AAV-2 Infection," *J. Virol.*, vol. 74, no. 19, pp. 9281–93, Oct. 2000.
- [87] M. Bartel, D. Schaffer, and H. Büning, "Enhancing the Clinical Potential of AAV Vectors by Capsid Engineering to Evade Pre-Existing Immunity.," *Front. Microbiol.*, vol. 2, no. October, p. 204, Jan. 2011.

- [88] G.-P. Gao, M. R. Alvira, L. Wang, R. Calcedo, J. Johnston, and J. M. Wilson, "Novel adeno-associated viruses from rhesus monkeys as vectors for human gene therapy.," *Proc. Natl. Acad. Sci. U. S. A.*, vol. 99, no. 18, pp. 11854–9, Sep. 2002.
- [89] Z. Wu, A. Asokan, J. C. Grieger, L. Govindasamy, M. Agbandje-McKenna, and R. J. Samulski, "Single amino acid changes can influence titer, heparin binding, and tissue tropism in different adeno-associated virus serotypes.," *J. Virol.*, vol. 80, no. 22, pp. 11393–7, Nov. 2006.
- [90] S. Mori, L. Wang, T. Takeuchi, and T. Kanda, "Two novel adeno-associated viruses from cynomolgus monkey: pseudotyping characterization of capsid protein.," *Virology*, vol. 330, no. 2, pp. 375–83, Dec. 2004.
- [91] M. Schmidt, L. Govindasamy, S. Afione, N. Kaludov, M. Agbandje-McKenna, and J. A. Chiorini, "Molecular characterization of the heparin-dependent transduction domain on the capsid of a novel adeno-associated virus isolate, AAV(VR-942).," *J. Virol.*, vol. 82, no. 17, pp. 8911–6, Sep. 2008.
- [92] M. Schmidt, A. Voutetakis, S. Afione, C. Zheng, D. Mandikian, and J. A. Chiorini, "Adeno-associated virus type 12 (AAV12): a novel AAV serotype with sialic acid- and heparan sulfate proteoglycan-independent transduction activity.," *J. Virol.*, vol. 82, no. 3, pp. 1399–406, Feb. 2008.
- [93] C. Summerford and R. J. Samulski, "Membrane-associated heparan sulfate proteoglycan is a receptor for adeno-associated virus type 2 virions.," *J. Virol.*, vol. 72, no. 2, pp. 1438–45, Feb. 1998.
- [94] Z. Wu, E. Miller, M. Agbandje-McKenna, and R. J. Samulski, "Alpha2,3 and alpha2,6 N-linked sialic acids facilitate efficient binding and transduction by adeno-associated virus types 1 and 6.," *J. Virol.*, vol. 80, no. 18, pp. 9093–103, Sep. 2006.
- [95] A. Kern, K. Schmidt, C. Leder, O. J. Müller, C. E. Wobus, C. W. Von Der Lieth, J. A. King, O. J. Mu, K. Bettinger, and J. A. Kleinschmidt, "Identification of a Heparin-Binding Motif on Adeno-Associated Virus Type 2 Capsids," *J. Virol.*, vol. 77, no. 20, pp. 11072–81, Oct. 2003.
- [96] S. R. Opie, K. H. Warrington, M. Agbandje-mckenna, S. Zolotukhin, and N. Muzyczka, "Identification of Amino Acid Residues in the Capsid Proteins of Adeno-Associated Virus Type 2 That Contribute to Heparan Sulfate Proteoglycan Binding †," vol. 77, no. 12, pp. 6995–7006, 2003.
- [97] P. Wu, W. Xiao, T. Conlon, J. Hughes, M. Agbandje-McKenna, T. Ferkol, T. Flotte, and N. Muzyczka, "Mutational analysis of the adeno-associated virus type 2 (AAV2) capsid gene and construction of AAV2 vectors with altered tropism.," *J. Virol.*, vol. 74, no. 18, pp. 8635–47, Sep. 2000.
- [98] N. Kaludov, K. E. Brown, R. W. Walters, J. Zabner, and J. A. Chiorini, "Adeno-associated virus serotype 4 (AAV4) and AAV5 both require sialic acid binding for hemagglutination and efficient transduction but differ in sialic acid linkage specificity.," *J. Virol.*, vol. 75, no. 15, pp. 6884–93, Aug. 2001.
- [99] R. W. Walters, S. M. Yi, S. Keshavjee, K. E. Brown, M. J. Welsh, J. A. Chiorini, and J. Zabner, "Binding of adeno-associated virus type 5 to 2,3-linked sialic acid is required for gene transfer.," *J. Biol. Chem.*, vol. 276, no. 23, pp. 20610–6, Jun. 2001.

- [100] A. Asokan, J. B. Hamra, L. Govindasamy, M. Agbandje-McKenna, and R. J. Samulski, "Adeno-associated virus type 2 contains an integrin alpha5beta1 binding domain essential for viral cell entry.," *J. Virol.*, vol. 80, no. 18, pp. 8961–9, Sep. 2006.
- [101] K. Qing, C. Mah, J. Hansen, S. Zhou, V. Dwarki, and A. Srivastava, "Human fibroblast growth factor receptor 1 is a co-receptor for infection by adeno-associated virus 2.," *Nat. Med.*, vol. 5, no. 1, pp. 71–7, Jan. 1999.
- [102] Y. Kashiwakura, K. Tamayose, K. Iwabuchi, Y. Hirai, T. Shimada, K. Matsumoto, T. Nakamura, M. Watanabe, K. Oshimi, and H. Daida, "Hepatocyte growth factor receptor is a coreceptor for adeno-associated virus type 2 infection.," *J. Virol.*, vol. 79, no. 1, pp. 609–14, Jan. 2005.
- [103] B. Akache, D. Grimm, K. Pandey, S. R. Yant, H. Xu, and M. A. Kay, "The 37/67-kilodalton laminin receptor is a receptor for adeno-associated virus serotypes 8, 2, 3, and 9.," *J. Virol.*, vol. 80, no. 19, pp. 9831–6, Oct. 2006.
- [104] C. Summerford, J. S. Bartlett, and R. J. Samulski, "AlphaVbeta5 integrin: a co-receptor for adeno-associated virus type 2 infection.," *Nat. Med.*, vol. 5, no. 1, pp. 78–82, Jan. 1999.
- [105] W. P. Parks, J. L. Melnick, R. Rongey, and H. D. Mayor, "Physical assay and growth cycle studies of a defective adeno-satellite virus.," *J. Virol.*, vol. 1, no. 1, pp. 171–80, Feb. 1967.
- [106] U. Bantel-Schaal and H. zur Hausen, "Characterization of the DNA of a defective human parvovirus isolated from a genital site.," *Virology*, vol. 134, no. 1, pp. 52–63, Apr. 1984.
- [107] E. A. Rutledge, C. L. Halbert, and D. W. Russell, "Infectious clones and vectors derived from adeno-associated virus (AAV) serotypes other than AAV type 2.," *J. Virol.*, vol. 72, no. 1, pp. 309–19, Jan. 1998.
- [108] A. Bello, K. Tran, A. Chand, M. Doria, M. Allocca, M. Hildinger, D. Beniac, C. Kranendonk, A. Auricchio, and G. P. Kobinger, "Isolation and evaluation of novel adeno-associated virus sequences from porcine tissues.," *Gene Ther.*, vol. 16, no. 11, pp. 1320–8, Nov. 2009.
- [109] M. Schmidt, E. Grot, P. Cervenka, S. Wainer, C. Buck, and J. A. Chiorini, "Identification and characterization of novel adeno-associated virus isolates in ATCC virus stocks.," *J. Virol.*, vol. 80, no. 10, pp. 5082–5, May 2006.
- [110] A. Asokan, D. V Schaffer, and R. J. Samulski, "The AAV vector toolkit: poised at the clinical crossroads.," *Mol. Ther.*, vol. 20, no. 4, pp. 699–708, Apr. 2012.
- [111] M. Nonnenmacher and T. Weber, "Intracellular transport of recombinant adeno-associated virus vectors.," *Gene Ther.*, no. November 2011, pp. 1–10, Feb. 2012.
- [112] S. Uhrig, O. Coutelle, T. Wiehe, L. Perabo, M. Hallek, and H. Büning, "Successful target cell transduction of capsid-engineered rAAV vectors requires clathrin-dependent endocytosis.," *Gene Ther.*, vol. 19, no. 2, pp. 210–8, Feb. 2012.
- [113] M. Nonnenmacher and T. Weber, "Adeno-associated virus 2 infection requires endocytosis through the CLIC/GEEC pathway.," *Cell Host Microbe*, vol. 10, no. 6, pp. 563–76, Dec. 2011.

- [114] U. Bantel-Schaal, I. Braspenning-Wesch, and J. Kartenbeck, "Adeno-associated virus type 5 exploits two different entry pathways in human embryo fibroblasts.," *J. Gen. Virol.*, vol. 90, no. Pt 2, pp. 317–22, Feb. 2009.
- [115] U. Bantel-Schaal, B. Hub, and J. Kartenbeck, "Endocytosis of adeno-associated virus type 5 leads to accumulation of virus particles in the Golgi compartment.," *J. Virol.*, vol. 76, no. 5, pp. 2340–9, Mar. 2002.
- [116] S. Sanlioglu, P. K. Benson, J. Yang, E. Morrey, T. Reynolds, J. F. Engelhardt, and E. M. Atkinson, "Endocytosis and Nuclear Trafficking of Adeno-Associated Virus Type 2 Are Controlled by Rac1 and Phosphatidylinositol-3 Kinase Activation," *J. Virol.*, vol. 74, no. 19, pp. 9184–96, Oct. 2000.
- [117] J. S. Bartlett, R. Wilcher, and R. J. Samulski, "Infectious Entry Pathway of Adeno-Associated Virus and Adeno-Associated Virus Vectors Infectious Entry Pathway of Adeno-Associated Virus and Adeno-Associated Virus Vectors," *J. Virol.*, vol. 74, no. 6, pp. 2777–85, Mar. 2000.
- [118] W. Ding, L. N. Zhang, C. Yeaman, and J. F. Engelhardt, "rAAV2 traffics through both the late and the recycling endosomes in a dose-dependent fashion.," *Mol. Ther.*, vol. 13, no. 4, pp. 671–82, Apr. 2006.
- [119] W. Xiao, K. H. W. Jr, P. Hearing, J. Hughes, N. Muzyczka, and K. H. Warrington, "Adenovirus-Facilitated Nuclear Translocation of Adeno-Associated Virus Type 2," *J. Virol.*, vol. 76, no. 22, pp. 11505–17, Nov. 2002.
- [120] G. Seisenberger, M. U. Ried, T. Endress, H. Büning, M. Hallek, and C. Bräuchle, "Real-time single-molecule imaging of the infection pathway of an adeno-associated virus.," *Science*, vol. 294, no. 5548, pp. 1929–32, Nov. 2001.
- [121] A. M. Douar, K. Poulard, D. Stockholm, and O. Danos, "Intracellular trafficking of adeno-associated virus vectors: routing to the late endosomal compartment and proteasome degradation.," *J. Virol.*, vol. 75, no. 4, pp. 1824–33, Feb. 2001.
- [122] K. Pajusola, M. Gruchala, H. Joch, T. F. Lüscher, S. Ylä-Herttuala, and H. Büeler, "Cell-type-specific characteristics modulate the transduction efficiency of adeno-associated virus type 2 and restrain infection of endothelial cells.," *J. Virol.*, vol. 76, no. 22, pp. 11530–40, Nov. 2002.
- [123] J. Hansen, K. Qing, and A. Srivastava, "Infection of purified nuclei by adeno-associated virus 2.," *Mol. Ther.*, vol. 4, no. 4, pp. 289–96, Oct. 2001.
- [124] S. Kronenberg, J. a Kleinschmidt, and B. Böttcher, "Electron cryo-microscopy and image reconstruction of adeno-associated virus type 2 empty capsids.," *EMBO Rep.*, vol. 2, no. 11, pp. 997–1002, Nov. 2001.
- [125] H.-J. Nam, B. L. Gurda, R. McKenna, M. Potter, B. Byrne, M. Salganik, N. Muzyczka, and M. Agbandje-McKenna, "Structural studies of adeno-associated virus serotype 8 capsid transitions associated with endosomal trafficking.," *J. Virol.*, vol. 85, no. 22, pp. 11791–9, Nov. 2011.
- [126] D. Mudhakar and H. Harashima, "Learning from the viral journey: how to enter cells and how to overcome intracellular barriers to reach the nucleus.," *AAPS J.*, vol. 11, no. 1, pp. 65–77, Mar. 2009.

- [127] S. Stahnke, K. Lux, S. Uhrig, F. Kreppel, M. Hösel, O. Coutelle, M. Ogris, M. Hallek, and H. Büning, "Intrinsic phospholipase A2 activity of adeno-associated virus is involved in endosomal escape of incoming particles.," *Virology*, vol. 409, no. 1, pp. 77–83, Jan. 2011.
- [128] Z. Zádori, J. Szelei, M. C. Lacoste, Y. Li, S. Gariépy, P. Raymond, M. Allaire, I. R. Nabi, and P. Tijssen, "A viral phospholipase A2 is required for parvovirus infectivity.," *Dev. Cell*, vol. 1, no. 2, pp. 291–302, Aug. 2001.
- [129] L. Denby, S. a Nicklin, and a H. Baker, "Adeno-associated virus (AAV)-7 and -8 poorly transduce vascular endothelial cells and are sensitive to proteasomal degradation.," *Gene Ther.*, vol. 12, no. 20, pp. 1534–8, Oct. 2005.
- [130] D. Duan, Y. Yue, Z. Yan, J. Yang, and J. F. Engelhardt, "Endosomal processing limits gene transfer to polarized airway epithelia by adeno-associated virus.," *J. Clin. Invest.*, vol. 105, no. 11, pp. 1573–87, Jun. 2000.
- [131] U. T. Hacker, L. Wingenfeld, D. M. Kofler, N. K. Schuhmann, S. Lutz, T. Herold, S. B. S. King, F. M. Gerner, L. Perabo, J. Rabinowitz, D. M. McCarty, R. J. Samulski, M. Hallek, and H. Büning, "Adeno-associated virus serotypes 1 to 5 mediated tumor cell directed gene transfer and improvement of transduction efficiency.," *J. Gene Med.*, vol. 7, no. 11, pp. 1429–38, Nov. 2005.
- [132] W. Ding, L. Zhang, Z. Yan, and J. F. Engelhardt, "Intracellular trafficking of adeno-associated viral vectors.," *Gene Ther.*, vol. 12, no. 11, pp. 873–80, Jun. 2005.
- [133] Z. Yan, R. Zak, G. W. G. Luxton, T. C. Ritchie, U. Bantel-Schaal, and J. F. Engelhardt, "Ubiquitination of both adeno-associated virus type 2 and 5 capsid proteins affects the transduction efficiency of recombinant vectors.," *J. Virol.*, vol. 76, no. 5, pp. 2043–53, Mar. 2002.
- [134] Z. Yan, R. Zak, Y. Zhang, W. Ding, S. Godwin, K. Munson, R. Peluso, and J. F. Engelhardt, "Distinct classes of proteasome-modulating agents cooperatively augment recombinant adeno-associated virus type 2 and type 5-mediated transduction from the apical surfaces of human airway epithelia.," *J. Virol.*, vol. 78, no. 6, pp. 2863–74, Mar. 2004.
- [135] L. Zhong, B. Li, C. S. Mah, L. Govindasamy, M. Agbandje-McKenna, M. Cooper, R. W. Herzog, I. Zolotukhin, K. H. Warrington, K. A. Weigel-Van Aken, J. A. Hobbs, S. Zolotukhin, N. Muzyczka, and A. Srivastava, "Next generation of adeno-associated virus 2 vectors: point mutations in tyrosines lead to high-efficiency transduction at lower doses.," *Proc. Natl. Acad. Sci. U. S. A.*, vol. 105, no. 22, pp. 7827–32, Jun. 2008.
- [136] J. Pang, X. Dai, S. E. Boye, I. Barone, S. L. Boye, S. Mao, D. Everhart, A. Dinculescu, L. Liu, Y. Umino, B. Lei, B. Chang, R. Barlow, E. Strettoi, and W. W. Hauswirth, "Long-term retinal function and structure rescue using capsid mutant AAV8 vector in the rd10 mouse, a model of recessive retinitis pigmentosa.," *Mol. Ther.*, vol. 19, no. 2, pp. 234–42, Feb. 2011.
- [137] C. Qiao, W. Zhang, Z. Yuan, J.-H. Shin, J. Li, G. R. Jayandharan, L. Zhong, A. Srivastava, X. Xiao, and D. Duan, "Adeno-associated virus serotype 6 capsid tyrosine-to-phenylalanine mutations improve gene transfer to skeletal muscle.," *Hum. Gene Ther.*, vol. 21, no. 10, pp. 1343–8, Oct. 2010.

- [138] C. Qiao, Z. Yuan, J. Li, R. Tang, J. Li, and X. Xiao, "Single tyrosine mutation in AAV8 and AAV9 capsids is insufficient to enhance gene delivery to skeletal muscle and heart.," *Hum. Gene Ther. Methods*, vol. 23, no. 1, pp. 29–37, Feb. 2012.
- [139] B. Akache, D. Grimm, X. Shen, S. Fuess, S. R. Yant, D. S. Glazer, J. Park, and M. A. Kay, "A two-hybrid screen identifies cathepsins B and L as uncoating factors for adeno-associated virus 2 and 8.," *Mol. Ther.*, vol. 15, no. 2, pp. 330–9, Feb. 2007.
- [140] K. Lux, N. Goerlitz, S. Schlemminger, D. Goldnau, J. Endell, K. Leike, M. Kofler, S. Finke, M. Hallek, L. Perabo, and D. M. Kofler, "Green Fluorescent Protein-Tagged Adeno-Associated Virus Particles Allow the Study of Cytosolic and Nuclear Trafficking," *J. Virol.*, vol. 79, no. 18, pp. 11776–87, Sep. 2005.
- [141] J. S. Johnson and R. J. Samulski, "Enhancement of adeno-associated virus infection by mobilizing capsids into and out of the nucleolus.," *J. Virol.*, vol. 83, no. 6, pp. 2632–44, Mar. 2009.
- [142] C. E. Thomas, T. A. Storm, Z. Huang, and M. A. Kay, "Rapid uncoating of vector genomes is the key to efficient liver transduction with pseudotyped adeno-associated virus vectors.," *J. Virol.*, vol. 78, no. 6, pp. 3110–22, Mar. 2004.
- [143] J. C. Grieger, S. Snowdy, and R. J. Samulski, "Separate basic region motifs within the adeno-associated virus capsid proteins are essential for infectivity and assembly.," *J. Virol.*, vol. 80, no. 11, pp. 5199–210, Jun. 2006.
- [144] K. J. Fisher, G. P. Gao, M. D. Weitzman, R. DeMatteo, J. F. Burda, and J. M. Wilson, "Transduction with recombinant adeno-associated virus for gene therapy is limited by leading-strand synthesis.," *J. Virol.*, vol. 70, no. 1, pp. 520–32, Jan. 1996.
- [145] F. K. Ferrari, T. Samulski, T. Shenk, and R. J. Samulski, "Second-strand synthesis is a rate-limiting step for efficient transduction by recombinant adeno-associated virus vectors.," *J. Virol.*, vol. 70, no. 5, pp. 3227–34, May 1996.
- [146] D. Grimm, M. A. Kay, and J. A. Kleinschmidt, "Helper virus-free, optically controllable, and two-plasmid-based production of adeno-associated virus vectors of serotypes 1 to 6.," *Mol. Ther.*, vol. 7, no. 6, pp. 839–50, Jun. 2003.
- [147] S. Weger, A. Wistuba, D. Grimm, and J. A. Kleinschmidt, "Control of adeno-associated virus type 2 cap gene expression: relative influence of helper virus, terminal repeats, and Rep proteins.," *J. Virol.*, vol. 71, no. 11, pp. 8437–47, Nov. 1997.
- [148] D. Grimm, A. Kern, K. Rittner, and J. A. Kleinschmidt, "Novel tools for production and purification of recombinant adenoassociated virus vectors.," *Hum. Gene Ther.*, vol. 9, no. 18, pp. 2745–60, Dec. 1998.
- [149] D. M. McCarty, H. Fu, P. E. Monahan, C. E. Toulson, P. Naik, and R. J. Samulski, "Adeno-associated virus terminal repeat (TR) mutant generates self-complementary vectors to overcome the rate-limiting step to transduction in vivo.," *Gene Ther.*, vol. 10, no. 26, pp. 2112–8, Dec. 2003.
- [150] D. M. McCarty, "Self-complementary AAV vectors; advances and applications.," *Mol. Ther.*, vol. 16, no. 10, pp. 1648–56, Oct. 2008.

- [151] Stephan Mockenhaupt, "Alleviation of shRNA off target effects via rAAV vector encoded sense strand decoys," Ruberto Carola University of Heidelberg, 2011.
- [152] W. Xiao, S. C. Berta, M. M. Lu, A. D. Moscioni, J. Tazelaar, and J. M. Wilson, "Adeno-associated virus as a vector for liver-directed gene therapy.," *J. Virol.*, vol. 72, no. 12, pp. 10222–6, Dec. 1998.
- [153] D. Grimm and M. A. Kay, "From virus evolution to vector revolution: use of naturally occurring serotypes of adeno-associated virus (AAV) as novel vectors for human gene therapy.," *Curr. Gene Ther.*, vol. 3, no. 4, pp. 281–304, Aug. 2003.
- [154] D. Grimm, K. Pandey, H. Nakai, T. A. Storm, and M. A. Kay, "Liver transduction with recombinant adeno-associated virus is primarily restricted by capsid serotype not vector genotype.," *J. Virol.*, vol. 80, no. 1, pp. 426–39, Jan. 2006.
- [155] C. Zincarelli, S. Soltys, G. Rengo, and J. E. Rabinowitz, "Analysis of AAV serotypes 1-9 mediated gene expression and tropism in mice after systemic injection.," *Mol. Ther.*, vol. 16, no. 6, pp. 1073–80, Jun. 2008.
- [156] A. C. Nathwani, M. Cochrane, J. McIntosh, C. Y. C. Ng, J. Zhou, J. T. Gray, and A. M. Davidoff, "Enhancing transduction of the liver by adeno-associated viral vectors.," *Gene Ther.*, vol. 16, no. 1, pp. 60–9, Jan. 2009.
- [157] S. Ponnazhagan, P. Mukherjee, M. C. Yoder, X. S. Wang, S. Z. Zhou, J. Kaplan, S. Wadsworth, and A. Srivastava, "Adeno-associated virus 2-mediated gene transfer in vivo: organ-tropism and expression of transduced sequences in mice.," *Gene*, vol. 190, no. 1, pp. 203–10, Apr. 1997.
- [158] D. D. Koeberl, I. E. Alexander, C. L. Halbert, D. W. Russell, and A. D. Miller, "Persistent expression of human clotting factor IX from mouse liver after intravenous injection of adeno-associated virus vectors.," *Proc. Natl. Acad. Sci. U. S. A.*, vol. 94, no. 4, pp. 1426–31, Feb. 1997.
- [159] T. C. Harding, K. E. Koprivnikar, G. H. Tu, N. Zayek, S. Lew, A. Subramanian, A. Sivakumaran, D. Frey, K. Ho, M. J. VanRoey, T. C. Nichols, D. A. Bellinger, S. Yendluri, J. Waugh, J. McArthur, G. Veres, and B. A. Donahue, "Intravenous administration of an AAV-2 vector for the expression of factor IX in mice and a dog model of hemophilia B.," *Gene Ther.*, vol. 11, no. 2, pp. 204–13, Jan. 2004.
- [160] R. O. Snyder, C. H. Miao, G. A. Patijn, S. K. Spratt, O. Danos, D. Nagy, A. M. Gown, B. Winther, L. Meuse, L. K. Cohen, A. R. Thompson, and M. A. Kay, "Persistent and therapeutic concentrations of human factor IX in mice after hepatic gene transfer of recombinant AAV vectors.," *Nat. Genet.*, vol. 16, no. 3, pp. 270–6, Jul. 1997.
- [161] K. Inagaki, S. Fuess, T. A. Storm, G. A. Gibson, C. F. Mctiernan, M. A. Kay, and H. Nakai, "Robust systemic transduction with AAV9 vectors in mice: efficient global cardiac gene transfer superior to that of AAV8.," *Mol. Ther.*, vol. 14, no. 1, pp. 45–53, Jul. 2006.
- [162] C. A. Pacak, Y. Sakai, B. D. Thattaliyath, C. S. Mah, and B. J. Byrne, "Tissue specific promoters improve specificity of AAV9 mediated transgene expression following intra-vascular gene delivery in neonatal mice.," *Genet. Vaccines Ther.*, vol. 6, p. 13, Jan. 2008.

- [163] C. A. Pacak, C. S. Mah, B. D. Thattaliyath, T. J. Conlon, M. A. Lewis, D. E. Cloutier, I. Zolotukhin, A. F. Tarantal, and B. J. Byrne, "Recombinant adeno-associated virus serotype 9 leads to preferential cardiac transduction in vivo.," *Circ. Res.*, vol. 99, no. 4, pp. e3–9, Aug. 2006.
- [164] H. Fechner, I. Sipo, D. Westermann, S. Pinkert, X. Wang, L. Suckau, J. Kurreck, H. Zeichhardt, O. Müller, R. Vetter, V. Erdmann, C. Tschöpe, and W. Poller, "Cardiac-targeted RNA interference mediated by an AAV9 vector improves cardiac function in coxsackievirus B3 cardiomyopathy.," *J. Mol. Med. (Berl.)*, vol. 86, no. 9, pp. 987–97, Sep. 2008.
- [165] Z. Wang, T. Zhu, C. Qiao, L. Zhou, B. Wang, J. Zhang, C. Chen, J. Li, and X. Xiao, "Adeno-associated virus serotype 8 efficiently delivers genes to muscle and heart.," *Nat. Biotechnol.*, vol. 23, no. 3, pp. 321–8, Mar. 2005.
- [166] K. D. Foust, A. Poirier, C. A. Pacak, R. J. Mandel, and T. R. Flotte, "Neonatal intraperitoneal or intravenous injections of recombinant adeno-associated virus type 8 transduce dorsal root ganglia and lower motor neurons.," *Hum. Gene Ther.*, vol. 19, no. 1, pp. 61–70, Jan. 2008.
- [167] Z. Wang, T. Zhu, K. K. Rehman, S. Bertera, J. Zhang, C. Chen, G. Papworth, S. Watkins, M. Trucco, P. D. Robbins, J. Li, and X. Xiao, "Widespread and stable pancreatic gene transfer by adeno-associated virus vectors via different routes.," *Diabetes*, vol. 55, no. 4, pp. 875–84, Apr. 2006.
- [168] C. Rivière, O. Danos, and A. M. Douar, "Long-term expression and repeated administration of AAV type 1, 2 and 5 vectors in skeletal muscle of immunocompetent adult mice.," *Gene Ther.*, vol. 13, no. 17, pp. 1300–8, Sep. 2006.
- [169] S. Lorain, D.-A. Gross, A. Goyenvalle, O. Danos, J. Davoust, and L. Garcia, "Transient immunomodulation allows repeated injections of AAV1 and correction of muscular dystrophy in multiple muscles.," *Mol. Ther.*, vol. 16, no. 3, pp. 541–7, Mar. 2008.
- [170] B. Sun, H. Zhang, L. M. Franco, T. Brown, A. Bird, A. Schneider, and D. D. Koeberl, "Correction of glycogen storage disease type II by an adeno-associated virus vector containing a muscle-specific promoter.," *Mol. Ther.*, vol. 11, no. 6, pp. 889–98, Jun. 2005.
- [171] L. Du, M. Kido, D. V Lee, J. E. Rabinowitz, R. J. Samulski, S. W. Jamieson, M. D. Weitzman, and P. A. Thistlethwaite, "Differential myocardial gene delivery by recombinant serotype-specific adeno-associated viral vectors.," *Mol. Ther.*, vol. 10, no. 3, pp. 604–8, Sep. 2004.
- [172] J. Palomeque, E. R. Chemaly, P. Colosi, J. A. Wellman, S. Zhou, F. Del Monte, and R. J. Hajjar, "Efficiency of eight different AAV serotypes in transducing rat myocardium in vivo.," *Gene Ther.*, vol. 14, no. 13, pp. 989–97, Jul. 2007.
- [173] C. Towne, C. Raoul, B. L. Schneider, and P. Aebischer, "Systemic AAV6 delivery mediating RNA interference against SOD1: neuromuscular transduction does not alter disease progression in fALS mice.," *Mol. Ther.*, vol. 16, no. 6, pp. 1018–25, Jun. 2008.
- [174] B. L. Davidson, C. S. Stein, J. A. Heth, I. Martins, R. M. Kotin, T. A. Derksen, J. Zabner, A. Ghodsi, and J. A. Chiorini, "Recombinant adeno-associated virus type 2, 4, and 5 vectors: transduction of variant cell types and regions in the mammalian central nervous system.," *Proc. Natl. Acad. Sci. U. S. A.*, vol. 97, no. 7, pp. 3428–32, Mar. 2000.

- [175] D. Lin, C. R. Fantz, B. Levy, M. A. Rafi, C. Vogler, D. A. Wenger, and M. S. Sands, "AAV2/5 vector expressing galactocerebrosidase ameliorates CNS disease in the murine model of globoid-cell leukodystrophy more efficiently than AAV2.," *Mol. Ther.*, vol. 12, no. 3, pp. 422–30, Sep. 2005.
- [176] C. Burger, O. S. Gorbatyuk, M. J. Velardo, C. S. Peden, P. Williams, S. Zolotukhin, P. J. Reier, R. J. Mandel, and N. Muzyczka, "Recombinant AAV viral vectors pseudotyped with viral capsids from serotypes 1, 2, and 5 display differential efficiency and cell tropism after delivery to different regions of the central nervous system.," *Mol. Ther.*, vol. 10, no. 2, pp. 302–17, Aug. 2004.
- [177] J. M. Alisky, S. M. Hughes, S. L. Sauter, D. Jolly, T. W. Dubensky, P. D. Staber, J. A. Chiorini, and B. L. Davidson, "Transduction of murine cerebellar neurons with recombinant FIV and AAV5 vectors.," *Neuroreport*, vol. 11, no. 12, pp. 2669–73, Aug. 2000.
- [178] M. Weber, J. Rabinowitz, N. Provost, H. Conrath, S. Folliot, D. Briot, Y. Chérel, P. Chenuaud, J. Samulski, P. Moullier, and F. Rolling, "Recombinant adeno-associated virus serotype 4 mediates unique and exclusive long-term transduction of retinal pigmented epithelium in rat, dog, and nonhuman primate after subretinal delivery.," *Mol. Ther.*, vol. 7, no. 6, pp. 774–81, Jun. 2003.
- [179] M. Gorbatyuk, V. Justilien, J. Liu, W. W. Hauswirth, and A. S. Lewin, "Preservation of photoreceptor morphology and function in P23H rats using an allele independent ribozyme.," *Exp. Eye Res.*, vol. 84, no. 1, pp. 44–52, Jan. 2007.
- [180] G. S. Yang, M. Schmidt, Z. Yan, J. D. Lindbloom, T. C. Harding, B. A. Donahue, J. F. Engelhardt, R. Kotin, and B. L. Davidson, "Virus-mediated transduction of murine retina with adeno-associated virus: effects of viral capsid and genome size.," *J. Virol.*, vol. 76, no. 15, pp. 7651–60, Aug. 2002.
- [181] R. L. Klein, R. D. Dayton, J. B. Tatom, K. M. Henderson, and P. P. Henning, "AAV8, 9, Rh10, Rh43 vector gene transfer in the rat brain: effects of serotype, promoter and purification method.," *Mol. Ther.*, vol. 16, no. 1, pp. 89–96, Jan. 2008.
- [182] B. P. De, A. Heguy, N. R. Hackett, B. Ferris, P. L. Leopold, J. Lee, L. Pierre, G. Gao, J. M. Wilson, and R. G. Crystal, "High levels of persistent expression of alpha1-antitrypsin mediated by the nonhuman primate serotype rh.10 adeno-associated virus despite preexisting immunity to common human adeno-associated viruses.," *Mol. Ther.*, vol. 13, no. 1, pp. 67–76, Jan. 2006.
- [183] R. W. Herzog, E. Y. Yang, L. B. Couto, J. N. Hagstrom, D. Elwell, P. A. Fields, M. Burton, D. A. Bellinger, M. S. Read, K. M. Brinkhous, G. M. Podsakoff, T. C. Nichols, G. J. Kurtzman, and K. A. High, "Long-term correction of canine hemophilia B by gene transfer of blood coagulation factor IX mediated by adeno-associated viral vector.," *Nat. Med.*, vol. 5, no. 1, pp. 56–63, Jan. 1999.
- [184] G. P. Niemeyer, R. W. Herzog, J. Mount, V. R. Arruda, D. M. Tillson, J. Hathcock, F. W. van Ginkel, K. A. High, and C. D. Lothrop, "Long-term correction of inhibitor-prone hemophilia B dogs treated with liver-directed AAV2-mediated factor IX gene therapy.," *Blood*, vol. 113, no. 4, pp. 797–806, Jan. 2009.
- [185] V. R. Arruda, J. Schuettrumpf, R. W. Herzog, T. C. Nichols, N. Robinson, Y. Lotfi, F. Mingozzi, W. Xiao, L. B. Couto, and K. A. High, "Safety and efficacy of factor IX gene transfer to skeletal

- muscle in murine and canine hemophilia B models by adeno-associated viral vector serotype 1.," *Blood*, vol. 103, no. 1, pp. 85–92, Jan. 2004.
- [186] H. Jiang, D. Lillicrap, S. Patarroyo-White, T. Liu, X. Qian, C. D. Scallan, S. Powell, T. Keller, M. McMurray, A. Labelle, D. Nagy, J. A. Vargas, S. Zhou, L. B. Couto, and G. F. Pierce, "Multiyear therapeutic benefit of AAV serotypes 2, 6, and 8 delivering factor VIII to hemophilia A mice and dogs.," *Blood*, vol. 108, no. 1, pp. 107–15, Jul. 2006.
- [187] R. Sarkar, M. Mucci, S. Addya, R. Tetreault, D. A. Bellinger, T. C. Nichols, and H. H. Kazazian, "Long-term efficacy of adeno-associated virus serotypes 8 and 9 in hemophilia a dogs and mice.," *Hum. Gene Ther.*, vol. 17, no. 4, pp. 427–39, Apr. 2006.
- [188] H. B. Dodiya, T. Bjorklund, J. Stansell, R. J. Mandel, D. Kirik, and J. H. Kordower, "Differential transduction following basal ganglia administration of distinct pseudotyped AAV capsid serotypes in nonhuman primates.," *Mol. Ther.*, vol. 18, no. 3, pp. 579–87, Mar. 2010.
- [189] A. K. Bevan, S. Duque, K. D. Foust, P. R. Morales, L. Braun, L. Schmelzer, C. M. Chan, M. McCrate, L. G. Chicoine, B. D. Coley, P. N. Porensky, S. J. Kolb, J. R. Mendell, A. H. M. Burghes, and B. K. Kaspar, "Systemic gene delivery in large species for targeting spinal cord, brain, and peripheral tissues for pediatric disorders.," *Mol. Ther.*, vol. 19, no. 11, pp. 1971–80, Nov. 2011.
- [190] G. Le Meur, K. Stieger, A. J. Smith, M. Weber, J. Y. Deschamps, D. Nivard, A. Mendes-Madeira, N. Provost, Y. Péréon, Y. Cherel, R. R. Ali, C. Hamel, P. Moullier, and F. Rolling, "Restoration of vision in RPE65-deficient Briard dogs using an AAV serotype 4 vector that specifically targets the retinal pigmented epithelium.," *Gene Ther.*, vol. 14, no. 4, pp. 292–303, Feb. 2007.
- [191] G. Gao, M. R. Alvira, S. Somanathan, Y. Lu, L. H. Vandenberghe, J. J. Rux, R. Calcedo, J. Sanmiguel, Z. Abbas, and J. M. Wilson, "Adeno-associated viruses undergo substantial evolution in primates during natural infections.," *Proc. Natl. Acad. Sci. U. S. A.*, vol. 100, no. 10, pp. 6081–6, May 2003.
- [192] R. Calcedo, L. H. Vandenberghe, G. Gao, J. Lin, and J. M. Wilson, "Worldwide epidemiology of neutralizing antibodies to adeno-associated viruses.," *J. Infect. Dis.*, vol. 199, no. 3, pp. 381–90, Feb. 2009.
- [193] C. L. Halbert, A. D. Miller, S. McNamara, J. Emerson, R. L. Gibson, B. Ramsey, and M. L. Aitken, "Prevalence of neutralizing antibodies against adeno-associated virus (AAV) types 2, 5, and 6 in cystic fibrosis and normal populations: Implications for gene therapy using AAV vectors.," *Hum. Gene Ther.*, vol. 17, no. 4, pp. 440–7, Apr. 2006.
- [194] N. Chirmule, W. Xiao, A. Truneh, M. A. Schnell, J. V. Hughes, P. Zoltick, and J. M. Wilson, "Humoral immunity to adeno-associated virus type 2 vectors following administration to murine and nonhuman primate muscle.," *J. Virol.*, vol. 74, no. 5, pp. 2420–5, Mar. 2000.
- [195] C. S. Manno, G. F. Pierce, V. R. Arruda, B. Glader, M. Ragni, J. J. Rasko, J. Rasko, M. C. Ozelo, K. Hoots, P. Blatt, B. Konkle, M. Dake, R. Kaye, M. Razavi, A. Zajko, J. Zehnder, P. K. Rustagi, H. Nakai, A. Chew, D. Leonard, J. F. Wright, R. R. Lessard, J. M. Sommer, M. Tigges, D. Sabatino, A. Luk, H. Jiang, F. Mingozzi, L. Couto, H. C. Ertl, K. A. High, and M. A. Kay, "Successful transduction of liver in hemophilia by AAV-Factor IX and limitations imposed by the host immune response.," *Nat. Med.*, vol. 12, no. 3, pp. 342–7, Mar. 2006.

- [196] F. Mingozzi, M. V Maus, D. J. Hui, D. E. Sabatino, S. L. Murphy, J. E. J. Rasko, M. V Ragni, C. S. Manno, J. Sommer, H. Jiang, G. F. Pierce, H. C. J. Ertl, and K. A. High, "CD8(+) T-cell responses to adeno-associated virus capsid in humans.," *Nat. Med.*, vol. 13, no. 4, pp. 419–22, Apr. 2007.
- [197] R. W. Herzog, "Immune responses to AAV capsid: are mice not humans after all?," *Mol. Ther.*, vol. 15, no. 4, pp. 649–50, Apr. 2007.
- [198] A. T. Martino, E. Basner-Tschakarjan, D. M. Markusic, J. D. Finn, C. Hinderer, S. Zhou, D. A. Ostrov, A. Srivastava, H. C. J. Ertl, C. Terhorst, K. A. High, F. Mingozzi, and R. W. Herzog, "Engineered AAV vector minimizes in vivo targeting of transduced hepatocytes by capsid-specific CD8+ T cells.," *Blood*, vol. 121, no. 12, pp. 2224–33, Mar. 2013.
- [199] F. Mingozzi and K. A. High, "Immune responses to AAV vectors: overcoming barriers to successful gene therapy.," *Blood*, vol. 122, no. 1, pp. 23–36, Jul. 2013.
- [200] F. Mingozzi and K. a High, "Therapeutic in vivo gene transfer for genetic disease using AAV: progress and challenges.," *Nat. Rev. Genet.*, vol. 12, no. 5, pp. 341–55, May 2011.
- [201] M. O'Reilly, A. Shipp, E. Rosenthal, R. Jambou, T. Shih, M. Montgomery, L. Gargiulo, A. Patterson, and J. Corrigan-Curay, "NIH oversight of human gene transfer research involving retroviral, lentiviral, and adeno-associated virus vectors and the role of the NIH recombinant DNA advisory committee.," *Methods Enzymol.*, vol. 507, pp. 313–35, Jan. 2012.
- [202] J. C. Grieger and R. J. Samulski, "Adeno-associated virus vectorology, manufacturing, and clinical applications.," *Methods Enzymol.*, vol. 507, pp. 229–54, Jan. 2012.
- [203] S. Ponnazhagan, G. Mahendra, S. Kumar, J. A. Thompson, and M. Castillas, "Conjugate-based targeting of recombinant adeno-associated virus type 2 vectors by using avidin-linked ligands.," *J. Virol.*, vol. 76, no. 24, pp. 12900–7, Dec. 2002.
- [204] J. S. Bartlett, J. Kleinschmidt, R. C. Boucher, and R. J. Samulski, "Targeted adeno-associated virus vector transduction of nonpermissive cells mediated by a bispecific F(ab'gamma)2 antibody.," *Nat. Biotechnol.*, vol. 17, no. 2, pp. 181–6, Feb. 1999.
- [205] M. U. Ried, A. Girod, K. Leike, H. Büning, and M. Hallek, "Adeno-associated virus capsids displaying immunoglobulin-binding domains permit antibody-mediated vector retargeting to specific cell surface receptors.," *J. Virol.*, vol. 76, no. 9, pp. 4559–66, May 2002.
- [206] J. E. Rabinowitz, D. E. Bowles, S. M. Faust, J. G. Ledford, S. E. Cunningham, and R. J. Samulski, "Cross-dressing the virion: the transcapsidation of adeno-associated virus serotypes functionally defines subgroups.," *J. Virol.*, vol. 78, no. 9, pp. 4421–32, May 2004.
- [207] Z. Wu, A. Asokan, and R. J. Samulski, "Adeno-associated virus serotypes: vector toolkit for human gene therapy.," *Mol. Ther.*, vol. 14, no. 3, pp. 316–27, Sep. 2006.
- [208] L. Gigout, P. Rebollo, N. Clement, K. H. Warrington, N. Muzyczka, R. M. Linden, and T. Weber, "Altering AAV tropism with mosaic viral capsids.," *Mol. Ther.*, vol. 11, no. 6, pp. 856–65, Jun. 2005.
- [209] B. Hauck, R. R. Xu, J. Xie, W. Wu, Q. Ding, M. Sipler, H. Wang, L. Chen, J. F. Wright, and W. Xiao, "Efficient AAV1-AAV2 hybrid vector for gene therapy of hemophilia.," *Hum. Gene Ther.*, vol. 17, no. 1, pp. 46–54, Jan. 2006.

- [210] D. E. Bowles, J. E. Rabinowitz, and R. J. Samulski, "Marker rescue of adeno-associated virus (AAV) capsid mutants: a novel approach for chimeric AAV production.," *J. Virol.*, vol. 77, no. 1, pp. 423–32, Jan. 2003.
- [211] X. Shen, T. Storm, and M. A. Kay, "Characterization of the relationship of AAV capsid domain swapping to liver transduction efficiency.," *Mol. Ther.*, vol. 15, no. 11, pp. 1955–62, Nov. 2007.
- [212] D. Grimm, J. S. Lee, L. Wang, T. Desai, B. Akache, T. a Storm, and M. a Kay, "In vitro and in vivo gene therapy vector evolution via multispecies interbreeding and retargeting of adeno-associated viruses.," *J. Virol.*, vol. 82, no. 12, pp. 5887–911, Jun. 2008.
- [213] C. Stemmer, "DNA shuffling by random fragmentation and reassembly: In vitro recombination for molecular evolution.," *Proc. Natl. Acad. Sci. U. S. A.*, vol. 91, no. October, pp. 10747–51, 1994.
- [214] J. T. Koerber, J.-H. Jang, and D. V Schaffer, "DNA shuffling of adeno-associated virus yields functionally diverse viral progeny.," *Mol. Ther.*, vol. 16, no. 10, pp. 1703–9, Oct. 2008.
- [215] P. Ward and C. E. Walsh, "Chimeric AAV Cap sequences alter gene transduction.," *Virology*, vol. 386, no. 2, pp. 237–48, Apr. 2009.
- [216] L. Yang, J. Jiang, L. M. Drouin, M. Agbandje-McKenna, C. Chen, C. Qiao, D. Pu, X. Hu, D.-Z. Wang, J. Li, and X. Xiao, "A myocardium tropic adeno-associated virus (AAV) evolved by DNA shuffling and in vivo selection.," *Proc. Natl. Acad. Sci. U. S. A.*, vol. 106, no. 10, pp. 3946–51, Mar. 2009.
- [217] S. J. Gray, B. L. Blake, H. E. Criswell, S. C. Nicolson, R. J. Samulski, T. J. McCown, and W. Li, "Directed evolution of a novel adeno-associated virus (AAV) vector that crosses the seizure-compromised blood-brain barrier (BBB).," *Mol. Ther.*, vol. 18, no. 3, pp. 570–8, Mar. 2010.
- [218] J. T. Koerber, R. Klimczak, J.-H. Jang, D. Dalkara, J. G. Flannery, and D. V Schaffer, "Molecular evolution of adeno-associated virus for enhanced glial gene delivery.," *Mol. Ther.*, vol. 17, no. 12, pp. 2088–95, Dec. 2009.
- [219] J.-H. Jang, J. T. Koerber, J.-S. Kim, P. Asuri, T. Vazin, M. Bartel, A. Keung, I. Kwon, K. I. Park, and D. V Schaffer, "An evolved adeno-associated viral variant enhances gene delivery and gene targeting in neural stem cells.," *Mol. Ther.*, vol. 19, no. 4, pp. 667–75, Apr. 2011.
- [220] W. Shi and J. S. Bartlett, "RGD inclusion in VP3 provides adeno-associated virus type 2 (AAV2)-based vectors with a heparan sulfate-independent cell entry mechanism.," *Mol. Ther.*, vol. 7, no. 4, pp. 515–25, Apr. 2003.
- [221] O. J. Müller, F. Kaul, M. D. Weitzman, R. Pasqualini, W. Arap, J. a Kleinschmidt, and M. Trepel, "Random peptide libraries displayed on adeno-associated virus to select for targeted gene therapy vectors.," *Nat. Biotechnol.*, vol. 21, no. 9, pp. 1040–6, Sep. 2003.
- [222] M. Grifman, M. Trepel, P. Speece, L. B. Gilbert, W. Arap, R. Pasqualini, and M. D. Weitzman, "Incorporation of tumor-targeting peptides into recombinant adeno-associated virus capsids.," *Mol. Ther.*, vol. 3, no. 6, pp. 964–75, Jun. 2001.

- [223] S. Michelfelder, J. Kohlschütter, A. Skorupa, S. Pfennings, O. Müller, J. a Kleinschmidt, and M. Trepel, "Successful expansion but not complete restriction of tropism of adeno-associated virus by in vivo biopanning of random virus display peptide libraries.," *PLoS One*, vol. 4, no. 4, p. e5122, Jan. 2009.
- [224] S. Michelfelder, K. Varadi, C. Raupp, A. Hunger, J. Körbelin, C. Pahrman, S. Schrepfer, O. J. Müller, J. a Kleinschmidt, and M. Trepel, "Peptide ligands incorporated into the threefold spike capsid domain to re-direct gene transduction of AAV8 and AAV9 in vivo.," *PLoS One*, vol. 6, no. 8, p. e23101, Jan. 2011.
- [225] K. Varadi, S. Michelfelder, T. Korff, M. Hecker, M. Trepel, H. a Katus, J. a Kleinschmidt, and O. J. Müller, "Novel random peptide libraries displayed on AAV serotype 9 for selection of endothelial cell-directed gene transfer vectors.," *Gene Ther.*, vol. 19, no. 8, pp. 800–9, Aug. 2012.
- [226] D. A. Waterkamp, O. J. Müller, Y. Ying, M. Trepel, and J. A. Kleinschmidt, "Isolation of targeted AAV2 vectors from novel virus display libraries.," *J. Gene Med.*, vol. 8, no. 11, pp. 1307–19, Nov. 2006.
- [227] Y. Matsuoka, G. E. Moore, Y. Yagi, and D. Pressman, "Production of free light chains of immunoglobulin by a hematopoietic cell line derived from a patient with multiple myeloma.," *Proc. Soc. Exp. Biol. Med.*, vol. 125, no. 4, pp. 1246–50, 1963.
- [228] D. J. Giard, S. A. Aaronson, G. J. Todaro, P. Arnstein, J. H. Kersey, H. Dosik, and W. P. Parks, "In vitro cultivation of human tumors: establishment of cell lines derived from a series of solid tumors.," *J. Natl. Cancer Inst.*, vol. 51, no. 5, pp. 1417–23, Nov. 1973.
- [229] S. Shimizu, T. Takiguchi, M. Fukutoku, R. Yoshioka, Y. Hirose, S. Fukuhara, H. Ohno, Y. Isobe, and S. Konda, "Establishment of a CD4-positive plasmacytoma cell line (AMO1).," *Leukemia*, vol. 7, no. 2, pp. 274–80, Feb. 1993.
- [230] W. F. Benedict, J. E. Gielen, I. S. Owens, A. Niwa, and D. W. Bebert, "Aryl hydrocarbon hydroxylase induction in mammalian liver cell culture. IV. Stimulation of the enzyme activity in established cell lines derived from rat or mouse hepatoma and from normal rat liver.," *Biochem. Pharmacol.*, vol. 22, no. 21, pp. 2766–9, Nov. 1973.
- [231] F. L. Graham, J. Smiley, W. C. Russell, and R. Nairn, "Characteristics of a human cell line transformed by DNA from human adenovirus type 5.," *J. Gen. Virol.*, vol. 36, no. 1, pp. 59–74, Jul. 1977.
- [232] T. R. Chen, "Re-evaluation of HeLa, HeLa S3, and HEP-2 karyotypes.," *Cytogenet. Cell Genet.*, vol. 48, no. 1, pp. 19–24, Jan. 1988.
- [233] D. O. Morgan, J. C. Edman, D. N. Standring, V. A. Fried, M. C. Smith, R. A. Roth, and W. J. Rutter, "Insulin-like growth factor II receptor as a multifunctional binding protein.," *Nature*, vol. 329, no. 6137, pp. 301–7, 1987.
- [234] G. J. Darlington, H. P. Bernhard, R. A. Miller, and F. H. Ruddle, "Expression of liver phenotypes in cultured mouse hepatoma cells.," *J. Natl. Cancer Inst.*, vol. 64, no. 4, pp. 809–19, Apr. 1980.

- [235] K. Takahashi, K. Tanabe, M. Ohnuki, M. Narita, T. Ichisaka, K. Tomoda, and S. Yamanaka, "Induction of pluripotent stem cells from adult human fibroblasts by defined factors.," *Cell*, vol. 131, no. 5, pp. 861–72, Nov. 2007.
- [236] J. Fogh, W. C. Wright, and J. D. Loveless, "Absence of HeLa cell contamination in 169 cell lines derived from human tumors.," *J. Natl. Cancer Inst.*, vol. 58, no. 2, pp. 209–14, Feb. 1977.
- [237] H. Nakabayashi, K. Taketa, K. Miyano, T. Yamane, and J. Sato, "Growth of human hepatoma cells lines with differentiated functions in chemically defined medium.," *Cancer Res.*, vol. 42, no. 9, pp. 3858–63, Sep. 1982.
- [238] M. E. MacKay VL, "Immortalized dendritic cells. US Patent 5,648,219 dated Jul 15 1997," US Patent 5,648,2191997.
- [239] U. Schneider, H. U. Schwenk, and G. Bornkamm, "Characterization of EBV-genome negative 'null' and 'T' cell lines derived from children with acute lymphoblastic leukemia and leukemic transformed non-Hodgkin lymphoma.," *Int. J. Cancer*, vol. 19, no. 5, pp. 621–6, May 1977.
- [240] C. B. Lozzio and B. B. Lozzio, "Human chronic myelogenous leukemia cell-line with positive Philadelphia chromosome.," *Blood*, vol. 45, no. 3, pp. 321–34, Mar. 1975.
- [241] P. Fischer, E. Nacheva, D. Y. Mason, P. D. Sherrington, C. Hoyle, F. G. Hayhoe, and A. Karpas, "A Ki-1 (CD30)-positive human cell line (Karpas 299) established from a high-grade non-Hodgkin's lymphoma, showing a 2;5 translocation and rearrangement of the T-cell receptor beta-chain gene.," *Blood*, vol. 72, no. 1, pp. 234–40, Jul. 1988.
- [242] H. P. Koeffler and D. W. Golde, "Acute myelogenous leukemia: a human cell line responsive to colony-stimulating activity.," *Science*, vol. 200, no. 4346, pp. 1153–4, Jun. 1978.
- [243] M. Namba, T. Ohtsuki, M. Mori, A. Togawa, H. Wada, T. Sugihara, Y. Yawata, and T. Kimoto, "Establishment of five human myeloma cell lines.," *In Vitro Cell. Dev. Biol.*, vol. 25, no. 8, pp. 723–9, Aug. 1989.
- [244] V. Diehl, M. Schaadt, H. Kirchner, K. P. Hellriegel, F. Gudat, C. Fonatsch, E. Laskewitz, and R. Guggenheim, "Long-term cultivation of plasma cell leukemia cells and autologous lymphoblasts (LCL) in vitro: a comparative study.," *Blut*, vol. 36, no. 6, pp. 331–8, Jun. 1978.
- [245] H. D. Soule and C. M. McGrath, "A simplified method for passage and long-term growth of human mammary epithelial cells.," *In Vitro Cell. Dev. Biol.*, vol. 22, no. 1, pp. 6–12, Jan. 1986.
- [246] H. D. Soule, J. Vazquez, A. Long, S. Albert, and M. Brennan, "A human cell line from a pleural effusion derived from a breast carcinoma.," *J. Natl. Cancer Inst.*, vol. 51, no. 5, pp. 1409–16, Nov. 1973.
- [247] M. J. Siciliano, P. E. Barker, and R. Cailleau, "Mutually exclusive genetic signatures of human breast tumor cell lines with a common chromosomal marker.," *Cancer Res.*, vol. 39, no. 3, pp. 919–22, Mar. 1979.
- [248] Y. Matsuo, S. Nakamura, T. Adachi, and T. Tsubota, "Establishment and characterization of new IgD lambda type myeloma cell lines, MOLP-2 and MOLP-3, expressing CD28, CD33 antigens and the IL-6 receptor.," *Hum. Cell*, vol. 6, no. 4, pp. 310–3, Dec. 1993.

- [249] Y. Matsuo, H. G. Drexler, A. Harashima, A. Okochi, A. Hasegawa, K. Kojima, and K. Orita, "Induction of CD28 on the new myeloma cell line MOLP-8 with t(11;14)(q13;q32) expressing delta/lambda type immunoglobulin.," *Leuk. Res.*, vol. 28, no. 8, pp. 869–77, Aug. 2004.
- [250] S. Harada, Y. Koyanagi, and N. Yamamoto, "Infection of human T-lymphotropic virus type-I (HTLV-I)-bearing MT-4 cells with HTLV-III (AIDS virus): chronological studies of early events.," *Virology*, vol. 146, no. 2, pp. 272–81, Oct. 1985.
- [251] S. A. Aaronson and G. J. Todaro, "Development of 3T3-like lines from Balb-c mouse embryo cultures: transformation susceptibility to SV40.," *J. Cell. Physiol.*, vol. 72, no. 2, pp. 141–8, Oct. 1968.
- [252] M. J. Robertson, K. J. Cochran, C. Cameron, J. M. Le, R. Tantravahi, and J. Ritz, "Characterization of a cell line, NKL, derived from an aggressive human natural killer cell leukemia.," *Exp. Hematol.*, vol. 24, no. 3, pp. 406–15, Feb. 1996.
- [253] S. Katagiri, T. Yonezawa, J. Kuyama, Y. Kanayama, K. Nishida, T. Abe, T. Tamaki, M. Ohnishi, and S. Tarui, "Two distinct human myeloma cell lines originating from one patient with myeloma.," *Int. J. Cancer*, vol. 36, no. 2, pp. 241–6, Aug. 1985.
- [254] T. C. Hamilton, R. C. Young, W. M. McKoy, K. R. Grotzinger, J. A. Green, E. W. Chu, J. Whang-Peng, A. M. Rogan, W. R. Green, and R. F. Ozols, "Characterization of a human ovarian carcinoma cell line (NIH:OVCA-3) with androgen and estrogen receptors.," *Cancer Res.*, vol. 43, no. 11, pp. 5379–89, Nov. 1983.
- [255] M. Lieber, J. Mazzetta, W. Nelson-Rees, M. Kaplan, and G. Todaro, "Establishment of a continuous tumor-cell line (panc-1) from a human carcinoma of the exocrine pancreas.," *Int. J. Cancer*, vol. 15, no. 5, pp. 741–7, May 1975.
- [256] M. E. Kaighn, K. S. Narayan, Y. Ohnuki, J. F. Lechner, and L. W. Jones, "Establishment and characterization of a human prostatic carcinoma cell line (PC-3).," *Invest. Urol.*, vol. 17, no. 1, pp. 16–23, Jul. 1979.
- [257] J. V Pulvertaft, "Cytology of Burkitt's Tumour (African Lymphoma).," *Lancet*, vol. 1, no. 7327, pp. 238–40, Feb. 1964.
- [258] P. Ralph and I. Nakoinz, "Antibody-dependent killing of erythrocyte and tumor targets by macrophage-related cell lines: enhancement by PPD and LPS.," *J. Immunol.*, vol. 119, no. 3, pp. 950–54, Sep. 1977.
- [259] J. T. Rutka, J. R. Giblin, H. K. Høifødt, D. V Dougherty, C. W. Bell, J. R. McCulloch, R. L. Davis, C. B. Wilson, and M. L. Rosenblum, "Establishment and characterization of a cell line from a human gliosarcoma.," *Cancer Res.*, vol. 46, no. 11, pp. 5893–902, Nov. 1986.
- [260] J. L. Biedler, L. Helson, and B. A. Spengler, "Morphology and growth, tumorigenicity, and cytogenetics of human neuroblastoma cells in continuous culture.," *Cancer Res.*, vol. 33, no. 11, pp. 2643–52, Nov. 1973.
- [261] O. Saiki and P. Ralph, "Clonal differences in response to T cell replacing factor (TRF) for IgM secretion and TRF receptors in a human B lymphoblast cell line.," *Eur. J. Immunol.*, vol. 13, no. 1, pp. 31–4, Jan. 1983.

- [262] S. D. Smith, R. Morgan, M. P. Link, P. McFall, and F. Hecht, "Cytogenetic and immunophenotypic analysis of cell lines established from patients with T cell leukemia/lymphoma.," *Blood*, vol. 67, no. 3, pp. 650–6, Mar. 1986.
- [263] G. H. Stein, "T98G: an anchorage-independent human tumor cell line that exhibits stationary phase G1 arrest in vitro.," *J. Cell. Physiol.*, vol. 99, no. 1, pp. 43–54, Apr. 1979.
- [264] S. Tsuchiya, Y. Kobayashi, Y. Goto, H. Okumura, S. Nakae, T. Konno, and K. Tada, "Induction of maturation in cultured human monocytic leukemia cells by a phorbol diester.," *Cancer Res.*, vol. 42, no. 4, pp. 1530–6, Apr. 1982.
- [265] K. Nilsson, H. Bennich, S. G. Johansson, and J. Pontén, "Established immunoglobulin producing myeloma (IgE) and lymphoblastoid (IgG) cell lines from an IgE myeloma patient.," *Clin. Exp. Immunol.*, vol. 7, no. 4, pp. 477–89, Oct. 1970.
- [266] J. Pontén and E. H. Macintyre, "Long term culture of normal and neoplastic human glia.," *Acta Pathol. Microbiol. Scand.*, vol. 74, no. 4, pp. 465–86, Jan. 1968.
- [267] C. Sundström and K. Nilsson, "Establishment and characterization of a human histiocytic lymphoma cell line (U-937).," *Int. J. Cancer*, vol. 17, no. 5, pp. 565–77, May 1976.
- [268] M. Herlyn, J. Thurin, G. Balaban, J. L. Bennicelli, D. Herlyn, D. E. Elder, E. Bondi, D. Guerry, P. Nowell, W. H. Clark, and H. Koprowski, "Characteristics of Cultured Human Melanocytes Isolated from Different Stages of Tumor Progression," *Cancer Res.*, vol. 45, no. 11_Part_2, pp. 5670–76, Nov. 1985.
- [269] C. A. Schneider, W. S. Rasband, and K. W. Eliceiri, "NIH Image to ImageJ: 25 years of image analysis.," *Nat. Methods*, vol. 9, no. 7, pp. 671–5, Jul. 2012.
- [270] N. Schürmann, L. G. Trabuco, C. Bender, R. B. Russell, and D. Grimm, "Molecular dissection of human Argonaute proteins by DNA shuffling.," *Nat. Struct. Mol. Biol.*, vol. 20, no. 7, pp. 818–26, Jul. 2013.
- [271] A. Wistuba, S. Weger, A. Kern, and J. A. Kleinschmidt, "Intermediates of adeno-associated virus type 2 assembly: identification of soluble complexes containing Rep and Cap proteins.," *J. Virol.*, vol. 69, no. 9, pp. 5311–9, Sep. 1995.
- [272] A. Wistuba, A. Kern, S. Weger, D. Grimm, and J. A. Kleinschmidt, "Subcellular compartmentalization of adeno-associated virus type 2 assembly," *J. Virol.*, vol. 71, no. 2, pp. 1341–52, Feb. 1997.
- [273] S. Zolotukhin, M. Potter, W. W. Hauswirth, J. Guy, and N. Muzyczka, "A 'humanized' green fluorescent protein cDNA adapted for high-level expression in mammalian cells.," *J. Virol.*, vol. 70, no. 7, pp. 4646–54, Jul. 1996.
- [274] D. Grimm, K. L. Streetz, C. L. Jopling, T. A. Storm, K. Pandey, C. R. Davis, P. Marion, F. Salazar, and M. A. Kay, "Fatality in mice due to oversaturation of cellular microRNA/short hairpin RNA pathways.," *Nature*, vol. 441, no. 7092, pp. 537–41, May 2006.
- [275] T. Matsushita, T. Okada, T. Inaba, H. Mizukami, K. Ozawa, and P. Colosi, "The adenovirus E1A and E1B19K genes provide a helper function for transfection-based adeno-associated virus vector production.," *J. Gen. Virol.*, vol. 85, no. Pt 8, pp. 2209–14, Aug. 2004.

- [276] E. Kienle, E. Senís, K. Börner, D. Niopek, E. Wiedtke, S. Grosse, and D. Grimm, "Engineering and evolution of synthetic adeno-associated virus (AAV) gene therapy vectors via DNA family shuffling," *J. Vis. Exp.*, no. 62, Jan. 2012.
- [277] A. K. Zaiss and D. A. Muruve, "Immunity to adeno-associated virus vectors in animals and humans: a continued challenge.," *Gene Ther.*, vol. 15, no. 11, pp. 808–16, Jun. 2008.
- [278] S. Boutin, V. Monteilhet, P. Veron, C. Leborgne, O. Benveniste, M. F. Montus, and C. Masurier, "Prevalence of serum IgG and neutralizing factors against adeno-associated virus (AAV) types 1, 2, 5, 6, 8, and 9 in the healthy population: implications for gene therapy using AAV vectors.," *Hum. Gene Ther.*, vol. 21, no. 6, pp. 704–12, Jun. 2010.
- [279] D. F. Aschauer, S. Kreuz, and S. Rumpel, "Analysis of Transduction Efficiency, Tropism and Axonal Transport of AAV Serotypes 1, 2, 5, 6, 8 and 9 in the Mouse Brain.," *PLoS One*, vol. 8, no. 9, p. e76310, Jan. 2013.
- [280] H. Büning, M. U. Ried, L. Perabo, F. M. Gerner, N. a Huttner, J. Enssle, and M. Hallek, "Receptor targeting of adeno-associated virus vectors.," *Gene Ther.*, vol. 10, no. 14, pp. 1142–51, Jul. 2003.
- [281] K. White, H. Büning, a Kritz, H. Janicki, J. McVey, L. Perabo, G. Murphy, M. Odenthal, L. M. Work, M. Hallek, S. a Nicklin, and a H. Baker, "Engineering adeno-associated virus 2 vectors for targeted gene delivery to atherosclerotic lesions.," *Gene Ther.*, vol. 15, no. 6, pp. 443–51, Mar. 2008.
- [282] M. Bechtle, "Engineering of Adeno-associated Viral Vectors for Targeted Cell Infection," Ruberto Carola University of Heidelberg, 2010.
- [283] S. Shen, K. D. Bryant, S. M. Brown, S. H. Randell, and A. Asokan, "Terminal N-linked galactose is the primary receptor for adeno-associated virus 9.," *J. Biol. Chem.*, vol. 286, no. 15, pp. 13532–40, Apr. 2011.
- [284] C. L. Bell, L. H. Vandenberghe, P. Bell, M. P. Limberis, G. Gao, K. Van Vliet, M. Agbandjeh-mckenna, and J. M. Wilson, "The AAV9 receptor and its modification to improve in vivo lung gene transfer in mice," *J. Clin. Invest.*, vol. 121, no. 6, pp. 2427–35, Jun. 2011.
- [285] A. Sacher, "Targeting Adeno-Associated Virus to Immune Cells for Application as a Genetic Vaccine Vector.," Ruperto Carola University of Heidelberg. Heidelberg., 2013.
- [286] M. Richner, M. Ulrichsen, S. L. Elmegaard, R. Dieu, L. T. Pallesen, and C. B. Vaegter, "Peripheral Nerve Injury Modulates Neurotrophin Signaling in the Peripheral and Central Nervous System.," *Mol. Neurobiol.*, vol. Epub, Apr. 2014.
- [287] M. R. J. Mason, E. M. E. Ehlert, R. Eggers, C. W. Pool, S. Hermening, A. Huseinovic, E. Timmermans, B. Blits, and J. Verhaagen, "Comparison of AAV serotypes for gene delivery to dorsal root ganglion neurons.," *Mol. Ther.*, vol. 18, no. 4, pp. 715–24, Apr. 2010.
- [288] J. Oi, T. Terashima, H. Kojima, M. Fujimiya, K. Maeda, R. Arai, L. Chan, H. Yasuda, A. Kashiwagi, and H. Kimura, "Isolation of specific peptides that home to dorsal root ganglion neurons in mice.," *Neurosci. Lett.*, vol. 434, no. 3, pp. 266–72, Apr. 2008.

- [289] T. Terashima, K. Oka, A. B. Kritz, H. Kojima, A. H. Baker, and L. Chan, "DRG-targeted helper-dependent adenoviruses mediate selective gene delivery for therapeutic rescue of sensory neuronopathies in mice.," *J. Clin. Invest.*, vol. 119, no. 7, pp. 2100–112, Jul. 2009.
- [290] A. Geisler, A. Jungmann, J. Kurreck, W. Poller, H. A. Katus, R. Vetter, H. Fechner, and O. J. Müller, "microRNA122-regulated transgene expression increases specificity of cardiac gene transfer upon intravenous delivery of AAV9 vectors.," *Gene Ther.*, vol. 18, no. 2, pp. 199–209, Feb. 2011.
- [291] M. Karali, A. Manfredi, A. Puppo, E. Marrocco, A. Gargiulo, M. Allocca, M. Della Corte, S. Rossi, M. Giunti, M. L. Bacci, F. Simonelli, E. M. Surace, S. Banfi, and A. Auricchio, "MicroRNA-restricted transgene expression in the retina.," *PLoS One*, vol. 6, no. 7, p. e22166, Jan. 2011.
- [292] C. Qiao, Z. Yuan, J. Li, B. He, H. Zheng, C. Mayer, and X. Xiao, "Liver-specific microRNA-122 target sequences incorporated in AAV vectors efficiently inhibits transgene expression in the liver.," *Gene Ther.*, vol. 18, no. 4, pp. 403–10, Apr. 2011.
- [293] A. Geisler, C. Schön, T. Gröbl, S. Pinkert, E. A. Stein, J. Kurreck, R. Vetter, and H. Fechner, "Application of mutated miR-206 target sites enables skeletal muscle-specific silencing of transgene expression of cardiotropic AAV9 vectors.," *Mol. Ther.*, vol. 21, no. 5, pp. 924–33, May 2013.
- [294] F. Mingozzi, X. M. Anguela, G. Pavani, Y. Chen, R. J. Davidson, D. J. Hui, M. Yazicioglu, L. Elkouby, C. J. Hinderer, A. Faella, C. Howard, A. Tai, G. M. Podsakoff, S. Zhou, E. Basner-Tschakarjan, J. F. Wright, and K. A. High, "Overcoming preexisting humoral immunity to AAV using capsid decoys.," *Sci. Transl. Med.*, vol. 5, no. 194, p. 194ra92, Jul. 2013.
- [295] F. Mingozzi, Y. Chen, S. C. Edmonson, S. Zhou, R. M. Thurlings, P. P. Tak, K. A. High, and M. J. Vervoordeldonk, "Prevalence and pharmacological modulation of humoral immunity to AAV vectors in gene transfer to synovial tissue.," *Gene Ther.*, vol. 20, no. 4, pp. 417–24, Apr. 2013.
- [296] Z. Wang, C. S. Kuhr, J. M. Allen, M. Blankinship, P. Gregorevic, J. S. Chamberlain, S. J. Tapscott, and R. Storb, "Sustained AAV-mediated dystrophin expression in a canine model of Duchenne muscular dystrophy with a brief course of immunosuppression.," *Mol. Ther.*, vol. 15, no. 6, pp. 1160–6, Jun. 2007.
- [297] C. A. Maguire, D. Gianni, D. H. Meijer, L. A. Shaket, S. D. Rabkin, G. Gao, and M. Sena-esteves, "Directed evolution of adeno-associated virus for glioma cell transduction," *J. Neurooncol.*, vol. 96, no. 3, pp. 337–47, Feb. 2010.
- [298] H. N. Kei Adachi, "A New Recombinant Adeno Associated Virus (AAV)- Based Random Peptide Display Library System: Infection-Defective AAV1.9-3 as a Novel Detargeted Platform for Vector Evolution," *Gene Ther. Regul.*, vol. 5, no. 1, pp. 31–55, Oct. 2010.
- [299] L. Yang and X. Xiao, "Creation of a cardiotropic adeno-associated virus: the story of viral directed evolution.," *Virology*, vol. 10, no. 1, p. 50, Jan. 2013.
- [300] W. Li, A. Asokan, Z. Wu, T. Van Dyke, N. DiPrimio, J. S. Johnson, L. Govindaswamy, M. Agbandje-McKenna, S. Leichtle, D. E. Redmond, T. J. McCown, K. B. Petermann, N. E. Sharpless, and R. J. Samulski, "Engineering and selection of shuffled AAV genomes: a new strategy for producing targeted biological nanoparticles.," *Mol. Ther.*, vol. 16, no. 7, pp. 1252–60, Jul. 2008.

- [301] K. J. D. A. Excoffon, J. T. Koerber, D. D. Dickey, M. Murtha, S. Keshavjee, B. K. Kaspar, J. Zabner, and D. V Schaffer, "Directed evolution of adeno-associated virus to an infectious respiratory virus.," *Proc. Natl. Acad. Sci. U. S. A.*, vol. 106, no. 10, pp. 3865–70, Mar. 2009.
- [302] B. L. Ellis, M. L. Hirsch, J. C. Barker, J. P. Connelly, R. J. Steininger, and M. H. Porteus, "A survey of ex vivo/in vitro transduction efficiency of mammalian primary cells and cell lines with Nine natural adeno-associated virus (AAV1-9) and one engineered adeno-associated virus serotype.," *Viol. J.*, vol. 10, no. 1, p. 74, Jan. 2013.
- [303] M. Naumer, F. Sonntag, K. Schmidt, K. Nieto, C. Panke, N. E. Davey, R. Popa-Wagner, and J. A. Kleinschmidt, "Properties of the adeno-associated virus assembly-activating protein.," *J. Virol.*, vol. 86, no. 23, pp. 13038–48, Dec. 2012.
- [304] M. Ruffing, H. Heid, and J. a Kleinschmidt, "Mutations in the carboxy terminus of adeno-associated virus 2 capsid proteins affect viral infectivity: lack of an RGD integrin-binding motif.," *J. Gen. Virol.*, vol. 75, pp. 3385–92, Dec. 1994.
- [305] N. DiPrimio, A. Asokan, L. Govindasamy, M. Agbandje-McKenna, and R. J. Samulski, "Surface loop dynamics in adeno-associated virus capsid assembly.," *J. Virol.*, vol. 82, no. 11, pp. 5178–89, Jun. 2008.
- [306] E. D. Horowitz, K. S. Rahman, B. D. Bower, D. J. Dismuke, M. R. Falvo, J. D. Griffith, S. C. Harvey, and A. Asokan, "Biophysical and ultrastructural characterization of adeno-associated virus capsid uncoating and genome release.," *J. Virol.*, vol. 87, no. 6, pp. 2994–3002, Mar. 2013.
- [307] L. I. Zhong, W. Li, Z. Yang, K. Qing, M. Tan, J. Hansen, Y. Li, L. Chen, R. J. Chan, D. Bischof, N. Maina, K. A. Weigel-kelley, W. Zhao, S. H. Larsen, M. C. Yoder, W. Shou, and A. Srivastava, "Impaired Nuclear Transport and Uncoating Limit Recombinant Adeno Associated Virus 2 Vector Mediated Transduction of Primary Murine Hematopoietic Cells," vol. 1218, no. December, pp. 1207–1218, 2004.
- [308] B. Hauck, W. Zhao, K. High, and W. Xiao, "Intracellular viral processing, not single-stranded DNA accumulation, is crucial for recombinant adeno-associated virus transduction.," *J. Virol.*, vol. 78, no. 24, pp. 13678–86, Dec. 2004.
- [309] R. M. Tenney, C. L. Bell, and J. M. Wilson, "AAV8 capsid variable regions at the two-fold symmetry axis contribute to high liver transduction by mediating nuclear entry and capsid uncoating.," *Virology*, vol. 454–455, pp. 227–36, Apr. 2014.
- [310] F. Mingozzi and K. a High, "Immune responses to AAV in clinical trials.," *Curr. Gene Ther.*, vol. 11, no. 4, pp. 321–30, Aug. 2011.
- [311] L. Wang, R. Calcedo, P. Bell, J. Lin, R. L. Grant, D. L. Siegel, and J. M. Wilson, "Impact of pre-existing immunity on gene transfer to nonhuman primate liver with adeno-associated virus 8 vectors.," *Hum. Gene Ther.*, vol. 22, no. 11, pp. 1389–401, Nov. 2011.
- [312] C. H. Miao, "Advances in Overcoming Immune Responses following Hemophilia Gene Therapy.," *J. Genet. Syndr. Gene Ther.*, vol. S1, Dec. 2011.
- [313] V. Ferreira, H. Petry, and F. Salmon, "Immune Responses to AAV-Vectors, the Glybera Example from Bench to Bedside.," *Front. Immunol.*, vol. 5, no. 82, pp. 1–15, Jan. 2014.

- [314] Y.-S. Tseng and M. Agbandje-McKenna, "Mapping the AAV Capsid Host Antibody Response toward the Development of Second Generation Gene Delivery Vectors.," *Front. Immunol.*, vol. 5, no. 9, pp. 1–11, Jan. 2014.
- [315] R. M. Buller, J. E. Janik, E. D. Sebring, and J. A. Rose, "Herpes simplex virus types 1 and 2 completely help adenovirus-associated virus replication.," *J. Virol.*, vol. 40, no. 1, pp. 241–7, Oct. 1981.
- [316] N. Zeltner, E. Kohlbrenner, N. Clément, T. Weber, and R. M. Linden, "Near-perfect infectivity of wild-type AAV as benchmark for infectivity of recombinant AAV vectors.," *Gene Ther.*, vol. 17, no. 7, pp. 872–9, Jul. 2010.
- [317] J. D. Tratschin, M. H. West, T. Sandbank, and B. J. Carter, "A human parvovirus, adeno-associated virus, as a eucaryotic vector: transient expression and encapsidation of the procaryotic gene for chloramphenicol acetyltransferase.," *Mol. Cell. Biol.*, vol. 4, no. 10, pp. 2072–81, Oct. 1984.
- [318] B. J. Carter, B. A. Antoni, and D. F. Klessig, "Adenovirus containing a deletion of the early region 2A gene allows growth of adeno-associated virus with decreased efficiency.," *Virology*, vol. 191, no. 1, pp. 473–6, Nov. 1992.
- [319] P. Ward, F. B. Dean, M. E. O'Donnell, and K. I. Berns, "Role of the adenovirus DNA-binding protein in in vitro adeno-associated virus DNA replication.," *J. Virol.*, vol. 72, no. 1, pp. 420–7, Jan. 1998.
- [320] L. S. Chang and T. Shenk, "The adenovirus DNA-binding protein stimulates the rate of transcription directed by adenovirus and adeno-associated virus promoters.," *J. Virol.*, vol. 64, no. 5, pp. 2103–9, May 1990.
- [321] S. Pilder, M. Moore, J. Logan, and T. Shenk, "The adenovirus E1B-55K transforming polypeptide modulates transport or cytoplasmic stabilization of viral and host cell mRNAs.," *Mol. Cell. Biol.*, vol. 6, no. 2, pp. 470–6, Feb. 1986.
- [322] R. J. Samulski and T. Shenk, "Adenovirus E1B 55-Mr polypeptide facilitates timely cytoplasmic accumulation of adeno-associated virus mRNAs.," *J. Virol.*, vol. 62, no. 1, pp. 206–10, Jan. 1988.
- [323] M. H. West, J. P. Trempe, J. D. Tratschin, and B. J. Carter, "Gene expression in adeno-associated virus vectors: the effects of chimeric mRNA structure, helper virus, and adenovirus VA1 RNA.," *Virology*, vol. 160, no. 1, pp. 38–47, Sep. 1987.
- [324] S.-H. Chung, K. K. Frese, R. S. Weiss, B. V. V. Prasad, and R. T. Javier, "A new crucial protein interaction element that targets the adenovirus E4-ORF1 oncoprotein to membrane vesicles.," *J. Virol.*, vol. 81, no. 9, pp. 4787–97, May 2007.
- [325] J. Wang, J. Xie, H. Lu, L. Chen, B. Hauck, R. J. Samulski, and W. Xiao, "Existence of transient functional double-stranded DNA intermediates during recombinant AAV transduction.," *Proc. Natl. Acad. Sci. U. S. A.*, vol. 104, no. 32, pp. 13104–9, Aug. 2007.
- [326] I. Sipo, H. Fechner, S. Pinkert, L. Suckau, X. Wang, S. Weger, and W. Poller, "Differential internalization and nuclear uncoating of self-complementary adeno-associated virus

- pseudotype vectors as determinants of cardiac cell transduction.," *Gene Ther.*, vol. 14, no. 18, pp. 1319–29, Sep. 2007.
- [327] Y. Ying, O. J. Müller, C. Goehringer, B. Leuchs, M. Trepel, H. a Katus, and J. a Kleinschmidt, "Heart-targeted adeno-associated viral vectors selected by in vivo biopanning of a random viral display peptide library.," *Gene Ther.*, vol. 17, no. 8, pp. 980–90, Aug. 2010.
- [328] C. Raupp, M. Naumer, O. J. Müller, B. L. Gurda, M. Agbandje-McKenna, and J. a Kleinschmidt, "The threefold protrusions of adeno-associated virus type 8 are involved in cell surface targeting as well as postattachment processing.," *J. Virol.*, vol. 86, no. 17, pp. 9396–408, Sep. 2012.
- [329] S. Michelfelder and M. Trepel, "Adeno-associated viral vectors and their redirection to cell-type specific receptors.," *Adv. Genet.*, vol. 67, no. 09, pp. 29–60, Jan. 2009.
- [330] L. Perabo, D. Goldnau, K. White, J. Endell, J. Boucas, S. Humme, L. M. Work, H. Janicki, M. Hallek, A. H. Baker, and H. Büning, "Heparan sulfate proteoglycan binding properties of adeno-associated virus retargeting mutants and consequences for their in vivo tropism.," *J. Virol.*, vol. 80, no. 14, pp. 7265–9, Jul. 2006.
- [331] M. Naumer, Y. Ying, S. Michelfelder, A. Reuter, M. Trepel, O. J. Müller, and J. a Kleinschmidt, "Development and validation of novel AAV2 random libraries displaying peptides of diverse lengths and at diverse capsid positions.," *Hum. Gene Ther.*, vol. 23, no. 5, pp. 492–507, May 2012.
- [332] C. Liu, G. Bhattacharjee, W. Boisvert, R. Dilley, and T. Edgington, "In vivo interrogation of the molecular display of atherosclerotic lesion surfaces.," *Am. J. Pathol.*, vol. 163, no. 5, pp. 1859–71, Nov. 2003.
- [333] S. Daya and K. I. Berns, "Gene therapy using adeno-associated virus vectors.," *Clin. Microbiol. Rev.*, vol. 21, no. 4, pp. 583–93, Oct. 2008.
- [334] G. R. Nemerow, "Cell receptors involved in adenovirus entry.," *Virology*, vol. 274, no. 1, pp. 1–4, Aug. 2000.
- [335] M. Mietzsch, F. Broecker, A. Reinhardt, P. H. Seeberger, and R. Heilbronn, "Differential adeno-associated virus serotype-specific interaction patterns with synthetic heparins and other glycans.," *J. Virol.*, vol. 88, no. 5, pp. 2991–3003, Mar. 2014.
- [336] C. L. Bell, B. L. Gurda, K. Van Vliet, M. Agbandje-McKenna, and J. M. Wilson, "Identification of the galactose binding domain of the adeno-associated virus serotype 9 capsid.," *J. Virol.*, vol. 86, no. 13, pp. 7326–33, Jul. 2012.
- [337] K. Adachi, T. Enoki, Y. Kawano, M. Veraz, and H. Nakai, "Drawing a high-resolution functional map of adeno-associated virus capsid by massively parallel sequencing.," *Nat. Commun.*, vol. 5, no. 3075, pp. 1–14, Jan. 2014.
- [338] L. Perabo, H. Büning, D. M. Kofler, M. U. Ried, A. Girod, C. M. Wendtner, J. Enssle, and M. Hallek, "In vitro selection of viral vectors with modified tropism: the adeno-associated virus display.," *Mol. Ther.*, vol. 8, no. 1, pp. 151–7, Jul. 2003.

- [339] S. Michelfelder, M.-K. Lee, E. deLima-Hahn, T. Wilmes, F. Kaul, O. Müller, J. a Kleinschmidt, and M. Trepel, "Vectors selected from adeno-associated viral display peptide libraries for leukemia cell-targeted cytotoxic gene therapy.," *Exp. Hematol.*, vol. 35, no. 12, pp. 1766–76, Dec. 2007.
- [340] W. Shi, G. S. Arnold, and J. S. Bartlett, "Insertional mutagenesis of the adeno-associated virus type 2 (AAV2) capsid gene and generation of AAV2 vectors targeted to alternative cell-surface receptors.," *Hum. Gene Ther.*, vol. 12, no. 14, pp. 1697–711, Sep. 2001.

Remarks

I hereby declare that I have written the submitted dissertation myself and in this process have used no other sources or materials than those expressly indicated. Moreover I hereby declare that I have not applied to be examined at any other institution, nor have I used the dissertation in this or any other form at any other institution as an examination paper, nor submitted it to any other faculty as a dissertation.

Date: _____

Signature: _____

Danksagung

An erster Stelle möchte ich Dr. Dirk Grimm danken, der mich als mein Betreuer immer und auf jede erdenkliche Weise unterstützt hat. Seinem Einsatz ist es zu verdanken, dass wir von Anfang an jede Idee nachverfolgen und quasi jedes Experiment durchführen konnten. Zum einen war und ist er sehr erfolgreich darin die nötigen Gelder einzuwerben -mir ist sonst keine Arbeitsgruppe bekannt, deren Problem es am Ende des Jahres ist, die restlichen Gelder auszugeben-. Zum anderen durfte ich in meiner wissenschaftlichen Laufbahn noch mit niemandem zusammenarbeiten, der eine bessere Übersicht über die Biowissenschaften oder ein besseres wissenschaftliches Verständnis hat. Dabei steht Dirk auch heute noch ab und an an der Bench und zeigt, dass er nicht mehr nur noch die Theorie beherrscht. Mir bleibt zu sagen: Danke Dirk!

Ich danke auch ganz besonders Herrn Prof. Dr. Hans-Georg Kräusslich, dafür, dass er das Erstgutachten meiner Dissertation übernimmt und für die hilfreichen Vorschläge und Anregungen während meiner TAC Meetings und der Seminare in der Zeit meiner Doktorarbeit.

Gleichsam bedanken möchte ich mich noch einmal bei Dr. Dirk Grimm als Zweitgutachter meiner Arbeit und Mitglied meines TAC Komitees. Weiter gilt mein Dank auch Dr. Dirk Nettelbeck als weiterem, wertvollen Mitglied des TAC Komitees und für seine Bereitschaft an meiner Disputation als Prüfer teilzunehmen; sowie Dr. Ralf Bischoff als weiterem Mitglied meines Prüfungskomitees.

Danke auch an Prof. Dr. Ralf Bartenschlager, für die Bereitschaft mich in das Doktoranden-Programm der Abteilung Infektionskrankheiten der Uni Heidelberg aufzunehmen.

Danken möchte ich außerdem unseren Kooperationspartnern, durch die es mir erst möglich war meine Konstrukte und Vektoren zu entwickeln bzw. in die konkrete Anwendung zu bringen. Hier möchte ich nennen: Dr. Jörg Rippman, Dr. Silke Uhrig –die jetzt bei uns in Heidelberg ist- und besonders Dr. Sebastian Kreuz von Böhringer Ingelheim. Außerdem Prof. Dr. Armin Blesch und Julianne McCall aus der Abteilung Experimentelle Paraplegiologie – Neuroregeneration; Dr. Dirk Hose und Dr. Anja Seckinger aus dem Labor für Myelomforschung der Medizinischen Klinik V; Dr. Anna Sacher aus der Gruppe von Prof. Dr. Martin Müller am DKFZ und Christine Kammel, die am Helmholtz Zentrum in München arbeitet. Ich möchte hier auch noch Dr. Christian Bender erwähnen, dessen SALANTO Programm gerade bei der Analyse der geschuffelten Klone von unschätzbarem Wert war. Vielen Dank für die gute Zusammenarbeit.

Ein ganz großes Dankeschön geht an alle Mitglieder der AG Grimm -ehemalige und jetzige-. Mit Blick auf den Inhalt meiner Dissertation möchte ich dabei besonders hervorheben: Marina Bechtle, die mit unseren Peptid-Display Konstrukten die ersten Screens gemacht hat und damit u.a. die Grundlage

gelegt hat für etliche Erkenntnisse in dieser und anderen Arbeiten; und auch für zukünftige Anwendungen. Außerdem Dr. Kathleen Börner, ohne deren unermüdlichen Einsatz auch meine Arbeit nicht auf den Stand gekommen wäre, auf dem sie ist; und schließlich Stefanie Große mit der ich am DFS arbeiten durfte und die diese Projekte mittlerweile noch deutlich voran gebracht hat.

Neben diesen drei waren mir alle in dieser Arbeitsgruppe -fachlich wie menschlich- die besten Kollegen, die man sich wünschen kann. Stellvertretend für alle mit denen ich in der Zeit gearbeitet habe möchte ich also Danke sagen zu: Ellen Wiedtke, Dr. Nina Schürmann und Dr. Stefan Mockenhaupt, die drei 'der ersten Stunde' die mir auf so vielfältige Weise geholfen haben. Außerdem zu Elena Senis Herrero und Franziska Hentzschel, und noch einmal zu Stefanie Große, Dr. Kathleen Börner, Marina Bechtle und Silke Uhrig.

Ich danke auch Alexandra Kelp, die mir über viele Jahre eine gute Partnerin war und auch meinen Freunden. Stellvertretend für die möchte ich hier Thomas Flier, Inga- und Alexander Roß nennen. Diesen und anderen Freunden ist wahrscheinlich gar nicht klar, was sie zu dieser Doktorarbeit beigetragen haben, aber ich möchte sagen, ohne sie hätte ich meine Promotion nicht zum Ende bringen können.

An oberster Stelle möchte ich aber meiner Familie danken. Meinem Bruder Sören und seiner Frau/ meiner Schwägerin Heike. Zum größten Dank bin ich hier aber mit Sicherheit meinen Eltern verpflichtet. Meinem Vater Gernot und meiner Mutter Brigitte. Ihr habt mich in Schule, Studium, Promotion und allen anderen Lebenslagen immer und ohne Vorbehalte -zum Teil zu eurem persönlichen Nachteil- unterstützt. Ich hätte das alles ohne euch niemals geschafft. Dafür werde ich euch immer von ganzem Herzen dankbar sein!